The Preserve: Lehigh Library Digital Collections

Molecular Structure-reactivity Relationships For Supported Molybdenum Oxide Catalysts.

Citation

Hu, Hangchun. *Molecular Structure-Reactivity Relationships For Supported Molybdenum Oxide Catalysts*. 1995, https://preserve.lehigh.edu/lehigh-scholarship/graduate-publications-theses-dissertations/theses-dissertations/molecular-26.

Find more at https://preserve.lehigh.edu/

This document is brought to you for free and open access by Lehigh Preserve. It has been accepted for inclusion by an authorized administrator of Lehigh Preserve. For more information, please contact preserve@lehigh.edu.

INFORMATION TO USERS

This manuscript has been reproduced from the microfilm master. UMI films the text directly from the original or copy submitted. Thus, some thesis and dissertation copies are in typewriter face, while others may be from any type of computer printer.

The quality of this reproduction is dependent upon the quality of the copy submitted. Broken or indistinct print, colored or poor quality illustrations and photographs, print bleedthrough, substandard margins, and improper alignment can adversely affect reproduction.

In the unlikely event that the author did not send UMI a complete manuscript and there are missing pages, these will be noted. Also, if unauthorized copyright material had to be removed, a note will indicate the deletion.

Oversize materials (e.g., maps, drawings, charts) are reproduced by sectioning the original, beginning at the upper left-hand corner and continuing from left to right in equal sections with small overlaps. Each original is also photographed in one exposure and is included in reduced form at the back of the book.

Photographs included in the original manuscript have been reproduced xerographically in this copy. Higher quality 6" x 9" black and white photographic prints are available for any photographs or illustrations appearing in this copy for an additional charge. Contact UMI directly to order.

UMI

A Bell & Howell Information Company
300 North Zeeb Road, Ann Arbor, MI 48106-1346 USA
313/761-4700 800/521-0600

MOLECULAR STRUCTURE-REACTIVITY RELATIONSHIPS FOR SUPPORTED MOLYBDENUM OXIDE CATALYSTS

by
HANGCHUN HU

A Dissertation
Presented to the Graduate and Research Committee
of Lehigh University
in Candidacy for the Degree of
Doctor of Philosophy

in
Department of Chemistry

Lehigh University, Bethlehem, Pennsylvania
1994

UMI Number: 9530991

UMI Microform 9530991
Copyright 1995, by UMI Company. All rights reserved.

This microform edition is protected against unauthorized
copying under Title 17, United States Code.

UMI
300 North Zeeb Road
Ann Arbor, MI 48103

CERTIFICATE OF APPROVAL

Approved and recommended for acceptance as a dissertation in partial fulfillment of the requirements for the degree of Doctor of Philosophy.

November 23, 1994

Israel E. Wachs

Dr. Israel E. Wachs
Advisor and Committee Chairman

Nov. 23, 1994
Accepted Date

Committee Members:

11/23/94
Dr. Kenneth O. Haug Date

Larry L. Murrell 11/23/94
Dr. Larry L. Murrell Date

11-23-94
Dr. James E. Roberts Date

12/13/94
Dr. Gary W. Simmons Date

ACKNOWLEDGEMENT

I am deeply indebted to my advisor, Professor Israel E. Wachs, for his guidance, counsel, and patience throughout my doctoral work. Without his presence and insight this work would not have been possible. I am thankful to the members of my dissertation committee, Dr. Kenneth Haug, Dr. Larry L. Murrell, Dr. James E. Roberts, and Dr. Gary W. Simmons, for their valuable comments; to Dr. Simon R. Bare for running XANES experiments; to Dr. Miguel A. Bañares for running Raman spectra and methane oxidations of some of the MoO_3/SiO_2 samples; to Dr. N. D. Spencer for obtaining the ICP Mo analysis data; to the different research groups for kindly supplying silica-supported molybdenum oxide samples.

The National Science Foundation and Department of Chemistry of Lehigh University are gratefully acknowledged for their financial support.

My special thanks goes to J-M. Jehng, G. Deo, A. M. Turek, and D. S. Kim for their guiding me during my stay at Lehigh both professionally and personally. I feel so lucky that they were all here when I first started in a completely new field. They and other people in our group, N. Arora, M. Kellner, M. A. Bañares, Sopee, and M. Ostromecki, have been very special people and great friends to me.

I also want to give my thanks to Marge Sawyers for her great help for so many things. Thanks to A. Civitella, B. Kessler, A. Miller, S. Simmons, and K. Orlosky for their help. I like to thank the following friends for their dear friendships and support for so many years: to Xieming & Tongsuo, Yulily & Zhouyi, Chenxiaofen & Xiaqin, Zhouziqiang & Xiaochu for being around and having so much fun when we were together and for constantly giving me the environment of hometown.

To my family, to my husband Qun for his love and constant understanding, his helpful discussion and support, to my lovely daughter Xiangyi and little baby Liangliang. To my parents for their love and encouraging that get me all the way to here.

TABLE OF CONTENTS

Page

ACKNOWLEDGEMENTS iii

LIST OF TABLES viii

LIST OF FIGURES x

ABSTRACT 1

CHAPTERS

1. REVIEW OF SUPPORTED MOLYBDENUM OXIDE CATALYSTS 3

- 1.1. INTRODUCTION 4
- 1.2. LITERATURE REVIEW 5
  - 1.2.1 Structure of supported molybdenum oxide catalysts 5
  - 1.2.2 Reactivity of supported molybdenum oxide catalysts 10
- 1.3. CONCLUSIONS 12
- 1.4. OUTLINE AND CONTENT OF THIS THESIS 14
- REFERENCES 14

2. SURFACE STRUCTURES OF SUPPORTED MOLYBDENUM OXIDE CATALYSTS: CHARACTERIZATION BY RAMAN AND Mo $L_{2,3}$-EDGE XANES 21

- 2.1. SUMMARY 22
- 2.2. INTRODUCTION 24
- 2.3. EXPERIMENTAL SECTION 27
  - 2.3.1. Catalyst preparation 27
  - 2.3.2. Raman spectroscopy 28
  - 2.3.3. X-ray absorption near edge spectroscopy (XANES) 29
- 2.4. RESULTS 31
  - 2.4.1. Raman of supported molybdenum oxide species under ambient conditions 32

2.4.2. XANES spectra of reference compounds and hydrated catalysts 38
2.4.3 Raman of supported molybdenum oxide species under dehydrated conditions 40
2.4.4. XANES studies of the dehydrated catalysts 44
2.5. DISCUSSION 45
2.5.1. Surface structures of supported molybdenum oxides under ambient conditions 45
2.5.2. Surface structures of supported molybdenum oxides under dehydrated conditions 50
2.5.3. Monolayer coverage of surface molybdenum oxides on different oxide supports 57
2.6. CONCLUSIONS 60
REFERENCES 61

3. CATALYTIC PROPERTIES OF SUPPORTED MOLYBDENUM OXIDE CATALYSTS: *IN SITU* RAMAN AND METHANOL OXIDATION STUDIES 91
3.1. SUMMARY 92
3.2. INTRODUCTION 93
3.3. EXPERIMENTAL SECTION 95
3.3.1. Catalyst preparation 95
3.3.2. Methanol oxidation 95
3.3.3. *In situ* Raman spectroscopy 97
3.4. RESULTS 99
3.4.1. Catalytic properties of supported molybdenum oxide catalysts for methanol oxidation 99
3.4.2. *In situ* Raman spectra of supported molybdenum oxide catalysts during methanol oxidation 104
3.4.3. Reduction of surface molybdenum oxide species 109

3.5. DISCUSSION 110
  3.5.1. Factors influencing the selectivity of the supported molybdenum oxide catalysts 110
  3.5.2. Factors influencing the TOF of the supported molybdenum oxide catalysts 112
  3.5.3. *In situ* Raman studies of the supported molybdenum oxide catalysts 116
3.6. CONCLUSIONS 121
REFERENCES 123

4. MOLYBDENUM OXIDE ON SILICA: ROLE OF THE PREPARATION METHODS ON THE STRUCTURE-SELECTIVITY PROPERTIES FOR THE OXIDATION OF METHANOL 143
4.1. SUMMARY 144
4.2. INTRODUCTION 145
4.3. EXPERIMENTAL SECTION 149
  4.3.1. Catalyst preparation 149
  4.3.2. Elemental analysis 149
  4.3.3. Laser Raman spectroscopy 150
  4.3.4. Methanol oxidation 152
4.4. RESULTS 152
  4.4.1. Elemental analysis 152
  4.4.2. Laser Raman spectroscopy 153
  4.4.3. Methanol oxidation 156
4.5. DISCUSSION 157
  4.5.1. Effect of preparation methods and specific support 157
  4.5.2. Methanol oxidation over MoO_3/SiO_2 catalysts 165
  4.5.3. Agglomeration of surface molybdenum oxide species during methanol oxidation 167
4.6. CONCLUSIONS 170

REFERENCES 170

5. **GENESIS AND STABILITY OF SILICOMOLYBDIC ACID ON SILICA-SUPPORTED MOLYBDENUM OXIDE CATALYSTS: *IN SITU* STRUCTURAL-SELECTIVITY STUDY ON SELECTIVE OXIDATION REACTIONS** 190
    5.1. SUMMARY 191
    5.2. INTRODUCTION 192
    5.3. EXPERIMENTAL SECTION 193
        5.3.1. Sample preparation 193
        5.3.2. *In situ* Raman spectroscopy 194
        5.3.3. Thermal gravimetric analysis 195
        5.3.4. Methane oxidation 195
    5.4. RESULTS 196
        5.4.1. Formation of SMA on the SiO_2 support 196
        5.4.2. Stability of SMA on SiO_2 197
        5.4.3. Methane partial oxidation 199
    5.5. DISCUSSION 200
    5.6. CONCLUSIONS 204
    REFERENCES 204

6. **CONCLUSIONS** 214
    REFERENCES 219

CURRICULUM VITAE 221

LIST OF TABLES

Page

Table 2.1. The surface density of supported MoO_3 catalysts at monolayer coverage. 67

Table 2.2. Elemental analysis of molybdenum oxide contents for supported samples. 68

Table 2.3. Raman bands of molybdate species in aqueous solutions. 69

Table 2.4. Summary of XANES and Raman structures of surface molybdenum oxide species under ambient conditions. 70

Table 2.5. Summary of XANES and Raman structures of surface molybdenum oxide under dehydrated conditions. 71

Table 3.1. Structures of the surface Mo species at low and near monolayer coverage for supported molybdenum oxide catalyst. 126

Table 3.2. Reactivity of MoO_3/TiO_2 catalysts as a function of MoO_3 loading for methanol oxidation reaction. 127

Table 3.3. Reactivity of MoO_3/ZrO_2 catalysts as a function of MoO_3 loading for methanol oxidation reaction. 128

Table 3.4. Reactivity of MoO_3/Nb_2O_5 catalysts as a function of MoO_3 loading for methanol oxidation reaction. 129

Table 3.5. Reactivity of MoO_3/Al_2O_3 catalysts as a function of MoO_3 loading for methanol oxidation reaction. 130

Table 4.1. Classification of the silica-supported molybdenum oxide catalysts studied. 174

Table 4.2. Some characteristics of the MoO_3/SiO_2 catalysts. 175

Table 4.3. Molybdenum oxide loading and nominal surface molybdenum oxide coverage on the specific silica supports. 176

Table 4.4. Methanol oxidation over MoO_3/SiO_2 catalysts at 503 K. 177

Table 5.1. Methane conversion on silica-supported molybdenum oxide and silicomolybdic acid. 207

LIST OF FIGURES

		Page
Fig. 2.1.	The Raman spectra of MoO_3/Al_2O_3 catalysts as a function of MoO_3 loading under ambient conditions.	72
Fig. 2.2.	The Raman spectra of MoO_3/SiO_2 catalysts as a function of MoO_3 loading under ambient conditions.	73
Fig. 2.3.	The Raman spectra of MoO_3/TiO_2 catalysts as a function of MoO_3 loading under ambient conditions.	74
Fig. 2.4.	The Raman spectra of MoO_3/ZrO_2 catalysts as a function of MoO_3 loading under ambient conditions.	75
Fig. 2.5.	The Raman spectra of MoO_3/Nb_2O_5 catalysts as a function of MoO_3 loading under ambient conditions.	76
Fig. 2.6.	Fluorescence yield Mo L_3-edge XANES of a series of Mo (VI) reference compounds.	77
Fig. 2.7.	Fluorescence yield Mo L_3-edge XANES of ambient 1% and 18% MoO_3/Al_2O_3 catalysts at room temperature.	78
Fig. 2.8.	Fluorescence yield Mo L_3-edge XANES of an ambient 6% MoO_3/TiO_2 catalyst at room temperature.	79
Fig. 2.9.	Fluorescence yield Mo L_3-edge XANES of ambient 1% and 5% MoO_3/SiO_2 catalysts at room temperature.	80

Fig. 2.10. The Raman spectra of MoO_3/Al_2O_3 catalysts as a function of MoO_3 loading under dehydrated conditions. 81

Fig. 2.11. The Raman spectra of MoO_3/SiO_2 catalysts as a function of MoO_3 loading under dehydrated conditions. 82

Fig. 2.12. The Raman spectra of MoO_3/TiO_2 catalysts as a function of MoO_3 loading under dehydrated conditions. 83

Fig. 2.13. The Raman spectra of MoO_3/ZrO_2 catalysts as a function of MoO_3 loading under dehydrated conditions. 84

Fig. 2.14. The Raman spectra of MoO_3/Nb_2O_5 catalysts as a function of MoO_3 loading under dehydrated conditions. 85

Fig. 2.15. Fluorescence yield Mo L_3-edge XANES of dehydrated 1% (solid line) and 18% MoO_3/Al_2O_3 catalysts at 723 K. 86

Fig. 2.16. Fluorescence yield Mo L_3-edge XANES of dehydrated 1% (solid line) and 6% MoO_3/TiO_2 catalysts at 723 K. 87

Fig. 2.17. Fluorescence yield Mo L_3-edge XANES of dehydrated 1%, 3.5%, and 5% MoO_3/SiO_2 catalysts at 723 K. 88

Fig. 2.18. Raman spectra of 1% MoO_3 catalysts on different oxide supports under dehydrated conditions. 89

Fig. 2.19. Raman spectra of monolayer MoO_3 catalysts on different oxide supports under dehydrated conditions. 90

Fig. 3.1. The *in situ* Raman spectra of the 1% MoO_3/TiO_2 catalyst during methanol oxidation. 131

Fig. 3.2. The *in situ* Raman spectra of the 6% MoO_3/TiO_2 catalyst during methanol oxidation. 132

Fig. 3.3. The *in situ* Raman spectra of the 6% MoO_3/TiO_2 catalyst during methanol reaction at different temperatures. 133

Fig. 3.4. The *in situ* Raman spectra of the 1% MoO_3/ZrO_2 catalyst during methanol oxidation. 134

Fig. 3.5. The *in situ* Raman spectra of the 4% MoO_3/ZrO_2 catalyst during methanol oxidation. 135

Fig. 3.6. The *in situ* Raman spectra of the 3% MoO_3/ZrO_2 catalyst during methanol reaction at different temperatures. 136

Fig. 3.7. The *in situ* Raman spectra of the 1% MoO_3/Nb_2O_5 catalyst during methanol oxidation. 137

Fig. 3.8. The *in situ* Raman spectra of the 5% MoO_3/Nb_2O_5 catalyst during methanol oxidation. 138

Fig. 3.9. The *in situ* Raman spectra of the 20% MoO_3/Al_2O_3 catalyst during methanol oxidation. 139

Fig. 3.10. The *in situ* Raman spectra of the 20% MoO_3/Al_2O_3 catalyst during methanol reaction at different temperatures. 140

Fig. 3.11. The percent reduction for different oxide-supported molybdenum oxide catalysts during methanol oxidation at 503 K. 141

Fig. 3.12. The plot of TOF versus the T_{max} temperature of TPR for different oxide supports. 142

Fig. 4.1. Raman spectra of silica-supported molybdenum oxide catalysts prepared by different methods under dehydrated conditions. 178

Fig. 4.2. Raman spectra of silica-supported molybdenum oxide catalysts on different silica supports under dehydrated conditions. 179

Fig. 4.3. Effect of calcium impurities on the molecular structures of surface molybdenum oxide species on SiO_2 under dehydrated conditions by Raman spectroscopy. 180

Fig. 4.4. Raman spectra of the surface molybdenum oxide species on SiO_2 with different molybdenum oxide loadings under dehydrated conditions. 181

Fig. 4.5. *In situ* Raman spectra of catalyst I9 with 0.1 Mo/nm^2 during methanol oxidation. 182

Fig. 4.6. *In situ* Raman spectra of catalyst I9 with 0.3 Mo/nm^2 during methanol oxidation. 183

Fig. 4.7. *In situ* Raman spectra of catalyst I9 with 0.4 Mo/nm^2 during methanol oxidation. 184

Fig. 4.8. *In situ* Raman spectra of catalyst I9 with 0.8 Mo/nm^2 during Methanol oxidation. 185

Fig. 4.9. TOF of surface molybdenum oxide of the MoO_3/SiO_2 catalysts during methanol oxidation at 503 K. 186

Fig. 4.10. Evolution of apparent TOF(HCHO)/apparent-TOF($HCOOCH_3$) for catalyst I9 during the first stages of the reaction. 187

Fig. 4.11. Amount of dispersed surface molybdenum oxide species as a function of the Mo surface coverage. 188

Fig. 4.12. Evolution of the Raman band for the Mo=O bond versus the surface molybdenum loading. 189

Fig. 5.1. *In situ* Raman spectra of 5MoSi in flowing air saturated with water at different decreasing temperatures. 208

Fig. 5.2. *In situ* Raman spectra of 5SMA in flowing oxygen saturated with water at different increasing temperatures. 209

Fig. 5.3. *In situ* Raman spectra of 5SMA in flowing dry oxygen at different increasing temperatures. 210

Fig. 5.4. *In situ* Raman spectra of 5SMA during the methanol oxidation reactions at different increasing temperatures. 211

Fig. 5.5. TGA measurements of the weight loss patterns in dry air of the MoSi series and SMA series. 212

Fig. 5.6. Selectivity *vs*. methane conversion plots for the representative catalysts 5SMA and 5MoSi. 213

ABSTRACT

The molecular structures and the catalytic properties of the surface molybdenum oxide species supported on TiO_2, Al_2O_3, ZrO_2, SiO_2 and Nb_2O_5 were investigated using characterization techniques (Raman and X-ray absorption near edge spectroscopy (XANES)) and reaction probes (methanol oxidation, methane oxidation). The supported molybdenum oxide catalysts were prepared by the incipient-wetness impregnation method employing aqueous solutions of ammonium heptamolybdate ($(NH_4)_6Mo_7O_{24}\cdot 4H_2O$). The dispersion, molecular structure, and reactivity of the surface molybdenum oxide species and their dependence on the specific oxide support, surface coverage, hydration/dehydration state, and thermal treatments were investigated. Under ambient conditions, the structures of the hydrated surface molybdenum oxide species are controlled by the net surface pH at the point of zero charge (PZC) of the catalysts and are the same as those observed in aqueous solutions: MoO_4^{2-}, $Mo_7O_{24}^{6-}$, and $Mo_8O_{26}^{4-}$. Under dehydrated conditions, the structures of the surface molybdenum oxide species depend on both the specific oxide support as well as surface coverage. Monolayer coverage was achieved at the same surface density of molybdenum oxide (~ 4.6 Mo/nm^2) on the different oxide supports with the exception of SiO_2 (~ 0.8 Mo/nm^2).

The catalytic properties of the supported molybdenum oxide catalysts were probed by methanol oxidation and were found to depend on both the specific oxide support and surface molybdenum oxide loading. Aggregation of the surface molybdenum oxide species to crystalline β-MoO_3 particles during methanol oxidation and the formation of

silicomolybdic acid (SMA, $H_4SiMo_{12}O_{40}$) upon water treatment were observed. The redox turnover frequency (TOF) increased with surface molybdenum oxide coverage and for the monolayer catalysts followed the order of $ZrO_2 \sim TiO_2 > Nb_2O_5 > Al_2O_3$. The number of active sites participating in the methanol oxidation reaction at steady state (percent of reduction) was determined by *in situ* Raman spectroscopy and appears to be similar for all of the catalysts. The reactivity per site for the surface molybdenum oxide species on oxide supports appears to be the determining factor controlling the catalyst activity during methanol oxidation.

CHAPTER 1

REVIEW OF SUPPORTED MOLYBDENUM OXIDE CATALYSTS

1.1. INTRODUCTION

Supported metal oxide catalysts are one of the most important types of heterogeneous catalytic systems. They consist of one or more metal oxide components supported on the surface of a second metal oxide which usually possesses a high surface area. The deposited metal oxide component is dispersed on the support surface as a two-dimentional overlayer and is found to be the active center for many catalytic reactions. Molybdenum oxide is one of the most widely used active oxides for supported metal oxide catalytic systems. Typical high surface area oxide supports are alumina (Al_2O_3), silica (SiO_2), titania (TiO_2), zirconia (ZrO_2), and niobia (Nb_2O_5).

Supported molybdenum oxide catalysts are widely used in various catalytic processes. They are active catalysts for hydrodesulfurization and hydrocracking of heavy fractions of crude oil, metathesis, isomerization, hydrogenation and polymerization of alkenes in the petroleum industry, and the partial oxidation of aliphatic alcohols [1]. It is important to know the surface composition and local structure of these catalysts on a molecular level in order to understand the roles played by the surface molybdenum oxide species in the various catalytic reactions. Furthermore, correlation of the structural information with the catalyst performance will ultimately be useful in the molecular design of new catalysts.

The molecular structures of the surface molybdenum oxide species on different oxide supports have been extensively investigated by various techniques over the past decade [2]. These investigations have resulted in major contributions to both fundamental research and industrial development, particularly in the field of petroleum chemistry. Numerous literature studies have concluded from Raman, Fourier transform infrared (FTIR), solid-state ^{95}Mo-nuclear magnetic resonance (NMR), extended X-ray absorption fine structure (EXAFS), X-ray absorption near edge structure (XANES), X-ray photoelectron spectroscopy (XPS), and ultraviolet visible diffuse reflectance spectroscopies (DRS-UV/VIS) that the structures of the supported molybdenum oxide species are a function of the specific oxide support, extent of surface hydration and dehydration, surface molybdenum oxide coverage, surface impurities, and calcination temperatures [2-5]. A brief review of the previous studies will be helpful to summarize what information is currently known about the structures of the surface molybdenum oxide species as well as to further guide our studies in this area.

1.2. LITERATURE REVIEW

1.2.1. Structure of supported molybdenum oxide catalysts

MoO_3/Al_2O_3: The structures of supported molybdenum oxide on Al_2O_3 catalysts have been extensively studied due to the wide-spread use and technical importance of this catalytic system. The application of Raman spectroscopy in early investigations by Knözinger, Jeziorowski and coworkers [6-8] was an important contribution in the determination of the structures of the two-dimensional surface molybdenum oxide species on the Al_2O_3 support. Both γ- and η-Al_2O_3 were used to prepare different loadings of the MoO_3/Al_2O_3 catalysts. It was demonstrated that there are at least three different molybdenum oxide species (tetrahedral MoO_4^{2-}-like and octahedral $Mo_7O_{24}^{6-}$-like surface species, as well as crystalline MoO_3 phase) present on the Al_2O_3 surface, and that their relative concentrations depend on the molybdenum oxide coverage and the surface area of the Al_2O_3 support. The presence of tetrahedral monomeric species and octahedral polymolybdate species was also found by Hall and Wang [9-11] using Raman spectroscopy. They found that Raman features were essentially the same for the catalysts prepared by different methods: impregnation, equilibrium, and adsorption of $Mo(CO)_6$. Later experiments using IR [12,13], XPS [13-15], solid-state ^{95}Mo NMR [16,17], and EXAFS/XANES [18] as well as Raman spectroscopy [19] provided additional information about the three types of Mo species on the Al_2O_3 surfaces. It is now generally accepted that, tetrahedrally coordinated molybdenum oxide species with a structure resembling that of MoO_4^{2-} in aqueous solutions are present at low Mo coverages and octahedrally coordinated polymeric species with structures similar to $Mo_7O_{24}^{6-}$ /$Mo_8O_{26}^{4-}$ molybdate clusters are present at higher Mo coverages. Above monolayer coverage of the dispersed surface molybdenum oxide species, crystalline MoO_3 is also formed. The preparation method did not seem to affect the surface structures of molybdenum oxide on the Al_2O_3 support [19].

An effect of water vapor on the surface structures of the supported molybdenum oxide species, however, was found [20] and new surface molybdenum oxide structures for the MoO_3/Al_2O_3 catalysts under dehydrated conditions were demonstrated [21-26]. A highly distorted octahedral molybdenum oxide species at low Mo loadings and a moderately distorted octahedral coordinated molybdenum oxide species at higher Mo loadings were suggested by a Raman study to be the surface species present on the Al_2O_3 surface with the latter possibly being polymeric molybdates because of the presence of Mo-O-Mo bonds [23,24]. The assignment of the octahedral coordinations is mainly based on the Raman band positions of the terminal Mo=O bond which can not be unambiguously assigned [7]. In addition, Knözinger *et al.* [27-30] and other research groups [31-33] investigated crystalline MoO_3 and Al_2O_3 solid/solid mixtures and revealed a spontaneous dispersion of the MoO_3 crystalline component over the Al_2O_3 surface upon thermal treatment. However, the surface Mo species on Al_2O_3 possessed the same structures found with other preparation methods. Thus, the formation of two-dimensional surface molybdenum oxide overlayer on the Al_2O_3 support is demonstrated and the structures of the surface molybdenum oxide species depend on the surface of the oxide support, molybdenum oxide coverage, and hydration/dehydration conditions.

MoO_3/SiO_2: The molecular structures of molybdenum oxide on silica catalysts were found to be dependent on the preparation methods and types of silica. In spite of the large number of studies on the MoO_3/SiO_2 catalysts there remains a significant lack of agreement among the various research groups. The characterization of the MoO_3/SiO_2 catalysts prepared by conventional aqueous impregnation of ammonium heptamolybdate (AHM) solution [34-40] and aqueous equilibrium adsorption [41] found that crystalline MoO_3 was present on most of the SiO_2 supports, even for very low loading samples. It was proposed that the interaction between the precursor and the support depends on the sign of the surface charge of the support and of the dissolved complexes of the precursor [42]. Accordingly, silica (point of zero charge PZC = 4) behaves like an acid support.

At the pH of the AHM solution (~5.5), the silica surface is negatively charged which makes it hard to interact with the anionic heptamolybdate cluster $Mo_7O_{24}^{6-}$. Consequently, the lack of interaction between heptamolybdate and silica is responsible for the formation of MoO_3-crystallites in the MoO_3/SiO_2 catalysts at low loadings.

Alternative synthesis methods have also been employed in producing samples with high dispersions of surface molybdenum oxide species on SiO_2. These new methods focused on an improvement of the interaction between the molybdenum oxide precursors and the silica surface hydroxyl groups by the use of molybdenum compounds with labile ligand (such as $MoCl_5$, $Mo(\eta^3C_3H_5)_4$, $Mo_2(\eta^3C_3H_5)_4$ or $Mo_2(OAc)_4$) that would be easily hydrolyzed by the silanol groups [34,43-52]. Improving the acid/base interaction of the molybdenum oxide precursor with the silica support by using the less acidic Mo^{3+} species was also proposed [42]. Many authors suggested that the specific preparation method generated specific surface molybdenum oxide species with unique structures [43,49,53]. However, Ekerdt and co-workers [34] concluded from Raman spectroscopy that surface octahedral mono-oxo molybdenum oxide species were present for the allyl and $MoCl_5$ preparations.

Characterization of the structures of the MoO_3/SiO_2 catalysts by different techniques and under different conditions results in different assignments. Under ambient conditions, the presence of a polyanionic structure [42,44,45,54,55] and a silicomolybdic acid (SMA) Keggin structure [56-60] were reported. Consequently, the factors controlling the formation of different structures such as surface point of zero change (PZC), solution pH, and precursor interaction were argued. At low Mo loadings and under dehydrated conditions, the dispersed surface molybdenum oxide species were reported to have either an octahedrally coordinated mono-oxo structure as concluded from IR and Raman spectroscopy [34,42,61-66] or a tetrahedrally coordinated di-oxo structure as concluded from luminescence and UV/Visible spectroscopies [67,68]. Disagreement between isolated and polymerized structures for the surface molybdenum oxide species on the SiO_2 support upon dehydration also exists. Also, the simultaneous presence of different species [56] by incomplete treatment and laser induced dehydration further complicates the assignments. In summary, characterization of the structures of the molybdenum oxide species on the SiO_2 support requires additional effort to resolve the above disagreements.

MoO_3/TiO_2: Characterization of the MoO_3/TiO_2 catalysts by Raman spectroscopy provided only limited information about the structures of the surface molybdenum oxide species due to the interference of the intense Raman bands of the TiO_2 support (anatase at 144, 199, 399, 520, and 643 cm^{-1} and rutile at 144, 148, and 611 cm^{-1}). The Raman spectra obtained were usually limited to the region above 700 cm^{-1} [41,69-78]. Under ambient conditions, both tetrahedral and octahedral surface molybdenum oxide species have been assigned based on the Raman band position of the terminal $Mo=O$ bond. Fewer studies have been performed on the structures of the MoO_3/TiO_2 catalysts under dehydrated conditions [77,79]. XPS has been used to determine the monolayer coverage of the surface molybdenum oxide on TiO_2 [76] and the distribution of Mo oxidation states in reduced Mo/TiO_2 catalysts [69]. A detailed description of the molecular structures of the surface molybdenum oxide species in MoO_3/TiO_2 catalysts is still lacking.

MoO_3/ZrO_2: The characterization of the surface molybdenum oxide structures present in MoO_3/ZrO_2 catalysts is still incomplete [41,79-83]. An unequivocal assignment of the Raman bands of the terminal Mo=O bond of the surface molybdenum oxide species was not possible since the low frequency region of the Raman spectra is overwhelmed by the much stronger bands of ZrO_2 support. IR and Raman studies concluded the presence of polymolybdate species on the ZrO_2 surface under hydrated conditions [41,80-83] and distorted octahedral species under dehydrated conditions [79].

MoO_3/Nb_2O_5: The structural assignment of the MoO_3/Nb_2O_5 catalysts is dependent on comparisons with other oxide supported catalysts [84,85] since the Nb_2O_5 support gives a strong background in the Raman spectra. Jehng *et al.* [85] suggested that $Mo_8O_{26}^{4-}$ species are present on the Nb_2O_5 surface when the surface is hydrated, and both a highly distorted and a slightly distorted surface molybdenum oxide structures are present when the MoO_3/Nb_2O_5 catalyst surface is dehydrated. In conclusion, there is a strong need to perform a detailed study of this catalytic system as well as the other oxide supported molybdenum oxide catalysts to evaluate their structure-reactivity relationships.

1.2.2. Reactivity of supported molybdenum oxide catalysts

One of the most important applications of molybdenum oxide catalysts is in selective catalytic oxidation reactions. Supported molybdenum oxide catalysts or MoO_3-based bulk catalysts have been found application in the oxidation of methane to formaldehyde [38,57,86,87], conversion of methanol to formaldehyde [43,44,88], selective oxidation of propene to acrolein [81,89], and other reactions [55,81,82]. The oxidative properties of the supported molybdenum oxide catalysts have been extensively studied with various chemical techniques. The oxidative activity is often associated with the reducibility of the oxide catalyst and, thus, temperature programmed reduction (TPR) [73,90] and thermal gravimetric analysis (TGA) [91,92] are techniques widely used. Characterization of the reduced molybdenum oxide species present in the catalysts are frequently studied with *in situ* techniques such as XPS [73,75,76] and ESR [46,93]. However, there is still a lack of fundamental understanding of the catalytic properties of the supported molybdenum oxide catalysts, especially with regard to the elucidation of the structure-reactivity relationships during oxidation reactions.

Studies of catalytic properties of MoO_3/SiO_2 catalysts have given confusing results. For MoO_3/SiO_2, both redox properties for methanol partial oxidation to formaldehyde (FA) and methylformate (MF) [44,48,53] and acidic properties for dehydration of methanol to dimethylether (DME) [94] were reported. A higher activity for grafted MoO_3/SiO_2 catalysts was reported [43]. The turnover frequency (TOF), which is defined as the number of the methanol molecules converted per surface oxide site per second, of the MoO_3/SiO_2 catalysts was found to decrease with MoO_3 loading [55]. There were also attempts to associate the methylformade selectivity with the dispersion and structure of surface molybdenum oxide species on SiO_2 [44,48]. The great variety of preparation methods, types of silica supports, characterization methods and activity studies employing different probe reactions results in a significant lack of aggrement between the various authors.

Molybdenum oxides on TiO_2 and ZrO_2 were found to be very active catalysts and possess a high selectivity for the oxidative dehydrogenation of methanol to formaldehyde [76,81,88,95]. However, no further studies on the determining factors controlling the catalytic properties of the surface molybdenum oxide species on ZrO_2 and TiO_2 were found. Only a few studies on methanol oxidation reactions over molybdenum oxide on Al_2O_3 and Nb_2O_5 supports have been investigated due to the high acidity of the Al_2O_3 and Nb_2O_5 supports towards the dehydration reaction of methanol which dominates the catalytic activity of the surface molybdenum oxide species [32,84,85].

1.3. CONCLUSIONS

The enormous amount of studies on the supported molybdenum oxides reveal that the structures and reactivities of the supported molybdenum oxide catalysts are controlled by parameters such as preparation method, surface coverage, calcination temperature, specific oxide support, hydration/dehydration conditions, and the presence of impurity/promoters. Previous investigations [41,96,97] usually only examined the structures of those surface molybdenum oxide species under ambient conditions which are different from that under reaction conditions (dehydrated states). In addition, there is still a lack of general agreement on the dispersion of the surface molybdenum oxide species on different supports with loading, structure and coordination of the surface molybdenum oxide species, consequently, the factors controlling the dispersion and structures of supported molybdenum oxide catalysts are not well understood. A detailed fundemental study to discriminate between the structural dependence on the hydrated and dehydrated states, on the metal oxide supports, and on the molybdenum oxide loading is essential.

The current studies will systematically examine the molecular structure and catalytic property of the different oxide supported molybdenum oxide catalysts for methanol oxidation as a function of the oxide support and molybdenum oxide coverage. The main technique used to obtain the fundamental information about molecular structure of the surface molybdenum oxide species is Raman spectroscopy. Raman spectroscopy has been extremely useful in revealing the surface structures of supported molybdenum oxide catalysts because of its high sensitivity for discriminating different structures and its "*in situ*" capabilities [2-5]. X-ray absorption near edge spectroscopy at the Mo $L_{2,3}$-edges is also used for the first time to provide additional coordination information about the structure of the surface molybdenum oxide species. The main chemical probe used to examine the catalytic performance for oxidation catalysis of the surface molybdenum oxide catalysts is the methanol oxidation reaction. Additional insights into the structure-reactivity relationships of the supported molybdenum oxide catalysts will be obtained with *in situ* Raman spectroscopy during methanol oxidation. Thus, a detailed study of the catalytic properties with well understood surface molybdenum oxide structures will allow us to determine the factors which control the oxidative activity of the supported molybdenum oxide catalysts. A more complete view of the structural dependence on the oxide support, dispersion of surface species, and the hydration states should result from this investigation.

1.4. OUTLINE AND CONTENT OF THIS THESIS

A series of Al_2O_3, SiO_2, TiO_2, ZrO_2, and Nb_2O_5 supported molybdenum oxide catalysts with various molybdenum oxide loading, with emphasis on the formation of the surface molybdenum oxide phase is initially synthesized. Characterization of the structures of surface molybdenum oxide phases by Raman and XANES spectroscopies is described in chapter 2. The characterization investigation focuses on the effects of hydration/dehydration and surface coverage. The methanol chemical probe reaction and *in situ* Raman spectroscopy are used to investigate the catalytic reactivity and active sites of the surface molybdenum oxide species on the Al_2O_3, TiO_2, ZrO_2, and Nb_2O_5 supports towards oxidative reaction, and the results are presented in chapter 3. The dependence of reactivity and selectivity on the structure, surface coverage, specific oxide support will be discussed. The latter part of this thesis deals with the unique properties of molybdenum oxide supported on SiO_2 in more detail. The effect of preparation method and reaction conditions to the molybdenum oxide structures on SiO_2 is investigated in chapter 4. Finally, the phase transformation of surface molybdenum oxide on SiO_2 to silicomolybdic acid (SMA) is investigated in chapter 5 as well as the stability of the surface SMA.

REFERENCES

1. Haber, J., *The Role of Molybdenum in Catalysis*, Climax Molybdenum Co. 1981.

2. Wachs, I. E., Ed. *Characterization of Catalytic Materials*, Butterworth Heinemann, 1992.
3. Bartlett, J. R., and Cooney, R. P., In *Spectroscopy of Inorganic-Based Materials*, Clark, R. J. H. and Hester, R. E. Ed. John Wiley & Sons, 187 (1987).
4. Mehicic, M., *Analytical Raman Spectroscopy*, Grasselli, J. G. and Bulkin, B. J. Ed. John Wiley & Sons, 325 (1991).
5. Stencel, J. M., *Raman Spectroscopy for Catalysis*, Van Norstranel Reinhold, **5** (1990).
6. Knözinger, H., and Jeziorowski, H., *J. Phys. chem.*, **82**, 2002 (1978).
7. Jeziorowski, H., and Knözinger, H., *J. Phys. Chem.*, **83**, 1166 (1979).
8. Jeziorowski, H., Knözinger, H., Grange, P., and Gajardo, P., *J. Phys. Chem.*, **84**, 1825 (1980).
9. Wang, L., and Hall, W. K. *J. Catal.*, **66**, 251 (1980).
10. Hall, W. K., *J. Proc. Climax 4th Int. Conf. on Chem. and Uses of Molybdenum*, 224 (1982).
11. Wang, L., and Hall, W. K. *J. Catal.*, **83**, 242 (1983).
12. Cornac, M., Janin, A., and Lavalley, J. C., *Infrared Phys.*, **24**, 143 (1984).
13. Okamoto, Y., and Imanaka, T., *J. Phys. Chem.*, **92**, 7102 (1988).
14. Zingy, D. S., Makovsky, L. E., Tischer, R. E., Brown, F. R., and Hercules, D. M., *J. Phys. Chem.*, **84**, 2898 (1980).
15. Rodrigo, L., Marcinkowska, K., Adnot, A., Roberge, P. C., Kaliaguine, S., Stencel, J. M., Makovsky, L. E., and Diehl, J. R., *J. Phys. Chem.*, **90**, 2690 (1986).
16. Edwards, J. C., Adams, R. D., and Ellis, P. D., *J. Am. Chem. Soc.*, **112**, 8349 (1990).
17. Luthra, N. P., and Cheng, W. C. *J. Catal.* **107**, 154 (1987).
18. Shimada, H., Matsubayashi, N., Sato, T., Yoshimura, Y., Nishijama, A., Kosugi, N., and Kuroda, H., *J. Catal.* **138**, 746 (1992).
19. Williams, C. C., Ekerdt, J. G., Jehng, J-M., Hardcastle, F. D., and Wachs, I.

E., *J. Phys. Chem.*, **95**, 8791 (1991).

20. Stencel, J. M., Makovsky, L. E., Sarkus, T. A., de Vries, J., Thomas, R., and Moulijn, J. A., *J. Catal.*, **90**, 314 (1984).
21. Chan, S. S., Wachs, I. E., Murrell, L. L., Wang, L., and Hall, W. K., *J. Phys. Chem.*, **88**, 5831 (1984).
22. Payen, E., Kasztelan, S., Grimblot, J., and Bonnelle, J. P., *J. Raman Spectrosc.*, **17**, 233 (1986).
23. Vuurman, M. A., and Wachs, I. E., *J. Phys. Chem.*, **96**, 5008 (1992).
24. Vuurman, M. A., and Wachs, I. E., *J. Mol. Catal.*, **77**, 29 (1992).
25. Gao, X., and Xin, Q., *Catalysis Letters*, **18**, 409 (1993).
26. Diaz, A. L., and Bussell, M. E., *J. Phys. Chem.* **97**, 470 (1993).
27. Leyrer, J., Zaki, M. I., and Knözinger, H., *J. Phys. Chem.*, **90**, 4775 (1986).
28. Leyrer, J., Mey, D., and Knözinger, H., *J. Catal.*, **124**, 349 (1990).
29. Kisfaludi, G., Leyrer, J., Knözinger, H., and Prins, R, *J. Catal.*, **130**, 192 (1991).
30. Knözinger, H., and Taglaner, E., *Catalysis*, *Pre. Royal Society of Chemistry*, Vo.**10**, 1(1993).
31. Stampfl, S. R., Chen, Y., Dumesic, J. A., Niu, C., and Hill, C. G. Jr., *J. Catal.*, **105**, 445 (1987).
32. Reddy, B. M., Reddy, E. P., and Srinivas, S. T., *J. Catal.*, **136**, 50 (1992).
33. del Arco, M., Carrazán, S. R. G., Rives, V., Gill-Llambías, F. J., and Malet, P., *J. Catal.* **141**, 48 (1993).
34. Williams, C. C., Ekerdt, J. G., Jehng, J.-M., Hardcastle, F. D., Turek, A. M., and Wachs, I. E., *J. Phys. Chem.* **95**, 8781 (1991).
35. Cáceres, C. V., Fierro, J. L. G., Lázaro, J., López Agudo, A., and Soria, J., *J. Catal.*, **122**, 113 (1990).
36. Martín, C., Martín, M. J., and Rives, V., *Studies in Surface Science and Catalysis*. Ruiz, P. and Delmon, B. Ed. **72**, 415 (1992).
37. Spencer, N. D., Pereira, C. J., and Grasselli, R. K., *J. Catal.* **126**, 546 (1990).

38. Bañares, M. A. , Fierro, J. L. G., and Moffat, J. B., *J. Catal.* **142**, 406 (1993).

39. Desikan, A.N., and Oyama, S.T., *J.C.S. Chem. Comm.* **88**, 3357 (1992).

40. Srinivasan, S., and Datye , A. K., *Catal. Letters* **15**, 155 (1992).

41. Kim, D. S., Segawa, K., Soeya, T., and Wachs, I. E., *J. Catal.*, **136**, 539 (1992).

42. de Boer, M., van Dillen, A. J., Koningsberger, D. C., Geus, J. W., Vuurman, M. A., and Wachs, I. E., *Catal. Lett.* **11**, 227 (1991).

43. Che, M., Louis, C., and Tatibouët, J. M., *Polyhedron*, **5**, 123 (1986).

44. Williams, C. C., and Ekerdt, J. G., *J. Catal.*, **141**, 430 (1993).

45. Roark, R. D., Kohler, S. D., and Ekerdt, J. G. , *Catal. Letters* **16**, 71 (1992).

46. Louis, C., Che, M., and Anpo, M., *J. Catal.* **141**, 453 (1993).

47. Aigler, J. M., Brito, J. L., Leach, P. A., Houalla, M., Proctor, A., Cooper, N. J., Hall, W. K., and Hercules, D. M., *J. Phys. Chem.* **97**, 5699 (1993).

48. Louis, C., and Che, M., *J. Catal.*, **135**, 156 (1992).

49. Iwasawa, Y., *Adv. Catal.* **35**, 265 (1987).

50. Yermakov, Y. I., *Catal. Rev. & Sci. Eng.* **13**, 77 (1976).

51. Zhuang, Q., Fukoka, A., Fujimoto, T., Tanaka, K., and Ichikawa, M., *J. Chem. Soc. Chem. Commun.* **11**, 745 (1991).

52. Ichikawa, M., Zhuang, Q., Li, G.-J., Tanaka, K., Fujimoto, T., and Fukoka, K., in "New Frontiers in Catalysis", *Studs. in Surf, Sci. and Catalysis*, **75(A)**, 529 (1992). Ed. Guczi, L.

53. Louis, C., Tatibouët, J. M., and Che, M., *J. Catal.* **109**, 354 (1988).

54. Roark, R. D., Kohler, S. D., Ekerdt, J. G., Kim, D. S., and Wachs, I. E., *Catal. Letters*, **16**, 77 (1992).

55. Liu, T.-C., Forissier, M., Coudurier, G., and Védrine, J. C., *J. Chem. Soc. Faraday Trans. I*, **85**, 1607 (1989).

56. Rodrigo, L., Marcinkowska, K., Adnot, A., Roberge, P. C., Kaliaguine, S., Stencel, J. M., Makovsky, L. E., and Diehl, J. R., *J. Phys. Chem.* **90**, 2690 (1986).

57. Barbaux, Y., Elamrani, A. R., Payen, E., Gengembre, L.P Bonnelle, J. B., and Grzybowska, B., *Appl. Catal.* **44**, 117 (1988).

58. Kasztelan, S., Payen, E., and Moffat, J. B., *J. Catal.*, **112**, 320 (1988).

59. Rocchiccioli-Deltcheff, C., Amirouche, M., Che, M., Tatibouët, J. M. and Fournier, M., *J. Catal.* **125**, 292 (1990).

60. Stencel, J. M., Diehl, J. R., D'Este, J. R., Makovsky, L. E., Rodrigo, L., Marcinkowska, K., Adnot, A., Roberge, P. C., and Kaliaguine, S., *J. Phys. Chem.*, **90**, 4739 (1986).

61. Wachs, I. E., Deo, G., Vuurman, M. A., Kim, D. S., Hu, H., and Jehng, J-M., *J. Molec. Catal.* **82**, 443 (1993).

62. Smith, M. R., Zhang, L., Driscoll, S. A., and Ozkan, U. S., *Catalysis Letters*, **19**, 1 (1993).

63. Seyedmonir, S. R., Abdo, S., and Howe, R. F., *J. Phys. Chem.*, **86**, 1233 (1982).

64. Cornac, M., Janin, A., and Lavalley, J. C., *Infrared Phys.*, **24**, 143 (1984).

65. Cornac, M., Janin, A., and Lavalley, J. C., *Polyhedron*, **5**, 183 (1986).

66. Seyedmonir, S. R., and Howe, R. F., *J. Catal.*, **110**, 216 (1988).

67. Marcinkowska, K., Rodrigo, L., Kaliaguine, S., and Roberge, P. C., *J. Catal.*, **97**, 75 (1986).

68. Hazenkamp, M. F., Thesis, University of Utrecht (The Netherlands), 1992.

69. Quincy, R. B., Houalla, M., Proctor, A., and Hercules, D. M., *J. Phys. Chem.* **93**, 5882 (1989).

70. Ono, T., Nakagawa, Y., Miyata, H., and Kubokawa, Y., *Bull. Chem. Soc. Jpn.* **57**, 1205 (1984).

71. Ng, K. Y. S., and Gulari, E., *J. Catal.*, **92**, 340 (1985).

72. Liu, Y.C., Griffin, G.L., Chan, S. S., and Wachs, I.E. *J. Catal.* **94**, 108 (1985).

73. Bond, G. C., Flamerz, S., and Wijk, L. V., *Catalysis Today*, **1**, 229 (1987).

74. Machej, T., Doumain, B., Yasse, B., and Delmon, B., *J. Chem. Soc., Faraday Trans.* 1, **84**, 3905 (1988).

75. Quincy, R. B., Houalla, M., and Hercules, D. M., *J. Catal.*, **106**, 85 (1987).

76. Segawa, K., Soeya, T., and Kim, D. S., *Sekiyu Gakkaishi*, **33**, 347 (1990).

77. Machej, T., Haber, J., Turek, A. M., and Wachs, I. E., *Applied Catalysis*, **70**, 115 (1991).

78. Spanos, N., Matralis, H. K., Kordulis, C., and Lycourghiotis, A., *J. Catal.*, **136**, 432 (1992).

79. Kim, D. S., Wachs, I. E., and Segawa, K., *J. Catal.* **146**, 268 (1993).

80. Leyrer, J., Vielhaber, B., Zaki, M. I., Zhuang, S., Weitkamp, J., and Knözinger, H., *Mat. Chem. Phys.* **13**, 301 (1985).

81. Ono, T., Miyata, H., and Kubokawa, Y., *J. Chem. Soc. Faraday Trans.* 1, **83**, 1761 (1987).

82. Miyata, H., Tokuda, S., Ono, T., Ohno, T., and Hatayama, F., *J. Chem. Soc. Faraday Trans.* **86**, 2291 (1990).

83. Ohno, T., Miyata, H., and Kubokawa, Y., *J. Chem. Soc. Faraday Trans, 1*, **83**, 176 (1987).

84. Jin, Y. S., Ouqour, A., Auroux, A., and Védrine, J. C., *Structure and Reactivity of surfaces*, Morterra, C., Zecchina, A. and Costa, G. Ed. Elsevier, 525 (1989).

85. Jehng, J-M., Turek, A. M., and Wachs, I. E., *Applied Catalysis A. General*, **83**, 179 (1992).

86. Yang, T-J., and Lunsford, J. H., *J. Catal.* **103**, 55 (1987).

87. Bañares, M. A., Jones, M. D., Spencer, N. D., and Wachs, I. E., *J. Catal.* **146**, 204 (1994).

88. Brückman, K., Grzybowska, B., Che, M., and Tatibouët, J. M., *Applied Catalysis A: General*, **96**, 279 (1993).

89. Volta J. C., and Portefaix J. L. *Appl. Catal.* **18**, 1 (1985).

90. Bond, G. C., and Tahir, S. F. *Appl. Catal.* A, **105**, 281 (1993).

91. Gajardo, P., Pirotto, D., Grange, P., and Delmon, B., *J. Phys. Chem.* **83**, 1780 (1979).

92. de Boer, M., Thesis, The University of Utrecht (The Netherlands), 1992.

93. Louis, C., and Che, M., *J. Phys. Chem.* **91**, 2875 (1987).

94. Tatibouët, J-M., Che, M., Amirouche, M., Fournier, M., and Rocchiccioli-Deltcheff, C., *J. Chem. Soc., Chem. Commun.* 1260 (1988).

95. Matsuoka, Y., Niwa, M., and Murakami, Y., *J. Phys. Chem.* **94**, 1477 (1990).

96. Cáceres, C. V., Fierro, J. L. G., Lázaro, J., López Agudo, A., and Soria, J., *J. Catal.*, **122**, 113 (1990).

97. López Cordero, R., Gil-Lliambias, F. J., and López Agudo, A., *Applied Catalysis*, **74**, 125 (1991).

CHAPTER 2

SURFACE STRUCTURES OF SUPPORTED MOLYBDENUM OXIDE CATALYSTS: CHARACTERIZATION BY RAMAN AND Mo $L_{2,3}$-EDGE XANES

2.1. SUMMARY

Supported molybdenum oxide catalysts on TiO_2, Al_2O_3, ZrO_2, SiO_2 and Nb_2O_5 were prepared by the incipient-wetness impregnation method employing aqueous solutions of ammonium heptamolybdate ($(NH_4)_6Mo_7O_{24}\cdot 4H_2O$). The molecular structures of the surface molybdenum oxide species were investigated by Raman spectroscopy and their local site symmetry were determined by X-ray absorption near edge spectroscopy (XANES) at the Mo $L_{2,3}$-edges. Under ambient conditions, the structures of the hydrated surface molybdenum oxide species are controlled by the net surface pH at the point of zero charge (PZC) and are the same as observed in aqueous solutions: MoO_4^{2-}, $Mo_7O_{24}^{6-}$, and $Mo_8O_{26}^{4-}$.

Under dehydrated conditions, the structures of the surface molybdenum oxide species depend on both the specific oxide support as well as surface coverage. At low surface coverages of MoO_3 on Al_2O_3 and TiO_2, the primary species is isolated and tetrahedral coordinated. At high surface coverages of MoO_3, for TiO_2 the primary species is polymerized and octahedral coordinated, but for Al_2O_3 there is a mixture of tetrahedral and octahedral coordinated species. The MoO_3/ZrO_2 system appears to be similar to the MoO_3/Al_2O_3 system and the MoO_3/Nb_2O_5 system appears to be similar to the MoO_3/TiO_2 system. The surface molybdenum oxide species on SiO_2 is isolated and appears to possess a coordination that is in between tetrahedral and octahedral. Monolayer coverage was achieved at the same surface density of molybdenum oxide on the different oxide supports with the exception of SiO_2. Only low loadings of

molybdenum oxide can be dispersed on SiO_2 due to the low concentration and reactivity of the surface OH groups.

2.2. INTRODUCTION

Supported molybdenum oxide catalysts are widely used in various catalytic processes [1]. The molecular structures of the surface molybdenum oxide species on different oxide supports have been extensively investigated by various techniques over the past decade [2]. Numerous literature studies have concluded from Raman, Fourier transform infrared (FTIR), solid-state ^{95}Mo-nuclear magnetic resonance (NMR), extended X-ray absorption fine structure (EXAFS), X-ray absorption near edge structure (XANES), X-ray photoelectron spectroscopy (XPS), and ultraviolet visible diffuse reflectance spectroscopies (DRS-UV) that the structures of the supported molybdenum oxide species are a function of the specific support, extent of surface hydration and dehydration, surface molybdenum oxide coverage, surface impurities, and calcination temperatures [2-5]. It is now well recognized that the surface structures of the metal oxide overlayers on oxide supports have to be evaluated under two distinctly different environments: ambient and dehydrated conditions. Under ambient conditions, the surface metal oxides are extensively hydrated by water molecules adsorbed on the support surfaces and, therefore, possess structures affected by the surface water. At elevated temperatures, the catalyst surfaces are dehydrated and the surface metal oxides undergo significant structural changes [2,4].

The structures of supported molybdenum oxide on Al_2O_3 have been extensively studied under both ambient conditions [6-24] and dehydrated conditions [25-31]. Raman spectroscopy studies [6-11] demonstrated that there are at least three different molybdenum oxide species (tetrahedral and octahedral coordinated surface species as well as a crystalline MoO_3 phase) present on the Al_2O_3 surface under ambient conditions, and that their relative concentrations depend on the molybdenum oxide coverage. Subsequent characterization experiments using IR [12,13], XPS [13-15], solid state ^{95}Mo NMR [16,17], EXAFS/XANES [18] provided additional information about the three types of Mo species on the Al_2O_3 surfaces under ambient conditions (tetrahedral, octahedral species and MoO_3 crystal phase). Under dehydrated conditions, a highly distorted octahedral molybdenum oxide species at low Mo loadings and a moderately distorted octahedral coordinated molybdenum oxide species (possibly polymeric in nature) at higher Mo loadings were suggested by Raman study to be the surface species present on the Al_2O_3 surface [28,29].

There recently has been an increasing amount of interest in the MoO_3/SiO_2 catalyst [14,32-55] because of its use as a model catalyst system (especially for selective oxidation reactions). Under ambient conditions, the presence of the polyanionic structures [35-39] and silicomolybdic acid (SMA) Keggin structures [40-43] have been reported. Under dehydrated conditions, the dispersed surface molybdenum oxide species are reported to have either the octahedral structure [32,36-39,44-47] or the tetrahedral structure [48-50]. In comparison to the MoO_3/Al_2O_3 and MoO_3/SiO_2 catalyst systems, relatively few studies have been carried out on the structures of surface molybdenum oxides on TiO_2 [56-65], ZrO_2 [66,67] and Nb_2O_5 [68,69]. The molecular structures of these catalyst systems (MoO_3 on TiO_2, ZrO_2 and Nb_2O_5) are still not well characterized because of the relatively weak Raman signals from the surface Mo oxide species compared to the strong background Raman signals of these oxide supports, especially in the low frequency region.

Previous attempts at the systematic characterization of molybdenum oxide on different oxide supports [33,34,45,70,71] usually only investigated the structures of molybdenum oxide under ambient conditions [33], and in some cases even mixed up the hydrated and dehydrated conditions because of laser induced dehydration [70,71]. There is still a lack of general agreement on the dispersion of the surface molybdenum oxide species on different supports, the structures and coordinations of the surface molybdenum oxide species and their controlling factors. Therefore, a systematic investigation of the surface molybdenum oxides on different oxide supports is important in order to clarify the confusion surrounding the surface structures of the supported molybdenum oxide catalysts and to reveal their structural dependance on the specific support and hydration/dehydration conditions.

The objectives of this work are 1) to combine Raman and XANES spectroscopies to determine the molecular structures of the surface molybdenum oxide species deposited on different oxide supports (under both ambient and dehydrated conditions), 2) to compare the surface molybdenum oxide monolayer coverage for each support, and 3) for the first time, to determined the local site symmetry of the supported molybdenum oxide phases at different Mo loading by using XANES at the Mo $L_{2,3}$-edge. The current findings provide a more complete view of the surface molybdenum oxide species structural dependence on the specific oxide support, their dispersion on different supports, and the effect of hydration/dehydration.

2.3. EXPERIMENTAL SECTION

2.3.1. Catalyst preparation

The support materials used in this study were TiO_2 (Degussa P-25), ZrO_2 (Degussa), Nb_2O_5 (from $Nb_2O_5 \cdot 4H_2O$, Niobium Products Co., calcined in air at 773 K 6 hours), Al_2O_3 (Harshaw), and SiO_2 (Cabosil EH-5, water wetted and calcined in air at 773 K overnight). The BET surface areas of these supports are listed in Table 2.1. The supported molybdenum oxide catalysts were prepared by the incipient-wetness impregnation method with aqueous solutions of ammonium heptamolybdate ($(NH_4)_6Mo_7O_{24} \cdot 4H_2O$). After impregnation, the samples were dried overnight under ambient conditions and further dried in air at 293 K overnight. The molybdenum oxides supported on TiO_2 and ZrO_2 samples were finally calcined in air at 723 K for two hours and the molybdenum oxides supported on Nb_2O_5, Al_2O_3, and SiO_2 samples were calcined in air at 773 K for two hours. The molybdenum oxide loading of the catalysts is given as the nominal weight percent of the MoO_3 in the samples. The actual loadings of the catalysts after ICP elemental analysis are listed in Table 2.2. Only the MoO_3/SiO_2 catalyst possessed slightly less MoO_3 than the deposited MoO_3 loading, and the MoO_3 loading on the other supports are all slightly higher and close to the deposited MoO_3 loading. The BET surface areas of the catalysts with monolayer molybdenum oxide coverage are also listed in Table 2.1. Table 2.1 shows that the dispersion of molybdenum oxide species is only slightly dependent on the surface area of the oxide supports except for SiO_2. The deposition of molybdenum oxide on SiO_2 also drastically decreases the surface area of SiO_2.

2.3.2. Raman spectroscopy

Raman spectra of the supported molybdenum oxide catalysts were obtained with a laser Raman apparatus with the 514.5 nm line of an Ar^+ laser (Spectra Physics, Model 171) as the excitation source. The laser power at each sample was adjusted to ~ 10 mW for ambient spectral measurements and ~ 40 mW for the dehydrated sample measurements. The scattered radiation from the sample was directed into a Spex Triplemate spectrometer (model 1877) coupled to a Princeton Applied Research (Model 1463) OMA III optical multichannel photodiode array detector (1024 pixels). The detector was cooled thermoelectrically to 238 K to decrease the thermal noise. The Raman scattering in the 100 - 1200 cm^{-1} region was collected and the spectra were recorded using an OMA III computer and software. The instrument resolution was experimentally determined to be better than 2 cm^{-1}, but the experimental operation and catalyst preparation added additional error and the reproducibility was only better than 4 cm^{-1} found by measuring the same loading samples from various preparations at different times. About 0.2 g of each supported molybdenum oxide catalyst was pressed into a thin wafer of about 1 mm thickness. For the spectral measurements under ambient conditions, a spinning sample holder was used to hold the sample pellet exposed in air and was generally rotated at ~ 2000 rpm to avoid local heating by the laser beam. For the measurements of the dehydrated samples, a fixed sample holder inside a quartz tube was used which allowed for the continual flowing of dry oxygen gas and heating at ~633 K to dehydrate the samples. The spectra were measured after the samples were fully dehydrated and cooled to room temperature, but the Raman spectrum for supported molybdenum oxide is not depend on temperature. A scan of the entire vibrational region requires 30 seconds. Generally, an accumulation of 25 scans was used for stronger Raman signals (Mo on Al_2O_3, TiO_2, ZrO_2, and Nb_2O_5) and 50 scans for weaker Raman signals (Mo on SiO_2). Raman spectra under both hydrated and dehydrated conditions were obtained by subtracting background signals (obtained under no laser beam condition) and correcting for the detector response for different frequency region. To minimize fluorescence from the support, the MoO_3/SiO_2 samples were calcined in dry air at 773 K overnight and the MoO_3/Al_2O_3 samples were calcined in dry air at 923 K for two hours before the Raman measurements.

2.3.3. X-ray absorption near edge spectroscopy (XANES)

Synchrotron radiation based X-ray absorption near edge spectroscopy (XANES) at the Mo $L_{2,3}$-edges has previously been demonstrated to provide information on the local site symmetry of dispersed molybdenum oxide surface phases in a series of supported molybdenum oxide on MgO catalysts [72]. This catalyst characterization method was based on some initial data of Mo reference compounds [73] and enzymes [74]. The interpretation of the data is based on an empirical ligand field splitting description of the final state d-orbital. The initial state of $L_{2,3}$-edge transitions are **p**-levels, and the dipole allowed final states are predominantly of **d** character. A combination of small natural line widths and high monochromator resolution at 2500 eV results in an estimated 0.5 eV experimental resolution at the Mo $L_{2,3}$-edges. This permits any splitting of the white line at the Mo $L_{2,3}$-edges to be observed. For a tetrahedral coordinated Mo the magnitude of the splitting of the d-orbitals is less than that of Mo in an octahedral field (e, t_2 versus t_{2g}, e_g). The number of available orbitals should also be reflected in the relative intensity of each transition. A successful study was performed previously by Bare and coworkers where a direct comparison was made between a series of molybdenum (VI) reference compounds of known structure and the MoO_3/MgO catalysts as a function of weight loading of Mo [72].

The Mo XANES data were recorded at the National Synchrotron Light Source, Brookhaven National Laboratory, on beam line X19A. The storage ring operated at 2.5 GeV with a current between 110 and 230 mA. The X-ray photons were monochromatized with a NSLS boomerang-type flat crystal monochromator with Si (111) crystals. The slit width of the monochromator was fixed at 3 mm, estimated to give a resolution of 0.5 eV at the Mo L-edges. The harmonic content was reduced by detuning the monochromator crystals by approximately 90%. The X-ray absorption edges were measured as fluorescence yield excitation spectra using a Stern-Heald-Lytle detector with argon as the detector gas. The XANES of the reference compounds were measured as electron yield spectra. To minimize absorption by the air the path length from the end of the beam pipe to the sample chamber was made as short as possible. Prolene™ windows (4 μm thick) were used on the Io chamber and entrance window to the *in situ* cell.

The *in situ* EXAFS experiments used a commercially available EXAFS cell [75] which has been described in detail elsewhere [76]. Briefly, the device comprises a water cooled, helium flushed aluminum block into which a cylindrical insert for soft X-ray work can be inserted. This cylindrical insert consists of the sample holder and cylindrical housing. The sample holder is made of stainless steel and supports a disk shaped sample which is heated by a Kanthal resistance heater. The sample holder has a gas inlet and outlet in order to control the gas environment around the sample. The cylindrical housing is water cooled and has a 5 μm aluminized Mylar window. The gas inlet is connected to a versatile portable feed gas system equipped with electronic mass flow controllers and switching valves.

In the experiments reported here, the catalyst disks ($\sim$0.7 g) of each catalyst were pressed and loaded into the sample holder. Mo L-edge XANES spectra were acquired on these air exposed, hydrated samples. The catalyst disks were then heated to 723 K in a flow of 20% O_2 in He for a given amount of time (usually 30-45 min.) in order to dehydrate the samples. Mo L-edge XANES spectra were then acquired at 723 K in the flow of O_2/He. The spectra are normalized to a unit edge jump according to conventional methods. The monochromator was calibrated by setting the first inflection point of the L_3-edge of Mo foil to 2520.0 eV. In this manner the absorption edge of all the catalyst samples falls in the range 4.0-5.0 eV, as expected for Mo (VI) compounds [72,73]. However, chemical shifts have not been used in interpreting the data since the Mo in all of the reference materials and the catalysts is in the +6 oxidation state.

2.4. RESULTS

2.4.1. Raman of supported molybdenum oxide species under ambient conditions:

The supported molybdenum oxide catalysts possess significant amounts of moisture under ambient conditions and the surface molybdenum oxide species are in a hydrated environment [33]. The hydrated surface molybdenum oxide species are essentially indistinguishable from those found in aqueous solutions [2,33]. Consequently, the molybdenum oxide aqueous compounds will serve as the reference compounds for the supported molybdenum oxide catalysts under ambient conditions. Table 2.3 lists the Raman bands of the major aqueous molybdate compounds (MoO_4^{2-}, $Mo_7O_{24}^{6-}$, and $Mo_8O_{26}^{4-}$) [33] as well as their dependence on solution pH; the Raman spectra of these species have previously been reported [77]. The MoO_4^{2-} species is isolated, tetrahedral coordinated and exhibits Raman bands at 897, 837, and 317 cm^{-1}. The $Mo_7O_{24}^{6-}$ and $Mo_8O_{26}^{4-}$ species are polymerized, octahedral coordinated clusters with Raman bands at 943, 903, 570, 362, and 210 cm^{-1} for $Mo_7O_{24}^{6-}$ and $Mo_8O_{26}^{4-}$ possesses Raman bands at 965, 925, 590, 370, 230 cm^{-1}. The Raman bands in the 890 - 1000 cm^{-1} and 830 - 970 cm^{-1} region are attributed to the symmetric and asymmetric stretching modes of the terminal Mo=O bond, the bands around 310 - 370 cm^{-1} are the corresponding bending modes of the terminal Mo=O bond, and the bands at ~ 560 and 210 cm^{-1} are assigned to the Mo-O-Mo symmetric stretch and Mo-O-Mo deformation modes, respectively. The 570 cm^{-1} band is generally very weak and the formation of polymerized species is characterized by the presence of the 200 - 230 cm^{-1} Raman band of the Mo-O-Mo linkage.

MoO_3/Al_2O_3: The Raman spectra of the 1 - 20% MoO_3/Al_2O_3 catalysts at ambient conditions are presented in Fig. 2.1. The Raman spectrum of the Al_2O_3 support is essentially featureless in the 100 - 1200 cm^{-1} region and the surface molybdenum oxide species on the alumina support possess several Raman bands in the 100 - 1200 cm^{-1} region. The bands at 912, 846 and 320 cm^{-1} of the 1% MoO_3/Al_2O_3 match fairly well with the Raman bands of tetrahedral coordinated MoO_4^{2-} species in aqueous solutions (see Table 2.3). The slight up-field shift of the Raman frequencies of the surface molybdenum oxide species is probably due to the minor distortion of the hydrated tetrahedral molybdenum oxide structure on the Al_2O_3 surface. Accordingly, the 912, 846, and 320 cm^{-1} can be assigned to the symmetric stretch, asymmetric stretch, and bending modes of hydrated MoO_4 units, respectively.

There are several changes in the Raman features as the molybdenum oxide loading increases from 1 to 20% MoO_3: a) the major Raman band due to the terminal Mo=O stretch shifts from 912 cm^{-1} to 949 cm^{-1}; b) a new weak band at 561 cm^{-1} appears; c) the band at 320 cm^{-1} decreases and a new band at 360 cm^{-1} increases; and d) the band at 210 cm^{-1} significantly increases. The significant difference in the terminal Mo=O stretching frequency between the 1% and 6% MoO_3/Al_2O_3 samples suggests the presence of different surface molybdenum oxide species. The Raman bands of the higher loading samples are close to that of octahedral coordinated $Mo_7O_{24}^{6-}$ species in aqueous solutions. Thus, the bands observed at 949, 904, and 360 cm^{-1} are attributed to the symmetric stretch, asymmetric stretch, and bending modes of the terminal Mo=O bond of octahedral coordinated MoO_6 species for hydrated $Mo_7O_{24}^{6-}$, respectively [7]. In addition, the Raman bands at 561 and 210 cm^{-1} are assigned to the Mo-O-Mo symmetric stretch and Mo-O-Mo deformation of the MoO_6 unit in hydrated $Mo_7O_{24}^{6-}$, respectively [28]. The higher intensity of the Raman band at 846 cm^{-1} for the high loading ambient MoO_3/Al_2O_3 samples relative to the aqueous $Mo_7O_{24}^{6-}$ species might be due to a slightly different Mo-O-Mo bond angle on the alumina support [28]. The Raman bands due to the hydrated MoO_4^{2-} species disappear and the bands attributed to the $Mo_7O_{24}^{6-}$ species predominate upon further increasing the Mo loading. These Raman band changes suggest the presence of tetrahedral coordinated species at low Mo loading (hydrated MoO_4^{2-}) and an increase of octahedral coordinated species at higher Mo loading (hydrated $Mo_7O_{24}^{6-}$) under ambient conditions. Strong Raman bands due to crystalline MoO_3 appear for the samples above 20% MoO_3 loading and predominate at higher molybdenum oxide loading samples (not shown in Fig. 2.1) which indicates that monolayer coverage for this Al_2O_3 support (~180 m^2/g) is ~20% MoO_3 loading.

MoO_3/SiO_2: The Raman spectra of the 1 - 7% MoO_3/SiO_2 catalysts under ambient conditions are presented in Fig. 2.2. The Raman spectrum of SiO_2 possesses broad and weak features at 977, 810, 601 and a very broad band from 490 - 380 cm^{-1}. The 977 cm^{-1} band is due to the surface hydroxyl groups (Si-O-H), the 810 and 457 cm^{-1} bands are associated with siloxane linkages, and the 601 and 488 cm^{-1} bands are due to three- and four-fold siloxane rings [38,39]. As the molybdenum oxide loading increases, the Raman bands of the surface molybdenum oxide species at 947, 880, 381, and 232 cm^{-1} increase in intensity but do not change positions. The Raman features due to the

SiO_2 support decrease in intensity relative to the Raman bands of surface molybdenum oxide species as the molybdenum oxide coverage increases. The Raman features of hydrated surface molybdenum oxide species on SiO_2 match the Raman bands of $Mo_7O_{24}^{6-}$ clusters in aqueous solutions (see Table 2.3), but are shifted ~20 cm^{-1} to higher frequency with the exception of the 880 cm^{-1} band. This ~20 cm^{-1} shift could be due to a weak interaction between the slightly distorted hydrated $Mo_7O_{24}^{6-}$ clusters and the SiO_2 surface. The relatively high intensity and the somewhat lower band position of the 880 cm^{-1} band suggests that it could arise from more than one vibrational modes. The Mo-O-Mo stretching mode may also contribute to the 880 cm^{-1} band. The maximum dispersion is exceeded when the molybdenum oxide loading is higher than 5% MoO_3, and further addition of molybdenum oxide forms crystalline MoO_3 (major Raman bands at 992, 820, and 280 cm^{-1}). Therefore, molybdenum oxide can be dispersed on this silica support up to 5% MoO_3 loading with the current preparation method. The structure of surface molybdenum oxide species is octahedral coordinated hydrated $Mo_7O_{24}^{6-}$ species at all Mo loadings under ambient conditions.

MoO_3/TiO_2: The Raman spectra of the 1 - 7% MoO_3/TiO_2 catalysts under ambient conditions are presented in Fig. 2.3. Raman spectra below 700 cm^{-1} were not collected because of the very strong Raman background of the TiO_2 support. The weak band at 790 cm^{-1} is the first overtone of the 395 am^{-1} band of TiO_2 (anatase) [57], and the relative intensity of this band decreases as the molybdenum oxide coverage increases. The surface molybdenum oxide species possess the terminal Mo=O Raman stretch in the range of 934 to 954 cm^{-1} which shifts to higher frequency as the molybdenum oxide loading increases. The position of the terminal Mo=O stretch at higher Mo loadings suggests the presence of octahedral coordinated surface molybdenum oxide species with a structure similar to that of $Mo_7O_{24}^{6-}$ or $Mo_8O_{26}^{4-}$ clusters in aqueous solutions. At lower Mo loading, the Raman band position of the terminal Mo=O bond also suggests the presence of a tetrahedral hydrated MoO_4^{2-} component. A weak and broad band at ~875 cm^{-1} also increases in intensity as the molybdenum oxide coverage increases. The 875 cm^{-1} Raman band is probably due to the stretching mode of a Mo-O-Mo bond of the polymerized three-dimensional surface molybdenum oxide species (hydrated $Mo_8O_{26}^{4-}$ or $Mo_7O_{24}^{6-}$) [28]. Strong Raman bands of crystalline MoO_3 are present at 820 and 992 cm^{-1} for the 7% MoO_3/TiO_2 (55 m^2/g) sample which indicates that monolayer coverage of the surface molybdenum oxide species has been exceeded.

MoO_3/ZrO_2: The Raman spectra of the 1 - 5% MoO_3/ZrO_2 catalysts under ambient conditions are presented in Fig. 2.4. Raman spectra below 700 cm^{-1} were not collected due to the strong background of the ZrO_2 support. The weak band at 760 cm^{-1} is due to ZrO_2 support and decreases in relative intensity as the molybdenum oxide coverage increases. The Mo=O terminal Raman stretch for the 1% sample (924 cm^{-1}) suggests the presence of tetrahedral species. The Raman band position increases to 952 cm^{-1} as the molybdenum oxide coverage increases from 1 to 5% MoO_3 which corresponds to the range of the terminal stretching bands of polymolybdate species (hydrated $Mo_7O_{24}^{6-}$ and $Mo_8O_{26}^{4-}$). The broad band around 880 cm^{-1} increases with coverage, and increases further after reaching monolayer coverage as shown for the 5% MoO_3/ZrO_2 sample. Thus, molybdenum oxide monolayer on the ZrO_2 support at higher

Mo loading possesses hydrated surface hepta- and octamolybdate species under ambient conditions. Monolayer coverage for the surface molybdenum oxide species on this ZrO_2 (39 m^2/g) support is ~4% MoO_3 loading since crystalline MoO_3 (major Raman bands at 820 cm^{-1}) is present at higher loadings.

MoO_3/Nb_2O_5: The Raman spectrum of bulk niobium oxide possesses strong Raman bands at ~690 cm^{-1}, a shoulder at ~820 cm^{-1} and bands at ~300 and 220 cm^{-1} which are also quite intense. Thus, Raman spectra of the MoO_3/Nb_2O_5 catalysts below 800 cm^{-1} were not collected because the very strong scattering from the Nb_2O_5 support dominates this region. The surface molybdenum oxide Raman features are quite weak against the strong Nb_2O_5 background and, thus, the peak positions of surface niobium oxide species are difficult to determine precisely. The Raman spectra of the 1 - 6% MoO_3/Nb_2O_5 catalysts under ambient conditions shown in Fig. 2.5 were obtained by subtracting the spectrum of the Nb_2O_5 support background in order to enhance the surface molybdenum oxide signals. The major Raman bands for the Mo=O stretch increase slightly from 943 to 952 cm^{-1} as the molybdenum oxide coverage increases. The band position for the terminal Mo=O stretching mode suggests that the surface molybdenum oxide species is primarily present as polymolybdate species (hydrated $Mo_7O_{24}^{6-}$ and $Mo_8O_{26}^{4-}$) on the Nb_2O_5 support. The small 820 cm^{-1} band and a weak shoulder at 992 cm^{-1} characteristic of crystalline MoO_3 appear for 6% MoO_3/Nb_2O_5 sample which indicates that monolayer coverage for surface molybdenum oxide species has been slightly exceeded. Thus, the monolayer coverage of molybdenum oxide on this Nb_2O_5 support (55 m^2/g) is ~6% MoO_3, and the structure of the hydrated surface molybdenum oxide species is similar to hydrated

$Mo_7O_{24}^{6-}$ and $Mo_8O_{26}^{4-}$ clusters under ambient conditions.

2.4.2. XANES spectra of reference compounds and hydrated catalysts:

The Mo L_3-edge XANES, shown as electron yield signals, of a series of reference compounds, $CoMoO_6$, MoO_3, $(NH_4)_2Mo_2O_7$ and Na_2MoO_4, are shown in Fig. 2.6. The prominent feature in the spectra is the intense white line. At the Mo L_3-edge this white line is a result of transitions from the dipole allowed 2p → 4d transition. In addition, splitting of the line is observed, reflecting the ligand field splitting of the final state d-orbital [73,74]. The magnitude, and relative intensity, of the splitting can be understood using simple ligand field concepts. In a tetrahedral field the magnitude of the splitting of the d-orbital is smaller than in an octahedral field (e, t_2 vs. t_{2g}, e_g). The number of available orbitals is also consistent with the relative intensities observed (e:2 and t_2:3; t_{2g}:3 and e_g:2) [73,74]. In $CoMoO_6$ and MoO_3 the Mo is octahedral coordinated to six oxygen atoms, whereas in Na_2MoO_4 the Mo is tetrahedral coordinated. $(NH_4)_2Mo_2O_7$ has Mo atoms both tetrahedral and octahedral coordinated to oxygen. Both the magnitude of the splitting, and relative intensity of the peaks of the compounds shown in Fig. 2.6 are consistent with their symmetry. The fluorescence yield data for these compounds have previously been shown, but here the magnitudes are free of thickness effects [72]. The inset of Fig. 2.6 shows the second derivatives of the XANES which serve to highlight the differences between the spectra. The range of values for the splitting of tetrahedral coordinated Mo oxides is 1.8 - 2.4 eV, whereas for octahedral coordinated Mo oxides it is 3.1 - 4.5 eV [72].

The Mo XANES data under hydrated conditions indicate that there are significant differences in the local site symmetry of molybdenum oxide supported on alumina, titania and silica which depend on both the oxide support and surface coverage. The Mo L_3-edge XANES of 1 and 18 wt% MoO_3/Al_2O_3 catalysts in the ambient state are shown in Fig. 2.7. The inset shows the second derivatives of the XANES. The measured splitting of the peaks in the second derivative of 1% MoO_3/Al_2O_3 is 2.25 eV and that of the 18% MoO_3/Al_2O_3 is 3.5 eV. The intensity ratio of the first to second peaks is reversed between the two samples. In the 1% MoO_3/Al_2O_3 case the second peak is larger than the first, and for the 18% MoO_3/Al_2O_3 catalyst the first is slightly larger than the second. For the 1% MoO_3/Al_2O_3 catalyst both the splitting of the peaks and their relative intensity indicate that the molybdenum oxide species is tetrahedral coordinated. The XANES spectrum of the 18% MoO_3/Al_2O_3 under ambient conditions suggests that the coordination of the surface molybdenum oxide species in this sample is octahedral coordinated, as evidenced both by the large splitting of the peaks and their relative intensity ratio. Thus, the coordination of the surface molybdenum oxide species on Al_2O_3 changes from tetrahedral to octahedral with increasing Mo coverage under ambient conditions.

The Mo L_3-edge XANES data for the 6% MoO_3/TiO_2 sample under ambient conditions is shown in Fig. 2.8. No data were collected for the low coverage MoO_3/TiO_2 catalyst in its hydrated state. The spectrum shows a splitting of ~3.2 eV with the first peak larger than the second, and is consistent with an octahedral coordination of the hydrated surface molybdenum oxide species on TiO_2 at monolayer coverage. Therefore, the molybdenum oxide species on TiO_2 is octahedral coordinated at monolayer coverage under ambient conditions.

The 1% and 5% MoO_3/SiO_2 Mo L_3-edge XANES spectra and the corresponding second derivatives, shown as the inset, are presented in Fig. 2.9. The splitting of the white line is 3.5 eV for the 1% MoO_3/SiO_2 catalyst, and 3.25 eV for the 5% MoO_3/SiO_2 sample. In both cases the intensity of the first peak is larger than the second. From the splitting of the peaks at the white line and their relative intensity ratio the surface molybdenum oxide is octahedral coordinated at both low and high molybdenum oxide loadings. Thus, the coordination of the hydrated surface molybdenum oxide species is octahedral on SiO_2 at all coverages under ambient conditions.

2.4.3. Raman of supported molybdenum oxide species under dehydrated conditions:

Solid molybdate compounds possess both tetrahedral and octahedral coordination with the high frequency Raman bands ranging from 840 - 1060 cm^{-1} for the terminal Mo=O stretching modes. In general, higher frequencies of the Mo=O stretch suggest shorter Mo=O bonds and greater distortions in the structure [78,79]. Raman frequencies in the 200 - 300 cm^{-1} and 500 - 800 cm^{-1} regions are associated with Mo-O-Mo functionalities. The surface molybdenum oxide species on oxide supports, however, possess structures that are generally different from those found in bulk molybdenum oxide compounds and, consequently, appropriate model reference compounds are not available for the surface molybdate. The Raman spectra of the supported molybdenum oxide species under dehydrated conditions provide information about specific bond functionalities (Mo=O, Mo-O-Mo, etc.), but cannot determine the Mo coordination because of the unavailability of surface molybdate reference compounds.

MoO_3/Al_2O_3: The Raman spectra of the MoO_3/Al_2O_3 catalysts as a function of molybdenum oxide loading under dehydrated conditions are presented in Fig. 2.10. At all MoO_3 loadings, a sharp Raman band in the terminal Mo=O stretching region at ~1000 cm^{-1} and a weak Raman band in the Mo=O bending region at ~300 cm^{-1} are observed. With increasing molybdenum oxide loading, the sharp Raman band increases in intensity and shifts from 990 to 1006 cm^{-1} while a broad band at ~870 cm^{-1} also increases in intensity. The Raman spectrum of the 1% MoO_3/Al_2O_3 sample also possesses a broad band at 836 cm^{-1} and a band at 454 cm^{-1} which is due to the instrumental background [28]. The Raman spectra of the higher Mo loaded samples reveal additional bands at ~940, ~590, ~377 and ~210 cm^{-1}. The presence of the 210 and 590 cm^{-1} bands, characteristic of Mo-O-Mo vibrations, for the 12% to 20% samples indicate the presence of surface polymolybdate species for these higher molybdenum oxide loading samples. The high wavenumber shift of the terminal stretching band (990 - 1000 cm^{-1}) and the absence of the ~210 - 220 cm^{-1} band for the low Mo loading samples (1% and 6% MoO_3/Al_2O_3) suggest the presence of a highly distorted and isolated dehydrated surface species [80]. The Raman bands at ~940, 590, ~377, and 210 cm^{-1} for the high loading samples (12% - 20% MoO_3/Al_2O_3) are an indication of the presence of highly distorted surface polymolybdate species under dehydrated conditions.

MoO_3/SiO_2: The Raman spectra of the MoO_3/SiO_2 catalysts under dehydrated conditions as a function of MoO_3 loading are presented in Fig. 2.11. The terminal Mo=O stretching band is located in the 976 - 980 cm^{-1} region. The 977 cm^{-1} Raman band of the Si-O-H stretching mode is gradually replaced by the 980 cm^{-1} Raman band of the surface molybdenum oxide species. The asymmetric nature of this terminal band implies an unresolved shoulder at ~970 cm^{-1}. The 970 cm^{-1} band is more pronounced in samples from non-aqueous preparations [38] that achieved higher dispersions of molybdenum oxide on SiO_2. The 970 cm^{-1} band was also reported in an IR study [46] and was assigned to a second surface molybdenum oxide species. The Raman spectrum of the 5% MoO_3/SiO_2 sample also exhibits a band at 357 cm^{-1} which is due to the bending mode of the terminal Mo=O bond. The absence of the Mo-O-Mo deformation mode at ~220 cm^{-1} for all Mo loaded samples suggests that only isolated surface molybdenum oxide species is present on SiO_2 surfaces. There is a weak band at ~1040 cm^{-1} that increases with molybdenum oxide loading that originated from surface $Si\text{-}O^-$ functionalities [38] formed during the anchoring of the surface molybdenum oxide species to the SiO_2 support. Thus, the dehydrated surface molybdenum oxide species on SiO_2 possess an isolated and highly distorted structure.

MoO_3/TiO_2: The Raman spectra of the MoO_3/TiO_2 catalysts under dehydrated conditions as a function of molybdenum oxide loading are presented in Fig. 2.12. The Raman stretching mode of the terminal Mo=O bond is sharp and occurs at 993-998 cm^{-1} which suggests a highly distorted structure. A very weak and broad band at ~910 cm^{-1} increases as the molybdenum oxide loading increases and is assigned to the formation of polymerized surface molybdenum oxide species. There is no direct information about whether Mo-O-Mo linkages exist in the dehydrated surface molybdenum oxide species on TiO_2 because it is not possible to obtain Mo-O vibrational information below 700 cm^{-1}

due to the strong Raman scattering of the TiO_2 support.

MoO_3/ZrO_2: The Raman spectra of the MoO_3/ZrO_2 catalysts as a function of molybdenum oxide loading under dehydrated conditions are presented in Fig. 2.13. The stretching mode of the terminal Mo=O bond shifts from 980 to 997 cm^{-1} as the molybdenum oxide loading increases. At low molybdenum oxide coverage (1% MoO_3/ZrO_2), there is also a broad Raman band at 845 cm^{-1} along with the major 980 cm^{-1} band. As the molybdenum oxide coverage increases, the 845 cm^{-1} Raman band shifts to ~868 cm^{-1}. There is no Raman information about the low frequency region for the MoO_3/ZrO_2 catalysts due to the strong Raman scattering from the ZrO_2 support. However, comparison of the Raman spectra of the MoO_3/ZrO_2 catalysts with the corresponding MoO_3/Al_2O_3 catalysts reveals a similarity between them. Therefore, similar surface molybdenum oxide structures appear to be present on the ZrO_2 surface as that on the Al_2O_3 surface: e.g., highly distorted, isolated surface molybdenum oxide species present on the ZrO_2 surfaces for low loadings and distorted, polymerized surface molybdenum oxide species present on ZrO_2 at high loadings.

MoO_3/Nb_2O_5: The Raman spectra of the MoO_3/Nb_2O_5 catalysts as a function of molybdenum oxide loading under dehydrated conditions, after subtraction of the Nb_2O_5 support background, are presented in Fig. 2.14. The terminal Mo=O stretching Raman band shifts from 992 to 996 cm^{-1} with increasing Mo oxide coverage. A broad and weak band at ~900 cm^{-1} is also present and its intensity also increases as the molybdenum oxide loading increases. As above, the ~996 cm^{-1} Raman band can be assigned to the terminal Mo=O stretch mode of a dehydrated highly distorted surface molybdenum oxide species and the weak ~900 cm^{-1} Raman band is possibly due to the presence of polymolybdate species. The strong Raman scattering of the Nb_2O_5 support in the low frequency region prevents the collection of additional information about the surface molybdenum oxide species on Nb_2O_5.

4.4.4. XANES studies of the dehydrated catalysts:

The previously calcined catalyst wafers were dehydrated *in situ* by flowing dry 20% O_2 in He over the samples as they were heated to 723 K. After approximately 30 - 45 minutes, the Mo L_3-edge XANES was recorded on each catalyst at 723 K in the flow of O_2/He. The spectra for the 1% and 18% MoO_3/Al_2O_3 samples are shown in Fig. 2.15. The inset shows the second derivatives of the XANES spectra shown in the main Figure. The splitting of the two peaks for the 1% MoO_3/Al_2O_3 catalyst is 2.5 eV, and that for the 18% catalyst is 2.9 eV. The intensity of the split peaks in the white line for the high loading alumina-supported sample are of comparable magnitude. In fact the overall spectrum is quite similar to that of diammonium dimolybdate ($(NH_4)_2Mo_2O_7$), shown in Fig. 2.6. For the dehydrated 1% MoO_3/Al_2O_3 catalyst the second peak is still larger than the first, as in the hydrated case. Thus, the dehydrated 1% MoO_3/Al_2O_3 appears to possess tetrahedral coordinated surface molybdenum oxide species and the dehydrated 18% MoO_3/Al_2O_3 appears to possess a mixture of tetrahedral and octahedral coordinated surface molybdenum oxide species.

The Mo L_3-edge XANES data for the dehydrated titania-supported catalysts are shown in Fig. 2.16. The XANES spectra of the 1% MoO_3/TiO_2 and the 6% MoO_3/TiO_2

catalysts are quite different. For the 1% MoO_3/TiO_2 catalyst the measured splitting in the second derivative is 2.3 eV, with the second peak larger than the first in the normalized data. For the 6% MoO_3/TiO_2 sample, the spectrum looks quite similar to that of bulk MoO_3, shown in Fig. 2.6, and the splitting between the two peaks is 3.5 eV. The first peak is also larger than the second. Thus, the dehydrated 1% MoO_3/TiO_2 possesses a structure with tetrahedral coordination and the dehydrated 6% MoO_3/TiO_2 possesses an octahedral coordinated surface molybdenum oxide species.

In situ Mo L_3-edge XANES data were collected on three different weight loading of the MoO_3/SiO_2 catalysts. The 1% and 5% MoO_3/SiO_2 catalysts were prepared by the aqueous impregnation method in our laboratory, while the 3.5% sample was supplied from a different group and was prepared from a molybdenum allyl compound [37]. As shown in Fig. 2.17, the spectra of all three catalysts are identical. There is no clear splitting of the white line at the Mo L_3-edge, although the asymmetry of the white line clearly indicates the presence of two peaks. The second derivatives are shown in the inset of the Figure. The peaks in the second derivative indicate a "splitting" of $\sim$2.8 eV. Thus, the dehydrated surface structure of the MoO_3/SiO_2 catalysts is not simply tetrahedral or octahedral coordinated and may possess a coordination in between MoO_4 and MoO_6 units.

2.5. DISCUSSION

2.5.1. Surface structures of supported molybdenum oxides under ambient conditions:

Raman spectra of surface molybdenum oxide species under ambient conditions demonstrated that the structure of the molybdenum oxide species depends on the specific oxide support and the molybdenum oxide loading. For the MoO_3/Al_2O_3 catalysts, tetrahedral coordinated hydrated MoO_4^{2-}-like species are the major species on the surface at low loadings and octahedral, polymerized hydrated $Mo_7O_{24}^{6-}$ and $Mo_8O_{26}^{4-}$ species are the predominant surface species at high Mo loadings. For the MoO_3/SiO_2 and MoO_3/Nb_2O_5 catalysts, octahedral polymerized hydrated species are the major species present on the surface regardless of the molybdenum oxide loading. For the MoO_3/TiO_2 and MoO_3/ZrO_2 catalysts, at low loading there are some components of tetrahedral hydrated species due to the low Raman band positions (~930 cm^{-1}) and the amount of octahedral hydrated species increases as the molybdenum oxide loading increases (Raman band ~950 cm^{-1}). The ambient Mo L_3-edge XANES study of the molybdenum oxide coordination on the different oxide supports at low and high Mo loadings is in excellent agreement with the results derived from the ambient Raman study. The major surface molybdenum oxide species present on the oxide supports under ambient conditions at low and high Mo loading are listed in Table 2.4.

Molybdenum oxide ions are known to form isopolyanions in aqueous solutions, and the state of aggregation in these solutions is highly dependent on pH and Mo concentration. The solution chemistry of molybdenum oxide can be explained by the following equations [2,33]:

$$7MoO_4^{2-} + 8H^+ \rightleftharpoons Mo_7O_{24}^{6-} + 4H_2O \qquad (1)$$

$$Mo_7O_{24}^{6-} + 3H^+ + HMoO_4^- \rightleftharpoons Mo_8O_{26}^{4-} + 2H_2O \qquad (2)$$

Above a pH of 8.0, isolated and tetrahedrally coordinated MoO_4^{2-} is the major species present in aqueous solution. For pH values between 4.8 and 6.8, the predominate species is a polymerized and octahedrally coordinated $Mo_7O_{24}^{6-}$ cluster. For pH values of 1.7 - 2.2, octahedral $Mo_8O_{26}^{4-}$ species is the main species in aqueous solution (see Table 3.3).

The point of zero charge (PZC) of a supported metal oxide catalyst system depends on both the oxide support and the molybdenum oxide loading since the addition of molybdenum oxide decreases the surface pH of the oxide support (PZC of MoO_3 ~ 2.3) [81]. It has been proposed that the final pH of the solutions in the filled pores of support is close to the PZC of the support because of the fairly large buffer capacity of the support [9]. However, directly following the dependence of the PZC of the catalysts on the molybdenum oxide loading for MoO_3/Al_2O_3 catalysts by Kohler *et al.* [23] found that the PZC of the catalysts continuously decreases from ~ 9 to 3.8 as the molybdenum oxide loading increases from 0% to ~ 10% Mo loading. This decrease in the PZC is responsible for the structural changes from tetrahedral to octahedral coordinated hydrated molybdenum oxide species which is analogous to the structures formed by molybdenum oxide in an aqueous solution possessing solution pH equal to the sample PZC. Thus, at low Mo loadings the PZC of the oxide support primarily determines the structure of hydrated surface molybdenum oxide, but at high Mo loadings the surface molybdenum oxide drastically depresses the PZC of the system.

For low Mo loading catalysts, the surface molybdenum oxide species on the Al_2O_3 support (pH at PZC=8.9) possessed mainly monomeric species MoO_4^{2-} (Raman band at 912 cm^{-1}), and the surface molybdenum oxide species on SiO_2 (pH at PZC=3.7-4.3) and Nb_2O_5 (pH at PZC=4.0) were found to favor octahedral coordinated polymolybdate species such as $Mo_7O_{24}^{6-}$ and $Mo_8O_{26}^{4-}$ (Raman bands at 947 and 948 cm^{-1}, respectively. Also see Table 2.3, $Mo_7O_{24}^{6-}$ and $Mo_8O_{26}^{4-}$ coexist at pH 2.2 - 4.8). The surface molybdenum oxide species on TiO_2 (pH at PZC=6.0-6.4) and ZrO_2 (pH at PZC=5.9-6.1) formed both tetrahedral and isolated species (MoO_4^{2-}) and polymolybdate species ($Mo_7O_{24}^{6-}$) as shown in Table 2.4 (Raman bands at 934 and 924 cm^{-1}, respectively). Thus, the support pH at PZC controls the molecular structures of molybdenum oxide overlayer on different oxide supports under ambient conditions at low Mo loadings.

The structural changes of the hydrated molybdenum oxide species on different oxide supports with increasing molybdenum oxide loading confirm the dependence of the surface molybdenum oxide structures on the molybdenum oxide loading which corresponds to the changes in the PZC of the samples. It was found that [23] the pH of the catalysts decreases from ~9 to ~3.7 as the Mo loading increases. The $Mo_7O_{24}^{6-}$ species coexist with the $Mo_8O_{26}^{4-}$ species at pH ~3.7 as shown in Table 2.3. The Raman bands of the monolayer catalysts are all located at 947 - 954 cm^{-1} region which is only slightly higher than the Raman band of the $Mo_7O_{24}^{6-}$ species (943 cm^{-1}). Therefore, the species formed on the different supports at high Mo loadings under ambient conditions are listed in Table 2.4 and the dominant species is $Mo_7O_{24}^{6-}$. As the molybdenum oxide content increases, the pH of their aqueous solution decreases and the ratio of $Mo_7O_{24}^{6-}/MoO_4^{2-}$ for MoO_3/Al_2O_3, MoO_3/TiO_2, MoO_3/ZrO_2 on the support surfaces increases. The corresponding Raman shifts toward higher frequency of the terminal stretching bands of the surface molybdenum oxide species with increasing loading of the molybdenum oxides are due to these structural changes (e.g., for the MoO_3/Al_2O_3 catalysts from tetrahedral to octahedral). These trends are in excellent agreement with the net surface pH at PZC model of Deo and Wachs [79]. The good agreement between the surface molybdenum oxide coordination obtained from XANES and that of the structural information from the Raman study further confirms the pH dependence. In addition, Shimada *et* al. [18] characterized the hydrated structures of molybdenum oxide on different oxide supports with EXAFS and found that a tetrahedral structure is predominant on MgO (pH at PZC = 11), an octahedral molybdenum oxide structure is present on SiO_2 and high loading TiO_2, and for Al_2O_3 the molybdenum oxide structures are tetrahedral for low loading and octahedral for high loading. Shimada *et al.*'s findings are in perfect agreement with the current Raman and XANES Mo L_3-edge studies.

The current work further suggests that the hydrated structures of surface molybdenum oxide species under ambient conditions are independent of the preparation method. In this study, the Raman spectra of the samples prepared by the aqueous impregnation method show that the net surface pH at PZC of the sample controls the structure of surface molybdenum oxide species, and agrees with the studies done by Kim *et al.* [33] for supported molybdenum oxide catalysts prepared by the equilibrium adsorption method. Segawa *et al.* [57] investigated MoO_3/TiO_2 catalysts prepared by the equilibrium adsorption method by Raman and found that at high molybdenum oxide loading and ambient conditions, octahedral coordinated molybdenum oxide species exist which is in agreement with our results. Williams *et al.* [24,37] found that the structures of the MoO_3/Al_2O_3 and MoO_3/SiO_2 catalysts under ambient conditions were independent of the Mo precursors and the preparation pH. Machej *et al.* [64,65] found that the same hydrated molybdenum oxide structure was present for high coverage MoO_3/TiO_2 catalysts prepared by impregnation and grafting methods. Knözinger *et al.* [7] found that the same structures are also present for molybdenum oxide dispersed on both η- and γ-Al_2O_3 supports and demonstrates that the specific structure of the oxide support also does not alter the surface structure of the ambient surface molybdenum oxide species. Thus, the molecular structures of the ambient surface metal oxide overlayers are controlled by the thermodynamics of the interactions at the hydrated metal oxide-oxide support interface. Furthermore, the ability to make the same surface molybdenum oxide overlayers from physical mixtures of crystalline MoO_3 and supports demonstrates the high mobility of the Mo species and, consequently, the lack of dependence on the preparation method [80,82-87].

2.5.2. Surface structures of supported molybdenum oxides under dehydrated conditions:

As discussed above, under ambient conditions the molecular structures of the hydrated surface molybdenum oxide species are similar to those found in aqueous solutions. At elevated temperatures, however, the adsorbed moisture desorbs from the catalyst surface and the surface becomes dehydrated. Consequently, the structures of the surface metal oxides are drastically altered upon dehydration as was found for many supported metal oxide systems (V, Nb, Cr, Re, etc.) [2,27,64]. Unfortunately, the structures of the surface molybdenum oxide species are not the same as known solid molybdate reference compounds. As already mentioned in the results section, unambiguous assignment of the vibrational bands for Raman spectra of solid molybdate compounds is not always straightforward since inorganic molybdenum oxide compounds possess vibrational frequencies for the tetrahedral and octahedral terminal Mo=O bond stretches that can overlap [9,78]. In addition, the stretching modes of the terminal Mo=O groups at 1046-840 cm^{-1} and of bridging Mo-O-Mo groups at 946-820 cm^{-1} can also overlap [28,78]. Moreover, the structures of many molybdate compounds cannot be classified as having precisely octahedral or tetrahedral coordination of the molybdenum ions [78]. Therefore, a Raman study of the surface molybdenum oxide species on different oxide supports under dehydrated conditions cannot provide a complete structure, but only gives some information about the Mo=O and Mo-O-Mo functionalities. However, the Mo XANES under dehydrated conditions is complementary to Raman and provides important information about the coordination of the surface molybdenum oxide species.

The Mo XANES data under dehydrated conditions indicate that there are significant differences in the local site symmetry of the surface molybdenum oxide species supported on alumina, titania and silica brought about by dehydration. Table 2.5 lists the coordination of the surface molybdenum oxide species on different supports for the low loading and high loading catalysts under dehydrated conditions. For the 1% MoO_3/Al_2O_3 sample, both the splitting of the peaks and their relative intensities indicate that the surface molybdenum oxide species is tetrahedral coordinated in the dehydrated state. For the low loading MoO_3/TiO_2 sample, the spectrum also indicates that the surface molybdenum oxide species is primarily tetrahedral coordinated. However, the presence of some octahedral coordinated surface molybdenum oxide on TiO_2 cannot be excluded as the second derivative indicates the presence of a shoulder at a splitting of 3.6 eV, and the relative ratio of the intensities of the peaks is only weakly indicative of tetrahedral geometry. Thus, the dehydrated surface molybdenum oxide species present for low loading samples on Al_2O_3 and TiO_2 primarily possess tetrahedral coordination. The XANES and Raman studies of the dehydrated MoO_3/SiO_2 catalysts will be discussed separately below since the surface molybdenum oxide species on the SiO_2 support is very different from the other oxide supports.

The main Raman features upon dehydration for the supported molybdenum oxide catalysts are the disappearance of the terminal bands in the 930 - 960 cm^{-1} region and the appearance of very sharp bands at ~1000 cm^{-1}. The terminal Mo=O Raman stretching bands for the different supports are very similar for the dehydrated samples. At low surface coverage, the sharp Raman band at ~1000 cm^{-1} predominates and the high frequency position of this Raman band suggests a highly distorted structure. The absence of Raman bands in the Mo-O-Mo bending region (~220 cm^{-1}) in the spectrum of the 1% MoO_3/Al_2O_3 sample suggests that this species is isolated. The combined XANES and Raman data at low Mo loading suggest that the surface molybdenum oxide species on the Al_2O_3 support is isolated, highly distorted and tetrahedrally coordinated. For a tetrahedrally coordinated species on the surface, the most likely structure is that possessing two terminal Mo=O bonds and two bridging Mo-O-support bonds. Accordingly, the broad ~836 cm^{-1} Raman band can be assigned to the asymmetric stretching mode of the Mo=O bonds. The Raman spectra of 1% MoO_3 on different oxide supports in the 1100 - 700 cm^{-1} region are compared in Fig. 2.18 and reveal very similar features for the 1% MoO_3/ZrO_2 and 1% MoO_3/Al_2O_3 catalysts at low coverage which suggests similar structures for these two catalysts. In addition, the XANES and Raman spectrum of the 1% MoO_3/TiO_2 suggests that the structures of surface molybdenum oxide are primarily highly distorted and tetrahedral coordinated species with a minor component of distorted and octahedral coordinated species. The Raman spectrum of the 1% MoO_3/Nb_2O_5 appears very similar to that of the 1% MoO_3/TiO_2 and, thus, similar structures are presumably present also for these two catalysts (see Fig. 2.18). However, the coordinations of the dehydrated MoO_3/ZrO_2 and MoO_3/Nb_2O_5 catalysts at low loadings should be directly confirmed with further XANES measurements.

The XANES spectra for the monolayer coverage catalysts are quite different from their corresponding low loading catalysts. In the XANES spectrum of 18% MoO_3/Al_2O_3, the surface molybdenum oxide species appears to be octahedrally coordinated because of the large splitting of the peaks and their relative intensity ratio. However, the splitting decreases slightly compared to the spectrum of hydrated condition, and the relative ratio of the peaks becomes almost equal. While the second derivative does not clearly confirm the presence of two components in the XANES spectrum, the overall shape of the normalized spectrum is similar to that of diammonium dimolybdate in which there is an equal number of tetrahedrally and octahedrally coordinated molybdenum. On the basis of this fingerprint, at high loadings of molybdenum on alumina under dehydrated conditions there are both octahedral and tetrahedral surface molybdenum oxide species present. The XANES spectrum of the 6% MoO_3/TiO_2 sample clearly indicates the octahedral coordination of the surface molybdenum oxide species for this high loading sample. Thus, the coordination of the surface molybdenum oxide species depends on the specific oxide support.

The Raman spectra also reflect the structural changes with increasing surface molybdenum oxide coverage of the dehydrated samples. As the molybdenum oxide loading increases, a second molybdenum oxide species which possesses Raman bands at ~940, 865, 590, 377, and 210 cm^{-1} is formed on the MoO_3/Al_2O_3 catalysts at high Mo loading. The 590 and 210 cm^{-1} bands reflect the formation of Mo-O-Mo bridging bonds in the surface molybdenum oxide structure which suggests the formation of a polymerized species. For surface molybdenum oxide species on other supports, the formation of this second species is indicated by an increase of a broad Raman band at ~880 cm^{-1} that generally grows with surface molybdenum oxide coverage with the exception of SiO_2 which does not form a polymeric species (no Raman bands at ~880 and ~210 cm^{-1}). The polymeric surface molybdenum oxide species appear to be most pronounced on Al_2O_3 and ZrO_2 relative to TiO_2 and Nb_2O_5. Fig. 2.19 compares the Raman spectra of the monolayer molybdenum oxide species on different oxide supports in the 1100 - 700 cm^{-1} region. The similar Raman bands for the 4% MoO_3/ZrO_2 and the 20% MoO_3/Al_2O_3 catalysts, as well as between the 5% MoO_3/Nb_2O_5 and the 6% MoO_3/TiO_2 catalysts suggest similarities in the structures of the surface molybdenum oxide species on the respective supports. Therefore, it is concluded that for high loadings of MoO_3/Al_2O_3 and MoO_3/ZrO_2 catalysts, highly distorted, polymerized and octahedral coordinated surface molybdenum oxide species coexist with tetrahedral, isolated surface species. In general, the relative Raman intensity of the two dehydrated surface species, polymeric to monomeric species, increases with increasing metal oxide loading, but their relative Raman cross sections are not known. A surface highly distorted octahedral polymolybdate species is also present on the TiO_2 and Nb_2O_5 supports for high loading catalysts but does not appear to be as extensively polymerized.

From the Raman spectra of the MoO_3/SiO_2 catalysts, the surface molybdenum oxide species possesses an isolated and highly distorted structure under dehydrated conditions. De Boer et al. [36] found by EXAFS that total Mo-Mo coordination number decreased from 3.27 to 0.20 after dehydration which confirms that dehydration produces essentially isolated molybdenum oxide species on SiO_2. The XANES spectra at the Mo L_3-edge of the MoO_3/SiO_2 catalysts after dehydration change quite dramatically compared to the spectra under hydrated conditions. However, there is no clear indication of splitting of the XANES upon dehydration, although the asymmetry of the peak clearly indicates the presence of two peaks. At present a clear interpretation of these XANES spectra is not available. The spectra indicate that the symmetry of the molybdenum is clearly not in a slightly distorted tetrahedral or octahedral geometry as found for the other catalysts, and the range of model compounds investigated. However, the similarity between the XANES spectrum of the 3.5% MoO_3/SiO_2 sample made by the nonaqueous preparation method and the 1% and 5% samples made by the aqueous impregnation method confirms the independence of the structure of the surface molybdenum oxide species on the preparation method. The symmetry of a species between tetrahedral and octahedral coordination indicated by XANES data agrees with the mono-oxo model suggested by the IR study that employed ^{18}O - ^{16}O exchange to examine the MoO_3/SiO_2 catalysts [46]. According to Cornac *et al.*, the coordination of surface Mo species on SiO_2 is an octahedral species with one bridging Mo-O- bond which attaches to a surface site different from the other three Mo-O-Si bridging bonds. The remaining Mo=O bond and three Mo-O-Si bonds show tetrahedral feature. More XANES studies are needed on these samples as well as model reference compounds in order to come to a firm conclusion about the local symmetry of the dehydrated surface molybdenum oxide species on silica.

From the combined Raman and XANES data, the dehydrated structures of the surface molybdenum oxide species present on the different oxide supports at low and high loading were determined and are listed in Table 2.5. The results in Table 2.5 suggest that under dehydrated conditions, the surface molybdenum oxide species tend to form isolated species on the oxide supports at low Mo loadings. When the Mo loading increases, the more dense surface Mo coverages allows polymolybdate species to be formed. For the MoO_3/SiO_2 catalysts, higher surface coverages are not possible before the formation of crystalline MoO_3, and therefore, only isolated surface molybdenum oxide species are present on this support. The isolated structures of the surface molybdenum oxide species for the low loading catalysts also suggest that the breaking of precursor clusters has occurred upon the deposition of molybdenum oxide on all oxide supports. Furthermore, this study also confirms that there is no precursor or preparation effect to the final structure of the surface molybdenum oxide species.

The combined Raman and XANES characterization techniques provide a relatively dependable determination of the structure and local site symmetry for supported molybdenum oxide catalysts. There were several recent attempts at using solid state ^{95}Mo NMR to study the structures of the surface molybdenum oxide species [4,16,88]. However, the analysis of the ^{95}Mo NMR spectrum does not appear straightforward; the variation of octahedral and tetrahedral sites affects not only the chemical shift but also the line width and line shape, and the assignment of the line shape components requires a curve-fitting program to estimate many parameters [16,88]. It appears that additional progress in solid state ^{95}Mo NMR is required for the molecular structural assignments of supported molybdenum oxide catalysts.

2.5.3. Monolayer coverage of surface molybdenum oxides on different oxide supports:

As previously mentioned, the supported molybdenum oxide catalysts used in the present study were all prepared by the incipient-wetness impregnation method from an aqueous solution of ammonium heptamolybdate. Samples possessing only a very small Raman band at ~ 820 cm^{-1} are taken as representative of monolayer coverage of surface molybdenum oxide species on the specific oxide support. The Raman signal of crystalline MoO_3 is significantly stronger in comparison to the Raman signal of surface molybdenum oxide species [28], and crystalline MoO_3 generally forms above monolayer coverage. The molybdenum oxide monolayer coverage obtained in the present study via the aqueous impregnation preparation method are listed in Table 2.1 for each support.

Essentially the same surface density (dispersion per unit surface area) is obtained on all the oxide supports used (~ 4.6 Mo atoms/nm^2) with the exception of the SiO_2 support. The theoretical monolayer coverage of molybdenum oxide on an oxide support was estimated to be ~ 8.0 Mo atoms/nm^2 which was obtained by assuming full coverage of the support surface by a single layer of the MoO_3 crystal phase [60]. The current findings reveal that only ~ 57% of a theoretical monolayer is formed for molybdenum oxide species on the oxide supports and suggests that theoretical monolayer coverage is not achievable before the formation of crystalline MoO_3. This also indicates that the theoretical model which is based on a layer of crystalline MoO_3 is not realistic since the surface molybdenum oxide species usually possess a different structure and packing density than crystalline MoO_3. A benzaldehyde-ammonia titration (BAT) method used [89] to determine the monolayer coverages of the surface molybdenum oxide species on Al_2O_3, TiO_2, and ZrO_2 supports obtained a surface concentration of <7 Mo atoms/nm^2 since the BAT method is less sensitive to the microcrystalline MoO_3 formation than the Raman technique.

The present work has shown that the conventional impregnation preparation gives the same dispersion as other preparation methods for oxide supports. Segawa *et al.* [57] found from the XPS Mo(3d)/Ti(2p) ratio that ~ 6.6 wt% MoO_3 corresponds to monolayer coverage for the TiO_2 (Degussa P-25). The close agreement between Segawa *et al.*'s results based on the equilibrium adsorption preparation method and the present result from the aqueous impregnation method (~ 6% MoO_3) suggests that the preparation method does not affect the final monolayer coverage. A literature search of other studies of molybdenum oxide monolayer coverage on oxide supports did not reveal higher loadings when different preparation methods were employed with the exception of the SiO_2 support (see discussion below). The current study also demonstrates that monolayer coverage is only a function of the oxide support surface area and not a function of the specific molecular structure of the surface molybdenum oxide species (e.g., Oh for MoO_3/TiO_2 and Oh/Td for MoO_3/Al_2O_3).

The preparation methods and precursors do not seem to have much of an effect on the dispersion of the surface molybdenum oxide species on different oxide supports except for SiO_2 in which the non-aqueous preparation of MoO_3/SiO_2 catalysts by Williams *et al.* [37-39] did produce higher loadings of the dispersed molybdenum oxide on SiO_2. However, monolayer coverage has never been achieved on SiO_2, partially due to the low surface OH density of this support and the reactivity between adjacent silanol groups to form siloxane bridges. It has been proposed that the interaction between the precursor and the oxide support surface depends on the sign of the surface charge of the support and of the dissolved complexes of the precursor [36]. The silica surface is negatively charged at the pH of the AHM solution (~ 5.5) and is thought to account for the lack of interaction with the anionic heptamolybdate cluster. However, in the present study the same monolayer coverage of surface molybdenum oxide species on the Nb_2O_5 support (PZC ~ 4) as on the other oxide supports was also obtained which suggests that the surface charge of the support is not the controlling factor for the dispersion of molybdenum oxide. The spontaneous dispersion behavior [82-87] of molybdenum oxide on the surface of oxide supports with the exception of SiO_2, suggests it is more likely that there is a driving force for the dispersion of molybdenum oxide on the surface of oxide supports. The inability to form monolayer coverage of surface molybdenum oxide species on SiO_2, however, reflects a repulsion between the SiO_2 surface and metal oxides since physical mixtures of surface molybdenum oxide species on SiO_2 and other oxide supports (TiO_2, Al_2O_3, etc.) result in complete migration of the surface molybdenum oxide species away from the SiO_2 support upon heating (e.g., $MoO_3/SiO_2 + TiO_2 \rightarrow SiO_2 + MoO_3/TiO_2$) [90].

2.6. CONCLUSIONS

The molecular structures of the surface molybdenum oxide species on the Al_2O_3, TiO_2, ZrO_2, Nb_2O_5, and SiO_2 supports were investigated by Raman and XANES at the Mo $L_{2,3}$-edges spectroscopies as a function of Mo loading and hydration/dehydration states. Under ambient conditions, the structures of supported molybdenum oxide species resembles molybdate species in aqueous solutions. At low Mo loadings, the structure of surface molybdenum oxide species depends on the pH at the point of zero charge of the different supports. At high Mo loadings, the structure of surface molybdenum oxide species also depends on the molybdenum oxide coverage which decreases the pH at the point of zero charge of the catalyst surface. For molybdenum oxide supported on SiO_2 and Nb_2O_5 supports, hydrated polymolybdate clusters ($Mo_7O_{24}^{6-}$ and $Mo_8O_{26}^{4-}$) are the principle species present on the surfaces. For the TiO_2 and ZrO_2 supported molybdenum oxide, the major species are tetrahedral species (MoO_4^{2-}) at low Mo loadings and polymolybdates ($Mo_7O_{24}^{6-}$) at high Mo loadings. For the Al_2O_3 support, at low loadings the isolated and tetrahedral coordinated molybdenum oxides (MoO_4^{2-}) are the main species, and the polymeric species ($Mo_7O_{24}^{6-}$) increase with Mo loadings. The molecular structures of the hydrated surface molybdenum oxide species can be predicted by the pH at PZC model. Under dehydrated conditions, the structures of the surface molybdenum oxide species depend on both the specific oxide support and the Mo loading. A highly distorted and isolated structure are observed to be present on all supports at low loading. On the Al_2O_3 support, this species is tetrahedral coordinated, on the TiO_2 support the major species are also tetrahedrally coordinated. At high loadings, octahedral coordinated polymolybdate species as well as isolated tetrahedral species present on the surface of Al_2O_3, but the polymolybdate species predominate on the TiO_2 support. The structures of the MoO_3/ZrO_2 appear to be similar to that of the MoO_3/Al_2O_3, and the structures of the MoO_3/Nb_2O_5 appear to be similar to that of the MoO_3/TiO_2. The SiO_2 supported surface molybdenum oxide species are isolated and highly distorted at all loadings and possess a symmetry somewhat between octahedral and tetrahedral coordinations, and additional studies with molybdenum oxide reference compounds are required.

REFERENCES

1. Haber, J. *The Role of Molybdenum in Catalysis*, Climax Molybdenum Co. 1981.
2. Segawa, K., and Wachs, I. E. In *Characterization of Catalytic Materials*; Wachs, I. E.Ed., Butterworth Heinemann, 72, 1992.
3. Bartlett, J. R., and Cooney, R. P. *Spectroscopy of Inorganic-Based Materials*; Clark, R. J. H., and Hester, R. E., Eds.; John Wiley & Sons, , 187, 1987.

4. Han, O. H., Lin, C. Y., Sustache, N., McMillan, M., Carruthers, J. D., Zilm, K. W., and Haller, G. L. *Appl.Catal. A: General,* **98**, 195 (1993).

5. Stencel, J. M. In *Raman Spectroscopy for Catalysis*, Van Norstranel Reinhold, 51, 1990.

6. Medema, J., van Stam, C., de Beer, V. H. J., Konings, A. J. A., and Koningsberger, D. C. *J. Catal.*, **53**, 386 (1978).

7. Knözinger, H., and Jeziorowski, H. *J. Phys. chem.*, **82**, 2002 (1978).

8. Jeziorowski, H., and Knözinger, H. *J. Phys. Chem.*, **83**, 1166 (1979).

9. Wang, L., and Hall, W. *K. J. Catal.*, **66**, 251 (1980).

10. Wang, L., and Hall, W. K. *J. Catal.*, **83**, 242 (1983).

11. Jeziorowski, H., Knözinger, H., Grange, P., and Gajardo, P. *J. Phys. Chem.*, **84**, 1825 (1980).

12. Cornac, M., Janin, A., and Lavalley, J. C. *Infrared Phys.*, **24**, 143 (1984).

13. Okamoto, Y., and Imanaka, T. *J. Phys. Chem.*, **92**, 7102 (1988).

14. Rodrigo, L., Marcinkowska, K., Adnot, A., Roberge, P. C., Kaliaguine, S., Stencel, J. M., Makovsky, L. E., and Diehl, J. R. *J. Phys. Chem.*, **90**, 2690 (1986).

15. Zingg, D. S., Makovsky, L. E., Tischer, R. E., Brown, F. R., and Hercules, D. M. *J. Phys. Chem.*, **84**, 2898 (1980).

16. Edwards, J. C., Adams, R. D., and Ellis, P. D. *J. Am. Chem. Soc.*, **112**, 8349 (1990).

17. Luthra, N. P., and Cheng, W. -C. *J. Catal.*, **107**, 154 (1987).

18. Shimada, H., Matsubayashi, N., Sato, T., Yoshimura, Y., Nishijama, A. Kosugi, N., and Kuroda, H. *J. Catal.*, **138**, 746 (1992).

19. Cheng, C. P., and Schrader, G. L. *J. Catal.*, **60**, 276 (1979).

20. Ng, K. Y. S., Zhou, X., and Gulari, E. *J. Phys. Chem.*, **89**, 2477 (1985).

21. Hall, W. K. *J. Proc. of the Climax 4th Int. Conf. on the Chem. and Uses of Molybdenum*, 224, 1982.

22. Payen, E., Grimblot, J., and Kasztelan, S. *J. Phys. Chem.*, **91**, 6642 (1987).

23. Kohler, S. D., Ekerdt, J. G., Kim, D. S., and Wachs, I. E. *Catalysis Letters*, **16**, 231 (1992).

24. Williams, C. C., Ekerdt, J. G., Jehng, J-M., Hardcastle, F. D., and Wachs, I. E. *J. Phys. Chem.*, **95**, 8791 (1991).

25. Stencel, J. M., Makovsky, L. E., Sarkus, T. A., de Vries, J., Thomas, R., and Moulijn, J. A. *J. Catal.*, **90**, 314 (1984).

26. Payen, E., Kasztelan, S., Grimblot, J., and Bonnelle, J. P. *J. Raman Spectrosc.*, **17**, 233 (1986).

27. Chan, S. S., Wachs, I. E., Murrell, L. L., Wang, L.,and Hall, W. K. *J. Phys. Chem.* **88**, 5831 (1984).

28. Vuurman, M. A., and Wachs, I. E. *J. Phys. Chem.*, **96**, 5008 (1992).

29. Vuurman, M. A. and Wachs, I. E. *J. Mol. Catal.*, **77**, 29 (1992).

30. Gao, X., and Xin, Q. *Catalysis Letters*, **18**, 409 (1993).

31. Diaz, A. L., and Bussell, M. E. *J. Phys. Chem.* 97, 470 (1993).

32. Smith, M. R., Zhang, L., Driscoll, S. A., and Ozkan, U. S. *Catalysis Letters*, **19**, 1 (1993).

33. Kim, D. S., Segawa, K., Soeya, T., and Wachs, I. E. *J. Catal.*, **136**, 539 (1992).

34. Martín, C., Martín, M., and Rives, V. *Studies in Surface Science and Catalysis*. Ruiz, P. and Delmon, B. Eds., **72**, 415 (1992).

35. Liu, T. C., Forissier, M., Coudurier, G., and Védrine, J. C. *J. Chem. Soc. Faraday Trans.* I, 85, 1607 (1989).

36. de Boer, M., van Dillen, A. J., Koningsberger, D. C., Geus, J. W., Vuurman, M. A., and Wachs, I. E. *Catal. Letters*, **11**, 227 (1991).

37. Williams, C. C., Ekerdt, J. G., Jehng, J-M., Hardcastle, F. D., Turek, A. M., and Wachs, I. E. *J. Phys. Chem.*, 95, 8781 (1991).

38. Roark, R. D., Kohler, S. D., Ekerdt, J. G., Kim, D. S., and Wachs, I. E. *Catal. Letters*, **16**, 77 (1992).

39. Roark, R. D., Kohler, S. D., and Ekerdt, J. G. *Catal. Letters*, **16**, 71 (1992).

40. Barbaux, Y., Elamrani, A. R., Payen, E., Gengembre, L., Bonnelle, J. P., and Grzybowska, B. *Applied Catal.*, 44, 117 (1988).

41. Kasztelan, S., Payen, E., and Moffat, J. B. *J. Catal.*, **112**, 320 (1988).

42. Rocchiccioli-Deltcheff, C., Amirouche, M., Che, M., Tatibouët, J. M., and Fournier, M. *J. Catal.*, **125**, 292 (1990).

43. Stencel, J. M., Diehl, J. R., D'Este, J. R., Makovsky, L. E., Rodrigo, L. Marcinkowska, K., Adnot, A., Roberge, P. C., and Kaliaguine, S. *J. Phys. Chem.*, **90**, 4739 (1986).

44. Seyedmonir, S. R., and Howe, R. F. *J. Catal.*, **110**, 216 (1988).

45. Wachs, I. E., Deo, G., Kim, D. S., Vuurman, M. A., and Hu, H. *Proc. Int. Congr. Catal. 10th*, A, 543 (1992).

46. Cornac, M., Janin, A., and Lavalley, J. C. *Polyhedron*, **5**, 183 (1986).

47. Seyedmonir, S. R., Abdo, S., and Howe, R. F. *J. Phys. Chem.*, **86**, 1233 (1982).

48. Marcinkowska, K., Rodrigo, L., Kaliaguine, S., and Roberge, P. C. *J. Catal.*, **97**, 75 (1986).

49. Hazenkamp, M. F. Ph. D. Thesis, University of Utrecht (The Netherland), (1992).

50. Louis, C., Che, M., and Anpo, M. *J. Catal.* **141**, 453 (1993).

51. Bañares, M. A., and Fierro, J. L. G. *Catalysis Letters*, **17**, 205 (1993).

52. Aigler, J. M., Brito, J. L., Leach, P. A., Houalla, M., Proctor, A., Cooper, N. J., Hall, W. K., and Hercules, D. M.; *J. Phys. Chem.* **97**, 5699 (1993).

53. Louis, C., and Che, M. *J. Catal.*, **135**, 156 (1992).

54. Ono, T., Anpo, M., and Kubokawa, Y. *J. Phys. Chem.*, **90**, 4780 (1986).

55. Datta, A. K., Ha, J. W., and Regalbuto, J. R.; *J. Catal.*, **133**, 55 (1992).

56. Spanos, N. Matralis, H. K., Kordulis, C., and Lycourghiotis, A. *J. Catal.*, **136**, 432 (1992).

57. Segawa, K., Soeya, T., and Kim, D. S. *Sekiyu Gakkaishi*, **33**, 347 (1990).

58. Ng, K. Y. S., and Gulari, E. *J. Catal.*, **92**, 340 (1985).

59. Ono, T., Nakagawa, Y., Miyata, H., and Kubokawa, Y. *Bull. Chem. Soc. Jpn.* **57**, 1205 (1984).
60. Bond, G. C., and Flamerz, S.; Wijk, L. V. *Catalysis Today*, **1**, 229 (1987).
61. Quincy, R. B., Houalla, M., and Hercules, D. M. *J. Catal.*, **106**, 85 (1987).
62. Quincy, R. B., Houalla, M., Proctor, A., and Hercules, D. M. *J. Phys. Chem.* **93**, 5882 (1989).
63. van Hengstum, A. J., van Ommen, J. G., Bosch, H., and Gellings, P. J. *Appl. Catal.*, **5**, 207 (1983).
64. Machej, T., Doumain, B., Yasse, B., and Delmon, B. *J. Chem. Soc., Faraday Trans.*, *1*, **84**, 3905 (1988).
65. Machej, T., Haber, J., Turek, A. M., and Wachs, I. E. *Appl. Catal.*, **70**, 115 (1991).
66. Ono, T., Miyata, H., and Kubokawa, Y. *J. Chem. Soc. Faraday Trans.* 1, **83**, 1761 (1987).
67. Miyata, H., Tokuda, S., Ono, T., Ohno, T., and Hatayama, F. *J. Chem. Soc. Faraday Trans.* 1, **86**, 2291 (1990).
68. Jin, Y. S., Ouqour, A., Auroux, A., and Védrine, J. C. In *Structure and Reactivity of Surfaces*, Morterra, C.; Zecchina, A.; Costa, G. Eds., Elsevier, 525 (1989).
69. Jehng, J-M., Turek, A. M., and Wachs, I. E. *Appl. Catal. A. General*, **83**, 179 (1992).
70. López Cordero, R., Gil-Lliambias, F. J., and López Agudo, A. *Appl. Catal.*, **74**, 125 (1991).
71. Cáceres, C. V., Fierro, J. L. G., Lázaro, J., López Agudo, A., and Soria, J. *J. Catal.*, **122**, 113 (1990).
72. Bare, S. R., Mitchell, G. E., Maj, J. J., Vrieland, G. E., and Gland, J. L. *J. Phys. Chem.* **97**, 6048 (1993).
73. Hedman, B., Penner-Hahn, J. E., and Hodgson, K. O. In *EXAFS and near Edge structure III*; Hodgson, K. O., Hedman, B., and Penner-Hahn, J. E. Eds.,

Springer Verlag, Berlin, 1984.

74. George, G. N., Cleland, W. E., Enemark, J. H., Smith, B. E., Kipke, C. A., Roberts, S. A., and Cramer, S. P. *J. Am. Chem. Soc.*, **110**, 3798 (1988).

75. The EXAFS Company, Seattle, WA.

76. Lytle, F. W., Greegor, R. B.,and Marques, E. C. *Proc. 9th Int. Congr. Catal.*, Calgary, **5**, 54 (1988).

77. Jeziorowski, H., and Knözinger, H. *J. Phys. Chem.* **83**, 1166 (1979).

78. Hardcastle, F. D. and Wachs, I. E. *J. Raman Spectroc.* **21**, 683 (1990).

79. Deo, G., and Wachs, I. E. *J. Phys. Chem.* **95**, 5889 (1991).

80. Leyrer, J., Mey, D., and Knözinger, H. *J. Catal.*, **124**, 349 (1990).

81. Butler, M. A., and Ginley, D. S. *J. Electrochem. Soc.*, **125**, 228 (1978).

82. Stampfl, S. R., Chen, Y., Dumesic, J. A., Niu, C., and Hill, C. G. Jr. *J. Catal.*, **105**, 445 (1987).

83. Knözinger, H., and Taglaner, E. In *Catalysis*, *Pre. Royal Society of Chemistry*, Vo.***10***, 1 (1993).

84. Leyrer, J., Zaki, M. I., and Knözinger, H. *J. Phys. Chem.*, **90**, 4775 (1986).

85. Reddy, B. M., Reddy, E. P., and Srinivas, S. T. *J. Catal.*, **136**, 50 (1992).

86. Kisfaludi,G., Leyrer, J., Knözinger, H., and Prins, R. *J. Catal.*, **130**, 192 (1991).

87. del Arco, M., Carrazán, S. R. G., Rives, V., Gill-Llambías, F. J., and Malet, P. *J. Catal.* **141**, 48 (1993).

88. Edwards, J. C., Zubieta, J., Shaikh, S. N., Chen, Q., Bank, S., and Ellis, P. D. *Inorg. Chem.* **29**, 3381 (1990).

89. Matsuoka, Y., Niwa, M., and Murakami, Y. *J. Phys. Chem.* **94**, 1477 (1990).

90. Jehng, J-M., and Wachs, I. E. Unpublished results.

Table 2.1. The Surface Density of Supported MoO_3 Catalysts at Monolayer Coverage.

Support	Surface area (m^2/g)	Monolayer loading (wt% MoO_3)	Monolayer surface area (m^2/g)	Surface density (Mo/nm^2)
MoO_3	-	-	-	8.0[a]
Al_2O_3	180	20	175	4.6
TiO_2	55	6	53	4.6
ZrO_2	39	4	39	4.3
Nb_2O_5	55	6	47	4.6
SiO_2	380	5	275	0.8[b]

a: Theoretical monolayer coverage of MoO_3 catalyst from reference 60.

b: Based on final BET of the SiO_2 support.

Table 2.2. Elemental Analysis of Molybdenum Oxide Contents for Supported Samples

Sample	MoO_3 (wt%)
20% MoO_3/Al_2O_3	20.8
5% MoO_3/TiO_2	5.5
5% MoO_3/ZrO_2	5.3
5% MoO_3/Nb_2O_5	5.5
4% MoO_3/SiO_2	3.1

Table 2.3. Raman Bands of Molybdate Species in Aqueous Solutions

Molybdate species	Solution pH	Raman bands (cm^{-1})
MoO_4^{2-}	> 8.0	897, 837, 317
$Mo_7O_{24}^{6-}$	6.8 - 4.8	943, 903, 570, 362, 210
$Mo_8O_{26}^{4-}$	2.2 - 1.7	965, 925, 590, 370, 230

Table 2.4. Summary of XANES and Raman Structures of Surface Molybdenum Oxide Species Under Ambient Conditions

Oxide support	PZC of support	Structures at low coverage		Structures at high coverage	
		XANES	Raman	XANES	Raman
Al_2O_3	8.9	Td	MoO_4^{2-}	Oh	$Mo_7O_{24}^{6-}$*, $Mo_8O_{26}^{4-}$
TiO_2	6.0 - 6.4	-	$Mo_7O_{24}^{6-}$, MoO_4^{2-}	Oh	$Mo_7O_{24}^{6-}$*, $Mo_8O_{26}^{4-}$
ZrO_2	5.9 - 6.1	-	$Mo_7O_{24}^{6-}$, MoO_4^{2-}	-	$Mo_7O_{24}^{6-}$*, $Mo_8O_{26}^{4-}$
SiO_2	3.7 - 4.3	Oh	$Mo_7O_{24}^{6-}$*, $Mo_8O_{26}^{4-}$	Oh	$Mo_7O_{24}^{6-}$*, $Mo_8O_{26}^{4-}$
Nb_2O_5	4.0	-	$Mo_7O_{24}^{6-}$*, $Mo_8O_{26}^{4-}$	-	$Mo_7O_{24}^{6-}$*, $Mo_8O_{26}^{4-}$

* Major species.

Table 2.5. Summary of XANES and Raman Structures of Surface Molybdenum Oxide Under Dehydrated Conditions

Oxide support	Structures at low coverage		Structures at high coverage	
	XANES	Raman	XANES	Raman
Al_2O_3	Td	isolated	Td + Oh	polymolybdate
TiO_2	Td + Oh[a]	–	Oh	polymolybdate
ZrO_2	(Td)[b]	–	(Td+Oh)[b]	polymolybdate
Nb_2O_5	(Td+Oh[a])[b]	–	(Oh)[b]	polymolybdate
SiO_2	?	isolated	?	isolated

a: Minor species.
b: Based on similarity of Raman spectra.

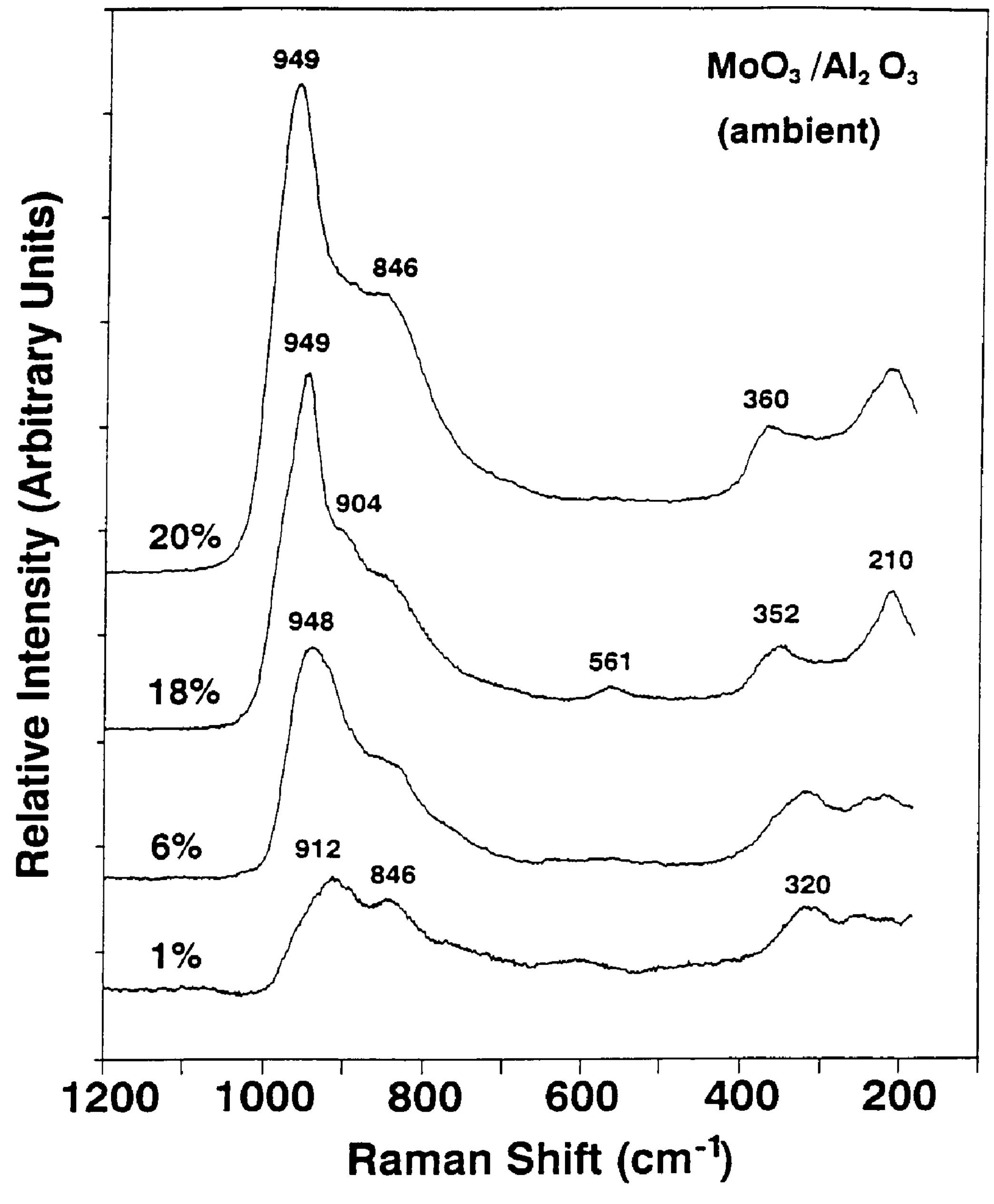

Fig. 2.1. The Raman spectra of MoO_3/Al_2O_3 catalysts as a function of MoO_3 loading. Spectra obtained under ambient conditions.

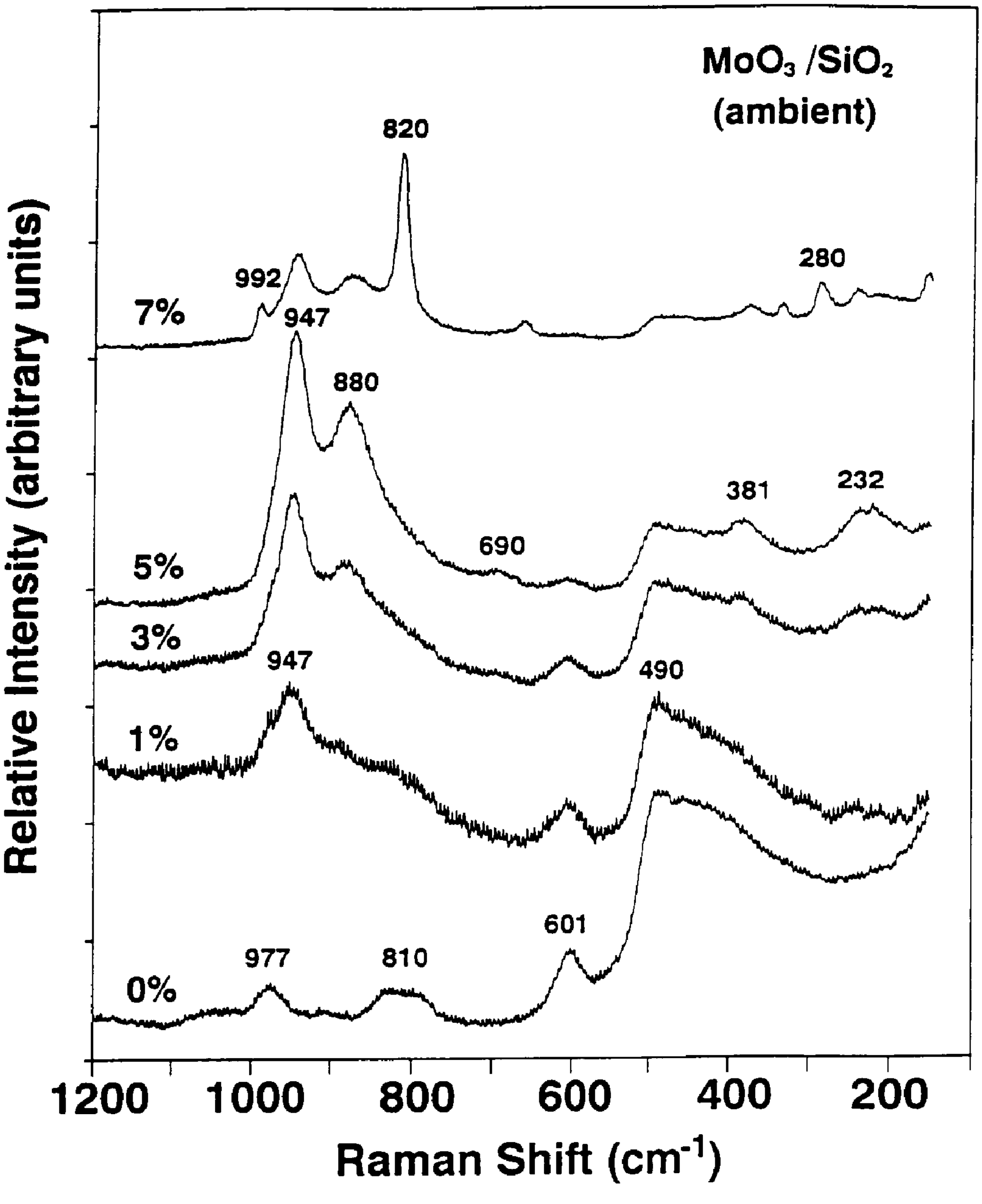

Fig. 2.2. The Raman spectra of MoO_3/SiO_2 catalysts as a function of MoO_3 loading. Spectra obtained under ambient conditions.

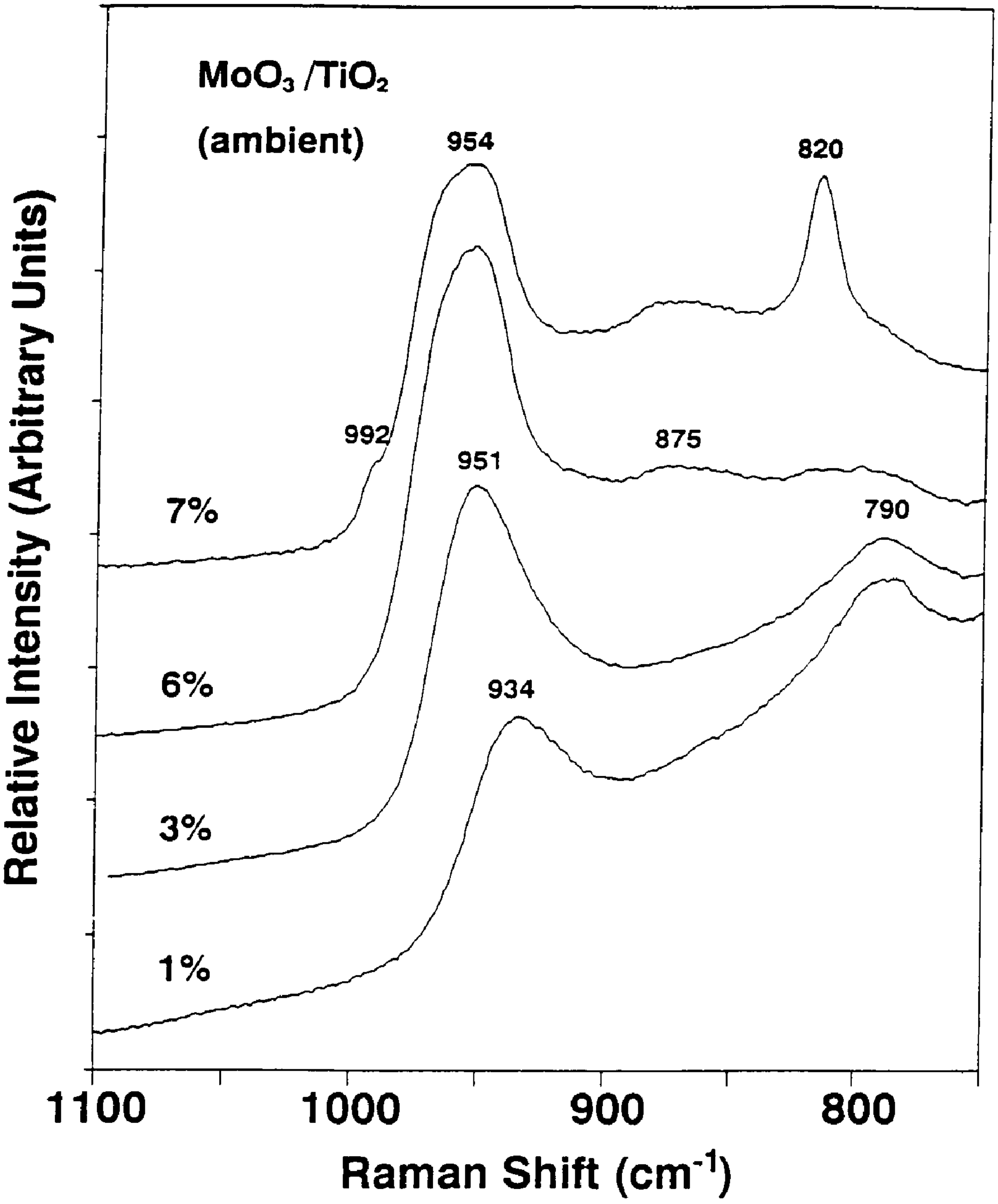

Fig. 2.3. The Raman spectra of MoO_3/TiO_2 catalysts as a function of MoO_3 loading. Spectra obtained under ambient conditions.

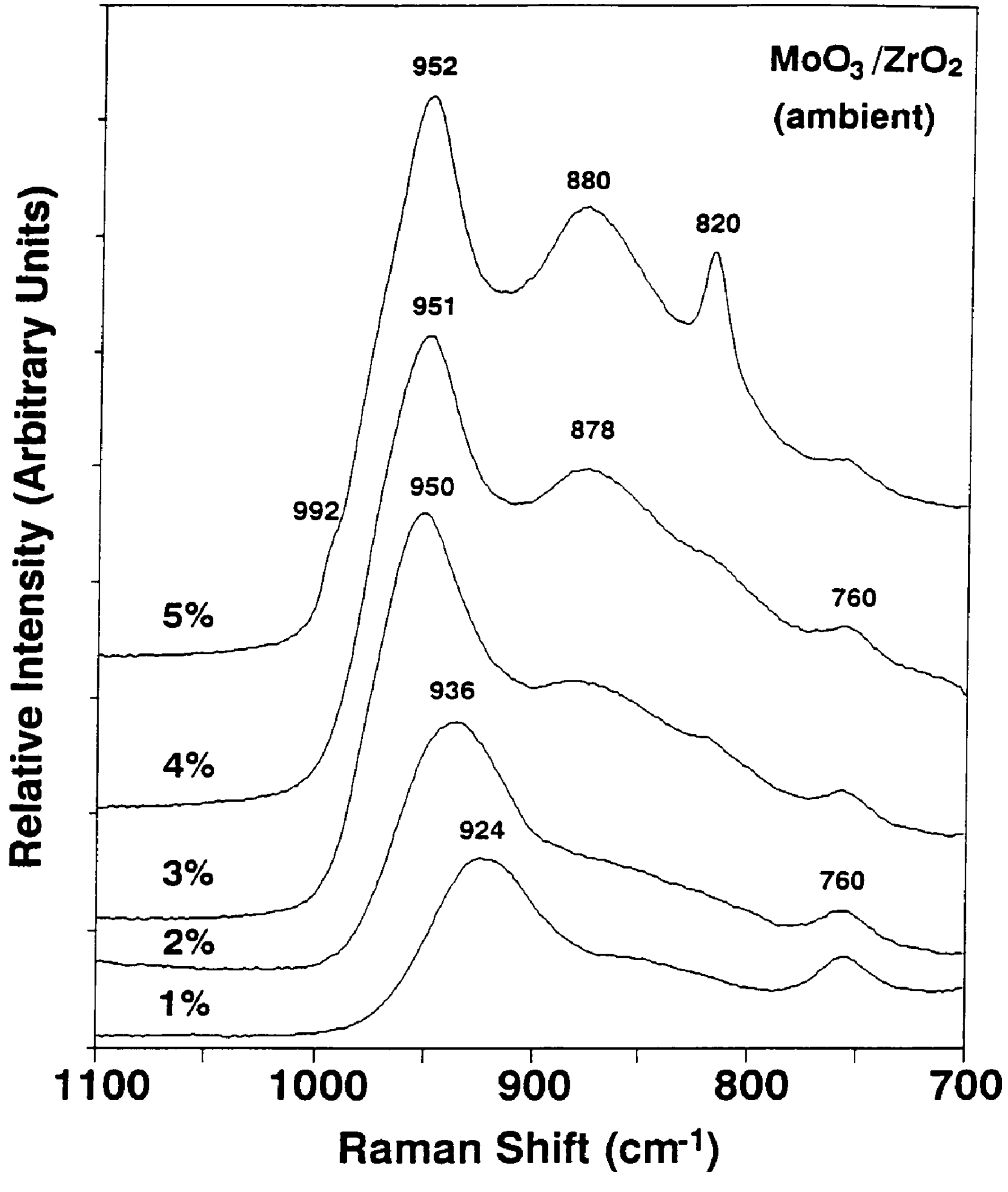

Fig. 2.4. The Raman spectra of MoO_3/ZrO_2 catalysts as a function of MoO_3 loading. Spectra obtained under ambient conditions.

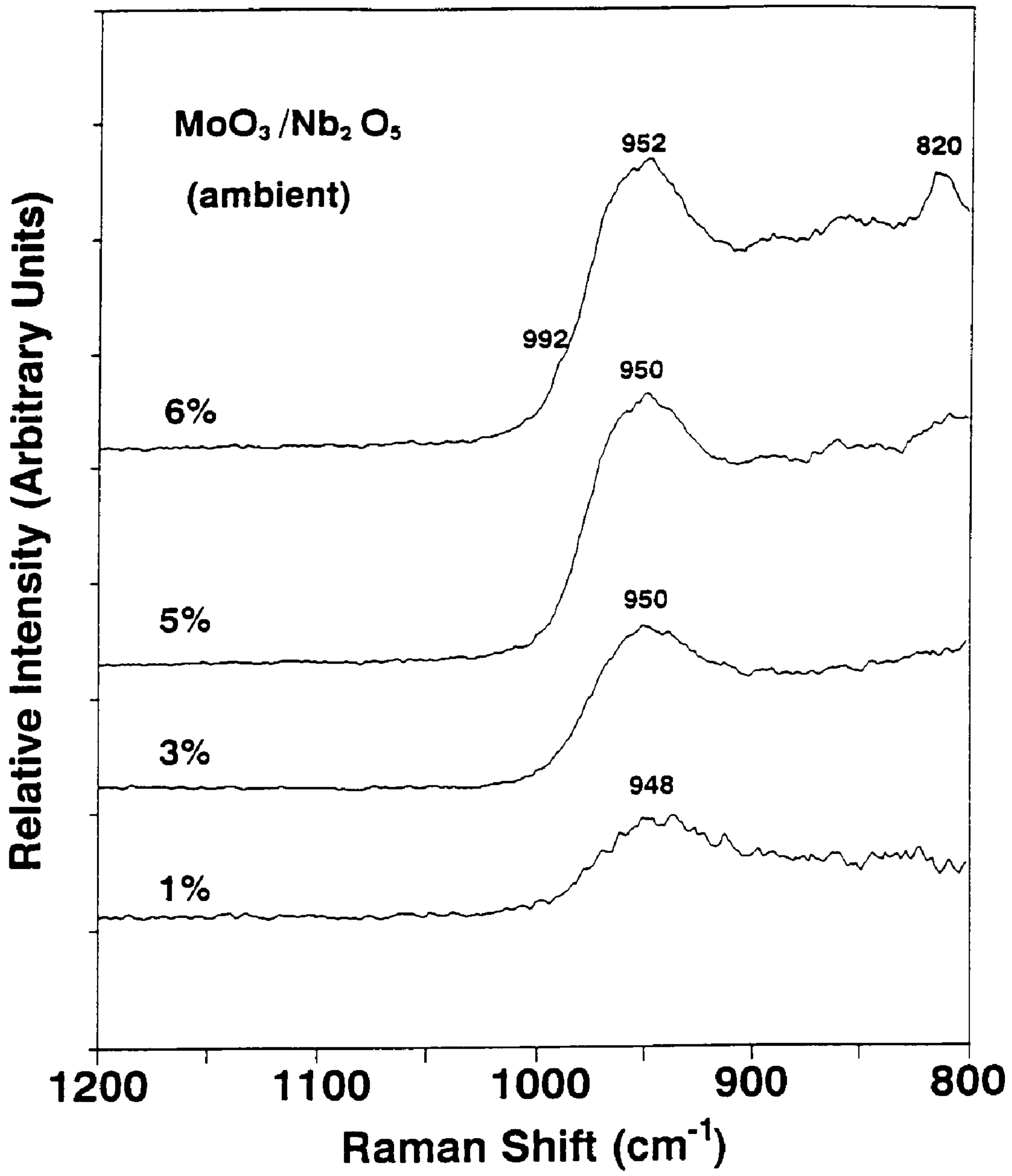

Fig. 2.5. The Raman spectra of MoO_3/Nb_2O_5 catalysts as a function of MoO_3 loading. Spectra obtained under ambient conditions.

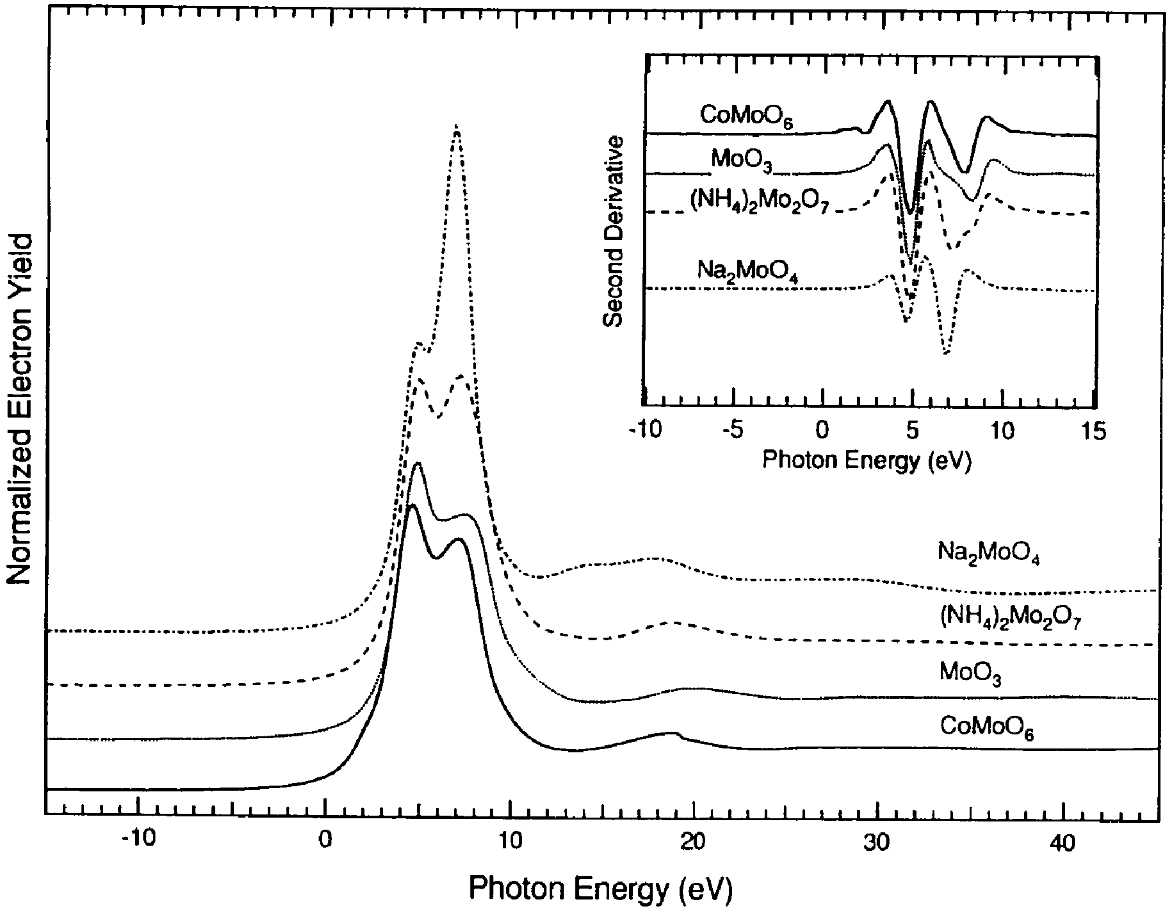

Fig. 2.6. Fluorescence yield Mo L_3-edge XANES of a series of Mo (VI) reference compounds. The spectra have been normalized as described in the text. The inset shows the second derivative of the spectra. In both cases the vertical scale is offset for clarity.

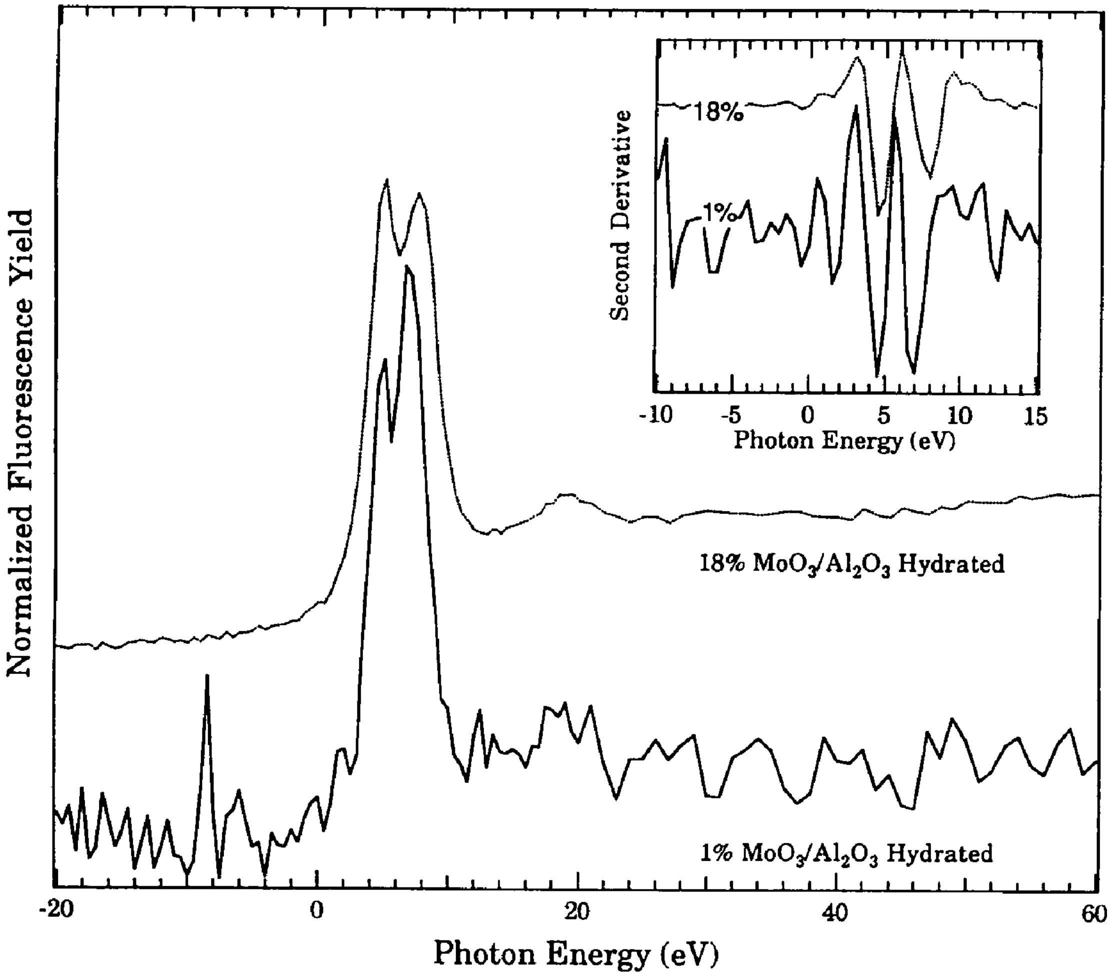

Fig. 2.7. Fluorescence yield Mo L_3-edge XANES of ambient 1% (solid line) and 18% (dotted line) MoO_3/Al_2O_3 catalysts at room temperature. The spectrum of the 1% MoO_3/Al_2O_3 sample has been normalized to the height of the white line of the 18% sample due to problems with background subtraction for the low loading sample. The inset shows the second derivative of the spectra. In both cases the vertical scale is offset for clarity.

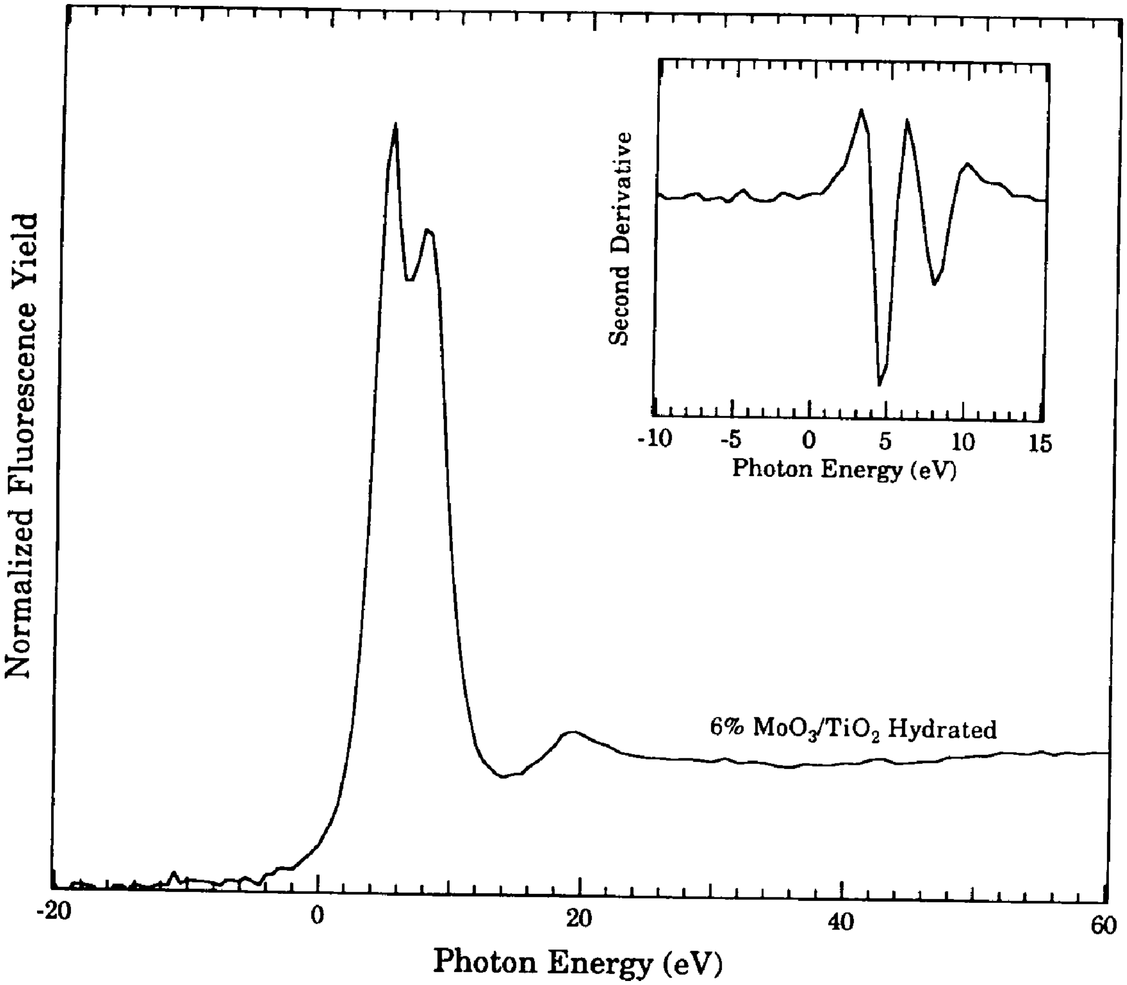

Fig. 2.8. Fluorescence yield Mo L_3-edge XANES of an ambient 6% MoO_3/TiO_2 catalyst at room temperature. The inset shows the second derivative of the spectrum.

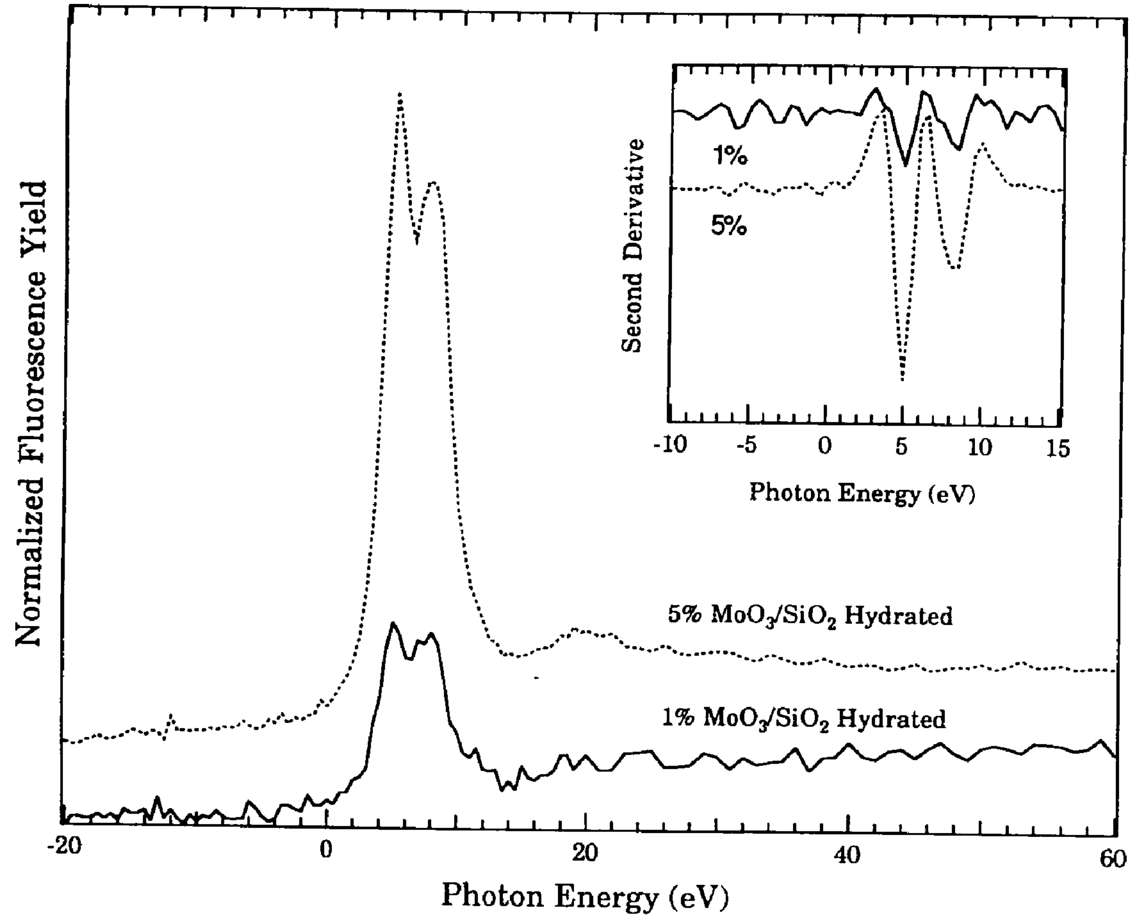

Fig. 2.9. Fluorescence yield Mo L_3-edge XANES of ambient 1% (solid line) and 5% (dotted line) MoO_3/SiO_2 catalysts at room temperature. The white line intensity of the 1% sample is reduced due to problems with background subtraction for the low loading sample. The inset shows the second derivative of the spectra. In both cases the vertical scale is offset for clarity.

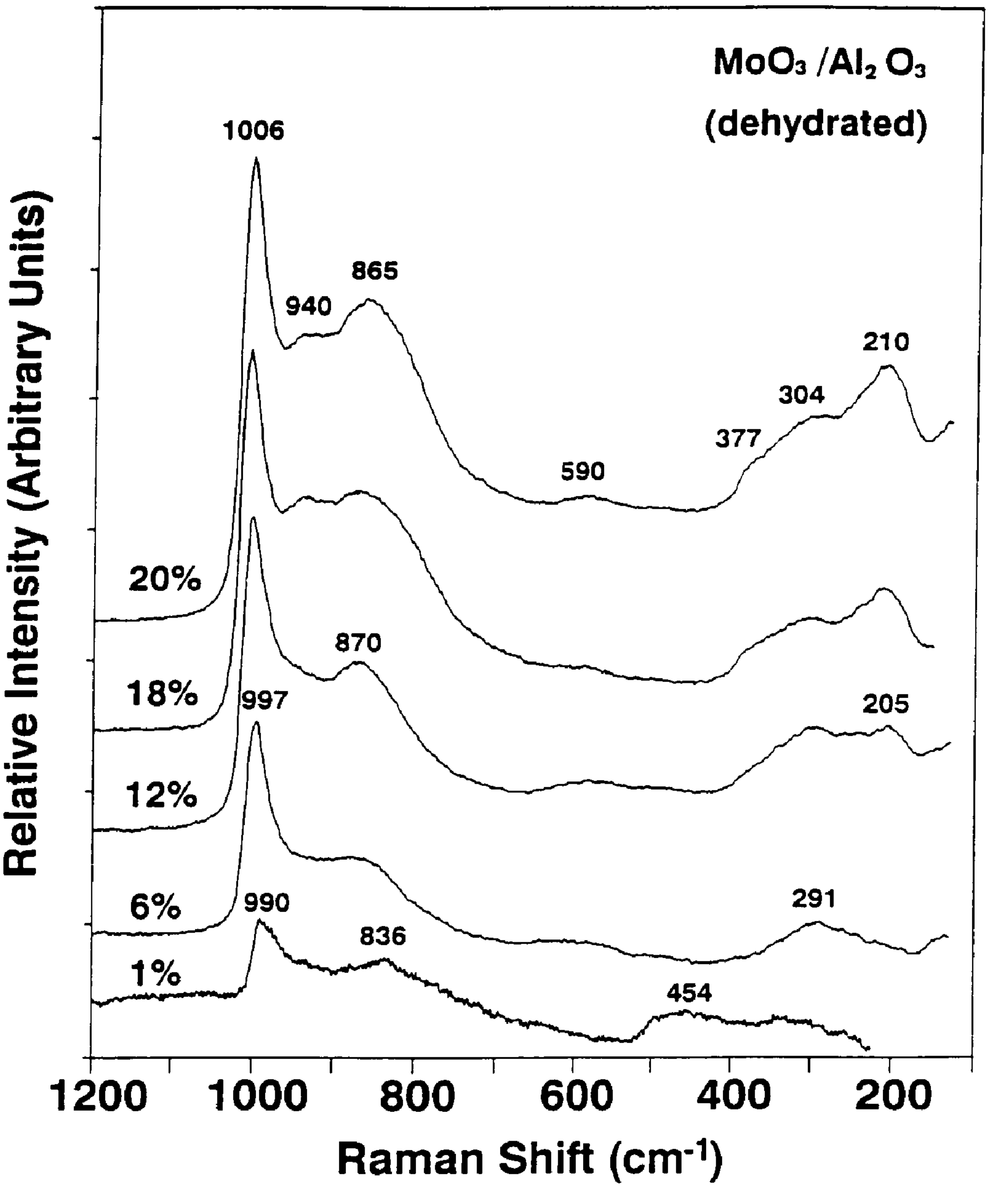

Fig. 2.10. The Raman spectra of MoO_3/Al_2O_3 catalysts as a function of MoO_3 loading. Spectra obtained under dehydrated conditions.

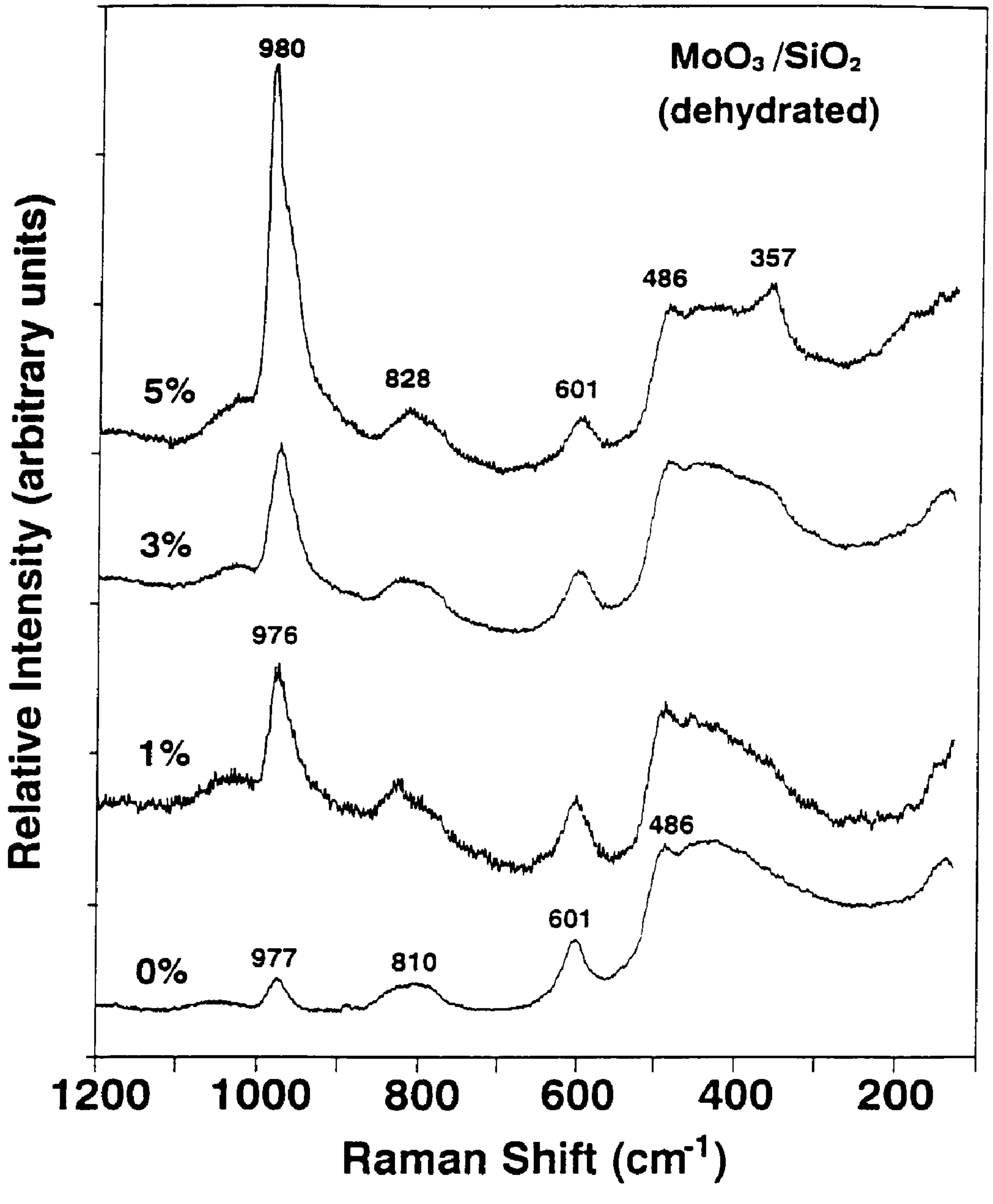

Fig. 2.11. The Raman spectra of MoO_3/SiO_2 catalysts as a function of MoO_3 loading. Spectra obtained under dehydrated conditions.

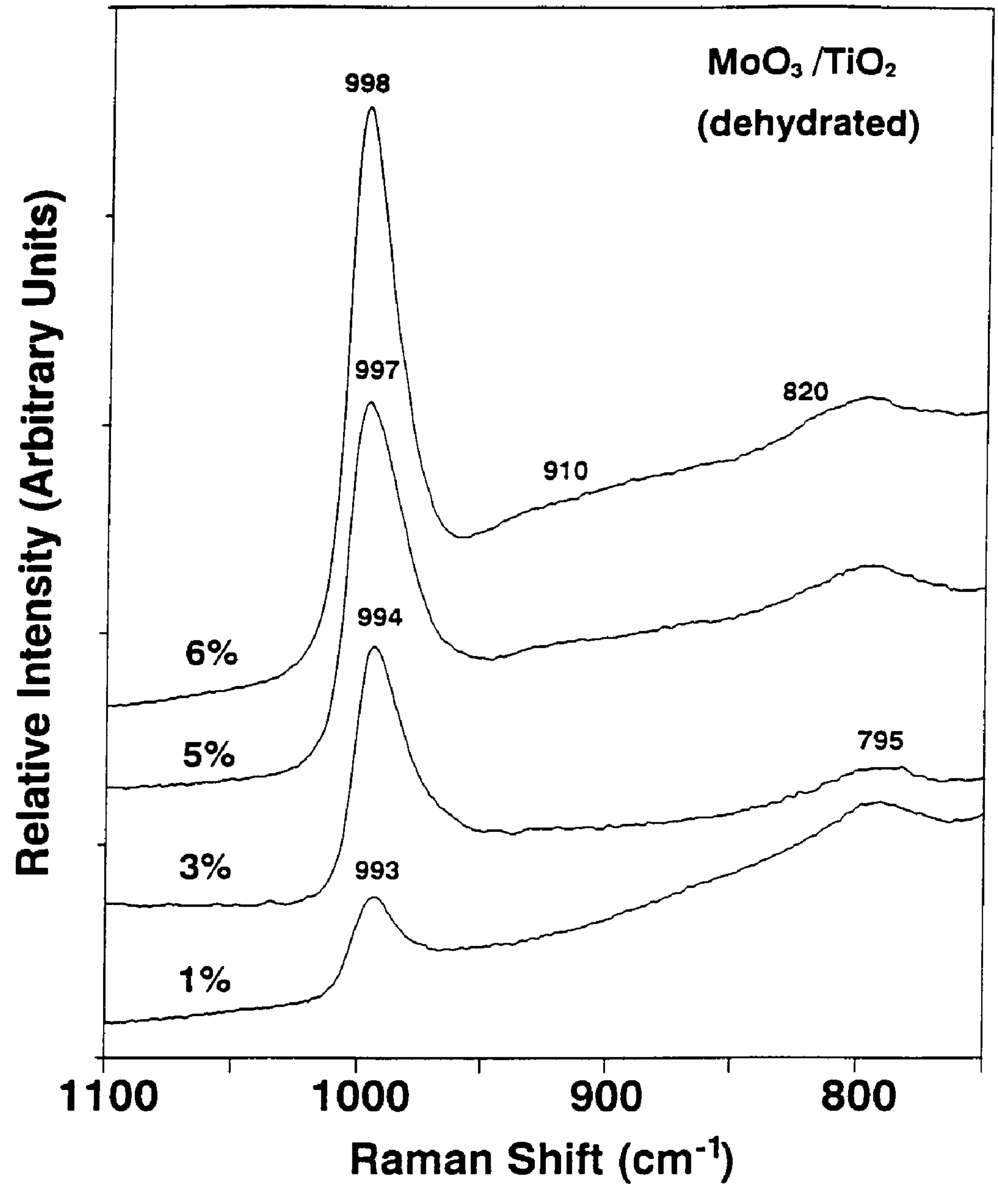

Fig. 2.12. The Raman spectra of MoO_3/TiO_2 catalysts as a function of MoO_3 loading. Spectra obtained under dehydrated conditions.

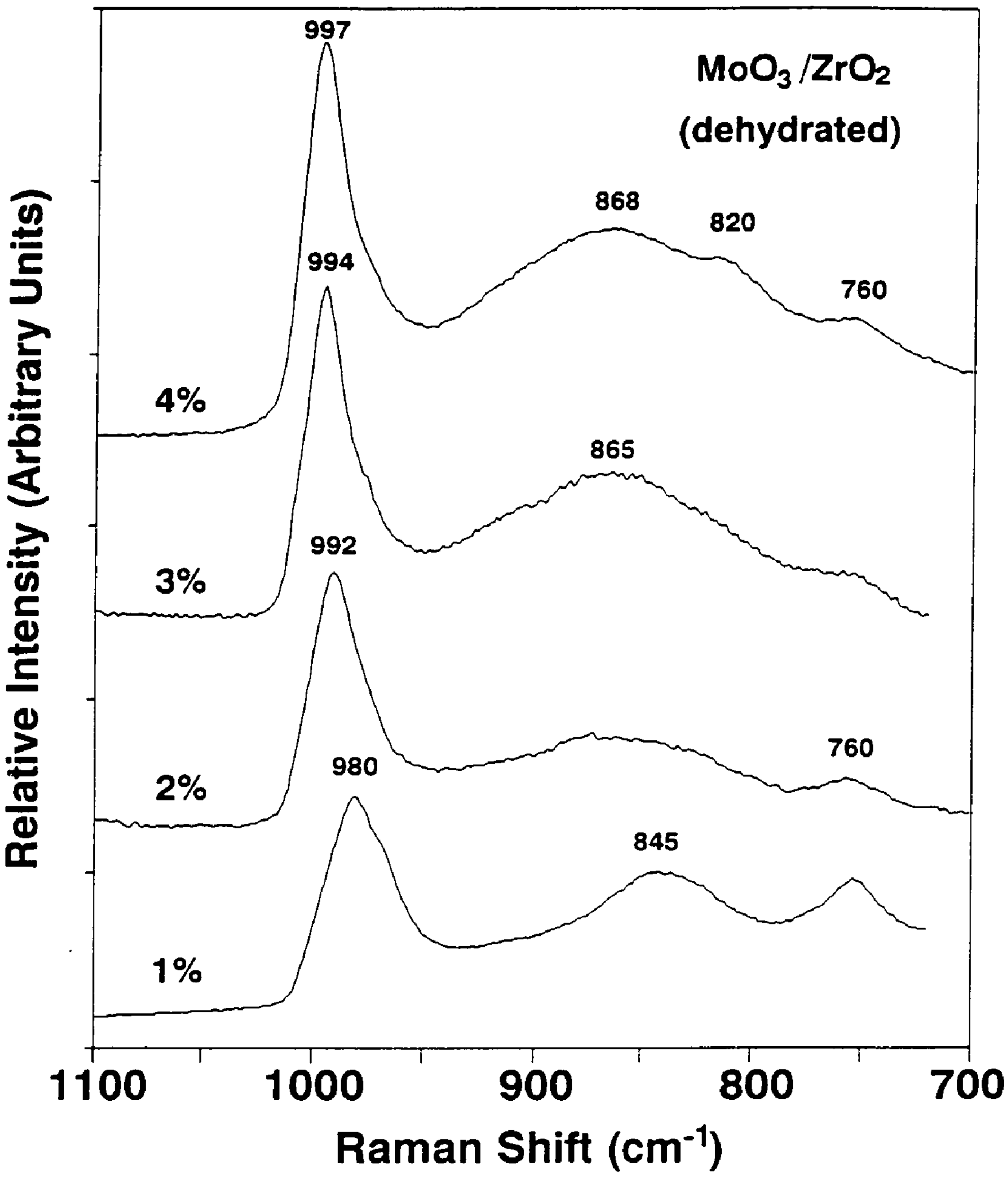

Fig. 2.13. The Raman spectra of MoO_3/ZrO_2 catalysts as a function of MoO_3 loading. Spectra obtained under dehydrated conditions.

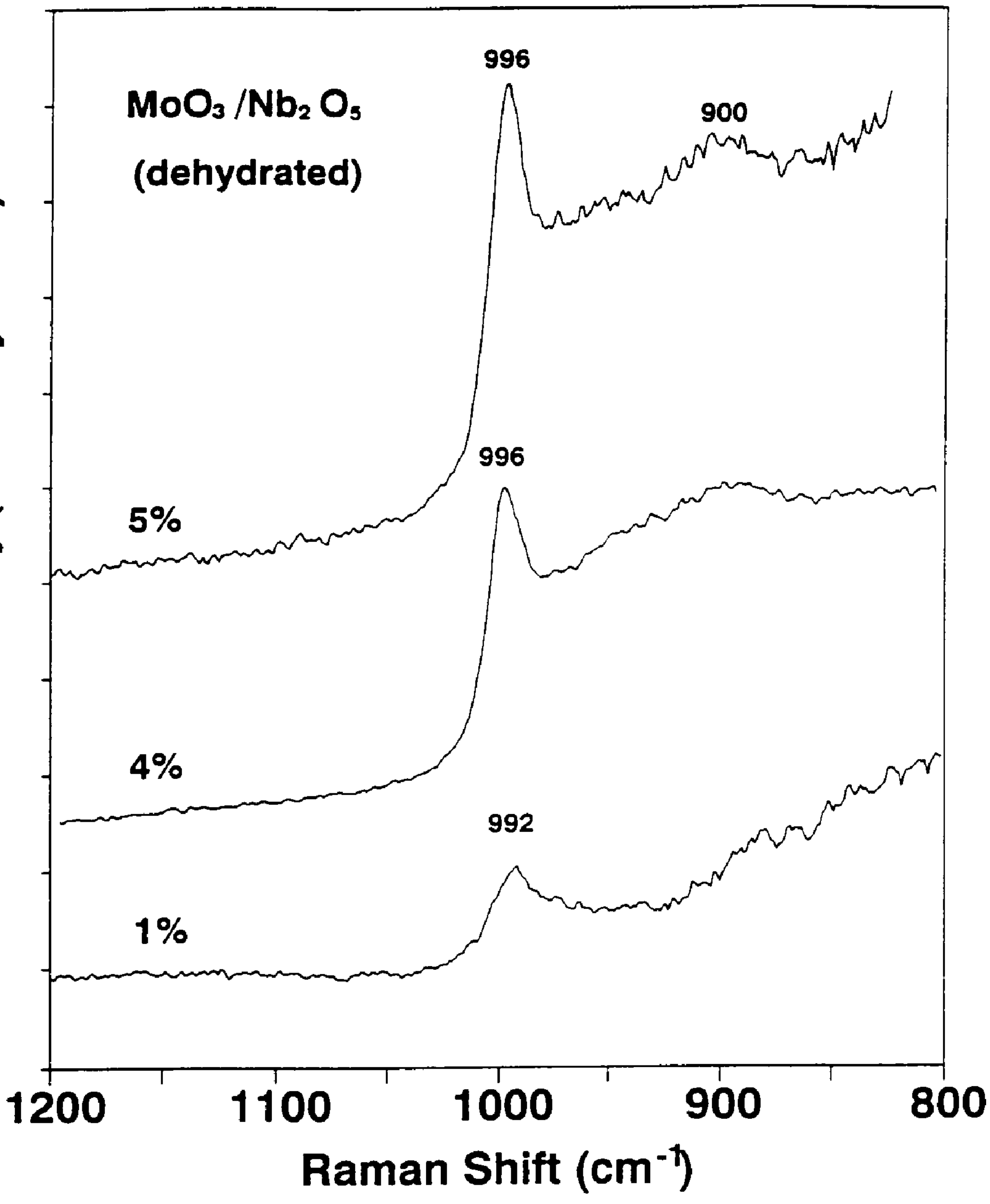

Fig. 2.14. The Raman spectra of MoO_3/Nb_2O_5 catalysts as a function of MoO_3 loading. Spectra obtained under dehydrated conditions.

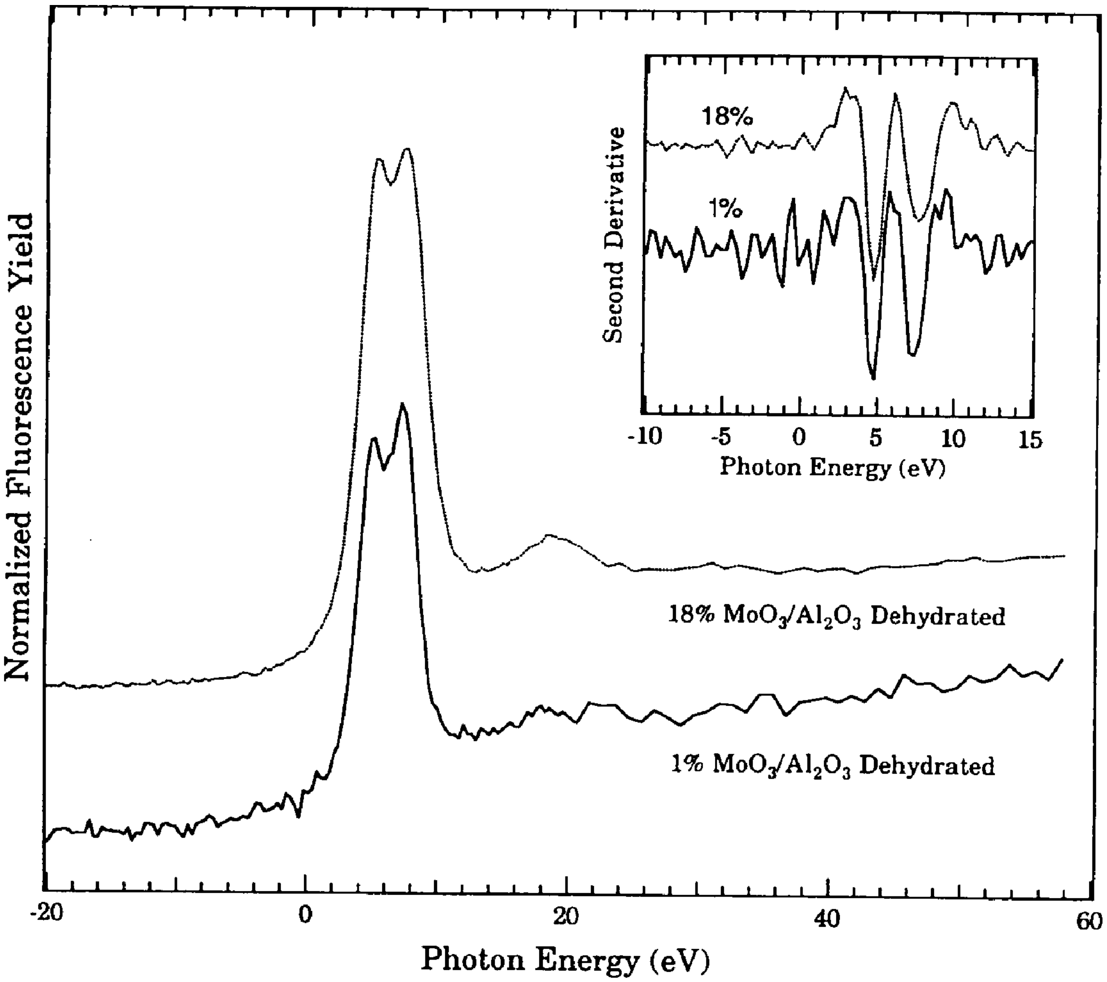

Fig. 2.15. Fluorescence yield Mo L_3-edge XANES of dehydrated 1% (solid line) and 18% (dotted line) MoO_3/Al_2O_3 catalysts at 723 K. The inset shows the second derivative of the spectra. In both cases the vertical scale is offset for clarity.

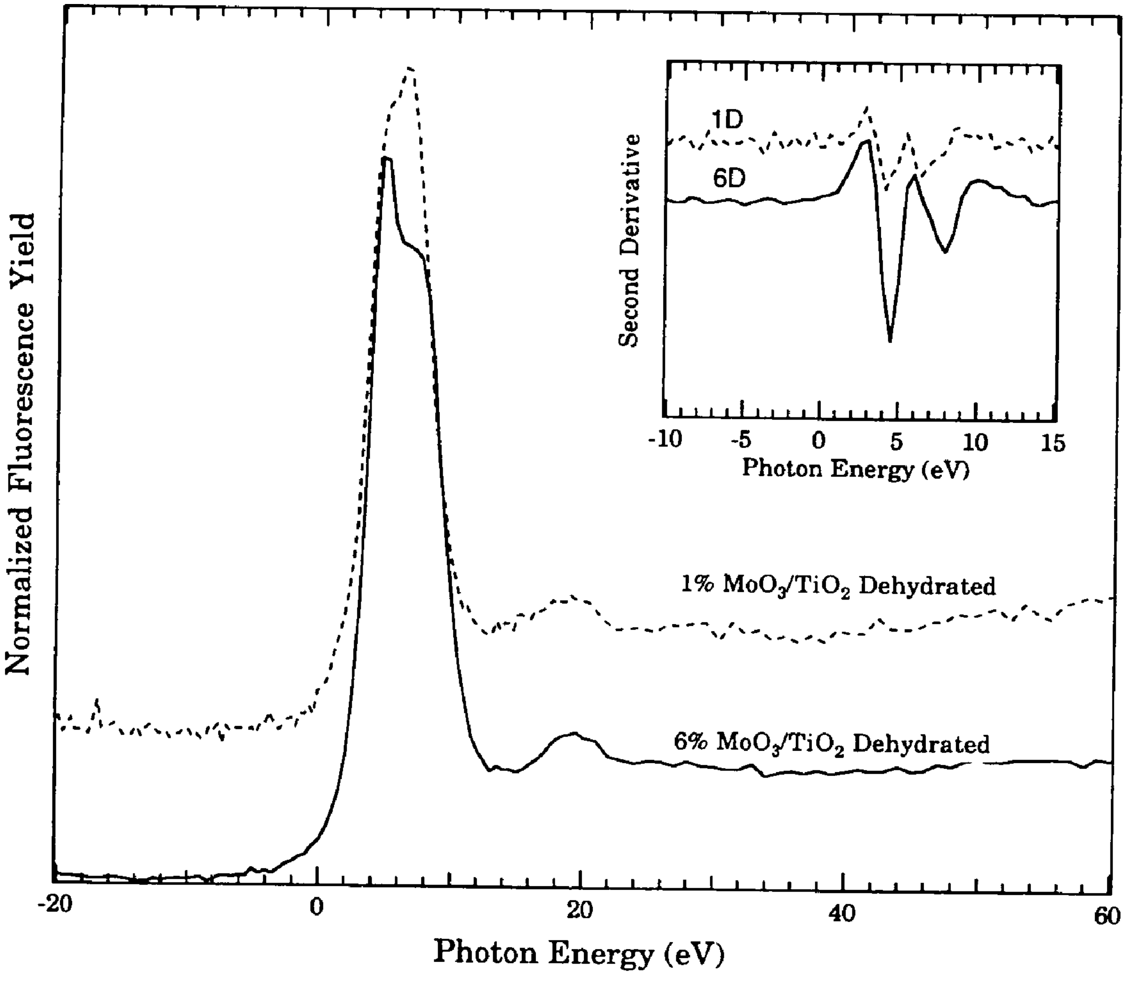

Fig. 2.16. Fluorescence yield Mo L_3-edge XANES of dehydrated 1% (solid line) and 6% (dotted line) MoO_3/TiO_2 catalysts at 723 K. The inset shows the second derivative of the spectra.

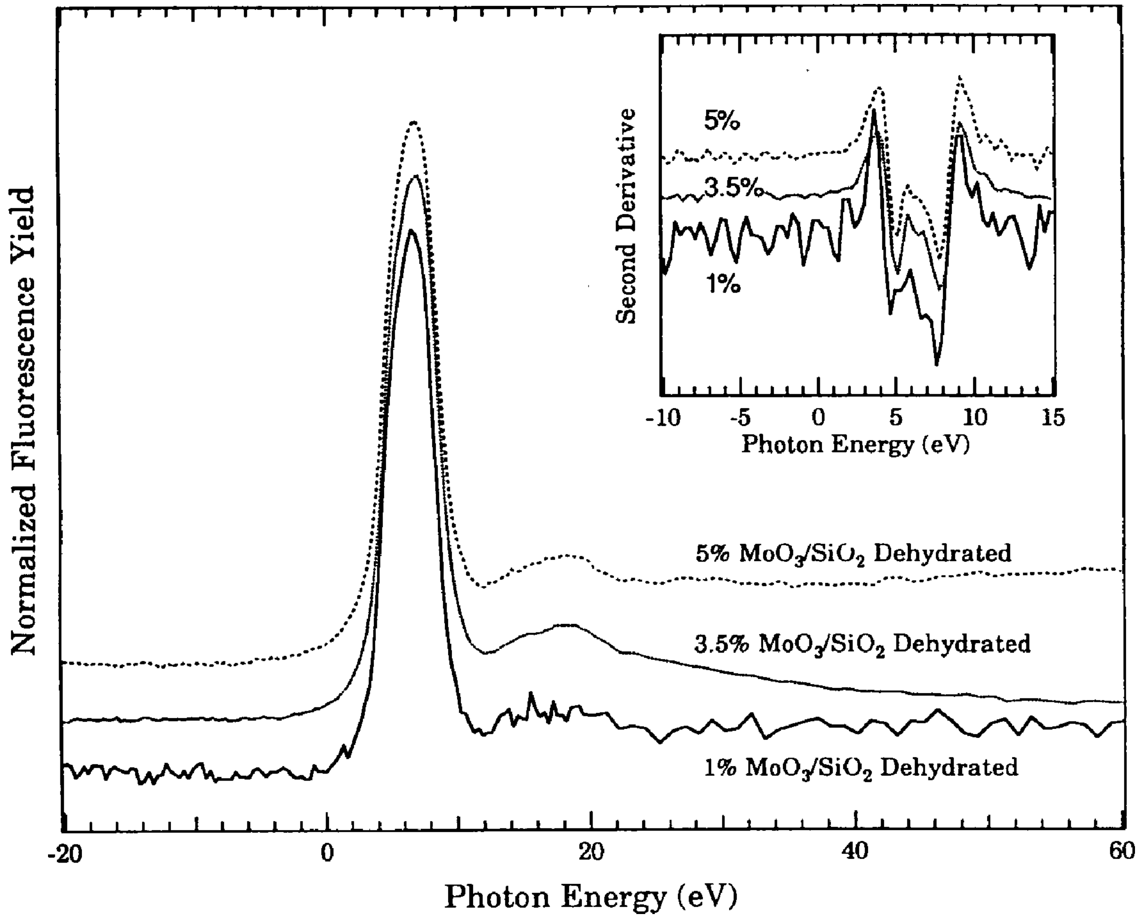

Fig. 2.17. Fluorescence yield Mo L_3-edge XANES of dehydrated 1% (solid line), 3.5% (dotted line), and 5% (dashed line) MoO_3/SiO_2 catalysts at 723 K. The spectra have all been normalized to the same intensity white line. The inset shows the second derivative of the spectra. In both cases the vertical scale is offset for clarity.

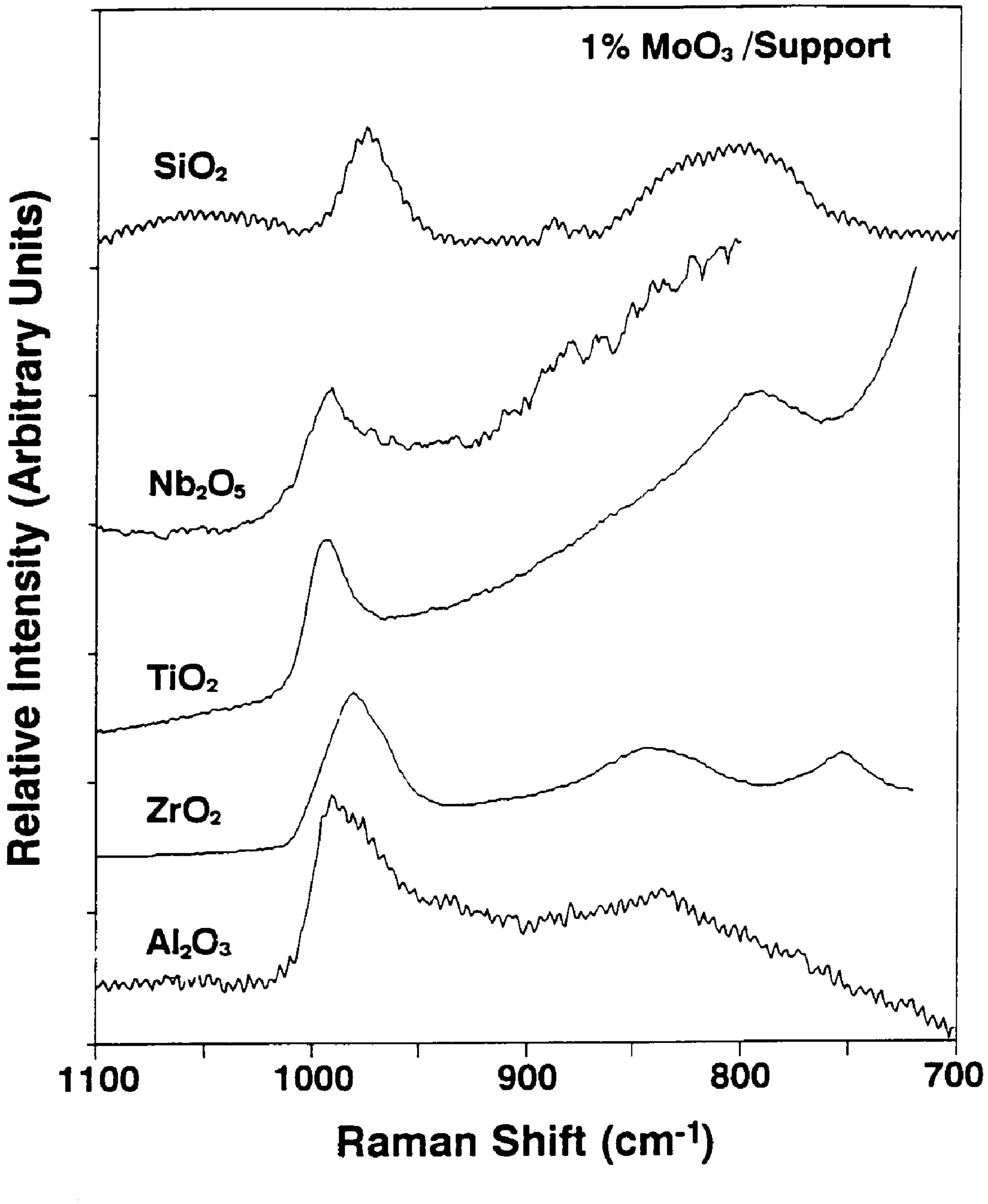

Fig. 2.18. Raman spectra of 1% MoO_3 catalysts on different oxide supports under dehydrated conditions.

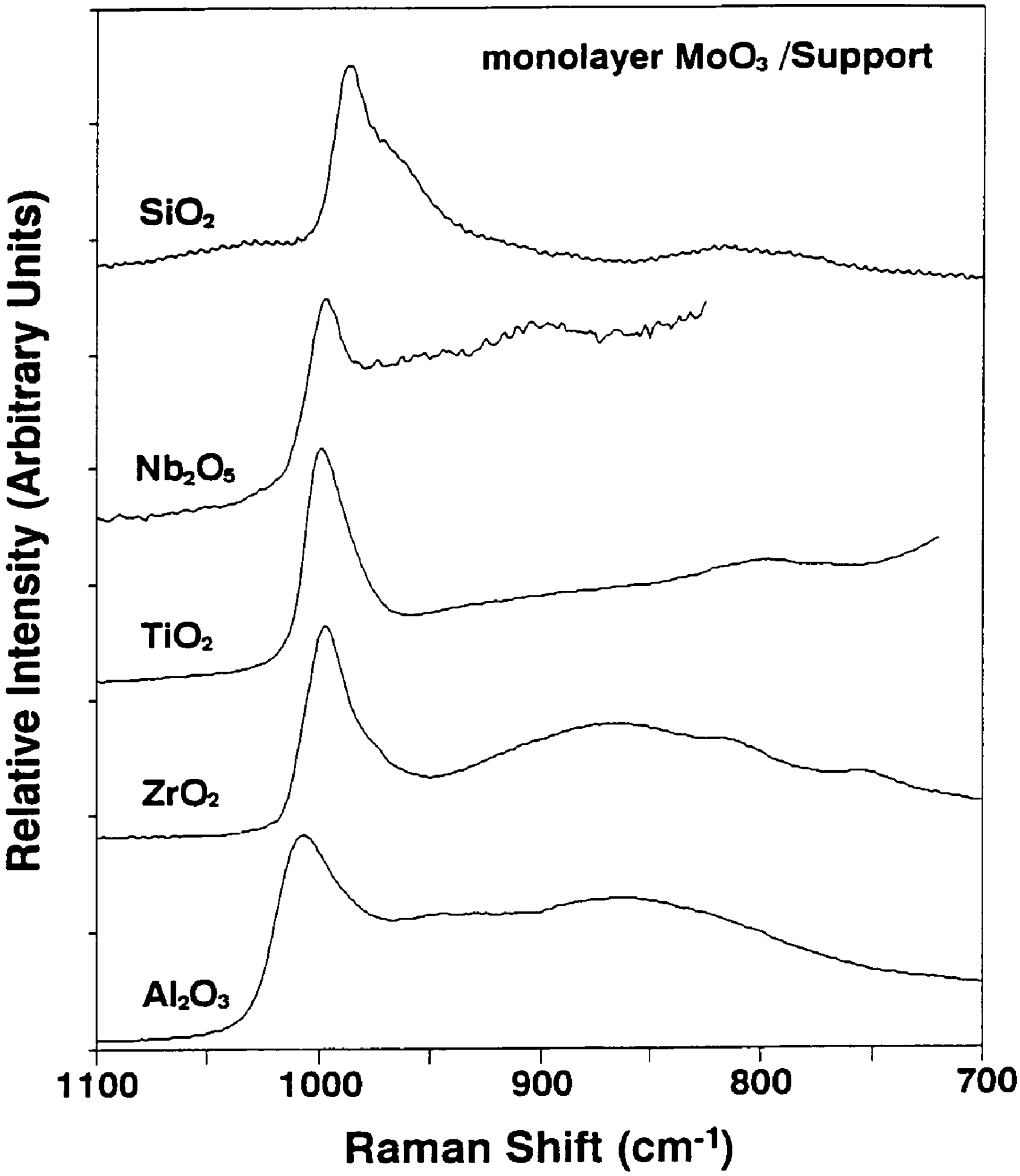

Fig. 2.19. Raman spectra of monolayer MoO_3 catalysts on different oxide supports under dehydrated conditions.

CHAPTER 3

CATALYTIC PROPERTIES OF SUPPORTED MOLYBDENUM OXIDE CATALYSTS: *IN SITU* RAMAN AND METHANOL OXIDATION STUDIES

3.1. SUMMARY

The oxidation of methanol was studied over supported molybdenum oxide catalysts as a function of the specific oxide support (TiO_2, ZrO_2, Nb_2O_5, and Al_2O_3) and molybdenum oxide loading (surface coverage). The surface molybdenum oxide species were selective for the production of formaldehyde and the oxide support sites yielded dimethylether (alumina and niobia), methylformate (zirconia) or were relatively inactive (titania). The turnover frequency (TOF) for the selective oxidation of methanol to formaldehyde varied by a factor of 2-4 with surface molybdenum oxide coverage and a factor of approximately 10 with the specific oxide support at monolayer coverage. The molecular structures of the surface molybdenum oxide species (isolated, tetrahedral at low coverages and polymerized, octahedral/tetrahedral at high coverages) did not affect the reaction selectivity, but did appear to influence the slight increase in TOF with surface coverage. The order of magnitude variation in TOF with the specific oxide support correlated with the reducibility of the support and suggests that the Mo-O-support bond is critical in controlling the TOF. *In situ* Raman studies during methanol oxidation revealed that the supported molybdenum oxide species were 100% dispersed up to monolayer coverage. The percent reduction of the surface molybdenum oxide species during methanol oxidation was not a strong function of surface coverage and the specific oxide support. This suggests that the order of magnitude variation in the TOF with the specific oxide support is primarily related to the activity per site of the surface molybdenum oxide species rather than variation in the number of participating sites.

3.2. INTRODUCTION

Following the previous study [1] on the molecular structure of the surface molybdenum oxide species on different oxide supports, this paper presents the studies of the catalytic properties of the same catalyst systems for the methanol oxidation reaction. Oxidation reactions play an increasingly important role in both the production of materials needed and in the destruction of undesired products by total catalytic oxidation. Supported molybdenum oxide catalysts are among the most useful oxidative catalysts [2]. The evaluation of reactivity of oxidative catalysts can be performed by the methanol oxidation reaction which is a valuable probe for studying the surface metal oxide redox sites [3-7]. During the partial oxidation of methanol, the methanol molecules are initially adsorbed on surface molybdenum sites as a methoxy (CH_3O) species [3-8]. The methoxy species subsequently react in various ways to form formaldehyde (FA, HCHO), methylformate (MF, $HCOOCH_3$), dimethoxymethane (DMM, $CH_2[OCH_3]_2$), dimethylether (DME, CH_3OCH_3), and carbon oxides (COx, CO and CO_2). The nature of the surface active sites determines the product distribution. Generally, surface acid sites produce the dehydration product DME, basic sites form carbon oxides, and redox sites produce FA, MF, and DMM [3,8,9].

Bulk molybdate catalysts have been studied in detail for methanol oxidation reactions by Sleight *et al.* [4-7], Tatibouët *et al.* [8-10], and Chung *et al.* [11,12] The breaking of the C-H bond was found to be the rate limiting step for the methanol oxidation over molybdate catalysts. The oxidative properties of supported molybdenum oxide catalysts have also been studied by many researchers, but most studies focused on the MoO_3/SiO_2 system [13-17]. Molybdenum oxides on TiO_2 and ZrO_2 were found to be the most active catalysts and possess higher selectivity for the oxidative dehydrogenation of methanol to formaldehyde [18-22]. Investigations of the oxidative properties of molybdenum oxides supported on Al_2O_3 and Nb_2O_5 are even rarer due to the high activity of the Al_2O_3 and Nb_2O_5 supports towards methanol dehydration reactions that dominate the catalytic activity of these catalysts [23-25]. The factors that influence the reactivity and selectivity of the supported molybdenum oxide catalysts and the relationships between the catalytic properties and the structure of the surface molybdenum oxide species present in such catalysts have not been extensively investigated.

The previous characterization studies using *in situ* Raman and XANES spectroscopies [1] revealed that the structure of the surface molybdenum oxide species on different oxide supports depends on both the specific oxide support and the surface molybdenum oxide coverage. Under dehydrated conditions, the surface molybdenum oxide species are primarily isolated, tetrahedrally coordinated at low loadings and tend toward polymerized, octahedrally coordinated at high loadings. At monolayer coverages, the structure of the surface molybdenum oxide species primarily possesses an octahedral coordination on TiO_2 but the structure is a mixture of tetrahedral and octahedral coordinations on Al_2O_3. The previous determinations of the structures of the dehydrated surface molybdenum oxide species on different oxide supports are summarized in Table 3.1 along with the corresponding Raman band positions of the terminal $Mo=O$ bond.

In the current study, the same catalyst systems were tested for their catalytic reactivity during methanol oxidation in order to gain information about the structure-reactivity relationships of the supported molybdenum oxide catalysts. In addition, *in situ* Raman spectra during methanol oxidation reaction were obtained to learn more about the nature of the surface molybdenum oxide species under reaction conditions.

3.3. EXPERIMENTAL SECTION

3.3.1. Catalyst preparation

The supported molybdenum oxide catalysts were prepared by the incipient-wetness impregnation method with aqueous solutions of ammonium heptamolybdate ($(NH_4)_6Mo_7O_{24} \cdot 4H_2O$) as described in detail in the previous study [1]. After impregnation, the samples were dried overnight under ambient conditions and further dried at 393 K in air overnight. The TiO_2 and ZrO_2 supported catalysts were finally calcined in dry air at 723 K for two hours. The Nb_2O_5, and Al_2O_3 supported catalysts were calcined in dry air at 773 K for two hours. The molybdenum oxide loading of the catalysts is given as the nominal weight percent of the MoO_3 in the samples.

3.3.2. Methanol oxidation

The reactivity of supported molybdenum oxide catalysts was probed by the methanol oxidation reaction. The reactor system consisted of a digital flow rate controller (Brooks, Model), a methanol reservoir, a condenser, a tube furnace

(Lindberg), and an on line gas chromatograph (HP 5840). The He and O_2 gaseous mixture, whose flow rate was adjusted by the mass flow rate controller, flowed through the methanol reservoir to the condenser maintained at 282.7 K. The methanol content in the flowing gas was obtained by calculating the partial pressure of methanol at this temperature. A 6.9/11.0/82.1 ratio of the $CH_3OH/O_2/He$ gaseous mixture was typically supplied to the reactor.

The catalysts were placed in the center of a 6 mm OD Pyrex microreactor of glass tubing supported by glass wool, placed in a vertical furnace, and preactivated under the flow of pure oxygen at 503 K for half an hour. The reaction was then run at the same temperature. The catalyst weight (1 - 50mg) was adjusted to maintain less than 10% methanol conversion in order to avoid complications due to heat and mass transfer limitations. The reaction products were analyzed on line after steady-state was reached (~10 minutes). The gas chromatograph (HP 5840) was modified to operate with two thermal conductivity detectors (TCD) and one flame ionization detector (FID), and programmed to perform automatic data acquisition and analysis. A Porapak R column was used at 408 K for the separation of CO_2, HCHO, $HCOOCH_3$, $CH_2(OCH_3)_2$ and CH_3OCH_3, and a Carbosieve SII column operating at room temperature for the analysis of CO. The catalytic activities were obtained by integrating the peak areas of the products and calculated according to mole products per hour per gram of catalyst used. The selectivities are expressed in mole percent for each product and defined as the ratio between the yield of this product and that of the total methanol reacted. Careful control of the total conversion is important for the study of selectivity since methylformate and dimethoxymethane are the secondary products of both formaldehyde and methanol and high conversion of methanol favors higher selectivity of methylformate and dimethoxymethane.

The redox turnover frequency (TOF) was normalized per surface molybdenum site since the Raman measurements demonstrated that the molybdenum oxide in the supported catalysts were 100% exposed on the support surface below monolayer coverage. The TOFs of the catalysts above monolayer coverage were also calculated assuming complete exposure of molybdenum oxide sites in order to make comparisons, but most of the present study focuses on monolayer or submonolayer coverages where 100% exposure is present. The TOFs of the surface molybdenum oxide active sites had to be corrected for the support reactivity since certain products resulted from the supports. The Al_2O_3, TiO_2, and Nb_2O_3 supports were essentially inactive for redox product formation, thus, the TOF of these catalysts was calculated from the amount of redox products (formaldehyde, methylformate, and dimethoxymethane) formed. However, the ZrO_2 support possesses some activity for the production of methylformate and the TOF of the MoO_3/ZrO_2 catalysts had to be corrected for the support reactivity.

3.3.3. *In situ* Raman spectroscopy

The *in situ* Raman spectra of the supported molybdenum oxide catalysts were obtained with a laser Raman apparatus equipped with an flow through sample cell. The 514.5 nm line of an Ar^+ laser (Spectra Physics, Model 171) was used as the excitation source. The laser power at the sample was ~50 mW. The scattered radiation from the sample was directed into a Spex Triplemate spectrometer (model 1877) coupled to a Princeton Applied Research (Model 1463) OMA III optical multichannel photodiode array detector. The detector was cooled thermoelectrically to 238 K to decrease thermal noise. The Raman spectra were recorded using a computer and OMA III software. The spectral resolution and reproducibility were experimentally determined to be better than 4 cm^{-1}. The *in situ* cell was equipped with a spinning sample holder, rotated at a speed of ~2000 rpm, and a quartz reaction cell which allowed the flowing of gases and heating of the samples. A cylindrical furnace was used to heat the sample cell to a controlled temperature which was measured by an internal thermocouple. About 0.2 g of each supported molybdenum oxide catalyst was pressed into a thin wafer of about 1 mm thickness and held onto the sample holder. The spectra were measured after dehydration at 723 - 773 K for 30 min and then cooled to 503 K which was the standard methanol oxidation reaction temperature. Different reaction temperatures were also used when studying the effect of temperature. The MoO_3/Al_2O_3 catalysts had to be calcined at 923 K for 2 h before the Raman measurements in order to eliminate fluorescence from the support. The *in situ* Raman spectra were obtained through the following procedure: the dehydrated Raman spectra before reaction were collected after heating the sample in a gaseous mixture of He/O_2, partial pressure ratio about 11/6, at 773 K (723 K for the TiO_2 and ZrO_2 supported catalysts) for 30 min and then cooled to 503 K. The Raman spectra during methanol oxidation were collected after passing the $CH_3OH/He/O_2$ gaseous mixture for at least 1h. The CH_3OH partial pressure was controlled by maintaining the methanol reservoir at 273 K with a water-ice bath. After the methanol oxidation reaction, the samples were reoxidized by the He/O_2 gas at 503 K for 1h and the Raman spectra were again collected. Raman spectra for some of the samples reoxidized at 773 K were also collected.

During the methanol oxidation reaction, the intensities of Raman signals from the surface molybdenum oxide species decreased due to the reduction of the oxidized surface molybdenum oxide species. The reduction also produced a systematic decrease in the Raman signals of the catalysts due to the darker color of the samples. To correct for the different sample colors, the overall Raman spectra were normalized to the Raman band intensities of the oxide supports which were used as internal intensity standards. The decrease in the normalized terminal Mo=O Raman band intensity of the catalysts during methanol oxidation is assumed to quantitatively represent the percent reduction of the supported molybdenum oxide species. The errors associated with the experimental and calculation procedures should not exceed 50%.

3.4. RESULTS

3.4.1. Catalytic properties of supported molybdenum oxide catalysts for methanol oxidation:

MoO_3/TiO_2: The reactivities and product selectivities of the MoO_3/TiO_2 catalysts as a function of molybdenum oxide loading during methanol oxidation at 503 K are listed in Table 3.2. Previous Raman characterization studies have demonstrated that monolayer coverage of the surface molybdenum oxide species on this TiO_2

corresponds to ~6 - 7% MoO_3/TiO_2 [1,26]. The properties of the pure TiO_2 support and the bulk MoO_3 are included for references. Formaldehyde is the major reaction product formed on the bulk MoO_3 catalyst, and there is some activity toward formation of dimethylether and dimethoxymethane. Trace amounts of COx and methylformate are also found. The turnover frequency (TOF) for bulk MoO_3 is $\sim 2.1 \times 10^{-2}$ s^{-1} based on the exposed surface area of the MoO_3 powder [27]. Bulk TiO_2 exhibits an extremely low activity towards methanol oxidation and produces mainly the dimethylether dehydration product as well as minor amounts of total oxidation products (COx). The specific activity of sample increases by one order of magnitude after only 0.5% molybdenum oxide is dispersed on the surface of the TiO_2 support, and the predominant product becomes formaldehyde (selectivity ~ 77%). The activity of the MoO_3/TiO_2 catalysts further increases ~50 times upon increasing the molybdenum oxide loading from 0.5 to 7% MoO_3 and there is also a slight increase in formaldehyde selectivity. Minor amounts of dimethoxymethane and methylformate are also formed from the surface molybdenum oxide redox sites. The yield of FA + MF + DMM was used to calculate the redox turnover frequency (TOF) of the surface molybdenum oxide sites on TiO_2. The TOF increases about four-fold as the molybdenum oxide loading increases. No further changes in the TOF and selectivity are observed in the vicinity of monolayer coverage (6 - 7% MoO_3/TiO_2). The methanol oxidation TOF of the surface molybdenum oxide species on TiO_2 at high surface coverages is more than one order of magnitude higher, as well as somewhat more selective to formaldehyde, than bulk MoO_3.

MoO_3/ZrO_2: The reactivities and selectivities of the MoO_3/ZrO_2 catalysts as a function of molybdenum oxide loading during methanol oxidation at 503 K are listed in Table 3.3 along with the pure ZrO_2 support for reference. Previous Raman characterization studies have demonstrated that monolayer coverage of the surface molybdenum oxide species on this ZrO_2 corresponds to ~4% MoO_3/ZrO_2 [1]. The ZrO_2 support exhibits some methanol oxidation activity towards methylformate, COx, and trace amounts of dimethylether. With increasing loadings of molybdenum oxide on ZrO_2, the main product formed by the surface molybdenum oxide sites is formaldehyde. A small amount of dimethoxymethane is also observed with the addition of molybdenum oxide to ZrO_2. The selectivity towards methylformate significantly decreases as the molybdenum oxide loading increases which suggests that the ZrO_2 surface is being covered by the surface molybdenum oxide species. The TOFs of the 0.5% and 1% MoO_3/ZrO_2 samples have not been calculated since the reactivity of these samples is close to that of the ZrO_2 support and it is difficult to separate the contribution of the support from the activity of the surface molybdenum oxide species. Furthermore, the ZrO_2 support competes not only with the surface molybdenum oxide species for the methanol reactant, but probably also functions together with surface molybdenum oxide species to form methylformate since isolated Mo species are present for the low loading MoO_3/ZrO_2 catalysts [1]. Thus, the redox TOF for the surface molybdenum oxide sites was calculated from the yield of formaldehyde and dimethoxymethane and did not take into consideration the minor amounts of methylformate produced from the combination of the ZrO_2 support and the surface molybdenum oxide species. At 2% MoO_3/ZrO_2 and higher Mo loadings, the reactivity and selectivity are both dominated by the surface molybdenum oxide species. The TOF varies from 2.4 to 6.1 × 10^{-1} s^{-1} for the 2% to 3% MOO_3/ZrO_2 samples. Above monolayer coverage (~4% MoO_3/ZrO_2), the TOF decreases because of the low exposure and specific activity of crystalline MoO_3 for methanol oxidation compared to the surface Mo species on ZrO_2.

MoO_3/Nb_2O_5: The reactivities and selectivities of the MoO_3/Nb_2O_5 catalysts as a function of molybdenum oxide loading during methanol oxidation at 503 K are listed in Table 3.4 along with the data for the Nb_2O_5 support for reference. Previous Raman characterization studies have demonstrated that monolayer coverage of the surface molybdenum oxide species on this Nb_2O_5 support corresponds to ~ 6% MoO_3/Nb_2O_5 [1]. The acidity of the Nb_2O_5 surface exclusively produces dimethylether. The surface molybdenum oxide species form oxidation products of formaldehyde and small amounts of methylformate and dimethoxymethane. The formaldehyde selectivity increases gradually and the dimethylether selectivity decreases as the molybdenum oxide loading increases. The yields of FA + MF + DMM were used to calculate the redox TOF of the surface molybdenum oxide species on Nb_2O_5. The TOFs of the 0.5% and 1% MoO_3/Nb_2O_5 samples were not calculated since the activity of the Nb_2O_5 support is comparable to these catalysts, and the Nb_2O_5 is competing with the surface molybdenum oxide species for the methanol reactant. At 2% MoO_3/Nb_2O_5 and higher Mo loadings, the activity of the surface molybdenum oxide species becomes more pronounced and dominates the reactivity for the higher Mo loading catalysts. The TOF varies within 0.9 - 1.9 × 10^{-1} s^{-1}, as the molybdenum oxide loading increases from 2 to 6% of surface molybdenum oxide species. No further increase in activity is observed for the sample containing more than monolayer coverage of surface molybdenum oxide species (7% MoO_3/Nb_2O_5) and the apparent TOF decreases slightly due to the presence of crystalline MoO_3 particles.

MoO_3/Al_2O_3: The reactivities and selectivities of the MoO_3/Al_2O_3 catalysts as a function of molybdenum oxide coverage for methanol oxidation at 503 K are listed in Table 3.5 along with the Al_2O_3 support as reference. Previous Raman studies have demonstrated that monolayer coverage of the surface molybdenum oxide species on Al_2O_3 corresponds to ~20% MoO_3/Al_2O_3 [1]. The Lewis acid sites of the Al_2O_3 support possess a very high activity for the dehydration of methanol to dimethylether. The formaldehyde partial oxidation product is only detected at molybdenum oxide loadings of 6% MoO_3 and above, and the selectivity to formaldehyde increases with increasing Mo loading. Only trace amounts of methylformate and dimethoxymethane were detected above 6% MoO_3/Al_2O_3 and COx was not a reaction product. The dimethylether formed from the Al_2O_3 support decreases as molybdenum oxide loading increases which indicates that the surface of the Al_2O_3 support has been covered by the deposition of surface molybdenum oxide species. As molybdenum oxide loading increases, the total activity remains essentially the same which suggests that the dehydration of methanol on the Al_2O_3 surface is faster than the partial oxidation of methanol over the surface molybdenum oxide sites. No TOF was calculated for the 6% and 12% MoO_3/Al_2O_3 samples since too much of the Al_2O_3 surface is exposed and the activity of Al_2O_3 dominates the reactivity of these catalysts. The Al_2O_3 acidity is very competitive with the surface molybdenum oxide sites and only ~21% selectivity towards formaldehyde formation was obtained at monolayer coverage (20% MoO_2/Al_2O_3). The amount of FA + MF + DMM produced were taken to represent the redox TOF of the surface molybdenum oxide sites of high loading catalysts, and a TOF of $\sim 1.1 \times 10^{-1}$ s^{-1} was obtained at monolayer coverage.

3.4.2. *In situ* Raman spectra of supported molybdenum oxide catalysts during methanol oxidation:

The Raman spectra of the dehydrated surface molybdenum oxide species possess bands in the 980 - 1006 cm^{-1} region corresponding to the terminal Mo=O stretching mode. The high loading catalysts possess additional Raman bands in the ~860 - 910 cm^{-1} region which were assigned to the stretching mode of the Mo-O-Mo bridging bond [1]. The Raman band at ~1000 cm^{-1} of the Mo=O terminal stretching mode is usually sharp and relatively strong, and the ~900 cm^{-1} Raman band of the Mo-O-Mo bond is usually very broad. The surface molybdenum oxide species become partially reduced during methanol oxidation which is reflected in a decrease in the normalized intensity of the Mo=O Raman band. It was assumed that the reduction of the catalysts is quantitatively reflected by the decrease in the normalized Raman intensity of the terminal Mo=O bond. Furthermore, Raman is more sensitive to the Mo=O double bonds than the Mo-O-Mo bridging bonds and the changes in the Raman intensity of the broad bridging bond were not substantial and may also be complicated by the overlap of the Raman band of the reduced surface molybdenum oxide species (for example, see the Raman spectra below of the MoO_3/Al_2O_3 catalyst during methanol oxidations). The vibrational modes of the bridging Mo-O-support bond are not Raman active due to the slight ionic character of these bonds. Therefore, the decrease in the terminal Mo=O Raman band intensity of the catalysts during methanol oxidation is used to represent the percent reduction of the supported molybdenum oxide catalysts, or the percent of surface molybdenum oxide species participating in the reaction.

MoO_3/TiO_2: The *in situ* Raman spectra of the 1 and 6% MoO_3/TiO_2 catalysts are presented in Figs. 3.1 and 3.2, respectively. The Raman spectra before, during, and after methanol oxidation were all normalized according to the synchronous Raman intensity changes of the crystalline TiO_2 support bands at 640, 520, and 399 cm^{-1}. During methanol oxidation, the Raman band of the terminal Mo=O stretching mode of the surface molybdenum oxide species of the 1% MoO_3/TiO_2 catalyst at 992 cm^{-1} decreases in intensity and shifts to 964 cm^{-1}, and that of the 6% MoO_3/TiO_2 catalyst also decreases in intensity and shifts from 997 to ~985 cm^{-1}. There is also a slight broadening for this Raman band during methanol oxidation. The decrease in the Raman signal of the terminal Mo=O bond reflects a certain extent of reduction of the surface molybdenum oxide species, and the broadening and shifts to lower frequency are probably partially due to the presence of methoxy species during methanol oxidation [28,29] (see discussion). The frequency shift of the terminal Mo=O Raman band for the low loading catalyst is more pronounced than that of the high loading catalyst. After the methanol flow is terminated and the samples are oxidized for 1h with a He/O_2 gas at the reaction temperature (503 K), the catalysts are only partially reoxidized (~10% differences to their initial states, compare Figs. 3.1a to 3.1c, and 3.2a to 3.2c). The catalysts are fully reoxidized to the original state after an oxidation treatment at 773 K (compare Figs.

3.2a and 3.2d), which suggests the reduction is the main cause of the Raman intensity decrease rather than reconstruction. The decrease in the Raman intensity of the terminal Mo=O bond of the surface molybdenum oxide species is ~23% under the methanol oxidation conditions. Unfortunately, no reduced surface molybdenum oxide species were identified in the Raman spectra.

The temperature dependence of the structure of the surface molybdenum oxide species during methanol oxidation was also studied by *in situ* Raman spectroscopy. Fig. 3.3 shows the Raman spectra of the 6% MoO_3/TiO_2 catalyst in the oxidized state and during methanol oxidation at 503 K, 573 K, and 633 K. Increasing the temperature during methanol oxidation results in sharper Raman bands and a decrease in the shift of the Raman band when comparing the spectra before and during reaction. These changes reflect less methoxy adsorption on the catalyst surface with increasing reaction temperature [28]. However, the decreases in the intensities of the Raman bands associated with the terminal Mo=O bonds at all temperatures are ~25% of the fully oxidized surface Mo species and do not show a strong dependence upon reaction temperature over the range investigated (503 - 633K).

MoO_3/ZrO_2: The *in situ* Raman spectra of the 1 and 4% MoO_3/ZrO_2 catalysts are presented in Figs. 3.4 and 3.5, respectively. The spectra were normalized according to the Raman intensity changes of the crystalline ZrO_2 support bands at 554, 532, and 497 cm^{-1}. During methanol oxidation at 503 K, the Raman band of the terminal Mo=O stretching mode of the 1% MoO_3/ZrO_2 catalyst decreases in intensity and shifts from 978 to ~957 cm^{-1}, and that of the 4% MoO_3/ZrO_2 catalyst also decreases in intensity and shifts from 995 to ~983 cm^{-1}. A substantial broadening of the terminal Mo=O Raman band is also observed for both MoO_3/ZrO_2 catalysts. Similar to the MoO_3/TiO_2 catalysts, the shift of the terminal Mo=O Raman band of the low loading sample upon methanol oxidation is larger than that of the high loading sample. The Mo=O Raman bands of the samples during methanol oxidation decrease ~33 and 43% compared to the fully oxidized surface molybdenum oxide species for the 1 and 4% MoO_3/ZrO_2 catalysts, respectively. After reoxidation with He/O_2 at 503 K, the reduced surface molybdenum oxide species partially recover their initial Raman intensities (~70%) and shift back towards their initial positions. No Raman bands due to the reduced Mo species are observed. The influence of temperature on the Raman spectrum during methanol oxidation was also studied for the 3% MoO_3/ZrO_2 sample and is shown in Fig. 3.6. The temperature dependence of the Raman spectra for the 3% MoO_3/ZrO_2 catalyst is similar to that of the MoO_3/TiO_2 catalyst (Fig. 3.3). Increasing the methanol oxidation reaction temperature sharpened the Raman bands and decreased the shift of the band. However, the changes in the surface area of the Mo=O Raman bands during methanol oxidations do not strongly depend on reaction temperature. The decreases of the Mo=O Raman band upon changing temperature are ~38% of their initial Raman intensities.

MoO_3/Nb_2O_5: The *in situ* Raman spectra of the 1% and 5% MoO_3/Nb_2O_5 catalysts are presented in Figs. 3.7 and 3.8, respectively, and were obtained by subtracting the background spectrum of the Nb_2O_5 support in order to enhance the surface molybdenum oxide signals. The normalization was made according to the Nb_2O_5 Raman band at ~220 cm^{-1}. During methanol oxidation a decrease in the intensity of the Raman band of the terminal Mo=O stretch mode occurs and the band shifts from 991 to 967 cm^{-1} for the 1% MoO_3/Nb_2O_5 catalyst and from 998 to 972 cm^{-1} for the 5% MoO_3/Nb_2O_5 catalyst. The decrease in Mo=O Raman intensity of the surface molybdenum oxide species for 5% MoO_3/Nb_2O_5 during methanol oxidation is determined to be ~20% according to the terminal Mo=O Raman band intensity of the fully oxidized Mo species. Reoxidation of the catalysts by He/O_2 at the reaction temperature (503 K) recovers the intensity of the Raman bands of the original surface molybdenum oxide species (~90%), and at 773 K the reoxidation is complete (Fig. 3.8d). Similar to the MoO_3/TiO_2 and MoO_3/ZrO_2 catalyst systems, the shifts to lower frequency during methanol oxidation is more pronounced for the lower loading catalyst.

MoO_3/Al_2O_3: The *in situ* Raman spectra of the 20% MoO_3/Al_2O_3 catalysts are presented in Fig. 3.9. The *in situ* Raman spectra of the lower loaded MoO_3/Al_2O_3 catalysts (1% and 6% sample) were not obtainable due to fluorescence of the samples during the methanol oxidation reaction conditions. The normalization of the *in situ* Raman signal for MoO_3/Al_2O_3 is difficult due to the lack of Raman bands from the Al_2O_3 support. Thus, the Raman spectra in Fig. 3.9 were normalized by adding ~0.5% TiO_2 (anatase, 20 m^2/g) as an internal standard that employs to the TiO_2 Raman band at 636 cm^{-1}. The migration of the surface molybdenum oxide species to the surface of the TiO_2 support can be neglected since the relative surface area of the TiO_2 internal standard is small (relative surface areas of Al_2O_3/TiO_2 ~ 2000/1). Exposure of the 20% MoO_3/Al_2O_3 to the reaction mixture results in the major Raman band at 1004 cm^{-1}, due to the terminal Mo=O stretching mode, to decrease in intensity and slightly shift to 998 cm^{-1}. However, new Raman bands at ~840, ~760, 491, and 274 cm^{-1} simultaneously increase and dominate spectrum during the methanol oxidation. The decrease in the Mo=O Raman intensity of the surface molybdenum oxide species is determined to be ~24% during methanol oxidation. Reoxidation with He/O_2 at the reaction temperature (503 K) recovers only ~70% the oxidative species (compare spectra 3.9c and 3.9a). Reoxidation at 773 K recovers all of the oxidized species (spectrum is not shown). The ~760, 491, and 274 cm^{-1} Raman bands were previously assigned to reduced surface molybdenum oxide species on Al_2O_3, but the ~840 cm^{-1} Raman band was previously assigned to the microcrystalline MoO_3 phase [30]. However, the current Raman spectra, after normalization with the internal TiO_2 standard, reveal that the 840 cm^{-1} band has actually increased in intensity and shifted position compared to the oxidized Mo species and, thus, it should be due to a reduced surface molybdenum oxide species. A similar trend was found for the temperature dependence of the 20% MoO_3/Al_2O_3 catalyst, shown in Fig. 3.10, as that for the MoO_3/TiO_2 and the MoO_3/ZrO_2 catalysts. No strong dependence of the Mo=O Raman intensity upon reaction temperature is found. The 640 cm^{-1} band in Fig. 3.10 is due to the TiO_2 anatase added as an internal standard for normalization of the Raman signals of the surface molybdenum oxide species. A shift of the Raman band at ~840 cm^{-1} to ~826 cm^{-1} is also observed upon increasing the reaction temperature. Note that the Raman spectra in Figs. 3.9 and 3.10 are plotted in different cm^{-1} regions.

3.4.3. Reduction of surface molybdenum oxide species:

The decreases in the normalized and integrated intensities of the terminal Mo=O

Raman bands of the surface molybdenum oxide species during methanol oxidation are compared in Fig. 3.11. The decreases in the Mo=O Raman band intensity of the surface molybdenum (VI) oxide species during methanol oxidation is approximately 20-24% on titania, niobia, and alumina and slightly higher on zirconia, 33-43%. As previously discussed, it is assumed that the decrease in the normalized Mo=O Raman band intensity is proportional to the extent of reduction. Nevertheless, the decrease in the normalized Mo=O Raman band intensities is about the same for all catalysts. Therefore, the percent reduction of the surface molybdenum oxide species during methanol oxidation does not appear to be a strong function of surface coverage or the specific oxide support.

3.5. DISCUSSION

3.5.1. Factors influencing the selectivity of the supported molybdenum oxide catalysts

The overall selectivity of the supported molybdenum oxide catalysts was determined by the reactivity properties of both the surface molybdenum oxide species and the specific oxide support. The surface molybdenum oxide species primarily were responsible for the formation of formaldehyde, but could also yield small amounts of methylformate (see MoO_3/TiO_2 data in Table 3.2) and dimethoxymethane (see MoO_3/ZrO_2 data in Table 3.3). The Lewis acid sites on the alumina and niobia supports were very active and resulted in significant amounts of dimethylether production (see data in Tables 3.4 and 3.5). In contrast, the Lewis acid sites on the titania support were not very active and resulted in only small amounts of dimethylether production. The small dimethylether production observed for the MoO_3/TiO_2 catalysts may even have originated from acid sites associated with the surface molybdenum oxide species rather than the titania support. The redox sites on the zirconia support possessed a modest activity and yielded methylformate from either pairs of Zr-Zr sites or Zr-Mo sites. The competitive reactions between the surface molybdenum oxide species and the specific oxide support determined the final overall reaction selectivity. The relative contribution of these two reactive sites was a strong function of the surface molybdenum oxide coverage since the surface molybdenum oxide species covered the reactive oxide support sites at high surface coverages. The primary reaction product formed at monolayer coverage of the surface molybdenum oxide species on the different supports was formaldehyde with approximately 80% selectivity. However, the very active Lewis acid sites on the alumina support, and possibly even acid sites associated with the surface molybdenum oxide species on alumina [31], were responsible for the catalyst exhibiting a formaldehyde selectivity of 21% at monolayer coverage. The generally high selectivity of the supported molybdenum oxide catalysts towards formaldehyde production during methanol oxidation demonstrates that this is the primary redox product from the surface molybdenum oxide species.

The selective production of formaldehyde during methanol oxidation over the supported molybdenum oxide catalysts does not appear to be dependent on the molecular structure of the surface molybdenum oxide species. The product selectivity for the 1% and 6% MoO_3/TiO_2 catalysts is essentially identical (see Table 3.2), however, these catalysts possess different surface molybdenum oxide structures [1]. The surface molybdenum oxide species primarily possess tetrahedral coordination for the 1% MoO_3/TiO_2 catalyst and octahedral coordination for the 6% MoO_3/TiO_2 catalyst, and the extent of polymerization of the surface molybdenum oxide species also increases with surface coverage (see Table 3.1). The zirconia-supported samples appear to possess both tetrahedral and octahedral coordinated surface molybdenum oxide species at monolayer coverage (see Table 3.1), and this catalyst also yields a comparable formaldehyde selectivity during methanol oxidation. Thus, the specific molecular structure of the surface molybdenum oxide species is not a critical parameter affecting the rate of selective oxidation of methanol oxidation to formaldehyde.

3.5.2. Factors influencing the TOF of the supported molybdenum oxide catalysts

The redox TOFs of the supported molybdenum oxide catalysts increase by a factor of about 2-4 as the coverage of the surface molybdenum oxide species increases towards monolayer coverage (see Tables 3.2-3.4). The most extensive catalytic data exist for the MoO_3/TiO_2 system since the titania support was relatively inactive towards methanol oxidation at low surface molybdenum oxide coverages, and the TOF for this system increases approximately four-fold with coverage. Comparison of the methanol oxidation reactivity data with the corresponding structural data for the surface molybdenum oxide species (see Table 3.1) suggests that this slight increase in reactivity may be related to structural differences of the surface molybdenum oxide species. The surface molybdenum oxide species on titania are predominantly isolated, tetrahedral species at low loadings and predominantly polymerized, octahedral species at high loadings.

Similar structural and catalytic trends for the surface molybdenum oxide species are also observed for the other supported molybdenum oxide catalysts, but are somewhat overshadowed by the contributions of the oxide supports at low surface coverages. Thus, it appears that polymerized, octahedral/tetrahedral surface molybdenum oxide species may be slightly more active, by a factor of 2-4, than isolated, tetrahedral surface molybdenum oxide species on oxide supports.

The redox TOFs of the supported molybdenum oxide catalysts at monolayer coverage increase by a factor of about 6 as the specific oxide support is changed (see Tables 3.2-3.5). Furthermore, the TOF for methanol oxidation over low coverage MoO_3/SiO_2 is a factor of two lower than for MoO_3/Al_2O_3, but only isolated surface molybdenum oxide species are present on silica [27]. The relative TOFs follow the pattern: Zr ~ Ti > > Nb > Al > Si. The current findings for the reactivity patterns of the supported molybdenum oxide catalysts have much in common with a similar series of studies on methanol oxidation over supported vanadium oxide catalysts [3]. The TOFs of the supported vanadium oxide catalysts were also found to vary with the specific oxide support: Zr ~ Ti > Nb > > Al > > Si. This trend in reactivity with the specific oxide support is the same for both the supported vanadium oxide and molybdenum oxide catalysts. However, the TOFs for the supported molybdenum oxide catalysts vary by approximately one order of magnitude, whereas, the TOFs for the supported vanadium oxide catalysts vary by approximately three orders of magnitude. Furthermore, the trend in TOF for the supported vanadium oxide catalysts was found to inversely correlate with the reduction temperature during temperature programmed reduction experiments: the more active catalysts reduce at lower temperature [3]. The same correlation is also found when the TOFs of the supported molybdenum oxide catalysts at monolayer coverage are compared with the reduction temperatures during temperature programmed reduction experiments [26] (see Fig. 3.12). The line drawn in Fig. 3.12 is not a curve fitting and is meant to illustrate that the oxidation activity is inversely related to the T_{max} temperature of TPR. Thus, these correlations suggest that the oxide support acts as a very important ligand for the surface metal oxide species and that its reducibility is a critical parameter in the redox activity of the supported metal oxide catalysts. It has been proposed for the supported vanadium oxide catalysts that the reducibility of the bridging V-O-support bonds control the TOF during methanol oxidation [3], and a similar conclusion appears to be valid for the supported molybdenum oxide catalysts. A molecular orbital study for the oxidative dehydrogenation of methanol over metal transition metal oxide surfaces by Weber [32] suggested that the bridging oxygens are more labile than the terminal oxygens which is consistent with the current results.

Additional support for the above conclusion that the bridging Mo-O-support bond controls the TOF is provided by the current Raman data and literature data on methanol oxidation over various molybdenum oxide containing catalysts. Comparison of the Raman data in Table 3.1 with the corresponding methanol oxidation TOFs, Tables 3.2-3.5, reveals that a correlation does not exist between the terminal Mo=O bond strength, higher frequencies correspond to shorter and stronger bonds [33], and the methanol oxidation TOF. The Raman Mo=O band position of the fully oxidized surface molybdenum oxide species is essentially the same for the surface molybdenum oxide species on titania, zirconia, and niobia, but the TOF varies by a factor of 3. The Raman Mo=O band position difference is the greatest between the alumina and silica supports (approximately 20 cm^{-1}) [27], but these two systems are the least active catalysts. The surface molybdenum oxide species also possess the same structures on titania and niobia, but the TOF varies by a factor of 3. Similarly, the surface molybdenum oxide species are similar on zirconia and alumina, but the TOF varies by a factor of about 6. Thus, the change in the TOF of the surface molybdenum oxide species with the specific oxide support, about a factor of 10 when silica is included, appears to be related to a property of the support rather than the structure of the surface molybdenum oxide overlayer. Methanol adsorption studies over the MoO_3 single crystal (010) basal plane, which possesses the surface containing the most saturated Mo=O bonds in the layered MoO_3 structure, found no chemisorption of methanol. It was, thus, hypothesized that methanol adsorption leading to reaction is favored by the coordinatively unsaturated Mo sites (the edge planes possessing Mo-O-Mo and Mo-OH bonds) [5,7,34]. Eguchi *et al.* [35] observed with *in situ* IR during methanol oxidation over heteropolyanion Keggin units that the bridging Mo-O-Mo bond was reduced at low degrees of reduction of the heteropolyanions and that the terminal Mo=O oxygen was consumed only at high extent of reduction. Thus, there currently is no supporting evidence that the terminal Mo=O bond controls the TOF during methanol oxidation.

Matsuoka *et al.* [21] were the first to study the activity of a series of supported molybdenum oxide catalysts (Al_2O_3, TiO_2, ZrO_2, and CeO_2 supports) for methanol oxidation. The dependence of the TOF on the surface molybdenum oxide coverage and the specific oxide support was reported (see Fig. 3.12 of reference 21). Their investigation found that the TOF increases with surface Mo coverage and the activity sequence for the supports, $ZrO_2 > TiO_2 > Al_2O_3$, agrees with the current findings. However, the larger increase of the TOF with the surface Mo loading in the prior studies compared to the current investigation may have been caused by the extremely low activities of the oxide supports in the earlier studies. The overall TOFs of the monolayer catalysts reported by Matsuoka *et al.* were also much lower than our results, even after taking into account the lower reaction temperature and lower partial pressure of the methanol employed. Kim *et al.* [26] also studied methanol oxidation over different supported molybdenum oxide catalysts, under similar reaction conditions as Matsuoka's, and reported TOFs of the surface molybdenum oxide species which are very close to the current findings. Matsuoka *et al.* did not give an explanation for the TOF dependence and a structure-reactivity relationship was not discussed since only the ambient structures of the surface molybdenum oxide species, rather than the structures under reaction conditions, were studied.

3.5.3. *In Situ* Raman studies of supported molybdenum oxide catalysts

Additional insights into the states of the surface molybdenum oxide species during the methanol oxidation reaction were provided by *in situ* Raman spectroscopy studies. The *in situ* Raman studies demonstrated that the surface molybdenum oxide species on ZrO_2, TiO_2, Nb_2O_5 and Al_2O_3 were stable during methanol oxidation and did not agglomerate into crystalline MoO_3 particles. Thus, the exposure of the surface molybdenum oxide species on these oxide supports remained 100% during methanol oxidation below monolayer surface coverage (see Figs. 3.1-3.10). This is in contrast to methanol oxidation over MoO_3/SiO_2 where the surface molybdenum oxide species agglomerate into crystalline β-MoO_3 particles at high loadings [27].

The *in situ* Raman studies also revealed that the surface molybdenum oxide species are influenced by the methanol oxidation reaction. The Mo=O Raman bands of the surface molybdenum oxides decrease in intensity, become broader, and are usually shifted to lower frequencies by ~ 10 cm^{-1}. These changes are primarily attributed to the participation of the surface molybdenum oxide species in the methanol oxidation reaction as well as coordination by surface methoxy species (the reaction intermediate [5-7]). Shifting to lower frequency and broadening of the Mo=O Raman bands can also be caused by adsorbed moisture [28]. However, the low water partial pressures in the *in situ* cell during methanol oxidation and the elevated reaction temperatures, 503 to 633 K, should minimize the perturbation of adsorbed moisture upon the Raman Mo=O band. In fact, moisture does not perturb the Raman Mo=O band of MoO_3/SiO_2 because of the hydrophobic nature of the silica support and this band also broadens and shifts to lower frequencies during methanol oxidation [27]. Thus, the changes in the Mo=O Raman bands are associated with the surface methoxy intermediates. The lifetime of the reactive methoxy intermediates on the surface Mo sites appears too short to be detected by normal Raman and the stable methoxy species readily seen by Raman during methanol oxidation are located on exposed sites of the oxide support [28,29]. The Raman signals of these stable surface methoxy species decrease with metal oxide loading and becomes undetectable when monolayer metal oxide coverage is approached. The presence of these stable surface methoxy species on the exposed sites of the oxide support affects the Raman Mo=O band of the surface molybdenum oxide: the Mo=O Raman bands shift to lower frequencies and become broader. This accounts for the decreases in the frequency shift and broadening of the Raman band with increasing surface molybdenum oxide coverage. The Mo=O Raman band features of the surface molybdenum oxide species during methanol oxidation were also sensitive to reaction temperature (see Figs. 3.3, 3.6, and 3.10) and generally became sharper and shifted to higher frequencies as a consequence of reduction in the number of surface methoxy species with increasing reaction temperature [28]. However, the integrated and normalized intensities of the Mo=O Raman bands did not change significantly from 503 to 633 K and the differences were within 15% for all temperatures. Thus, over the temperature range investigated, the percent reduction of the surface molybdenum oxide species was not significantly influenced by temperature.

The decrease in the normalized intensity of the Raman Mo=O band during methanol oxidation was taken as a reflection of reduction of the surface molybdenum (VI) oxide species to lower oxidation states. This assumption needs to be quantitatively confirmed with experiments such as *in situ* UV/Vis diffuse reflectance spectroscopy which can measure the distribution of oxidation states under reaction conditions. The reduced surface molybdenum oxide species are apparently not Raman active or give rise to weak signals on titania, zirconia, and niobia, but in the case of MoO_3/Al_2O_3 the reduced surface molybdenum oxide species are readily observable (see Fig. 3.9). This observation is consistent with previous XPS measurements that demonstrated that surface molybdenum oxide species are more readily reduced in hydrogen on titania than on alumina [36,37]. For MoO_3/TiO_2, it was found that no Mo(+6) species remained after reduction at 503 K [37]. However, for MoO_3/Al_2O_3, significant amounts of Mo(+6) remained even after a reduction treatment at 773 K [36]. The absence of observable Raman bands for the reduced surface molybdenum oxide species on zirconia, titania, and niobia may be a consequence of their lower oxidation states during methanol oxidation.

The *in situ* Raman studies during methanol oxidation also provide additional insights into the determine factors controlling the TOFs for methanol oxidation over the different supported molybdenum oxide catalysts. The *in situ* Raman studies reveal that the number of surface molybdenum oxide sites participating in the methanol oxidation reaction at steady state, reflected by the percent reduction of the normalized Mo=O Raman bands in Fig. 3.11, is approximately the same for all the supported molybdenum oxide catalysts (~25%). As discussed above, the percent reduction of the surface molybdenum oxide species during methanol oxidation was also not significantly influenced by the reaction temperature. These observations reveal that only approximately one-quarter of the surface molybdenum oxide species simultaneously participate in the methanol oxidation reaction under steady state, even though the surface molybdenum oxide species are 100% dispersed up to monolayer coverage. All the surface molybdenum oxide species appear to participate in the methanol oxidation reaction since all the surface Mo=O Raman bands are reduced when only methanol (in helium) is passed over the catalysts. Details of the extent of participation would require *in situ* isotope experiments to be carried out. A similar situation was found for methanol oxidation over supported vanadium oxide catalysts where approximately 50% of the surface vanadia species were reduced under the same reaction conditions [29]. The *in situ* Raman studies also reveal that the differences in reactivity among the oxide supports are not generally related to different quantities of surface molybdenum oxide species participating in the methanol oxidation reaction. This suggests that the increase in reactivity with the specific oxide support, as well as reaction temperature, is associated with an increase in the specific reactivity of the surface molybdenum oxide active sites.

The constant number of surface molybdenum oxide sites participating on the different oxide supports during the methanol oxidation reaction, under the standard reaction conditions, has significant implications for the kinetics of this reaction. The kinetics of methanol oxidation to formaldehyde have been extensively investigated over many different types of catalysts (molybdenum oxide [5-9,12,34], supported vanadia [3], and metals [38]), and the same mechanism and activation energy were always found. The oxidation of methanol to formaldehyde proceeds via a surface methoxy intermediate and the rate determining step is the breaking of the C-H bond which typically requires about 85 kJ/mole. Furthermore, under the present standard conditions of methanol oxidation, the reaction was first order in methanol concentration and zero order in oxygen because of the excess oxygen employed. The constant activation energy for the methanol oxidation reaction, as well as the constant number of participating surface molybdenum oxide sites as discussed above, reveals that the order of magnitude difference observed in the TOF of the supported molybdenum oxide catalysts originates with the pre-exponential factor of the Arrhenius rate constant and is associated with an entropy term for the activated transition state complex. The increase in entropy of the transition state complex may be related to the more labile Mo-O-support bridging oxygen present for supported molybdenum oxide species on ZrO_2 and TiO_2 compared to Nb_2O_5, Al_2O_3 and SiO_2. The increase in TOF with molybdenum oxide surface coverage can be accounted by an increase in the density of electronic states which increases the entropy of the activated complex during the methanol oxidation reaction. The current findings are in agreement with the molecular orbital study of surface methoxy C-H bond breaking by metal oxide surfaces by Weber, which indicated that the electron delocalization to the support increases the activation entropy of the methanol oxidation reaction [32]. A similar conclusion was reached for the corresponding supported vanadia catalysts during methanol oxidation [29].

3.6. CONCLUSIONS

The final overall selectivity during methanol oxidation over the supported molybdenum oxide catalysts was determined by the competitive reactions between the surface molybdenum oxide species and the specific oxide support. The surface molybdenum oxide redox sites selectively yielded formaldehyde, the Lewis acid sites on the alumina and niobia supports resulted in dimethylether production, the surface redox sites on zirconia formed methylformate, and the titania surface sites were relatively inactive. At monolayer coverage of the surface molybdenum oxide species, formaldehyde selectivities of approximately 80% were achieved on titania, zirconia and niobia. The high activity of the alumina support resulted in a maximum formaldehyde selectivity of only 21% at monolayer coverage. The molecular structure of the surface molybdenum oxide species (isolated, tetrahedral or polymerized, octahedral/tetrahedral) did not correlate with the selectivity of methanol oxidation to formaldehyde.

The redox TOFs of the supported molybdenum oxide catalysts increased by a factor of 2-4 with surface molybdenum oxide coverage. This suggests that polymerized, octahedral/tetrahedral surface molybdenum oxide species may be slightly more active than isolated, tetrahedral surface molybdenum oxide species. The redox TOFs of the supported molybdenum oxide catalysts increased by a factor of about 10 as the specific oxide support was changed: Zr ~ Ti > > Nb > Al > Si. This suggests that the oxide support acts as an important ligand that controls the reactivity of the surface molybdenum oxide overlayer. It was proposed that the reducibility of the bridging Mo-O-support bond controls the TOF during methanol oxidation.

In situ Raman studies during methanol oxidation demonstrated that the dispersion of the surface molybdenum oxide species was 100% below monolayer coverage. The surface molybdenum oxide Mo=O Raman bands decreased in intensity, became broader, and shifted to lower frequencies during methanol oxidation. These changes were due to the adsorption of surface methoxy species on the catalysts and partial reduction of the surface molybdenum oxide species (reflected in the decreased normalized intensity of the MO=O Raman bands). The percent reduction of the surface molybdenum oxide species during methanol oxidation was not found to be a strong function of surface coverage and the specific oxide support. This suggests that the order of magnitude variation in the TOF with the specific oxide support is primarily related to the specific reactivity of the bridging bond between the surface molybdenum oxide species and the oxide support. The results agree with Weber's proposal that the entropy of the activated complex is affected by the density of accessible electronic states associated with the support [32].

REFERENCES

1. Hu, H., Wachs, I. E., and Bare, S. R., *J. Phys. Chem.* Accepted for publication.
2. Haber, J., "*The Role of Molybdenum in Catalysis*", Climax Molybdenum Co. 1981.
3. Deo, G. and Wachs, I. E. *J. Catal.* **146**, 323 (1994).
4. Machiels, C. J., and Sleight, A. W. *J. Catal.* **76**, 238 (1982).
5. Cheng, W. H., Chowdhry, U., Ferretti, A., Firment, L. E., Groff, R. P., Machiels, C. J., McCarron, E. M., Ohuchi, F., Staley, R. H., and Sleight, A. W. In "*Heterogeneous Catalysis*", Shapiro, B. L. Ed. Texas A&M Univ. Press, 165 (1984).
6. Chowdhry, U., Ferretti, A., Firment, L. E., Machiels, C. J., Ohuchi, F., Sleight, A. W., and Staley, R. H. *Appl. Surf. Sci.* **19**, 360 (1984).
7. Machiels, C. J., Cheng, W. H., Chowdhry, U., Farneth, W. E., Hong, F., McCarron, E. M., and Sleight, A. W. *Appl. Catal.* **25**, 249 (1986).
8. Tatibouët, J. M. and Germain, J. E., *J. Catal.*, **72**, 375 (1981).
9. Tatibouët, J. M., Germain, J. E. and Volta, J. C., *J. Catal.*, **82**, 240 (1983).
10. Louis, C., Tatibouët, J. M. and Che, M., *J. Catal.*, **109**, 354 (1988).
11. Chung, J. S., and Bennett, C. O., In "*Adsorption and Catalysis on Oxide Surfaces*", Che, M., and Bond, G. C., Eds., Elsevier, 185 (1985).
12. Chung, J. S., Miranda, R., and Bennett, C. O. *J. Catal.* **114**, 398 (1988).

13. Rocchiccioli-Deltcheff, C., Amirouche, M., Che, M., Tatibouët, J. M. and Fournier, M., *J. Catal.*, **125**, 292 (1990).
14. Liu, T. C., Forissier, M., Coudurier, G., and Védrine, J. C. *J. Chem. Soc. Faraday Trans.* I, **85**, 1607 (1989).
15. Che, M., Louis, C. and Tatibouët, J. M., *Polyhedron*, **5**, 123 (1986).
16. Louis, C. and Che, M., *J. Catal.*, **135**, 156 (1992).
17. Williams, C. C. and Ekerdt, J. G., *J. Catal.*, **141**, 430 (1993).
18. Segawa, K., Soeya, T. and Kim, D. S., *Sekiyu Gakkaishi*, **33**, 347 (1990).
19. Ono, T., Miyata, H. and Kubokawa, Y., *J. Chem. Soc. Faraday Trans.* 1, **83**, 1761 (1987).
20. Wachs, I. E., Deo, G., Kim, D. S., Vuurman, M. A. and Hu, H., *Proc. Int. Congr. Catal. 10th*, A, 543 (1992).
21. Matsuoka, Y., Niwa, M. and Murakami, Y., *J. Phys. Chem.*, **94**,1477 (1990).
22. Brückman, K., Grzybowska, B., Che, M. and Tatibouët, J. M., *Applied Catalysis A: General*, **96**, 279 (1993).
23. Reddy, B. M., Reddy, E. P. and Srinivas, S. T., *J. Catal.*, **136**, 50 (1992).
24. Jehng, J-M., Turek, A. M. and Wachs, I. E., *Applied Catalysis A. General*, **83**, 179 (1992).
25. Jin, Y. S., Ouqour, A., Auroux, A. and Védrine, J. C., *Structure and Reactivity of surfaces*, Morterra, C., Zecchina, A. and Costa, G. Ed. Elsevier, 525 (1989).
26. Kim, D. S., Wachs, I. E., and Segawa, K., *J. Catal.* **146**, 268 (1994).
27. Bañares, M. A., Hu, H., and Wachs, I. E., *J. Catal.*, **150** (1994).
28. Jehng, J-M., and Wachs, I. E. Unpublished results.
29. Deo, G., and Wachs, I. E., Unpublished results.
30. Gao, X., and Xin, Q. *J. Catal.* **146**, 306 (1994).
31. Turek, A. M., Wachs, I. E., and DeCanio, E. *J. Phys. Chem.* **96**, 5000 (1992).
32. Weber, R. S., *J. Phys. Chem.* **98**, 2999 (1994).
33. Hardcastle, F. D., and Wachs, I. E., *J. Raman Spectroc.* **21**, 683 (1990).
34. Ohuchi, F., Firment, L. E., Chowdhry, U., and Ferretti, A., *J. Vac. Sci.*

Technol. **A2**, 1022 (1984).

35. Eguchi, K., Toyozawa, Y., Yamazoe, N., and Seiyama, T., *J. Catal.* **83**, 32 (1983).
36. Yamada, M., Yasumaru, J., Houalla, M., and Hercules, D. M., *J. Phys. Chem.* **95**, 7037 (1991).
37. Quincy, R. B., Houalla, M., Proctor, A., and Hercules, D. M., *J. Phys. Chem.* **94**, 1520 (1990).
38. Wachs, I. E., and Madix, R. J., *Surface Science*, **76**, 531 (1978).

Table 3.1. Structures of the Surface Mo Species at Low and Near Monolayer Coverage for Supported Molybdenum Oxide Catalyst[1]

Catalyst	Low coverage (1%)		Monolayer coverage	
	Raman band of Mo=O(cm^{-1})	Structure	Raman band of Mo=O(cm^{-1})	Structure
MoO_3/TiO_2	993	Td	998	Oh,polymer
MoO_3/ZrO_2	980	(Td)	997	(Td+Oh,polymer)
MoO_3/Nb_2O_5	992	(Td)	996	(Oh, polymer)
MoO_3/Al_2O_3	990	Td, isolated	1006	Td+Oh, polymer

Table 3.2. Reactivity of the MoO_3/TiO_2 Catalysts as a Function of MoO_3 Loading for Methanol Oxidation Reaction.

Sample	Density Mo atom /nm^2	Activity mmole/ g.hr	TOF^a (redox) ($10^{-1}s^{-1}$)	Selectivity^b %				
				FA	MF	DMM	DME	COx
MoO_3	-	10	0.2^c	76	tr	6	16	2
TiO_2	-	2	-	-	-	-	91	9
0.5%MoO_3/TiO_2	0.4	20	1.3	77	tr	6	13	4
1% MoO_3/TiO_2	0.8	61	2.2	85	1	5	5	4
2% MoO_3/TiO_2	1.5	159	3.0	87	1	7	2	3
3% MoO_3/TiO_2	2.3	370	4.7	91	tr	5	3	1
5% MoO_3/TiO_2	3.8	786	5.8	85	3	4	6	2
6% MoO_3/TiO_2	4.6	942	5.7	85	tr	5	6	4
7% MoO_3/TiO_2	5.3	1082	5.7^e	90	tr	2	6	2

a: Redox TOF is based on the formation of FA + MF + DMM.

b: FA = formaldehyde (HCHO); MF = methylformate ($HCOOCH_3$);
DMM = dimethoxymethane ($CH_2(OCH_3)_2$); DME = dimethylether (CH_3OCH_3);
COx = CO + CO_2.

c: Based on the exposed MoO_3 surface area.

d: Reaction temperature at 503 K, $CH_3OH/O_2/He$ = 6.9/11/82.1.

e: Apparent TOF since dispersion is not 100% due to presence of crystalline MoO_3 particles.

Table 3.3. Reactivity of the MoO_3/ZrO_2 Catalysts as a Function of MoO_3 Loading for Methanol Oxidation Reaction.

Sample	Density Mo atom /nm^2	Activity mmole/ g.hr	TOF[a] (redox) ($10^{-1}s^{-1}$)	Selectivity %				
				FA	MF	DMM	DME	COx
ZrO_2	-	20	-	-	86	-	tr	14
0.5% MoO_3/ZrO_2	0.5	21	-[b]	4	51	-	3	42
1% MoO_3/ZrO_2	1.1	38	-[b]	18	48	tr	4	30
2% MoO_3/ZrO_2	2.1	185	2.4	63	27	1	2	7
3% MoO_3/ZrO_2	3.2	612	6.1	74	18	1	2	5
5% MoO_3/ZrO_2	5.4	754	5.1[c]	82	12	2	3	1
7% MoO_3/ZrO_2	7.5	811	3.9[c]	83	11	1	3	2

a: Redox TOF is based on the formation of FA + DMM.

b: Not calculated due to significant contribution from the ZrO_2 support.

c: Apparent TOF since dispersion is not 100% due to presence of crystalline MoO_3 particles.

Table 3.4. Reactivity of the MoO_3/Nb_2O_5 Catalysts as a Function of MoO_3 Loading for Methanol Oxidation Reaction.

Sample	Density Mo atom /nm^2	Activity mmole/ g.hr	TOF^a (redox) ($10^{-2}s^{-1}$)	Selectivity %				
				FA	MF	DMM	DME	COx
Nb_2O_5	-	15.7	-	-	-	-	100	-
0.5% MoO_3/Nb_2O_5	0.4	17.3	-^{b}	10	-	2	88	tr
1% MoO_3/Nb_2O_5	0.8	24.8	-^{b}	30	tr	1	68	tr
2% MoO_3/Nb_2O_5	1.5	66.3	8.8	65	tr	2	32	tr
3% MoO_3/Nb_2O_5	2.3	134.5	14.0	76	tr	2	22	tr
4% MoO_3/Nb_2O_5	3.0	124.0	9.4	72	tr	4	23	tr
5% MoO_3/Nb_2O_5	3.8	271.6	17.8	80	tr	2	18	tr
6% MoO_3/Nb_2O_5	4.6	351.7	19.2	80	tr	2	18	tr
7% MoO_3/Nb_2O_5	5.3	323.3	15.3^c	80	tr	3	17	tr

a: Redox TOF is based on the formation of FA + MF + DMM.

b: Not calculated due to the high activity of the Nb_2O_5 support.

c: Apparent TOF since dispersion is not 100% due to presence of crystalline MoO_3 particles.

Table 3.5. Reactivity of the MoO_3/Al_2O_3 Catalysts as a Function of MoO_3 Loading for Methanol Oxidation Reaction.

Sample	Density Mo atom /nm^2	Activity mmole/g.hr (10^3)	TOF[a] (redox) ($10^{-2}s^{-1}$)	Selectivity %				
				FA	MF	DMM	DME	COx
Al_2O_3	-	3.7	-	-	-	-	100	-
1% MoO_3/Al_2O_3	0.2	1.8	-	-	-	-	100	-
6%MoO_3/Al_2O_3	1.4	3.0	-[b]	0.5	-	tr	99.5	-
12%MoO_3/Al_2O_3	2.8	1.4	-[b]	4	tr	tr	96	-
18%MoO_3/Al_2O_3	4.2	1.6	9.4	11	tr	tr	89	-
20%MoO_3/Al_2O_3	4.6	2.6	1.1	21	tr	tr	79	-

a: Redox TOF is based on oxidation products (FA + MF + DMM) formed.

b: Not calculated due to the high activity of the Al_2O_3 support.

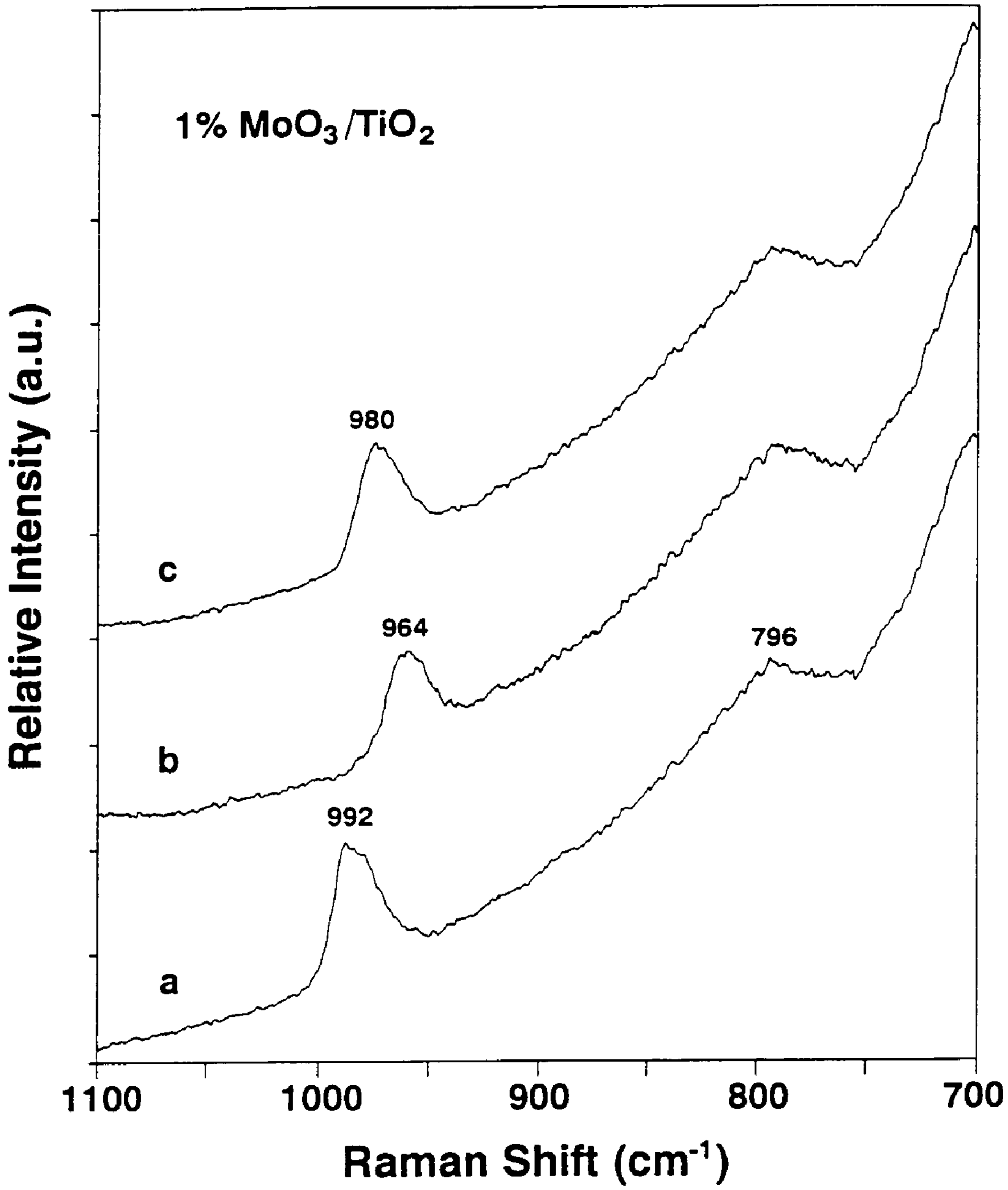

Fig. 3.1. *In situ* Raman spectra of the 1% MoO_3/TiO_2 catalyst during methanol oxidation. a) 503 K, He/O_2, b) 503K, CH_3OH/He/O_2, and c) 503 K, He/O_2 after reaction.

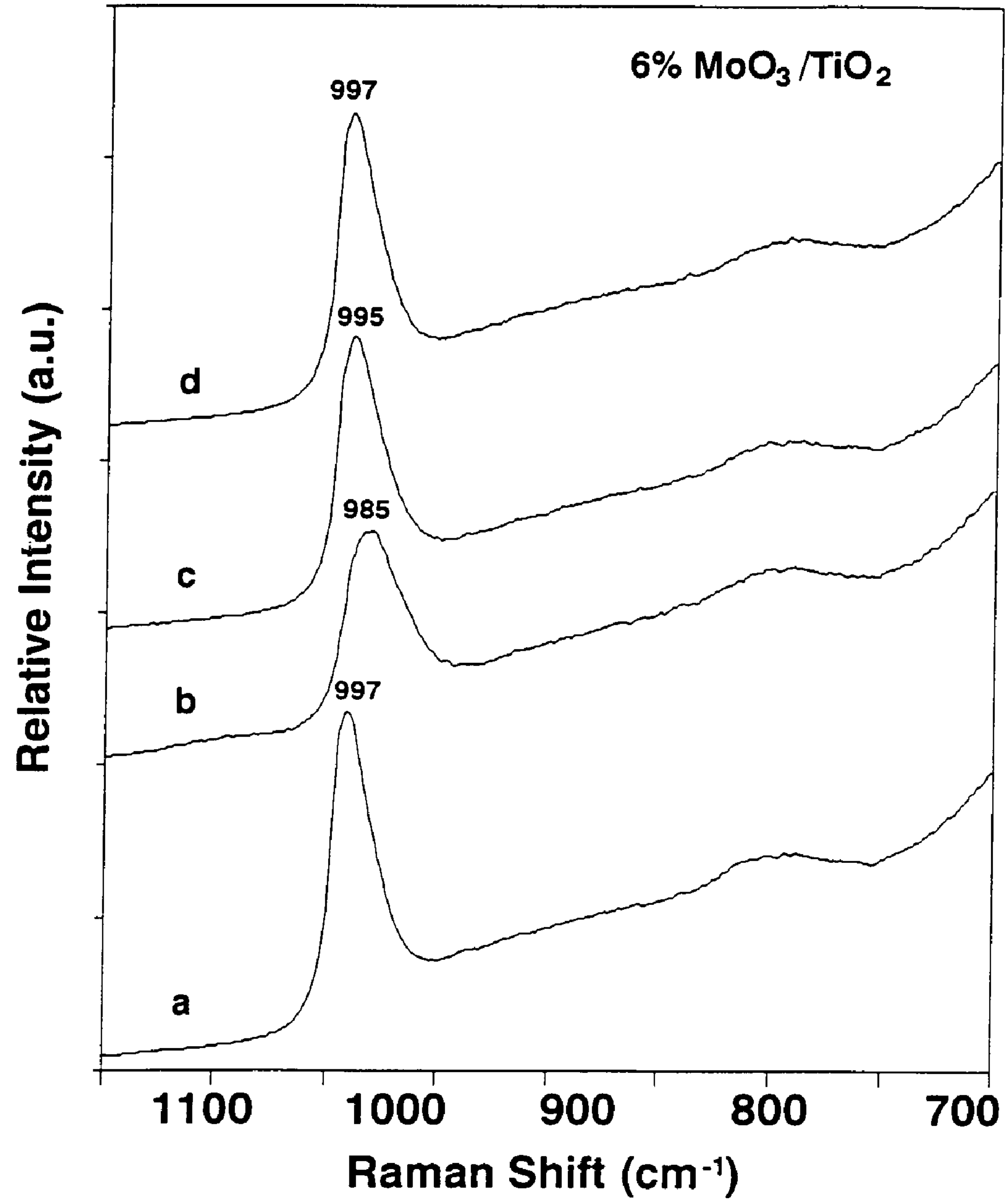

Fig. 3.2. *In situ* Raman spectra of the 6% MoO_3/TiO_2 catalyst during methanol oxidation. a) 503 K, He/O_2, b) 503K, CH_3OH/He/O_2, c) 503 K, He/O_2 after reaction, and d) 773 K, He/O_2.

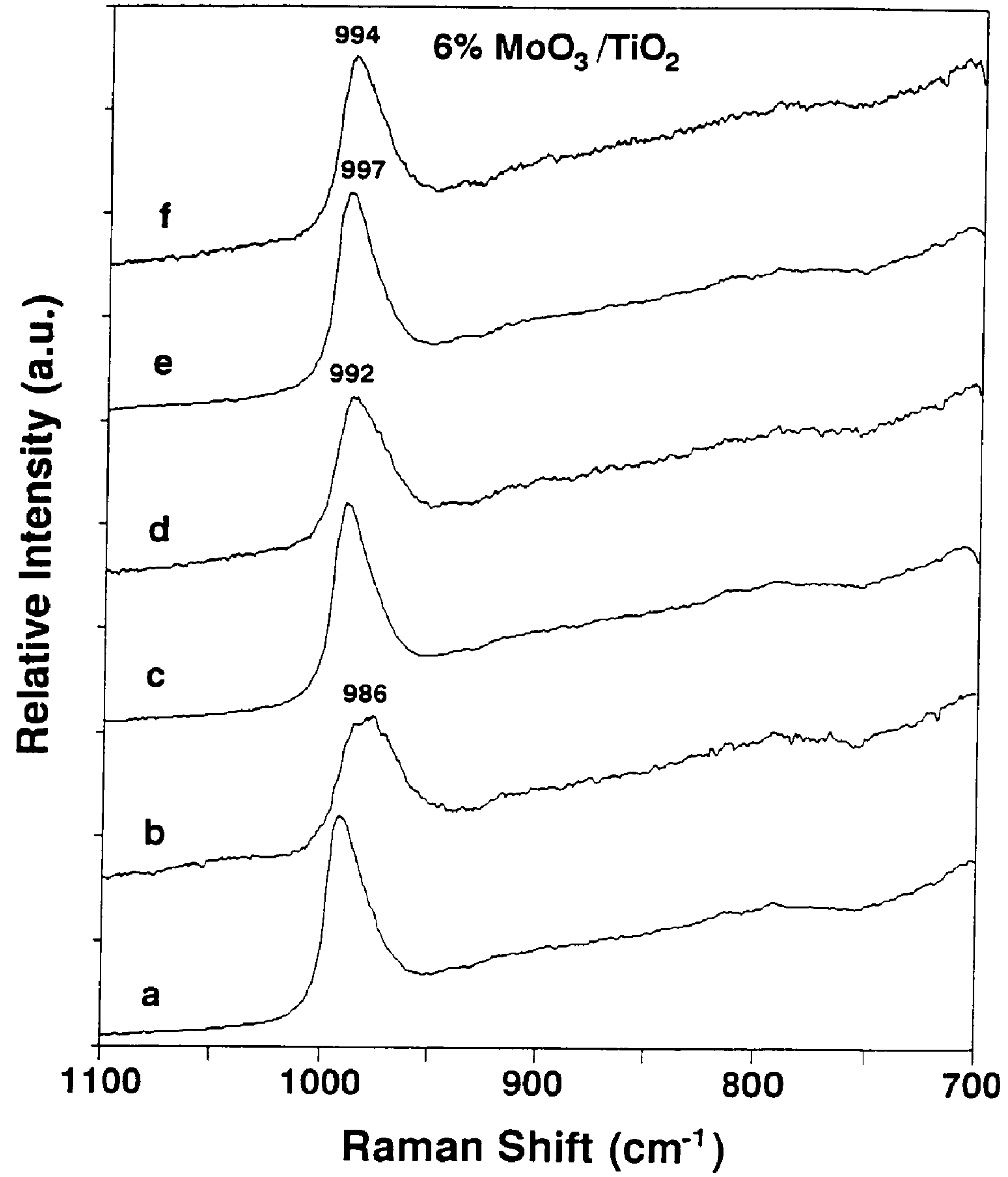

Fig. 3.3. *In situ* Raman spectra of the 6% MoO_3/TiO_2 catalyst during methanol reaction at a) and b) 503 K, c) and d) 573 K, and e) and f) 633 K. Where a), c), and e) are taken before reactions and b), d), and f) are taken during the reactions.

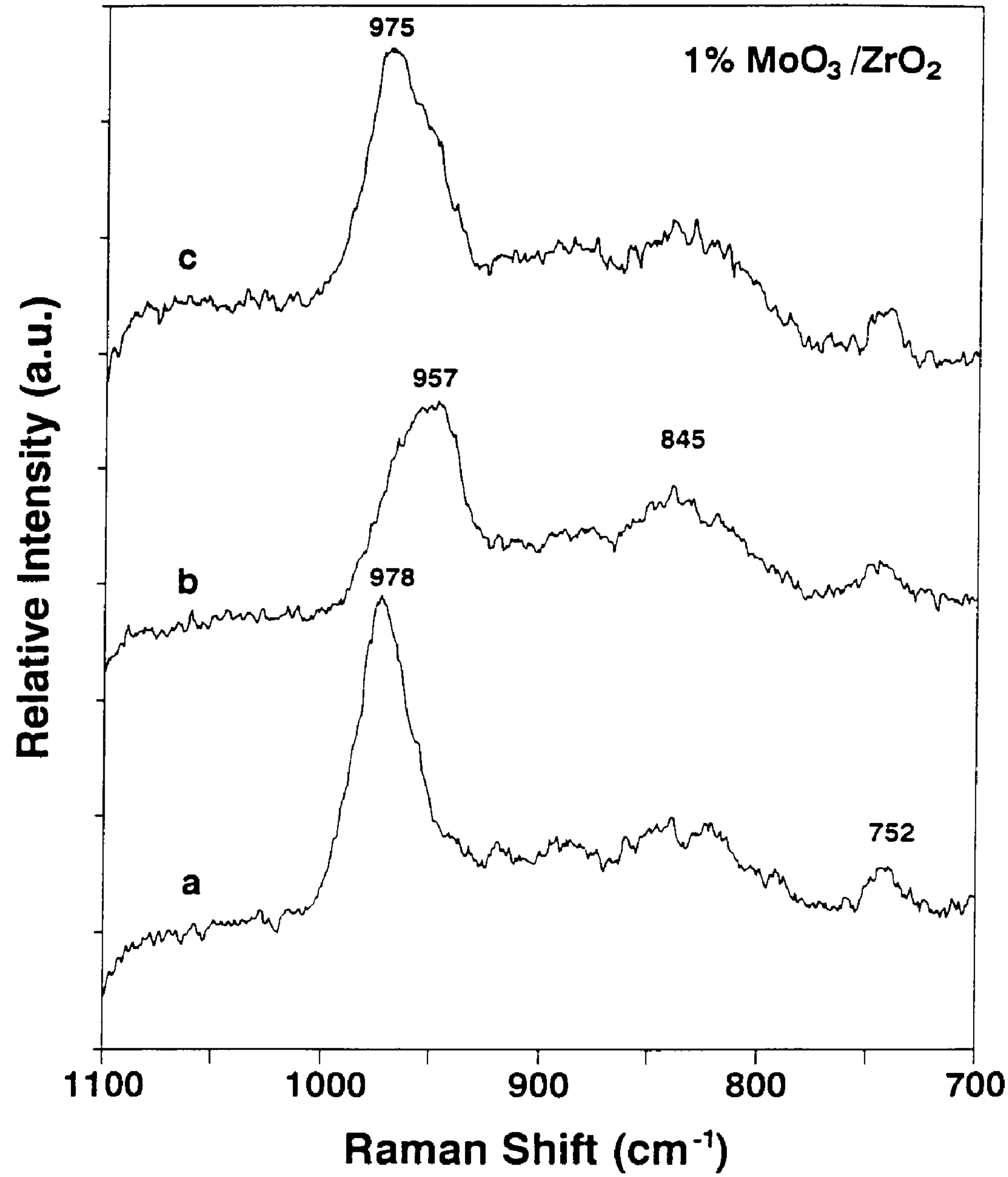

Fig. 3.4. *In situ* Raman spectra of the 1% MoO_3/ZrO_2 catalyst during methanol oxidation. a) 503 K, He/O_2, b) 503K, $CH_3OH/He/O_2$, and c) 503 K, He/O_2 after reaction.

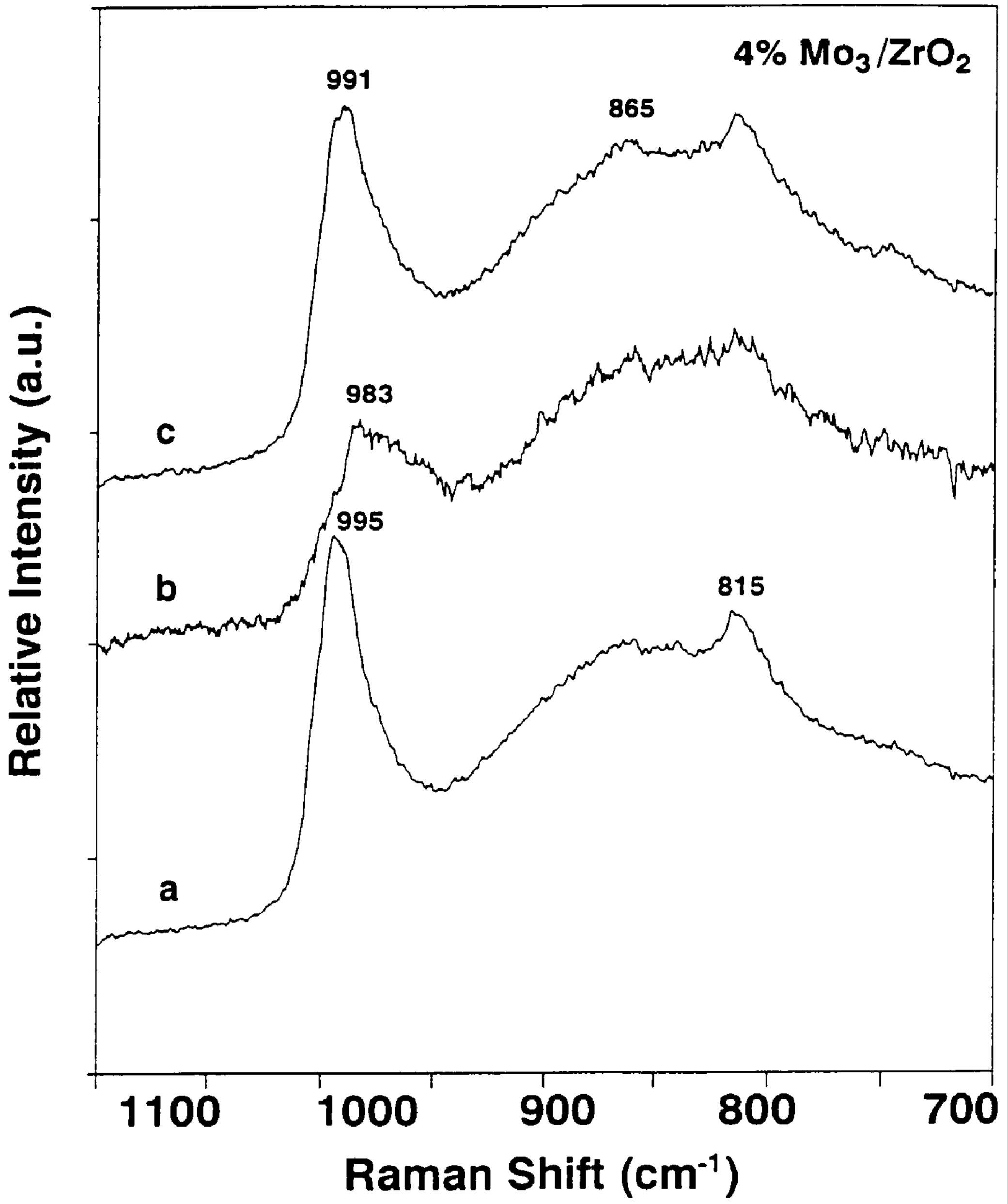

Fig. 3.5. *In situ* Raman spectra of the 4% MoO_3/ZrO_2 catalyst during methanol oxidation. a) 503 K, He/O_2, b) 503K, $CH_3OH/He/O_2$, and c) 503 K, He/O_2 after reaction.

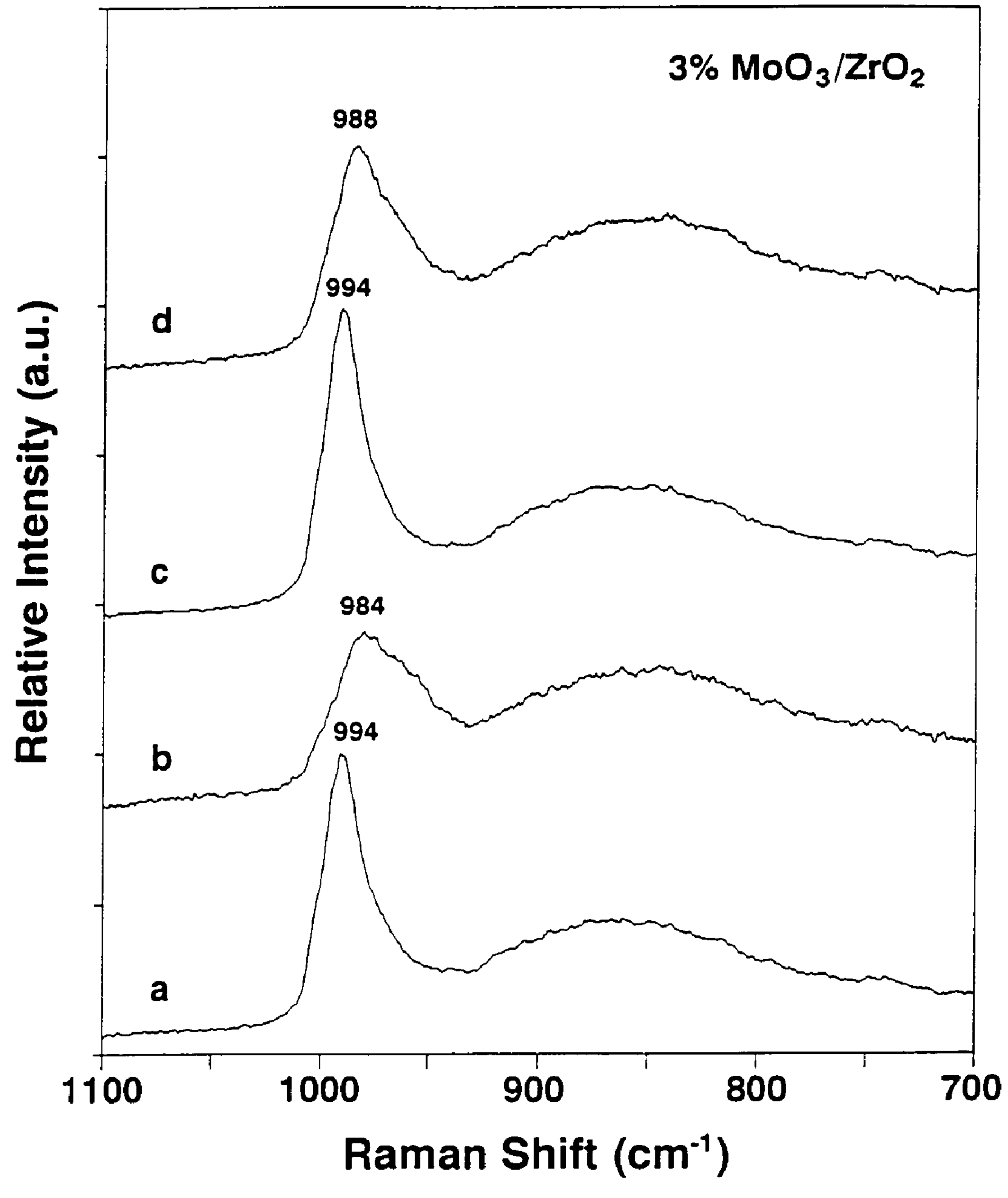

Fig. 3.6. *In situ* Raman spectra of the 3% MoO_3/ZrO_2 catalyst during methanol reaction at a) and b) 573 K; c) and d) 633 K, where a) and c) are before reactions and b) and d) are during reactions.

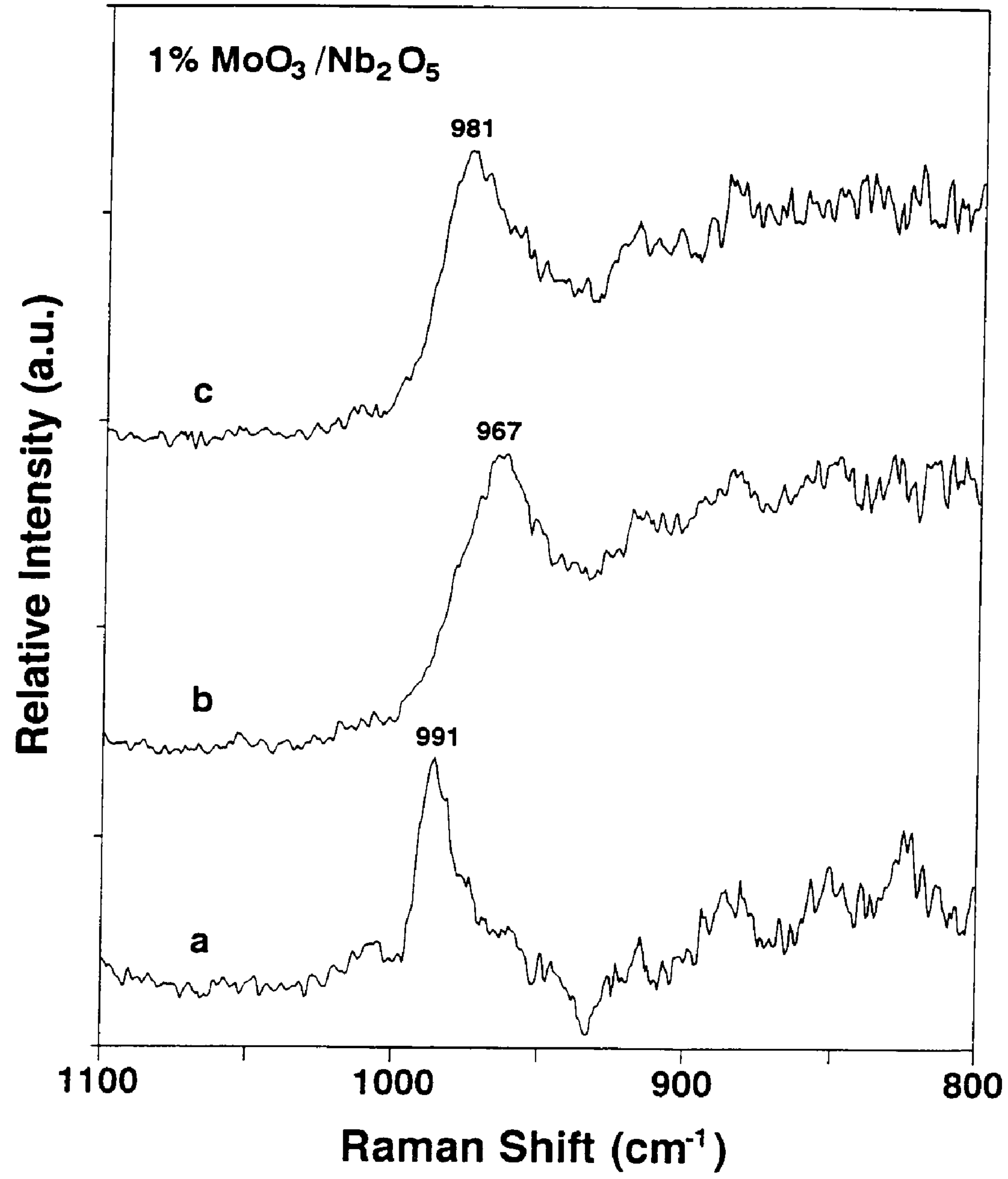

Fig. 3.7. *In situ* Raman spectra of the 1% MoO_3/Nb_2O_5 catalyst during methanol oxidation. a) 503 K, He/O_2, b) 503K, $CH_3OH/He/O_2$, and c) 503 K, He/O_2 after reaction.

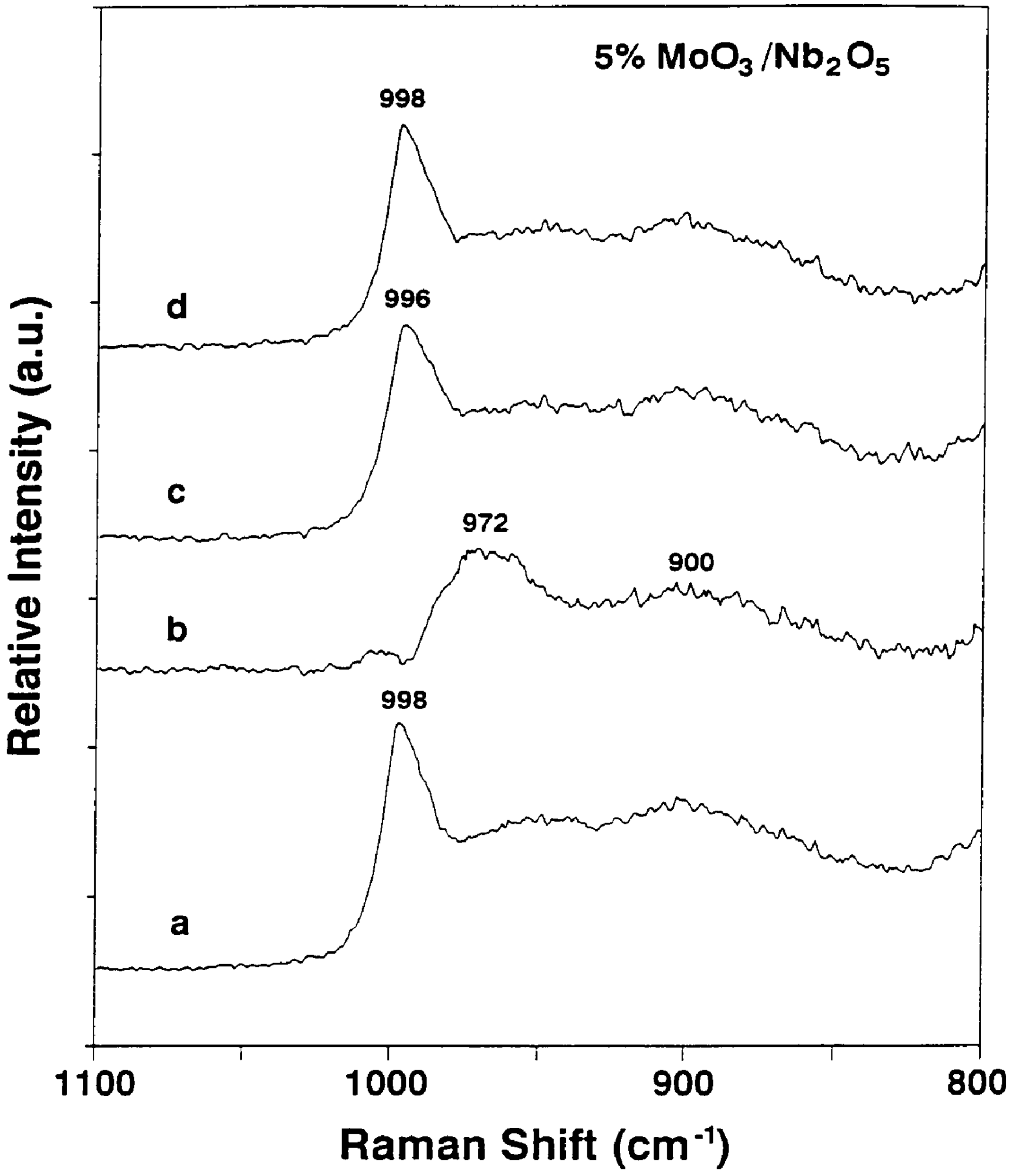

Fig. 3.8. *In situ* Raman spectra of the 5% MoO_3/Nb_2O_5 catalyst during methanol oxidation. a) 503 K, He/O_2, b) 503K, CH_3OH/He/O_2, c) 503 K, He/O_2 after reaction, and d) 773 K, He/O_2.

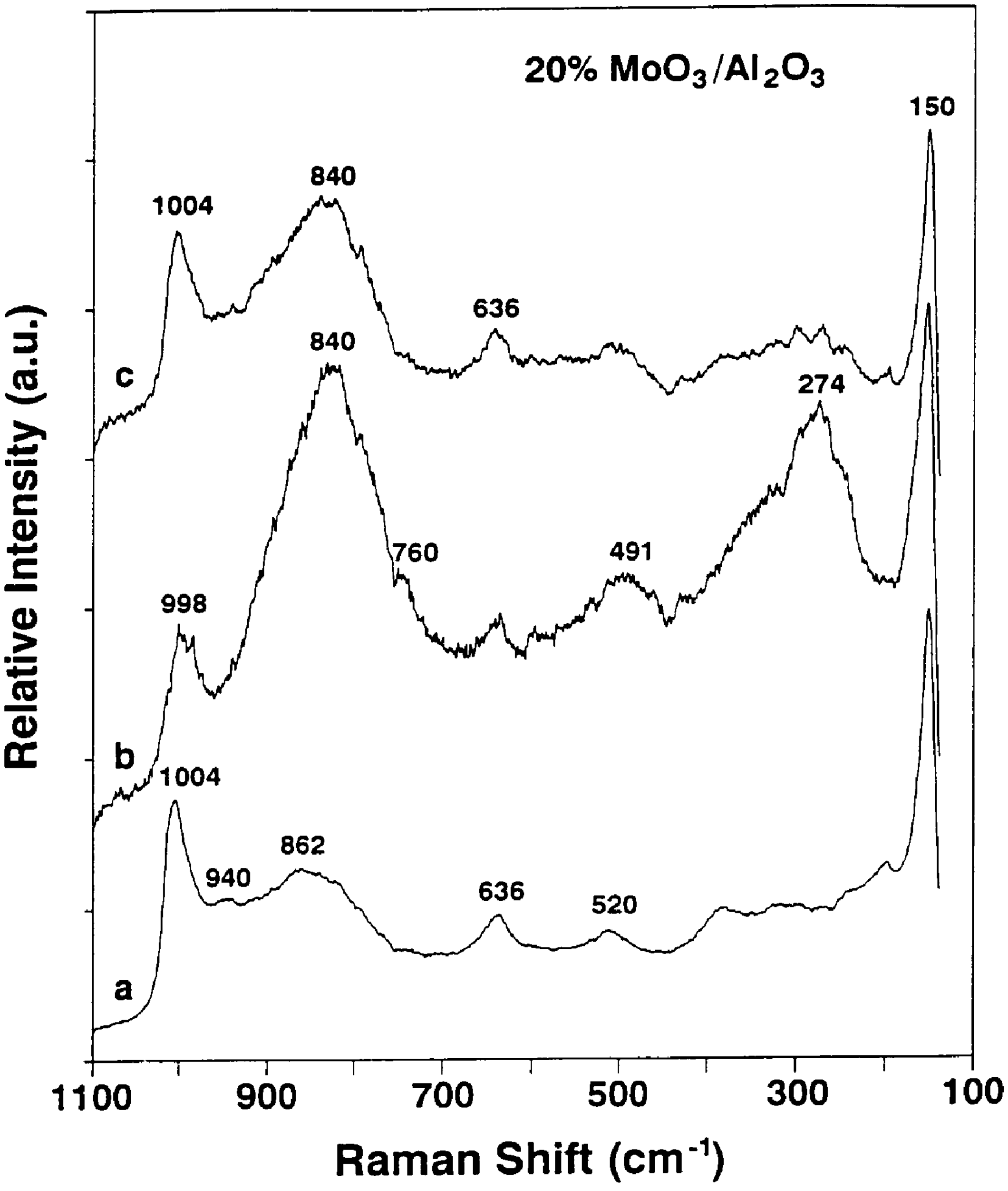

Fig. 3.9. *In situ* Raman spectra of the 20% MoO_3/Al_2O_3 catalyst during methanol oxidation. a) 503 K, He/O_2, b) 503K, CH_3OH/He/O_2, and c) 503 K, He/O_2 after reaction.

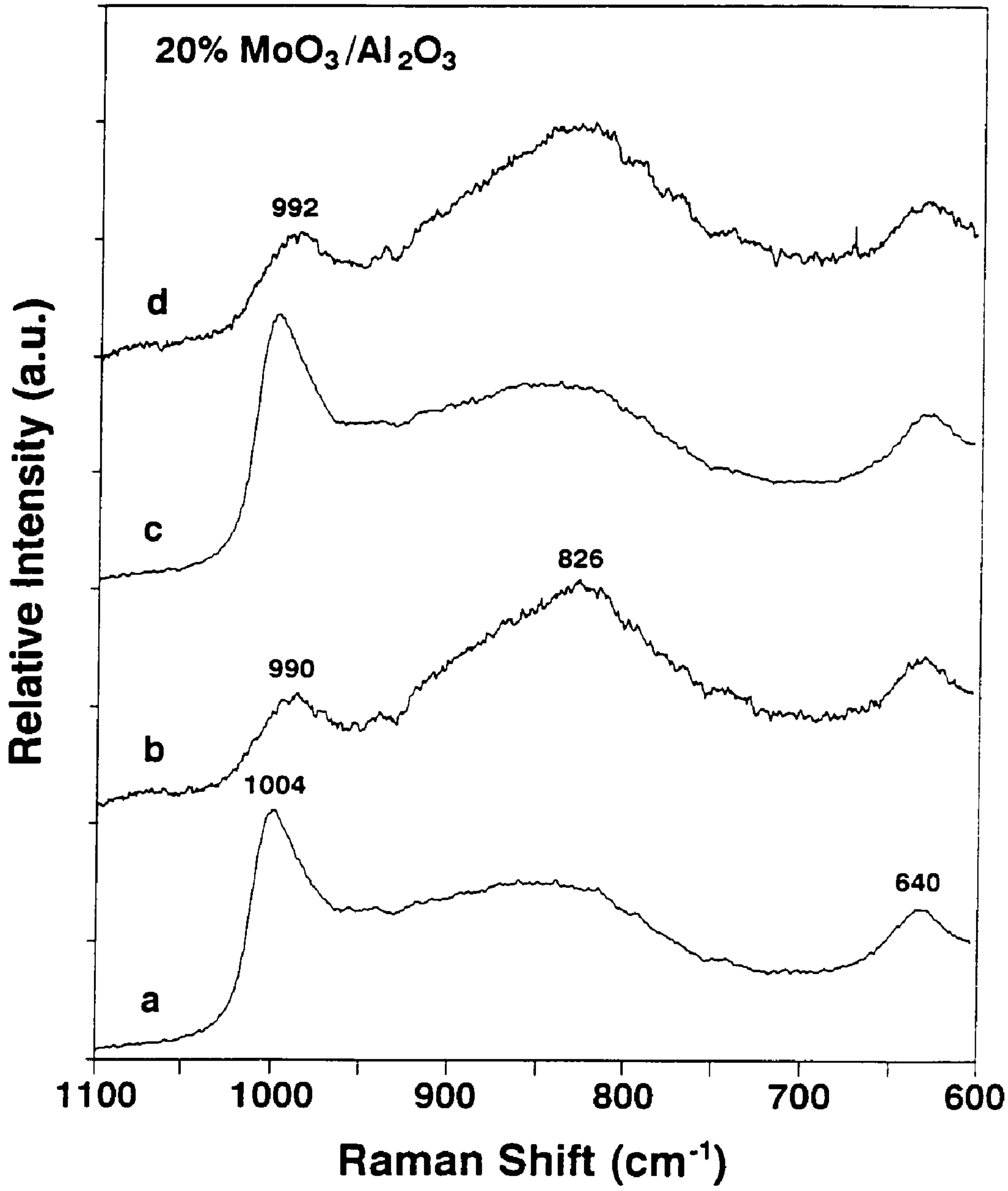

Fig. 3.10. *In situ* Raman spectra of the 20% MoO_3/Al_2O_3 catalyst during methanol reaction at a) and b) 573 K, and c) and d) 633 K, where a) and c) are before reactions and b) and d) are during reactions.

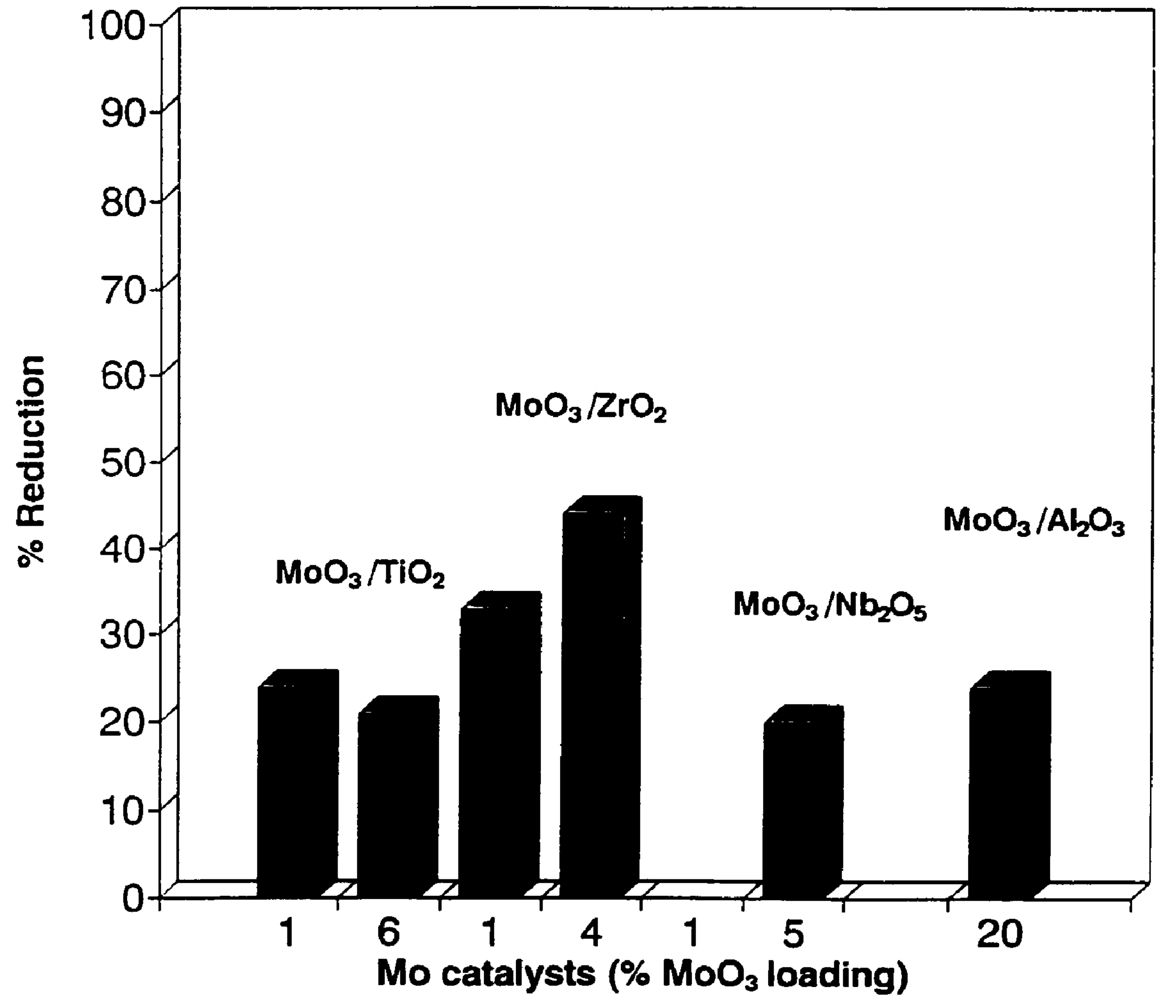

Fig. 3.11. The percent reduction (decrease in the Raman Mo=O band intensity) for different oxide-supported molybdenum oxide catalysts during methanol oxidation at 503 K.

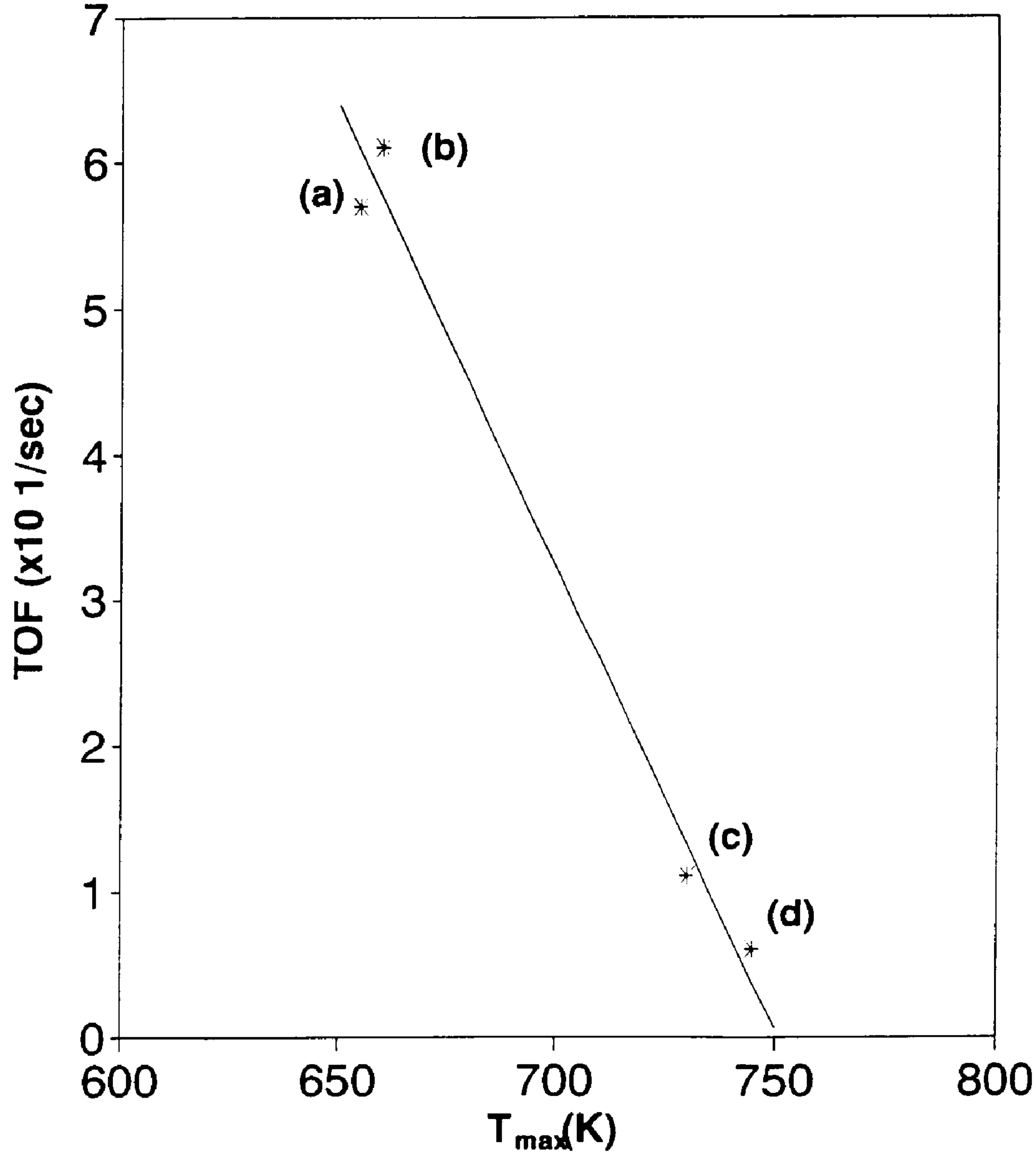

Fig. 3.12. Plot of TOF versus the T_{max} temperature of TPR for the (a) MoO_3/TiO_2, (b) MoO_3/ZrO_2, (c) MoO_3/Al_2O_3, and (d) MoO_3/SiO_2 catalysts. T_{max} is from reference 26, and the TOF of MoO_3/SiO_2 is from reference 27.

CHAPTER 4

MOLYBDENUM OXIDE ON SILICA: ROLE OF THE PREPARATION METHODS ON THE STRUCTURE-SELECTIVITY PROPERTIES FOR THE OXIDATION OF METHANOL

4.1. SUMMARY

A series of MoO_3/SiO_2 samples prepared by several research groups, employing different silicas and preparation methods, have been studied by *in situ* Raman spectroscopy, X-ray photoelectron spectroscopy, and methanol oxidation as a probe reaction. The *in situ* Raman spectroscopy studies show that under dehydrated conditions the molecular structure of the silica-supported molybdenum oxide surface species is independent of the preparation methods used in the present study. The surface molybdenum oxide species is assigned to an isolated, highly distorted octahedral mono-oxo Mo structure. The appearance of new structures in some samples is due to the presence of calcium impurities in the silica supports which result in the formation of calcium molybdate. Neither the preparation method nor the specific silica used affected the methanol oxidation activity of the MoO_3/SiO_2 catalysts. The surface molybdenum oxide coverage on silica is the only relevant factor that determines the catalytic properties during methanol oxidation. *In situ* Raman spectroscopy during methanol oxidation shows aggregation of surface molybdenum oxide species to crystalline β-MoO_3. The extent of aggregation increases with the surface molybdenum coverage, even at very low coverages, and accounts for the decrease in the methanol oxidation catalytic activity with increasing surface molybdenum coverage.

4.2. INTRODUCTION

Molybdenum oxide on silica catalysts are widely used in a number of reactions such as propene metathesis [1,2], propene oxidation [3], methanol oxidation [4], ethanol oxidative dehydrogenation [1], and ammonia selective oxidation to nitrogen [5], and in the selective oxidation of methane [6,7]. These numerous catalytic applications have generated much interest in the structures of these catalysts and their relevance to their catalytic properties [1,2,8,9]. Furthermore, there has developed an interest in tailoring the structures of the surface molybdenum species to improve their catalytic properties for specific applications.

In the past few years, many authors have reported various structures or synthesis methods which are proposed to generate a specific surface molybdenum oxide species at low coverage: isolated dioxo surface MoO_4 species [4,10], isolated mono-oxo MoO_6 species [5,11], or dimeric surface Mo_2O_8 compounds [12] (see Scheme 4.1).

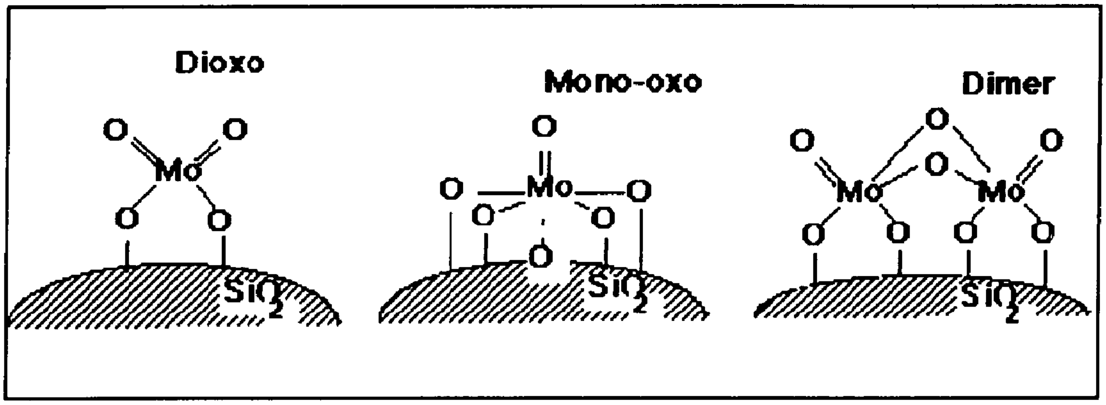

Scheme 4.1

Some synthesis methods have been reported to result in a better dispersion and catalytic activity than other preparation methods [4,11,12]. Unfortunately, disagreements are quite frequently found in the literature in the structures obtained even when using the same preparation methods. Possible reasons for these discrepancies may be the use of different characterization techniques, conditions of characterization, or the presence of impurities in the catalysts.

The most common method employed to deposit molybdenum oxide on the silica support surface is by aqueous impregnation with ammonium heptamolybdate ($(NH_4)_6Mo_7O_{24}\bullet 4H_2O$) solutions [6,7,10,11,13]. In this preparation method, the water solvent is removed by drying and the dry precursor is calcined at temperatures ranging from 723 to 873 K. At low Mo loadings and under dehydrated conditions, the dispersed surface molybdenum oxide species are reported to have either the hexacoordinated mono-oxo structure as concluded from Raman spectroscopy [11] or the tetracoordinated dioxo structure as concluded from luminescence [14,15]. Alternative synthesis methods have also been employed due to the poor effectiveness of this conventional impregnation method in producing samples with high dispersions of Mo. These new methods focused on an improvement of the interaction between the molybdenum oxide precursors and the silica surface hydroxyl groups by the use of molybdenum compounds with labile ligands (such as $MoCl_5$, $Mo(\eta^3C_3H_5)_4$, $Mo_2(\eta^3C_3H_5)_4$, or $Mo_2(OAc)_4$) that would be easily hydrolyzed by the silanol groups [11,12,15-18]. Another approach is to improve the acid/base interaction of the molybdenum oxide precursor with the silica support by using the less acidic Mo^{3+} species [5].

Several research groups have claimed that the allyl-derived Mo/SiO_2 species possess unique structures which are preparation dependent. Yermakov reported that the preparation with $Mo(\eta^3C_3H_5)_4$ results in surface molybdenum oxide species bonded to the silica through two Si-O-Mo bridges (dioxo structure) [16] for the Mo(VI) oxidation state from infrared and ESR measurements. Iwasawa [12] reported that supporting $Mo(\eta^3C_3H_5)_4$ or $Mo_2(\eta^3C_3H_5)_4$ results in isolated or paired bidentate MoO_4 tetrahedra joined by bridging oxygen, respectively, as concluded from photoluminescence, DRS-UV/VIS and EXAFS studies of the dehydrated samples. Dimeric structures have also been reported by Ichikawa and co-workers [17,18] to result from the $Mo_2(OAc)_4$ precursors based on *in situ* FT-IR, DRS-UV/VIS and EXAFS studies of the samples under oxygen and water free conditions. The allyl-derived structures were reported to be stable under repeated oxidation (673 K) and reduction (773 and 813 K) cycles [12]. These structures, however, could not be reproduced by Ekerdt and co-workers [11] employing Raman spectroscopy.

The preparation of catalysts by the reaction of $MoCl_5$ with the silica surface hydroxyl groups has been proposed by Che and co-workers to present higher molybdenum oxide dispersions and better catalytic activity during methanol oxidation than catalysts prepared by impregnation with ammonium heptamolybdate [4,15]. In this preparation method, surface polymerization of the molybdenum precursor to dimeric Mo_2Cl_{10} is very important and only a very small amount is really hydrolyzed by the silanol groups. Consequently, an ammonium hydroxide washing step is required to remove the molybdenum species which have not been hydrolyzed by the silica hydroxyl groups and remain loosely bound. The ammonium hydroxide washing step, however, removes up to 90% of the molybdenum initially deposited [4]. After calcination, the remaining dispersed surface molybdenum oxide species is reported to have a tetrahedral geometry with two oxo groups (dioxo structure) based on luminescence studies. Ekerdt and co-workers [11] concluded from Raman spectroscopy that surface octahedral mono-oxo molybdenum oxide species were present after such a preparation. A new procedure to obtain well-dispersed molybdenum oxide on silica, by impregnating with Mo^{3+} aqueous solutions, has been proposed by de Boer *et al.* [5]. In this preparation method, Mo^{3+} interacts more strongly with silica than Mo(VI) species due to its basic properties. Oxidizing the surface Mo^{3+} species to Mo(VI) results in an isolated mono-oxo MoO_6 structure based on Raman, IR, and EXAFS/XANES characterization studies [5,26].

The great variety of preparation methods, types of silicas, characterization methods, and activity studies employing different probe reactions results in a significant lack of homogeneity and, therefore, agreement among the various authors. The objective of this work was to systematically characterize various MoO_3/SiO_2 catalysts obtained from different laboratories with one characterization technique (Raman spectroscopy) and one probe reaction (methanol oxidation) in order to address the origin of these disagreements. The selective oxidation of methanol was chosen as the probe reaction because it is very sensitive to the nature of the surface sites present in oxide catalysts. Surface redox sites form primarily formaldehyde and to a lesser extent methyl formate as the reaction products. Surface acid sites result in the formation of dimethyl ether.

Methyl formate results from the participation of CH_3OH adsorbed on the silica surface hydroxyl and adjacent surface molybdenum oxide sites [19]. The MoO_3/SiO_2 samples were supplied by nine different research groups, using four different synthesis methods (grafting with washing, allyl compounds of molybdenum, impregnation with ammonium heptamolybdate, and impregnation with Mo^{3+} solutions) and up to eight different silicas (porous and nonporous with BET surface areas ranging from 20 to 400 m^2/g) as shown in Tables 4.1 and 4.2.

4.3. EXPERIMENTAL SECTION

4.3.1. Catalyst preparation

The Mo/SiO_2 samples were provided by several research groups and Tables 4.1 and 4.2 identify all the samples used with information on the preparation method and the specific silica support. The codes used to identify the different series are as follows: **I**, impregnated samples; **E**, samples prepared by impregnation with electrochemically reduced molybdenum species (Mo^{3+}); **A**, samples prepared by interaction with the allyl molybdenum compound $Mo_2(\eta^3C_3H_5)_4$; and **G**, samples prepared by grafting with $MoCl_5$. The number is used to discriminate between the different research groups. Additional letters "a" or "b" identify different batches for the same method from a specific group.

4.3.2. Elemental analysis

The loading of molybdenum oxide on the catalysts was determined using a

Perkin-Elmer 3030 Atomic Absorption Spectrometer. The samples were prepared by dissolving in a HF, HCl, and HNO_3 solution and were further treated in a microwave oven at a power of 650 W.

Additional XPS measurements for surface chemical analysis were performed in a Fisons ESCALAB MkII 200R spectrometer fitted with a hemispherical electron analyzer and a Mg anode X-ray exciting source (Mg Kα = 1253.6 eV). The residual pressure in the analysis chamber was below 3×10^{-9} Torr (1 Torr = 133.3 Pa).

4.3.3. Laser Raman spectroscopy

The molecular structures of the surface molybdenum oxide species on silica were examined with Raman spectroscopy. The Raman spectrometer system possessed a Spectra-Physics Ar^+ laser (Model 2020-05) tuned to the exciting line at 514.5 nm. The radiation intensity at the samples was varied from 10 to 70 mW. The scattered radiation was passed through a Spex Triplemate spectrometer (Model 1877) coupled to a Princeton Applied Research OMA III optical multichannel analyzer (Model 1463) with an intensified photodiode array cooled to 238 K. Slit widths ranged from 60 to 550 μm. The overall resolution was better than 4 cm^{-1}. For the *in situ* Raman spectra of the dehydrated samples, a pressed wafer was placed into a stationary sample holder that was installed in an *in situ* cell which has previously been described [22]. Spectra were recorded in flowing oxygen at room temperature after the samples were dehydrated in flowing oxygen at 573 K. The MoO_3/SiO_2 samples had to be calcined for at least 2 h before the Raman measurements to eliminate the fluorescence from the support.

Essentially the same Raman spectra were obtained with lower calcination pretreatment temperatures, but the signal to noise ratio was usually low.

In situ Raman spectroscopy during methanol oxidation was also performed in order to study the structural changes taking place for the silica-supported molybdenum oxide catalysts. These spectra were performed with a second Raman apparatus consisting of an Ar^+ laser (Spectra Physics, Model 165), a triple grating spectrometer (Spex, Model 1877), a photodiode array detector (EG&G, Princeton Applied Research, Model 1420), and a specially designed *in situ* sample cell. The 514.5-nm line of the Ar^+ laser with 10-100 mW of power is focused on the sample disc in a right-angle scattering geometry. The *in situ* cell was equipped with a spinning sample holder which was generally rotated at ca.1000 rpm inside a quartz cell which allows working under controlled atmosphere and temperature. Sample discs of 100-200 mg are held by the cap of the metallic alloy sample holder. A cylindrical furnace surrounding the quartz cell heats the sample and is controlled by an internal thermocouple. The MoO_3/SiO_2 samples had to be calcined at 773-973 K for at least 2 h before the Raman measurement to eliminate the fluorescence from the support. The *in situ* Raman spectra were obtained under continuous flow of a gaseous mixture with a He/O_2 ratio near 11/6. The Raman spectra of the dehydrated samples were recorded after *in situ* heating the sample at 773 K for 30 min and cooling to 503 K, which is the methanol oxidation reaction temperature. The Raman spectra under reaction conditions were collected after passing the He/O_2 mixture gas through a methanol reservoir at 273 K for at least 30 min. After the methanol oxidation, the samples were reoxidized by the He/O_2 gas at 503 and 773 K for 1 h.

4.3.4. Methanol oxidation

The reactivities of the different silica-supported molybdenum oxide species were probed by the methanol oxidation reaction. The reactor consisted of a 6 mm o.d. glass tube containing ca. 50 mg of catalyst which provides differential reactor conditions by keeping conversion below 10%. The catalyst was held in place by a glass-wool sandwich. The catalysts were pretreated in flowing O_2 at 573 K prior to methanol oxidation. A methanol/oxygen/helium mixture of 6/13/81 (molar ratios) at 1 atm pressure was used as the reactant gas for all the data presented in this work. Volatilization of molybdenum in the samples with high molybdenum oxide loading was observed. The analysis of the reaction products was performed with an on-line gas chromatograph (HP-5840A) containing two packed columns (Porapack R and Carbosieve SII) and two detectors (TCD and FID). The catalytic values reported here are taken after running the reaction for a few hours when steady state has essentially been reached. The reaction temperature was maintained at 503 K and the results are presented as turnover frequency (TOF), which is defined as the number of moles of methanol converted or specific product formed per mole of molybdenum atom per second. The TOF values reported are apparent TOF values since all the supported molybdenum atoms are assumed to be active in the methanol oxidation and this may not always be the case.

4.4. RESULTS

4.4.1 Elemental analysis

The results of the elemental analyses of the catalysts are presented in Table 4.3. The molybdenum loadings are very close (typically better than 5%) to those reported by the different research groups.

Surface chemical analyses (XPS) show that most of the samples do not contain significant amount of impurities. However, the presence of alkali impurities was observed in the samples A4 (sodium) and G2b (calcium).

4.4.2. Laser Raman spectroscopy

The Raman spectra of dehydrated samples prepared by impregnation with ammonium heptamolybdate (I5), allylic compounds of molybdenum (A4), and grafting of $MoCl_5$ (G4), impregnated with Mo^{3+} (E6) solutions, and supported on Degussa Aerosil 200, Davidson-952, Davidson-952, and Degussa Aerosil 200 silicas, respectively, are shown in Fig. 4.1. The broad features at 800, 650, and 500-300 cm^{-1} are due to the silica support. All the samples show the same Raman band at 978-990 cm^{-1}. Another series of Raman spectra of samples prepared by impregnation with AHM (I1, I3, I7, I8, I9) and grafting with $MoCl_5$ (G2a) and using different silica supports (Strobe, 20 m^2/g; Cab-O-Sil, 90 m^2/g; Degussa Aerosil 200, 180 m^2/g; Cab-O-sil M5, 185 m^2/g; Cab-O-Sil EH5, 380 m^2/g; and Rhône-Poulenc XOA400, 400 m^2/g) is presented in Fig. 4.2. The Rhône-Poulenc sample gave a very weak Raman signal because of strong sample fluorescence. The Strobe silica presents a high number of silanol groups that result in very intense silica Raman bands at 970, 800, 600, and 485 cm^{-1} relative to the surface molybdenum species (Fig. 4.2f) due to its low temperature preparation. Again, the only molybdenum oxide Raman band observed is the one at ~982 cm^{-1}. Despite its very low intensity, the Raman band at 982 cm^{-1} could positively be assigned to surface molybdenum oxide species since exposure of this sample (I3) to ambient conditions resulted in the transformation of this Raman band to the Raman bands characteristic of heptamolybdate species at 965-940, 880, 380-370 and 240-210 cm^{-1}. Thus, the Raman studies reveal that the same surface molybdenum oxide species is present on all the Mo/SiO_2 samples examined and is independent of the specific silica support and the preparation method.

The presence of calcium impurities on the silica support results in the formation of new compounds ($CaMoO_4$) as seen by the presence of new Raman bands at 876, 844, 794, and 319 cm^{-1} which are not affected by hydration/dehydration processes [11]. This is shown in Fig. 4.3 for the sample prepared on Rhône-Poulenc silica. Along with these new Raman bands, the band characteristic of the dispersed surface molybdenum oxide species is also present at ~982 cm^{-1}.

Impregnation of silica with Mo^{3+} solutions is claimed to result in a better dispersion of surface molybdenum oxide species on the silica support. A sample prepared according to this method, shown in Fig. 4.4e [5], was compared with a series of MoO_3/SiO_2 catalysts with higher and lower molybdenum loadings, shown in Figs. 4.4a-4.4d and 4.4f. This series was prepared by impregnation with ammonium heptamolybdate [7], which is reported to give the worst dispersion and the same silica support (Aerosil-200 Degussa) was employed for all the samples. The dehydrated Raman spectra of these samples are shown in Fig. 4.4 and the only molybdenum oxide Raman band observed is at 978-990 cm^{-1} for all the samples as well as the broad features of the silica support. At loadings close to the maximum dispersion limit of molybdenum oxide on silica (ca. 1 Mo/nm^2), a new feature can be observed at ca. 968 cm^{-1} as a shoulder. The maximum amount of Mo dispersed on SiO_2 corresponds to the titration of all the silica silanols [23]. This new Raman band cannot be observed for the sample prepared from Mo^{3+} solutions, despite its high molybdenum loading. This could be indicative of a better local dispersion for the molybdenum species on this sample. In addition, preparations employing allyl molybdenum compounds also appear to result in a better dispersion than observed with the conventional AHM aqueous solutions [23].

The *in situ* Raman spectra during methanol oxidation of samples prepared by impregnation with ammonium heptamolybdate (I9) and surface molybdenum loadings of 0.1, 0.3, 0.5, and 0.7 Mo/nm^2 are presented in Fig. 4.5, 4.6, 4.7, and 4.8, respectively. The broad features near 800, 600 and 500-300 cm^{-1} are due to the silica support. In addition, all the samples show the Raman band near 980 cm^{-1} under dehydrated conditions prior to exposure to the methanol oxidation reaction conditions. During methanol oxidation, the Raman band of the dispersed surface molybdenum oxide species shifts to ca. 963 cm^{-1} and, in addition, new Raman bands near 894, 842, 768, 411, 347, 305, and 279 cm^{-1} appear. The new bands become more pronounced with increasing Mo loadings. These changes in the Raman spectra occurred as soon as the catalysts were exposed to the reaction environment. The Raman spectra in Figs. 4.5 - 4.8 were taken after 30 min of methanol oxidation. Switching from the methanol oxidation reaction conditions to the dehydrated conditions shifts the Raman band at 963 cm^{-1} to ca. 970

cm^{-1}, but does not alter the new Raman bands near 894, 842, 768, 411, 347, 305, and 279 cm^{-1}. These new Raman bands correspond to crystalline β-MoO_3 which is a low temperature structure of crystalline MoO_3 [40]. Further treatment of β-MoO_3 in oxygen at 773 K results in the appearance of sharp Raman bands at 991, 816, 662 , 334, 284, and 150 cm^{-1} which are due to orthorhombic crystalline α-MoO_3 (see Fig. 4.6d). Thus, the surface molybdenum oxide species on silica is not stable under methanol oxidation reaction conditions at surface densities greater than ca. 0.1 Mo/nm^2. Furthermore, even α-MoO_3 crystals initially present for loadings above 0.5 Mo/nm^2 are also unstable during methanol oxidation and are completely transformed to crystalline β-MoO_3 (see Fig. 4.8).

4.4.3. Methanol oxidation

The oxidation of methanol produced mainly formaldehyde and methyl formate. Minor amounts of carbon oxides were detected, and the production of dimethyl ether remained very low for most of the samples. The results for methanol oxidation on the different Mo/SiO_2 catalysts are presented in Figs. 4.9a-4.9d as a function of the surface molybdenum oxide loading. Table 4.3 identifies every sample by its initial surface molybdenum coverage, preparation method, and apparent TOF in order to facilitate identification of the different samples. An increase in the molybdenum loading generally results in a significant decrease of the apparent TOF and this is most pronounced in the case of the TOF toward methylformate. The apparent formaldehyde TOF decreases smoothly with Mo coverage and dimethyl ether production is generally low for all the molybdenum loadings studied. The dimethyl ether produced on several of the catalysts is probably the consequence of some trace acid impurities in the silica (G2a, G4, and I8). The ability to plot all the methanol oxidation catalytic data, obtained from different sources and preparation methods, essentially on a single curve as a function of Mo surface density suggests that the Mo surface coverage is the critical parameter in determining the catalytic properties of silica-supported molybdenum oxide catalysts. A similar conclusion has recently been reported by Williams and Ekerdt [24].

The catalysts show an initial transient period when the reaction is started. During this transition period, there is a very slight increase in activity and change in the selectivities to formaldehyde and methyl formate that depends on molybdenum oxide loading. The evolution of the ratio of the apparent TOF to formaldehyde *vs.* the apparent TOF to methyl formate for the same catalysts, which were characterized by ***in situ*** Raman spectroscopy during methanol oxidation, is shown in Fig. 4.10. The sample with the lowest surface molybdenum oxide loading (0.1 Mo/nm^2) does not show any transient behavior in the selectivity. However, the catalysts with the higher molybdenum oxide loadings (0.3 and 0.4 Mo/nm^2) exhibit an initial decrease in formaldehyde production and an initial increase in methylformate production.

4.5. DISCUSSION

4.5.1. Effect of preparation methods and specific support

The Raman spectra of the dehydrated samples presented in the results section demonstrate that the preparation method as well as the specific silica support does not appear to affect the structure of the silica-supported molybdenum oxide species. Only the presence of impurities in the silica support was found to affect the nature of the surface molybdenum oxide species. The present results suggest that the apparent discrepancies in the literature between different research groups studying the MoO_3/SiO_2 system are not due to different samples, but seem to be related to the different characterization methods with regard to spectral assignments.

The isolated surface molybdenum oxide species have been reported by most authors, but there is still disagreement as to whether this species is present as mono-oxo (octahedral) or dioxo (tetrahedral). Mono-oxo MoO_6 structures have been assigned from Raman spectroscopy [5,11,23], IR [25,26], and EXAFS/XANES [5]. *In situ* Raman and IR studies of the same MoO_3/SiO_2 sample by de Boer *et al.* [5,26] yield identical Mo=O vibrations at 986 cm^{-1}. This observation is significant since according to Raman/IR vibrational selection rules this coincidence should occur only for mono-oxo species [27]. This conclusion is further supported by ^{18}O-^{16}O isotope experiments that yield only two vibrational peaks consistent with mono-oxo species (dioxo species would be expected to yield three vibrational peaks) [25]. The isolated nature of the dehydrated surface molybdenum oxide species is supported by the absence of Mo-O-Mo vibrations at 220 cm^{-1} in Raman [5,11,28] and the extremely low Mo-Mo coordination ($SN_{Mo\text{-}Mo} = 0.30$) measured by EXAFS [5,26]. The highly distorted nature of the isolated MoO_6 unit is reflected in the pre-edge feature observed in the XANES spectra and the presence of a terminal Mo=O bond in Raman/IR.

The dioxo MoO_4 structures have been assigned from luminescence [29,30], UV-visible diffuse reflectance [29], ESR [29], and Raman spectroscopy [20]. Previous studies have demonstrated that UV-visible diffuse reflectance is not reliable in discriminating between MoO_4 and MoO_6 structures [11,31]. ESR can only detect Mo^{5+} species and it cannot be assumed that the same coordination is present for Mo(V) and Mo(VI) species on silica. The previous Raman spectroscopy study was reported on the same sample used in this study and the prior spectrum was not reproducible because of the adsorption of background moisture which affected the Raman features in the earlier investigation [32]. In the luminescence spectra, the assignment to a tetrahedral (dioxo) structure is based on the close agreement in the emission and excitation bands with those of the MoO_4^{2-} complex in the reference compound $CaMoO_4$ [14]. Calcium impurities observed in some of the samples could account for this, however, samples without $CaMoO_4$ (I1 and G2b) are also identified as dioxo by luminescence [4]. Unfortunately, octahedral molybdenum species possesses such a short lifetime that it is weakly detected by luminescence (approximately ten times weaker than tetrahedral molybdenum species [33]. Consequently, luminescence can be used to detect tetrahedral molybdenum oxide species, but may not give any information on the presence or absence of octahedral molybdenum oxide species. Thus, the evidence for concluding that dioxo MoO_4 species are present on the silica surface is not very strong.

Silica-attached molybdenum dimer structures have been reported to be obtained by reacting $Mo_2(\eta^3\text{-}C_3H_6)_4$ [12,34,35] with the OH groups of the silica support and activating in H_2 or in an inert atmosphere (N_2). The activation of allyl dinuclear molybdenum compounds in hydrogen has been proposed to result in dimeric structures of Mo(II) based on *in situ* EXAFS measurements [34]. After oxidation with molecular oxygen at 673 K, the Mo-Mo bond is not detected [34]. Two different structures have been claimed for the Mo(VI) oxide surface species depending on the specific silica support [34]. The silica supports employed (Snowtex-30, 120 m^2/g, SiO_2-1; and Snowtex-O, 285 m^2/g, SiO_2-2) had molybdenum loadings below 0.5 and 0.2 Mo/nm^2, respectively [35], which are well below the maximum dispersion limits of MoO_3/SiO_2 (~ 1 Mo/nm^2) and account for the homogeneity of the structures observed on each silica. On SiO_2-1, the Mo(VI) surface oxide species was reported to be tetrahedral dioxo molybdenum oxide monomers based on DRS-UV/VIS spectroscopy (band at 285 nm) of the dehydrated sample [35] and *in situ* EXAFS studies. On SiO_2-2, however, the observed DRS-UV/VIS spectrum shows a band at 306 nm characteristic of five- or six-coordinated Mo(VI) species. In addition, the XANES studies indicate that these species are highly distorted. This highly distorted structure is in agreement with the more recent XANES structures determined for samples prepared by impregnation of silica with Mo^{3+} solutions [5,26] or by impregnation of ammonium heptamolybdate solutions [21] on a different silica (Cab-O-Sil EH5).

The presence of different molybdenum oxide structures from the same precursor on different silicas is in contrast to the current findings that the specific silica support has no effect on the structure. However, the presence of impurities, especially basic, can influence the surface molybdenum structures [36]. Indeed, the presence of sodium impurities on SiO_2-1 is reported to be $< 0.5\%$ Na in a more recent work by the same authors [12]. This explains the structural differences observed between the Mo(VI) species on SiO_2-1 and SiO_2-2. We have found that even very low amounts of sodium (Na/Mo = 1/15 atomic ratio) will affect the catalytic activities and surface structures of the dehydrated Mo(VI) species on silica [36]. In the presence of alkali, the surface molybdenum oxide species react to form microcrystalline or molybdate phases containing tetrahedral MoO_4 species [11,36]. This effect will be even more pronounced in the case of preparations containing very low molybdenum loadings (from 0.6 to 1.5% MoO_3/SiO_2 on SiO_2-1) *(35)* since the Na/Mo atomic ratio varies from ~ 2 to 10. This high Na-to-Mo ratio accounts for the tetrahedral structure observed for molybdenum oxide on SiO_2-1.

On the sodium-free silica (SiO_2-2), no direct Mo-O-Mo bonding is observed above 200 K (dimeric surface molybdenum oxide species could be detected only at 80 K), but evidence is presented for the existence of two molybdenum oxide entities in close vicinity [12]. Similar results are reported on a third silica support (SiO_2-3, 510 m^2/g) [12]. This is most probably due to the dinuclear nature of the precursor which increases the probability of anchoring two Mo species in close proximity. It has recently been demonstrated with EXAFS and Raman spectroscopy that heptamolybdate clusters spread on the silica support upon dehydration resulting in dispersed, isolated mono-oxo molybdenum oxide species [5]. For these samples the molybdenum anchorage to the silica surface takes place at elevated temperatures, where the silanol population is significantly decreased and prevents the formation of molybdenum species in close vicinity. However, in the dimeric molybdenum-allyl samples the anchorage takes place at low temperatures and this may possibly account for their proximity with this preparation. More importantly, however, is that the XANES studies showed that the surface Mo(VI) structure on silica is the same from the allyl preparation and the samples used in the present study employing different preparation methods. The current study also found that the same surface Mo(VI) species was formed on silica from Raman spectroscopy when using the allyl preparation (Sample A4, Fig. 4.1). The preparation of derived dimeric molybdenum species could not be reproduced in the present study since dimeric features could not be detected in the EXAFS measurements of these samples taken by Iwasawa [51]. In fact, the synthesis of this dimeric species on silica has been attempted by several different research groups and all were unsuccessful [11,52,53]. Thus, it has been difficult to independently confirm that such a dimeric molybdenum oxide species can be formed on silica via the allyl preparation.

Formation of silicomolybdic acid in silica-supported molybdenum oxide samples has also been reported by several authors [8,38,44,45]. Our preliminary results show that silicomolybdic acid supported on silica is indeed formed at room temperature only after exposure to very moist air [38,46]. However, its formation requires a prolonged exposure to amounts of water larger than those present under standard ambient conditions. The silicomolybdic acid is stable at temperatures below 570 K [39] and it breaks up and spreads into isolated surface molybdenum oxide species when the temperature is higher than 570 K [38,46]. Thus, silicomolybdic acid formation requires special conditions which are usually not encountered in conventional studies and accounts for the absence of this species in most studies of the MoO_3/SiO_2 system. Actually, molybdenum oxide/silica samples prepared by Che *et al.* may have formed silicomolybdic acid during the washing step as well as samples prepared by impregnation of aqueous solutions of ammonium heptamolybdate. However, these samples are typically calcined above 570 K (see Table 4.2), which transforms the supported silicomolybdic acid to isolated surface molybdenum oxide species on silica.

An estimation of the degree of coverage of the surface molybdenum oxide species can be obtained from the increase in the intensity of the Mo=O Raman band at ca. 980 cm^{-1} with respect to the silica Raman band at 495 cm^{-1} since the silica band is essentially constant with molybdenum loading. This ratio is presented in Fig. 4.11 for the series of samples studied in Fig. 4.4. There is a linear increase of the Raman intensity at ~980 cm^{-1} with molybdenum loading at low coverages. The increase in the Raman intensity of the isolated surface molybdenum oxide species levels off at ca. 1 Mo/nm^2 since at this coverage there are very few available reactive silanol groups remaining which are required to stabilize the isolated surface molybdenum oxide species [2,23]. Consequently, additional isolated surface molybdenum oxide species would not be expected to form above ca. 1 Mo/nm^2 because of the unavailability of reactive silanol groups on the silica surface. A linear correlation between the molybdenum loading and the Raman shift of the Mo=O bond is also evident and is shown in Fig. 4.12. The Mo=O Raman band reaches a constant value at 990 cm^{-1} as a consequence of the onset of the crystalline orthorhombic MoO_3 at higher loadings. This scenario is in agreement with the appearance of a new Raman band at ca. 968 cm^{-1} which may represent a polymerized molybdenum oxide species such as a cluster [23] that cannot spread any more and may be the precursor to the formation of larger crystalline aggregates. This new molybdenum oxide species is different from the heptamolybdate species present in the hydrated state which gives a Raman band at ~945 cm^{-1} [11]. The availability of silanol groups is the determining factor for the dispersion of molybdenum oxide species on silica. The samples prepared by incorporation of Mo^{3+} and allyl-derivatives exhibit a somewhat lower wavenumber for the Mo=O bond than expected for the same loading from the samples prepared by impregnation. This may be indicative of a better local dispersion for these samples with respect to those prepared by impregnation. However, the estimation of the isolated surface molybdenum oxide species from the intensity of the Raman band at ca. 980 cm^{-1} fits well with the values obtained from the samples prepared by impregnation with ammonium heptamolybdate (Fig. 4.11). Catalyst I3 shows a much lower wavenumber for the very high molybdenum loading and the Raman band at 968 cm^{-1} is unusually pronounced for this sample. This Raman band is associated with the silica support since hydration treatments have no effect on this Raman band. Despite its very high surface molybdenum coverage, 2.3 Mo/nm^2, no aggregated molybdenum oxide species are observed. The high dispersion on this silica is achieved because of the high number of silanol groups present in this sample which resulted from the special low-temperature silica synthesis [13]. This is in agreement with the importance of availability of silanol groups in the formation of the dispersed surface molybdenum oxide species [2,23]. Consequently, the availability of reactive silanol groups for a specific molybdenum oxide loading is significantly higher for this sample than for the other silicas prepared or synthesized at elevated temperatures.

4.5.2. Methanol oxidation over MoO_3/SiO_2 catalysts

The selective oxidation of methanol on the silica supported molybdenum oxide samples, presented in Fig. 4.9, shows a continuous decrease in the apparent TOF for methanol oxidation with increasing molybdenum surface coverage for all the samples studied. The decrease in methanol conversion with surface molybdenum oxide coverage is mainly due to the sharp decrease in the apparent TOFs to methyl formate formation, and the apparent TOF for HCHO shows a smoother decrease with molybdenum oxide loading. The trends presented here essentially depend only on the surface molybdenum oxide coverage, and are essentially independent of preparation method and specific SiO_2 support. The product formation trends agree with the mechanistic model proposed by Che and co-workers [4]. There are two active sites in the oxidation of methanol over silica-supported catalysts: surface molybdenum oxide sites and silanol groups. Surface molybdenum oxide sites which interact with methanol form HCHO that may desorb or further interact with another methanol molecule anchored on the silanol groups of the silica surface resulting in the formation of methyl formate. The increase in the surface molybdenum coverage has a negative effect on the formation of methyl formate since the surface molybdenum oxide species aggregates to crystalline β-MoO_3. These effects account for the significant decrease in methanol conversion to methyl formate which requires both adjacent sites. It is interesting to note that the surface molybdenum oxide species on silica prepared by impregnation with ammonium heptamolybdate at very low coverages result in an activity very similar to that of samples prepared by grafting at similar surface molybdenum oxide loading. The grafting method is limited by the washing step, which eliminates most of the molybdenum and prevents high molybdenum loadings [37]. Consequently, the high activities reported for grafted samples toward methyl formate may be due primarily to the lower Mo loadings rather than to the preparation method. The reactivity trends observed for methanol conversion to formaldehyde also do not show any dependence on the preparation method, but also depend only on the molybdenum oxide surface coverage. The very high silanol population in sample I3 accounts for the very high selectivity to methyl formate observed (no formaldehyde is detected for this sample), according to the above mechanistic model.

The presence of basic impurities results in a lower TOF for the partial oxidation of methanol [37,24] due to the formation of alkali molybdates [11] with different redox properties [37]. In the case of the sample A4, where traces of sodium were found as impurities by XPS, no sodium molybdates were detected by Raman spectroscopy and the methanol oxidation results followed the expected trends. In sample G2b, however, Ca impurities were measurable by XPS and the presence of $CaMoO_4$ was observed by Raman spectroscopy. On the other hand, its homologue (G2a), prepared by the same group in a different batch, possessed no Ca-impurities as measured by XPS, and $CaMoO_4$ was not detected by Raman spectroscopy. The absence/presence of $CaMoO_4$ in these two samples results in different catalytic properties for the selective oxidation of methanol. The Ca-free sample (G2a) exhibited a high activity to methyl formate, as already reported [2], and the activity to methyl formate was significantly decreased by the presence of calcium impurities.

4.5.3. Agglomeration of surface molybdenum oxide species during methanol oxidation

The *in situ* methanol oxidation studies revealed that the surface molybdenum oxide species are not stable, for catalysts containing high surface Mo densities during methanol oxidation and agglomerated to crystalline β-MoO_3. The extent of agglomeration increased with Mo loading. When the dehydrated sample is exposed to methanol oxidation conditions, a significant shift in the Raman band at 980 cm^{-1}, characteristic of the surface molybdenum oxide species, to ca. 963 cm^{-1} is observed. This could be due to interaction with the methoxide groups [48] which alters the length of the Mo-O bond and, therefore, its frequency [54]. It is interesting to note that the Raman band at ca. 980 cm^{-1} is not affected during the selective oxidation of methane at 823 K [36], though water is formed, and no aggregation of the surface molybdenum oxide species is observed during the reaction [55]. In addition, the presence of water at temperatures higher than 373 K does not affect the Raman band of the isolated surface molybdenum oxide species and no aggregation is observed [46]. Thus, the interaction between the surface molybdenum oxide species and methanol must be the driving force for the aggregation into β-MoO_3. The fact that silicomolybdic and phosphomolybdic acids are converted to β-MoO_3 during methanol oxidation [56] provides further evidence for this model.

Another important factor associated with the aggregation of the surface molybdenum oxide species into crystalline β-MoO_3 is the volatilization of the active phase. Volatilization of aggregated crystalline molybdenum oxide (α-MoO_3) is higher than that of dispersed surface molybdenum oxide species [41,42], and its volatilization is further promoted in the presence of water [42,43] which is produced during the oxidation of methanol. The present work shows that increasing molybdenum loadings result in increasing degrees of aggregation of the surface molybdenum oxide species into β-MoO_3. This behavior parallels the higher volatility observed at higher loadings of molybdenum oxide on silica.

The extent of agglomeration of surface molybdenum oxide species can be estimated from the comparison of the apparent TOFs of the surface molybdenum oxide species and β-MoO_3. The true TOF for the dispersed surface molybdenum oxide species can be determined from the samples possessing the lowest molybdenum loadings in Table 4.4, 0.1 Mo/nm^2 where only a trace of β-MoO_3 is formed (Fig. 4.5), and corresponds to approximately $7 - 10\times10^{-2}$ s^{-1}. The true TOF for bulk α-MoO_3 powder was measured and found to be approximately 2×10^{-2} s^{-1} [48]; Chowdhry *et al.* [49] demonstrated that β-MoO_3 is about 2-3 times more active than α-MoO_3 [49-51], which gives a TOF of $4 - 6\times10^{-2}$ s^{-1} for β-MoO_3. The similar true TOFs for surface molybdenum oxide species on silica and β-MoO_3 suggest that the decrease in the apparent TOF is directly due to a lower fraction of exposed molybdenum sites because of agglomeration. The estimated dispersions for the silica-supported molybdenum oxide catalysts during methanol oxidation are presented in the seventh column of Table 4. The few catalysts that produced significant amounts of DME were omitted from these calculations since this acid product is not associated with the molybdenum oxide sites. The estimated calculations suggest that the molybdenum oxide dispersion decreased from approximately

100 to ca. 4% during steady state methanol oxidation as the Mo loading was increased. The formation of $HCOOCH_3$ for all Mo loadings suggests that either some surface molybdenum oxide species were still present or the microcrystalline β-MoO_3 particles interacted with adjacent surface silanols since unsupported bulk MoO_3 does not produce $HCOOCH_3$. Sample I3, which possesses a high surface density of silanols, again behaved differently, yielding almost exclusively $HCOOCH_3$.

The initial methanol oxidation catalytic studies showed that the catalysts with high surface Mo densities experienced a decrease in the $H_2CO/HCOOCH_3$ selectivity ratio during the first 30 min. The corresponding *in situ* Raman studies revealed that the transformation of the surface molybdenum oxide species to microcrystalline β-MoO_3 occurred as soon as the catalysts were exposed to the methanol/oxygen reaction environment and essentially did not significantly change with time. The decrease in initial $H_2CO/HCOOCH_3$ selectivity corresponds to an increase in the number of the surface molybdenum oxide species on the silica support. This suggests that a small amount of Mo from the β-MoO_3 microcrystals was being redispersed via volatilization. The absence of any initial selectivity changes for the 0.1 Mo/nm^2 catalyst is consistent with this conclusion since essentially no crystalline β-MoO_3 was formed on this catalyst and high density Mo/SiO_2 catalysts possessing crystalline β-MoO_3 exhibited this transient behavior. Thus, the molybdenum oxide in the MoO_3/SiO_2 catalyst can be both agglomerated and redispersed by exposure to the methanol oxidation reaction environment.

4.6. CONCLUSIONS

The preparation of silica-supported molybdenum oxide catalysts at low coverages by impregnation with an aqueous solution of ammonium heptamolybdate, Mo^{3+}, or grafting of $MoCl_5$ followed by washing results in the same surface molybdenum oxide species. The molecular structure of the surface molybdenum oxide species on silica is most likely that of an isolated, distorted mono-oxo MoO_6 species. The formation of dimeric molybdenum oxide species derived from allyl compounds is not observed. The formation of new molybdenum oxide compounds on silica is due to the presence of basic impurities like calcium or sodium. The selective oxidation of methanol is a sensitive probe reaction to study silica-supported molybdenum oxide catalysts. The surface molybdenum oxide coverage on silica and the availability of reactive silanol groups are the only factors affecting the nature of the surface molybdenum oxide species and the corresponding catalytic activity during methanol oxidation over the MoO_3/SiO_2 catalysts. Dispersed surface molybdenum oxide species aggregate during methanol oxidation into crystalline β-MoO_3 and the extent of agglomeration increases with surface Mo density. The methanol oxidation apparent TOF decreases proportionally to the number of expose Mo sites because the true TOFs for the surface molybdenum oxide species and supported β-MoO_3 are very similar: $7 - 10\times10^{-2}$ s^{-1} and $4 - 6\times10^{-2}$ s^{-1}, respectively.

REFERENCES

1. Ono, T., Anpo, M., and Kubokawa, Y. , *J. Phys. Chem.* **90**, 4780 (1986).

2. Liu, T-C., Forissier, M., Coudurier , G., and Védrine, J. C., *J. Chem. Soc., Faraday Trans. 1* **85**, 1607 (1989).
3. Giordano, N. ,Meazzo, M., Castellan, A., Bart, J. C., and Ragaini, V., *J. Catal.* **50**, 342 (1977).
4. Louis, C., Tatibouët, J. M., and Che, M., *J. Catal.* **109**, 354 (1988).
5. de Boer, M., van Dillen, A.J., Koningsberger, D.C., Geus, J. W., Vuurman, M.A., and Wachs, I.E., *Catal. Lett.* **11**, 227 (1991).
6. Spencer, N. D., Pereira, C. J., and Grasselli, R. K., *J. Catal.* **126**, 546 (1990).
7. Bañares, M. A. , Fierro, J. L. G., and Moffat, J. B., *J. Catal.* **142**, 406 (1993).
8. Barbaux, Y., Elamrani, A. R., Payen, E., Gengembre, L., Bonnelle, J. P., and Grzybowska, B., *Appl. Catal.* **44**, 117 (1988).
9. Che, M., Louis, C., and Tatibouët, J. M.,*Polyhedron* **5**, 123 (1986).
10. Desikan, A. N., and Oyama, S. T., *J.Chem.Soc., Chem. Commun.* **88**, 3357 (1992).
11. Williams, C. C., Ekerdt, J. G., Jehng, J.-M., Hardcastle, F. D., Turek, A. M., and Wachs, I. E., *J. Phys. Chem*, **95**, 8781 (1991).
12. Iwasawa, Y., *Adv. Catal.* **35**, 265 (1987).
13. Srinivasan, S., and Datye, A. K., *Catal. Lett.* **15**, 155 (1992).
14. Hazenkamp, M. F., Thesis, University of Utrecht, The Netherlands,1992.
15. Louis, C., Che, M., and Anpo, M., *J. Catal.*, **141**, 453 (1993).
16. Yermakov, Y. I., *Catal. Rev. Sci. Eng.* **13**, 77 (1976).
17. Zhuang, Q., Fukoka, A., Fujimoto, T., Tanaka, K., and Ichikawa, M., *J. Chem. Soc., Chem. Comm.* **11**, 745 (1991).
18. Ichikawa, M., Zhuang, Q., Li, G-J., Tanaka, K., Fujimoto, T., and Fukoka, K., In "New Frontiers in Catalysis", Guczi, L. Ed. *Stud. Surf. Sci. Catal.* **75(A)**, 529 (1992).
19. Kim, D. S., Tatibouët, J. M., and Wachs, I. E., *J. Catal.* **136**, 209 (1992).
20. Desikan, A. N., Huang, L., and Oyama, S. T., *J. Phys. Chem.* **95**, 10050 (1991).

21. Hu, H., Wachs, I. E., and Bare, S. R., to be submitteded.

22. Machej, T., Haber, J., Turek, A. M., and Wachs, I. E., *Appl. Catal.* **70**, 115 (1991).

23. Roark, R. D., Kohler, S. D., Ekerdt, J. G., Kim, D. S., and Wachs, I. E., *Catal. Lett.*, **16**, 77 (1992).

24. Williams, C. C., and Ekerdt, J. G., *J. Catal.* **141**, 430 (1993).

25. Cornac, M., Janin, A., and Lavalley, J. C., *Polyhedron* **5**, 183 (1986).

26. de Boer, M. Ph. D. Thesis, University of Utrecht, The Netherlands, 1992.

27. Cristiani, C., Forzatti, P., and Busca, G., *J. Catal.* **116**, 586 (1989).

28. Roark, R. D., Kohler, S. D., and Ekerdt, J. G., *Catal. Lett.* **16**, 71 (1992).

29. Louis, C., and Che, M., *J. Phys. Chem.* **91**, 2875 (1987).

30. Anpo, M., Kondo, M., Coluccia, S., Louis, C., and Che, M., *J. Am. Chem. Soc.* **111**, 8191 (1989).

31. Fournier, J., Louis, C., Che, M., Chaquin, P., and Masure, D., *J. Catal.* **119**, 400 (1989).

32. Oyama, S. T., personal communication.

33. Wiegel, M., and Blasse, G., *J. Solid State Chem.* **99**, 388 (1992).

34. Iwasawa, Y., In "Tailored Metal Catalysts" Iwasawa, Y., Ed. Reidel Dordrecht, 1986.

35. Iwasawa, Y., and Yamagishi, M., *J. Catal.* **82**, 373 (1983).

36. Bañares, M. A., Jones, M. D., Spencer, N. D., and Wachs, I. E., *J. Catal.* **146**, 204 (1994).

37. Louis, C., and Che, M., *J. Catal.* **135**, 156 (1992).

38. Rodrigo, L., Marcinkowska, K., Adnot, A., Roberge, P. C., Kaliaguine, S., Stencel, J. M., Makovsky, L. E., and Diehl, J. R., *J. Phys. Chem.* **90**, 2690 (1986).

39. Rocchiccioli-Deltcheff, C., Amirouche, M., Che, M., Tatibouët, J. M., and Fournier, M., *J. Catal.* **125**, 292 (1990).

40. McCarron, E. M. III, *J. Chem. Soc., Chem. Commun.* 336 (1986).

41. Hu, H., and Wachs, I. E., unpublished results.

42. Liu, D., Zhang, L., Yang, B., and Li, J., *Appl. Catal. A* **124**, 349 (1993).

43. Leyrer, J., Mey, D., and Knözinger, H., *J. Catal.* **124**, 349 (1990).

44. Castellan, A., Bart, J. C. J., Vaghi, A., and Giordano, N., *J. Catal.* **42**, 162 (1976).

45. Kasztelan, S., Payen, E., and Moffat, J. B., *J. Catal.* **112**, 320 (1988).

46. Bañares, M. A., Hu, H., and Wachs, I. E., in preparation.

47. Kim, D. S., Wachs, I. E., and Segawa, K., *J. Catal.* **146**, 268 (1994).

48. Farneth, W. E., McCarron E. M. III, Sleight, A. W., and Staley, R. H., *Langmuir* **3**, 217 (1987).

49. Chowdhry, U., Ferreti, A., Firment, L. E., Machiels, C. J., Ohuchi, F., Sleight, A. W., and Staley, R. H., *Appl. Surf. Sci.* **19**, 360 (1984).

50. Machiels, C. J., Cheng, W. H., Chowdhry, U., Farneth, W. E., Hong, F., McCarron, E. M. III, Sleight, A. W., *Appl. Catal.* **25**, 249 (1986).

51. Iwasawa, Y., personal communication.

52. Roberge, P. C., personal communication.

53. Hall, W. K., personal communication.

54. Hardcastle, F. D., and Wachs, I. E., *J. Raman Spectrosc.* **21**, 683 (1990).

55. Sun, Q., Klier, K., and Wachs, I. E., unpublished results.

56. Fournier, M., Aoussi, A., and Rocchiccioli-Deltcheff, C., *J. Chem. Soc., Chem. Commun.* 307 (1994).

Table 4.1. Classification of the Silica-Supported Molybdenum Oxide Catalysts Studied

Group	Preparation[a]	Molecular Characterization			Ref	Series code
		Technique	Conditions	Proposed structure		
1 Blasse	AHM	Photo luminescence	Vacuum	Dioxo	*(14)*	I1
2 Che[b]	Grafting	Photo luminescence ESR	Vacuum	Dioxo	*(4)*	G2a G2b
3 Datye	AHM	T.E.M.	Vacuum	Dispersed	*(13)*	I3
4 Ekerdt	Allyl	Raman IR NMR	*In situ*	Mono-oxo	*(11)*	A4
Ekerdt	Grafting	Raman IR NMR	*In situ*	Mono-oxo	*(11)*	G4
5 Fierro	AHM	XPS NO adsorption Raman	Ambient	Dispersed	*(7)*	I5
6 Geus	Mo^{3+}	EXAFS Raman IR	*In situ*	Mono-oxo	*(5)*	E6
7 Oyama	AHM	Raman	*In situ*	Dioxo	*(20)*	I7
8 Spencer	AHM				*(6)*	I8
9 Wachs	AHM	Raman	*In situ*	Mono-oxo	*(21)*	I9

a: AHM is impregnation with aqueous solutions of $(NH_4)_2Mo_7O_{24}\cdot 4H_2O$; Grafting is by reacting $MoCl_5$ with silica silanol groups; Allyl is by reaction of silica silanol groups with molybdenum ally derivatives and Mo^{3+} is impregnation of Mo^{3+} aqueous solutions.

b: Samples from two different batches were supplied by this group and are identified as G2a and G2b.

Table 4.2 . Some Characteristics of the MoO_3/SiO_2 Catalysts

Sample	Preparation method	Silica support	Calcination Temp. (K)	Silica BET surface Area (m^2/g)	Ref
I1	AHM impregnation	Degussa Aerosil-200	798	180	*(14)*
G2	$MoCl_5$	Rhône-Poulenc XOA-400	773	400	*(4)*
I3	AHM mpregnation	Strobe	573	<20	*(13)*
A4	Allyl compounds	Davidson-952^a	773	280	*(11)*
G4	$MoCl_5$	Davidson-952^a	773	280	*(11)*
I5	AHM impregnation	Degussa Aerosil-200	873	180	*(7)*
E6	Mo^{3+}	Degussa Aerosil-200	723	180	*(5)*
I7	AHM Impregnation	Cab-O-Sil		90	*(20)*
I8	AHM Impregnation	Cab-O-Sil M5^a	873	185	*(6)*
I9	AHM Impregnation	Cab-O-Sil EH5	773	380	*(21)*

a: Acid washed to remove impurities.

Table 4.3. Molybdenum Oxide Loading and Nominal Surface Molybdenum Oxide Coverage on the Specific Silica Supports.

Series Code	% MoO_3/SiO_2	Mo/nm^2 [a]
I1	0.62	0.1
G2a	1.31	0.1
G2b	1.29	0.1
I3	0.38	2.3
A4	2.90	0.7
G4	1.31	0.2
I5	1.40	0.3
	3.70	0.8
	6.01	1.3
E6	5.40	1.0
I7	0.98	0.5
I8	2.72	0.5
I9	1.0	0.1
	3.0	0.31
	4.0	0.42

a: The surface molybdenum loading has been calculated assuming a complete dispersion of the molybdenum oxide species on the surface of the silica support which is supported by the Raman characterization studies below.

Table 4.4. Methanol Oxidation at 503 K

	Apparent TOF (10^{-2} s^{-1})					Steady state	Series
Mo/nm^2	CH_3OH	HCHO	DME	$HCOOCH_3$	Ref.	%dispersion	code
0.1	7.8	1.7	1.8	0.7	*(4)*	-	G2b
0.1	10.0	1.5	0.1	4.0	*(4)*	100	G2a
0.1	7.0	1.5	0.1	2.2	*(21)*	-	I9
0.2	8.7	1.9	0.8	2.3	*(11)*	87	G4
0.3	3.6	0.7	0.6	0.9	*(21)*	36	I9
0.3	3.0	0.7	tr	0.9	*(7)*	30	I5
0.4	1.0	0.4	0.1	0.3	*(21)*	10	I9
0.5	3.8	1.6	0.6	0.4	*(6)*	-	I8
0.5	1.1	0.1	tr	0.5	*(20)*	38	I7
0.7	2.6	1.1	0.1	0.6	*(11)*	26	A4
0.8	1.4	0.4	tr	0.4	*(7)*	14	I5
1.0	0.9	0.3	tr	0.2	*(5)*	9	E6
1.3	0.5	0.1	tr	0.1	*(7)*	5	I5
2.3	0.4	0.0	tr	0.1	*(18)*	4	I3

Reaction conditions: 503 K, 0.01724 mol CH_3OH /h in 50 mg catalyst.

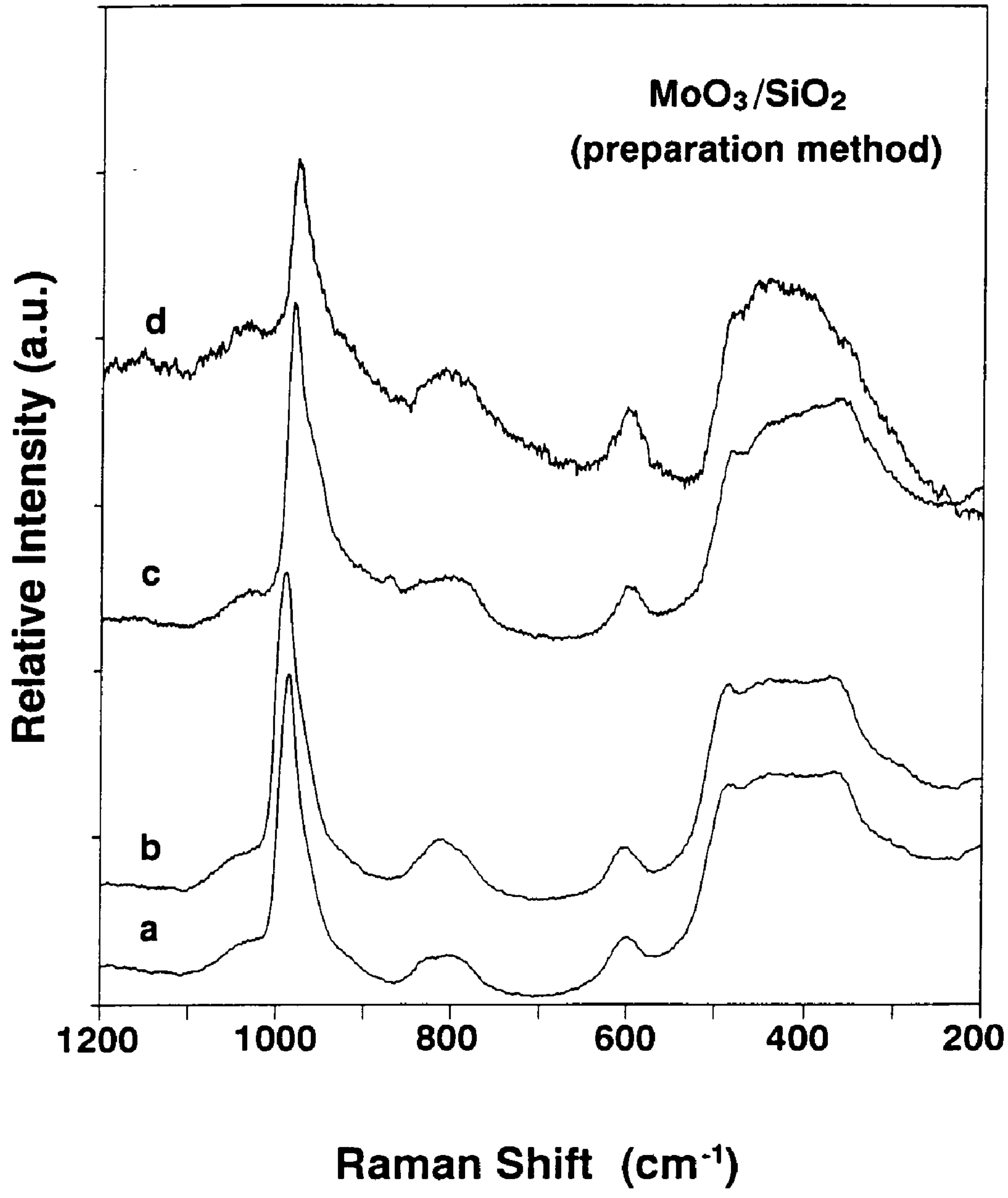

Fig. 4.1. *In situ* Raman spectra of dehydrated silica-supported molybdenum oxide catalysts prepared by (a) impregnation with Mo^{3+} solutions on Degussa Aerosil 200 silica, E6; (b) impregnation with AHM aqueous solutions on Degussa Aerosil 200 silica, I5; (c) allyl derivatives on Davidson-952 silica, A4; and (d) grafting on Davidson-952 silica, G4.

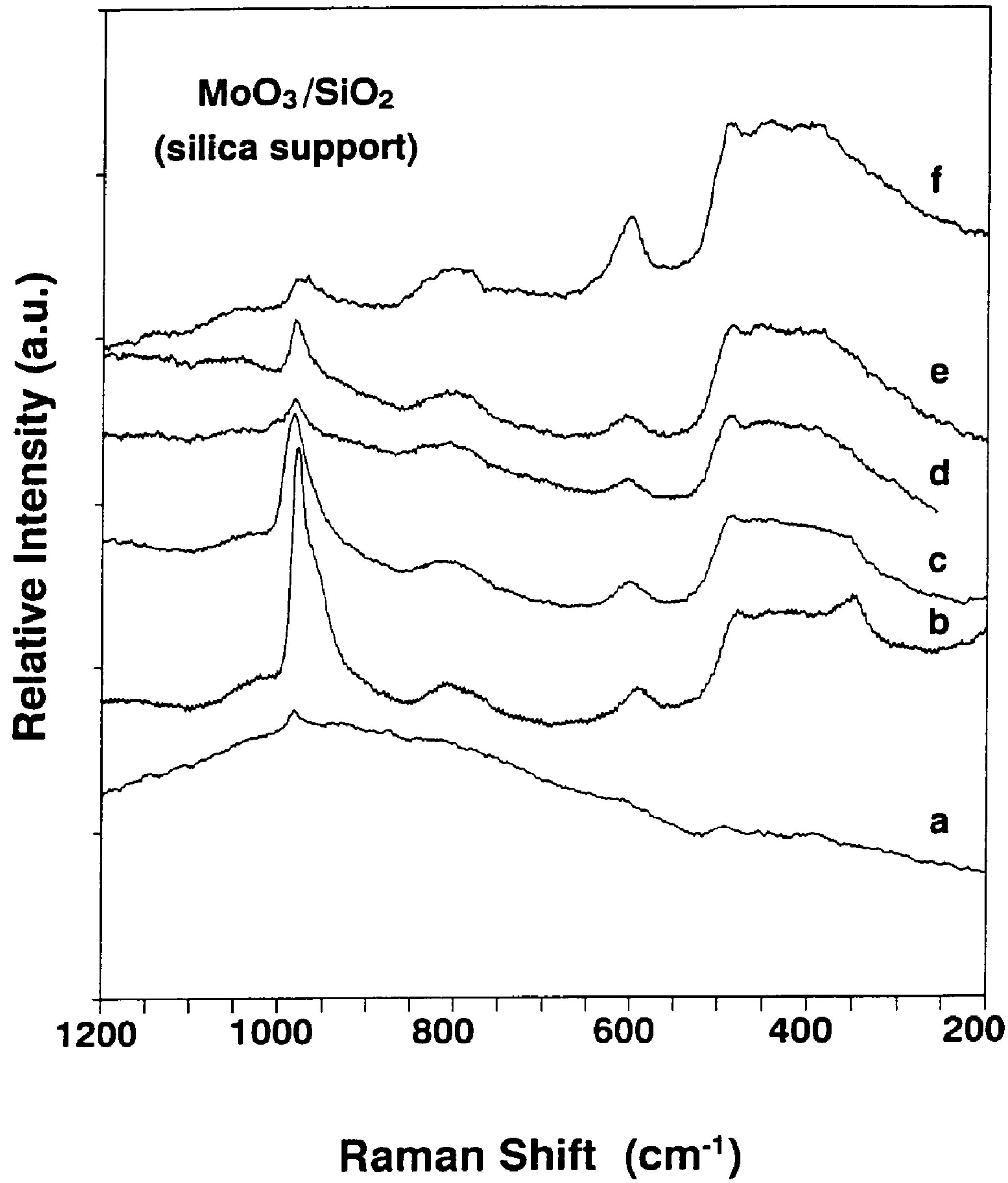

Fig. 4.2. *In situ* Raman spectra of dehydrated silica-supported molybdenum oxide catalysts (a) on Rhône-Poulenc XOA-400 silica, 400 m^2/g (G2a); (b) on Cab-O-Sil EH5 silica, 380 m^2/g (I9); (c) on Cab-O-Sil M5 silica, 185 m^2/g (I8); (d) on Cab-O-Sil silica, 90 m^2/g (I7); (e) on Degussa Aerosil-200 silica, 180 m^2/g (I1); and (f) on Strobe silica, < 20 m^2/g (I3).

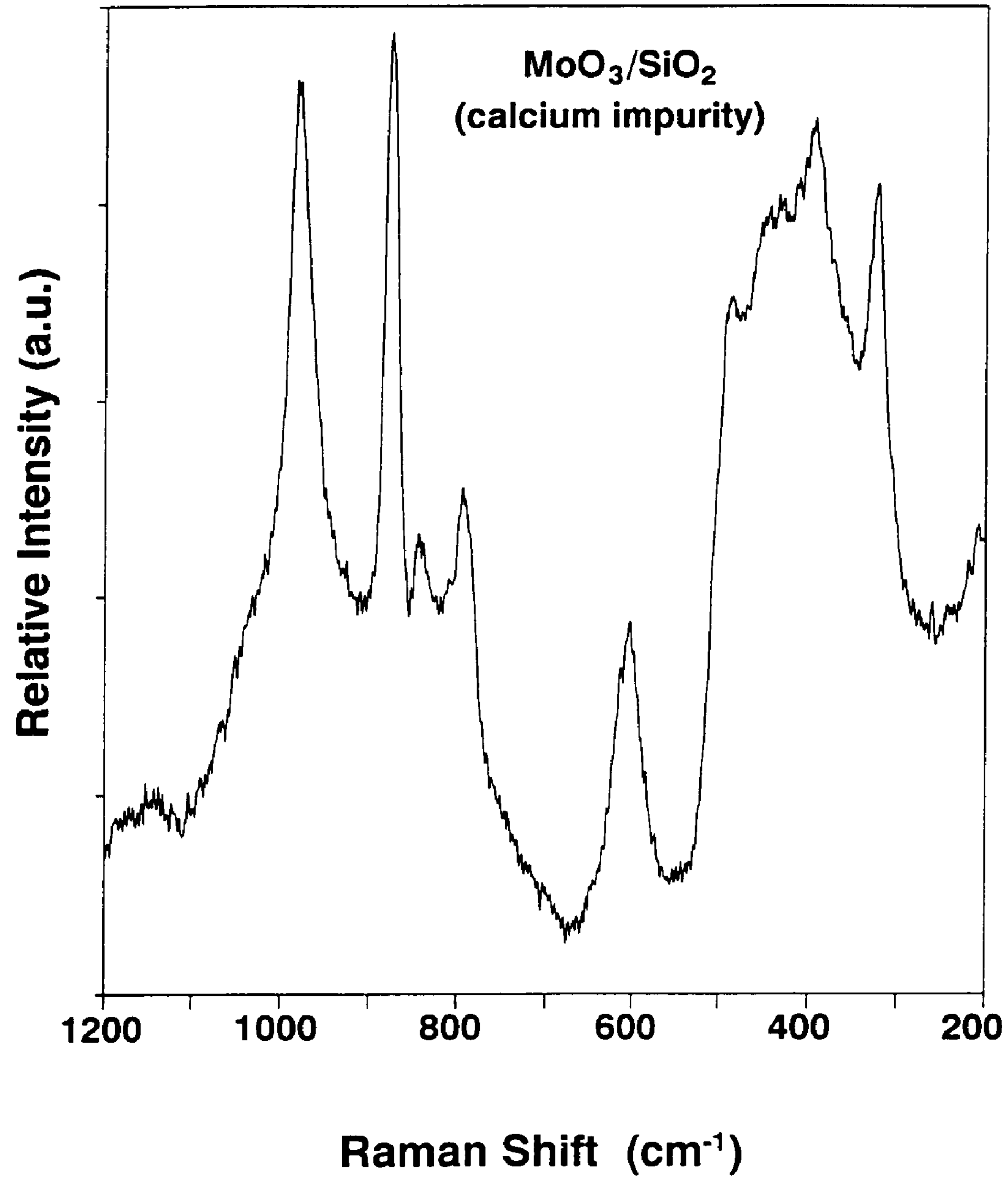

Fig. 4.3. Effect of calcium impurities on the molecular structures of dehydrated silica-supported surface molybdenum oxide species by means of *in situ* Raman spectroscopy of the dehydrated samples supported on Rhône-Poulenc XOA-400 silica with Ca impurities (G2b).

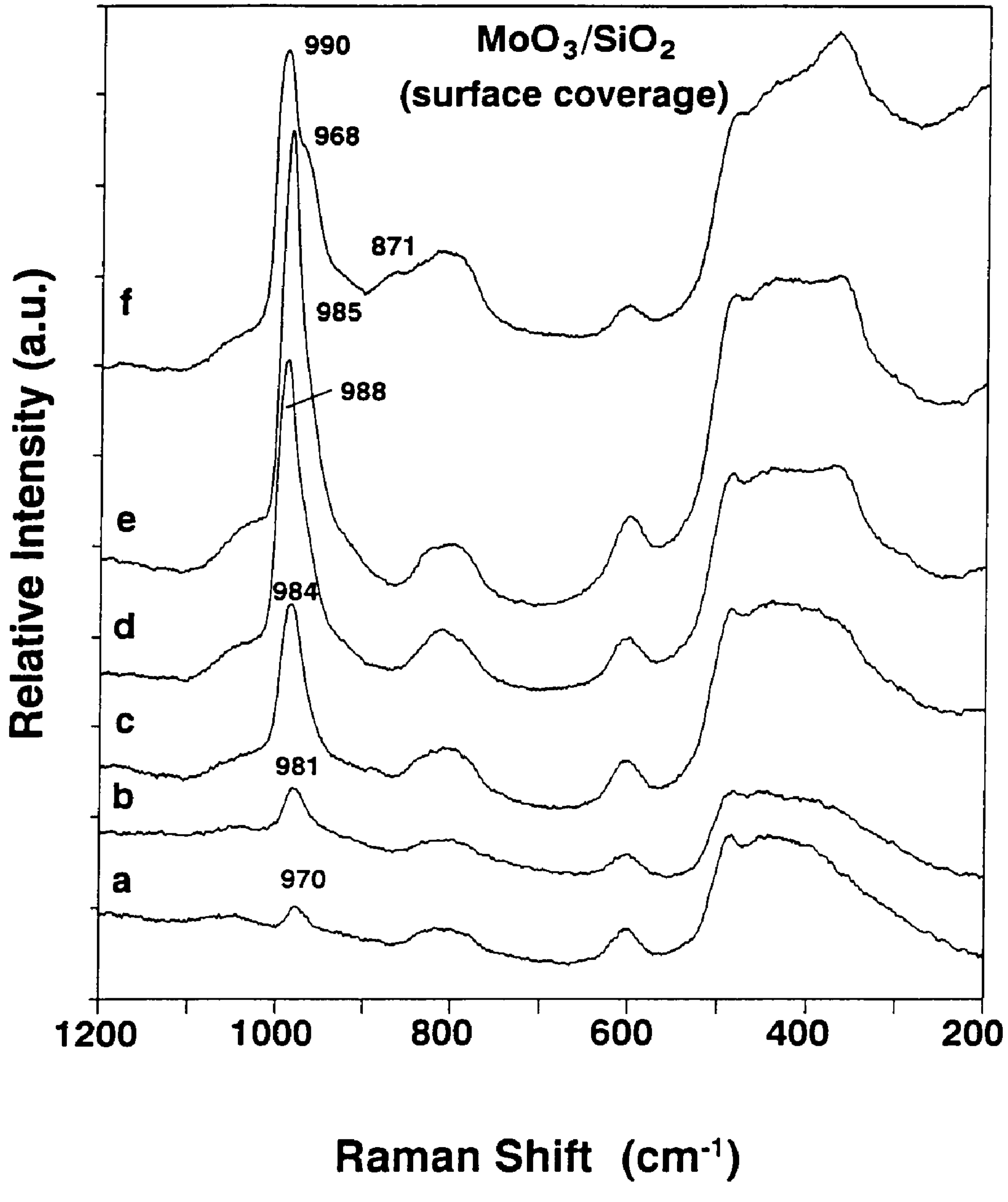

Fig. 4.4. *In situ* Raman spectra of the Degussa Aerosil 200 silica support and of the dehydrated silica-supported molybdenum oxide catalysts of the series I5 and E6 with surface molybdenum loadings of 0.3, 0.5, 0.8, and 1.3 Mo/nm^2 in series I5 and 1.0 Mo/nm^2 in series E6. (a) Aerosil 200; (b) 0.3I5; (c) 0.5I5; (d) 0.8I5; (e) 1.0E6; (f) 1.3I5.

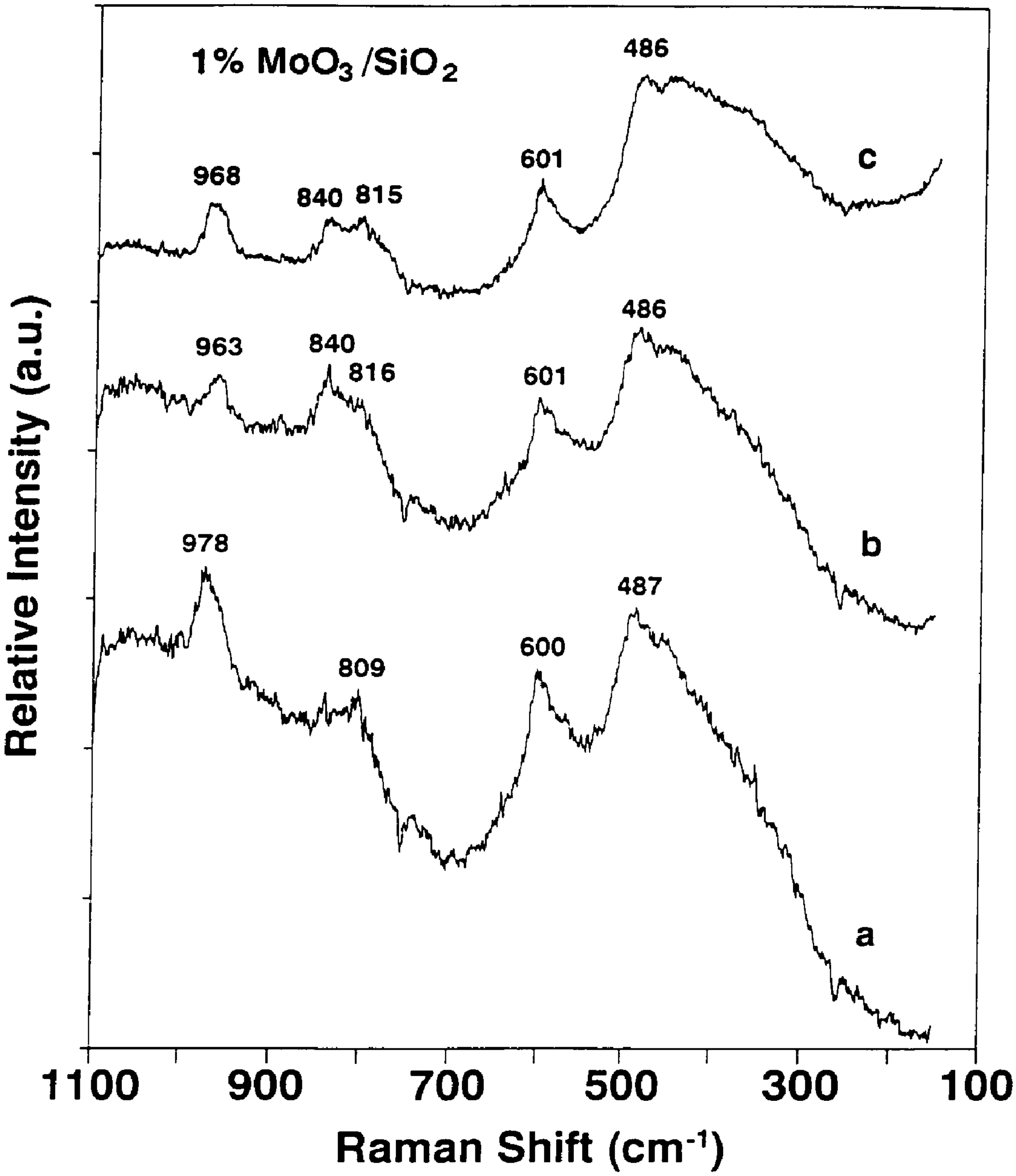

Fig. 4.5. *In situ* Raman spectra in reaction cell of catalysts I9 with 0.1 Mo/nm^2. a) dehydrated conditions, 503 K; b) methanol oxidation at 503 K; and c) dehydrated conditions after reaction, 503 K.

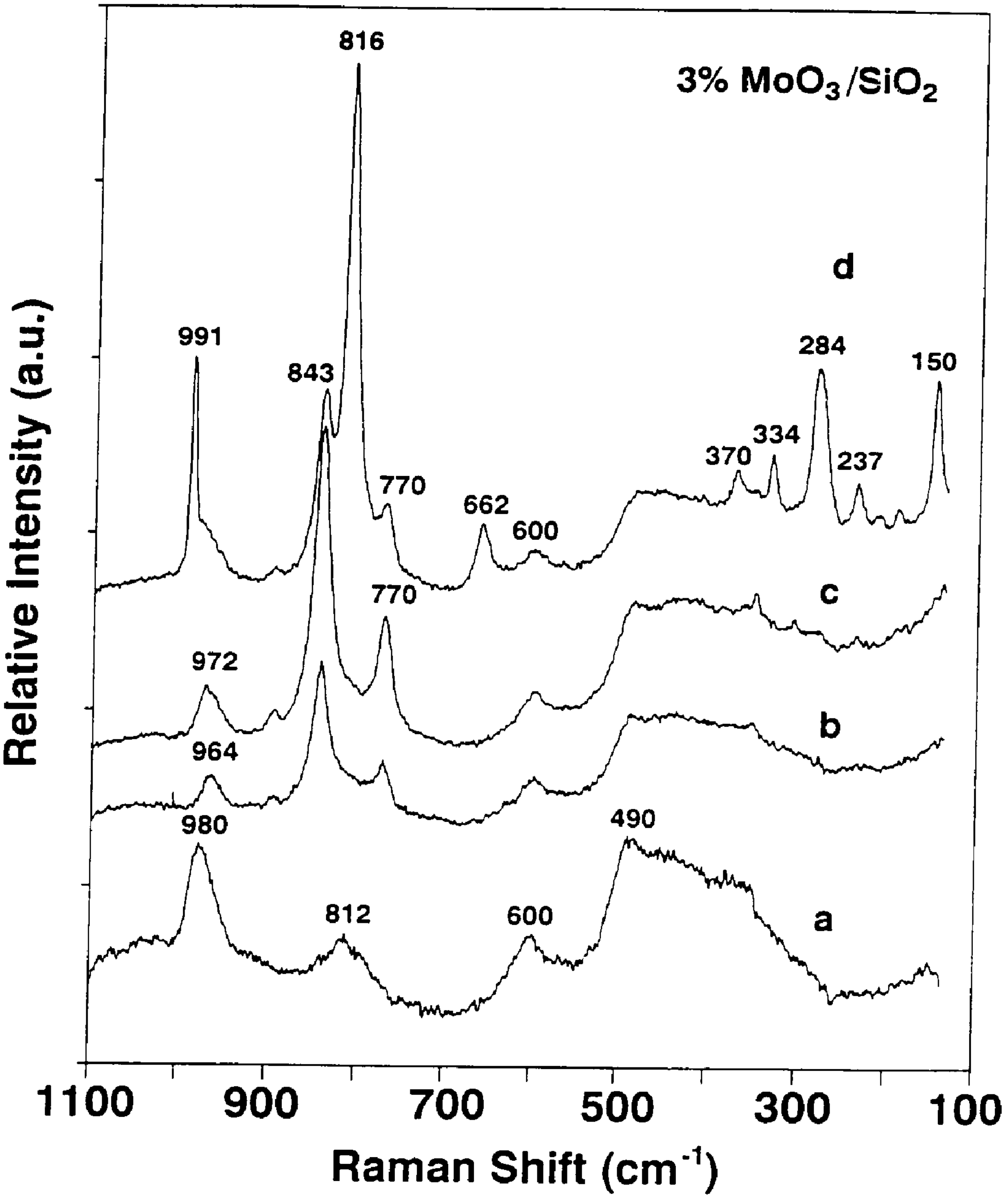

Fig. 4.6. *In situ* Raman spectra in reaction cell of catalyst I9 with 0.3 Mo/nm^2. a) dehydrated conditions, 503 K; b) methanol oxidation at 503 K; c) dehydrated conditions after reaction, 503 K; and d) dehydrated after reoxidation in He/O_2 at 773 K.

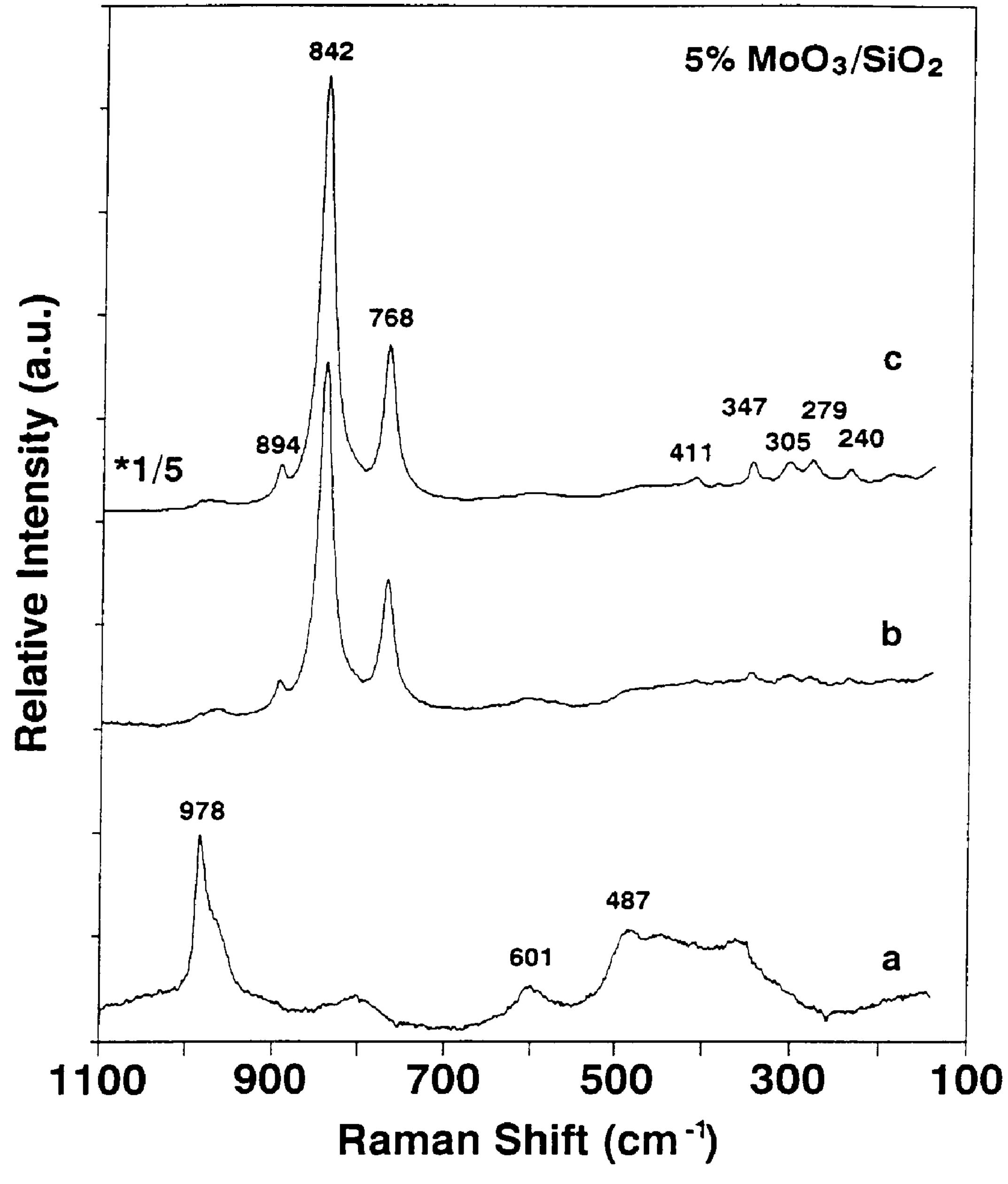

Fig. 4.7. *In situ* Raman spectra in reaction cell of catalyst I9 with 0.5 Mo/nm^2. a) dehydrated conditions, 503 K; b) methanol oxidation at 503 K; and c) dehydrated conditions after reaction, 503 K.

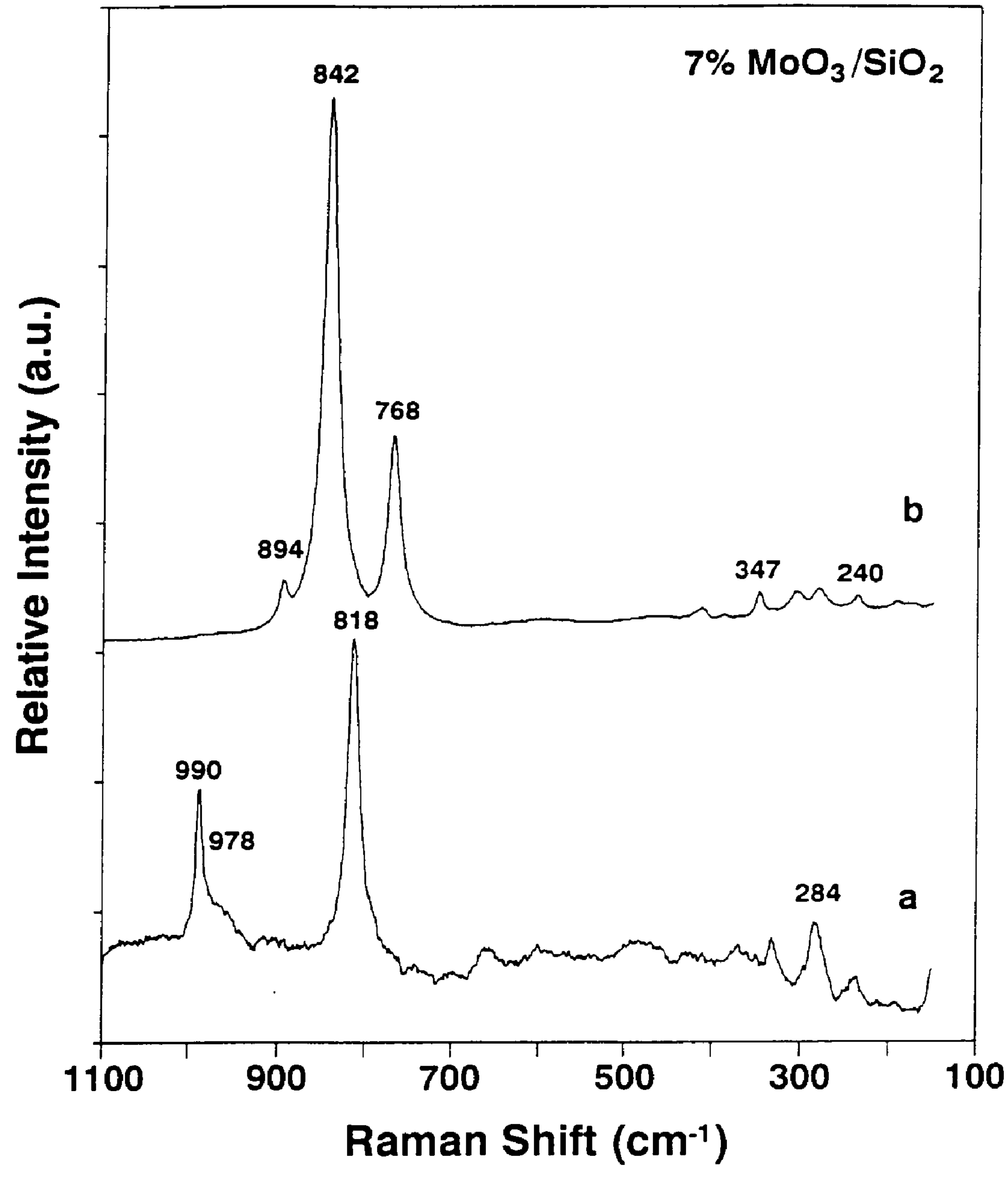

Fig. 4.8. *In situ* Raman spectra in reaction cell of catalyst I9 with 0.8 Mo/nm^2. a) dehydrated conditions, 503 K; b) methanol oxidation at 503 K.

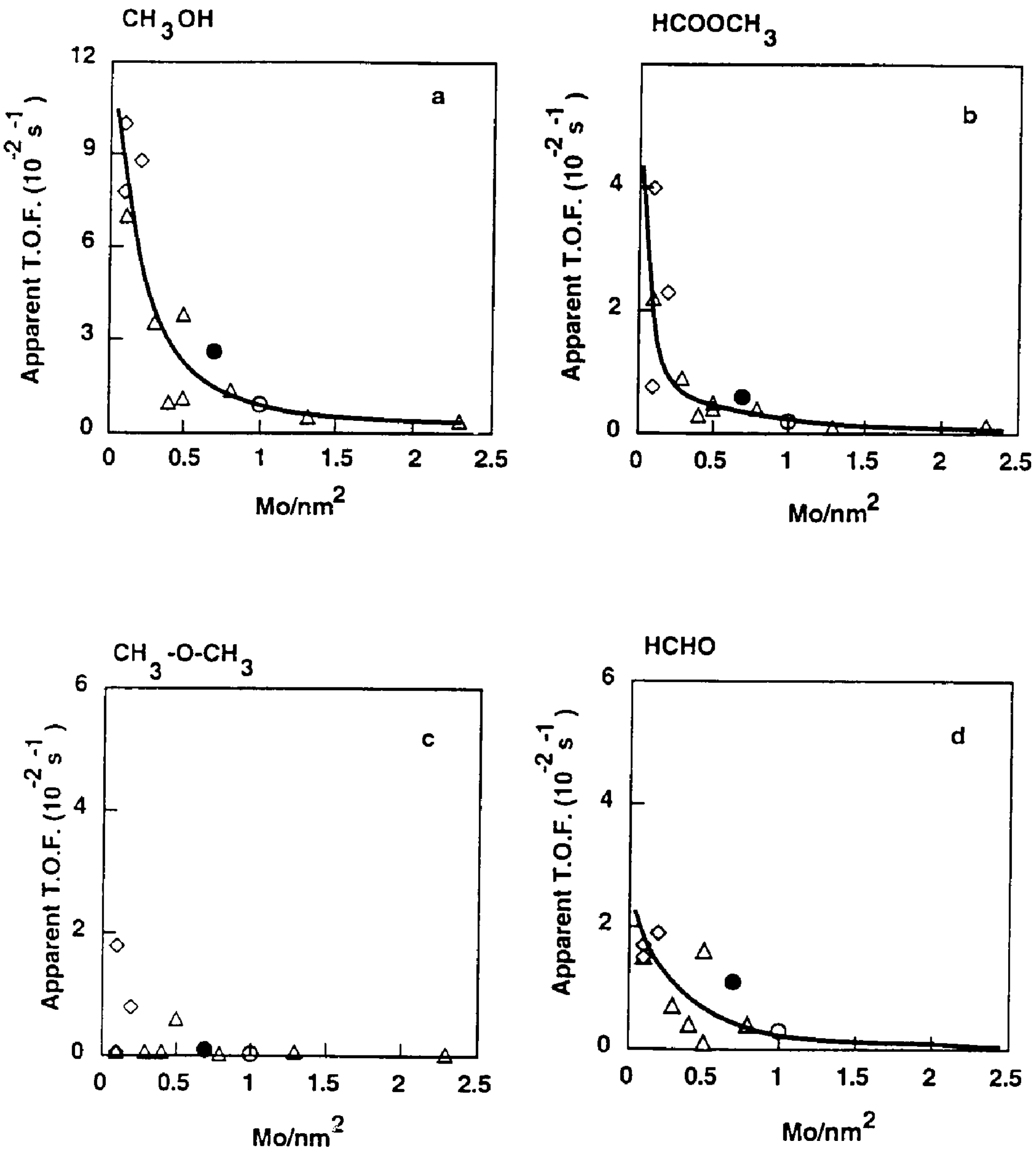

Fig. 4.9. Methanol oxidation on the MoO_3/SiO_2 catalysts at 503 K with a methanol/oxygen/helium feed of 6/13/81 (molar ratios) at 1 atm. Flow of 0.00035 mol-CH_3OH/h.g-cat. (a) Methanol TOF; TOF to (b) $HCOOCH_3$, (c) CH_3-O-CH_3, and (d) HCHO. (Δ) I-series, (◇) G-series, (O) E-series, and (●) A-series.

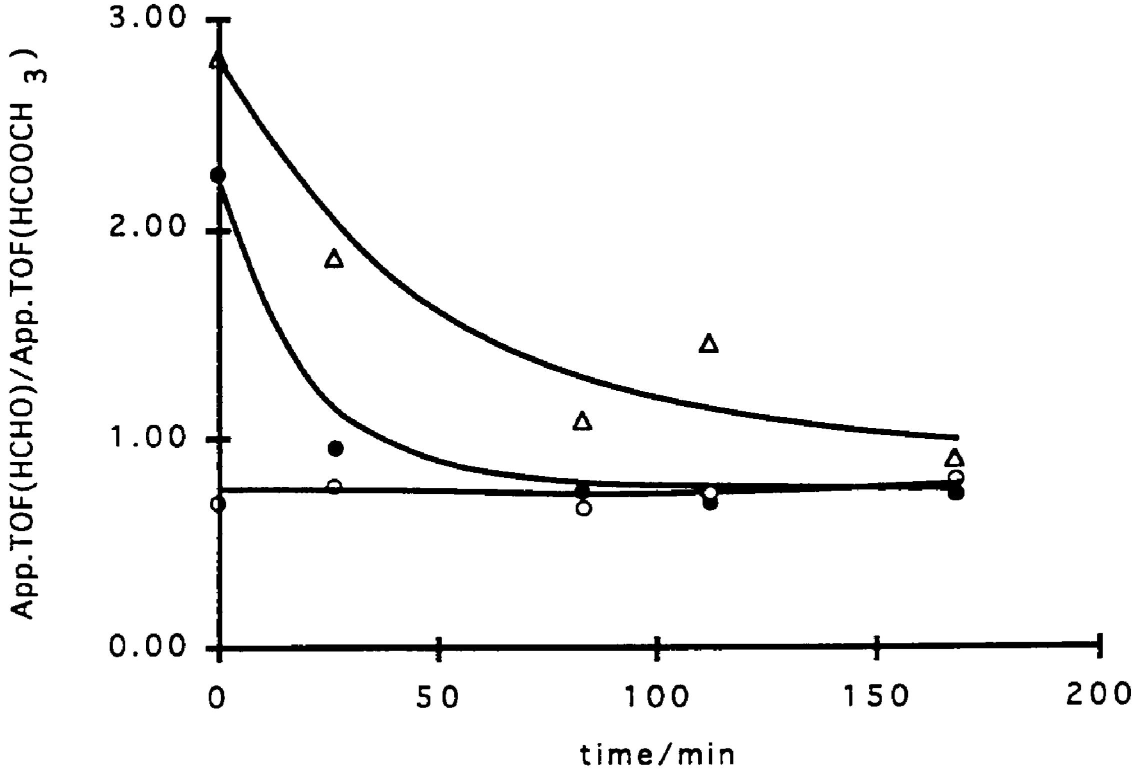

Fig. 4.10. Evolution of apparent TOF(HCHO)/apparent-TOF($HCOOCH_3$) for catalyst I9 during the first stages of the reaction. (O) 0.1 Mo/nm^2, (●) 0.3 Mo/nm^2, (▵) 0.4 Mo/nm^2. Zero time corresponds to the first sample analysis which was taken after 10 min of reaction.

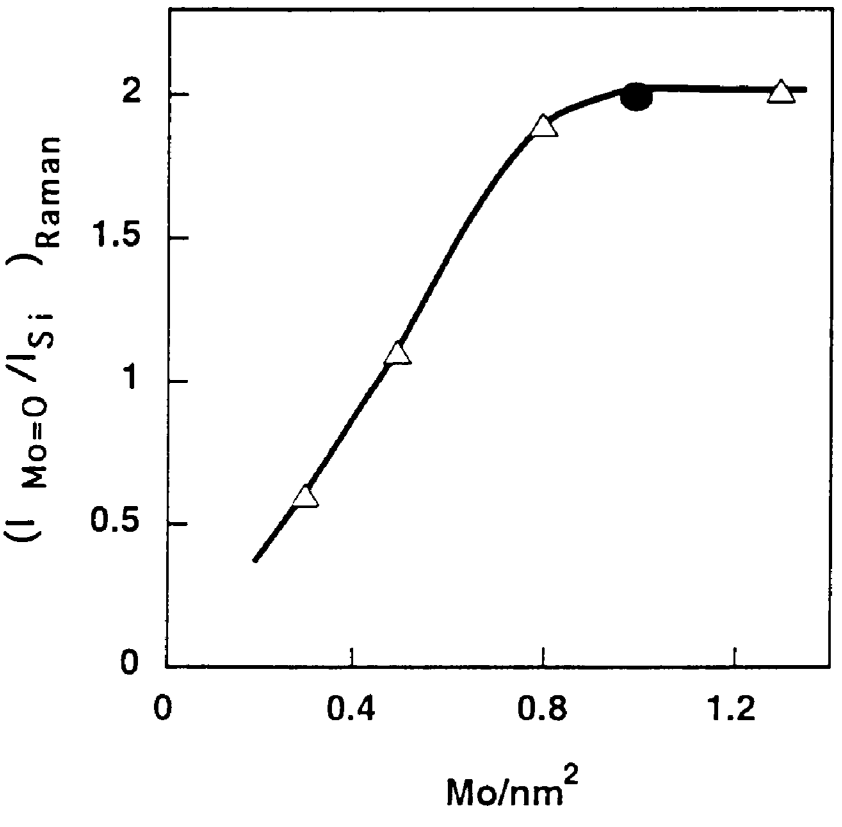

Fig. 4.11. Amount of dispersed surface molybdenum oxide mono-oxo species as a function of the Mo surface coverage on Degussa Aerosil 200 silica. (Δ) series I5, and (O) series E6.

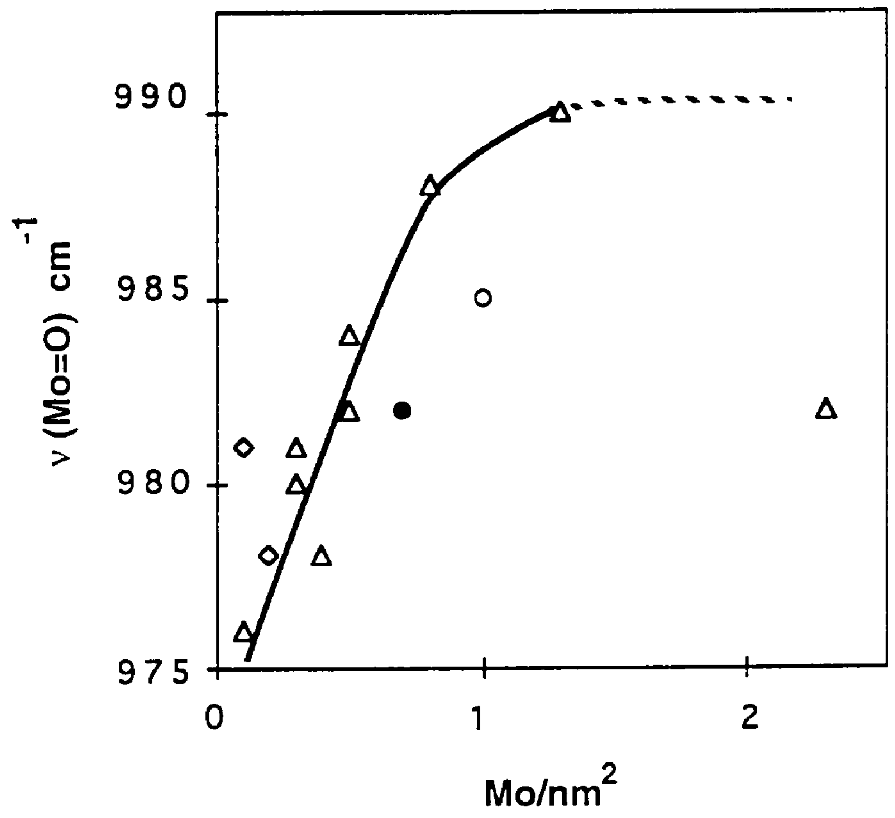

Fig. 4.12. Evolution of the Raman band for the Mo=O bond versus the surface molybdenum loading. (Δ) I-series, (◇) G-series, (O) E-series, and (●) A-series.

CHAPTER 5

GENESIS AND STABILITY OF SILICOMOLYBDIC ACID ON SILICA-SUPPORTED MOLYBDENUM OXIDE CATALYSTS: *IN SITU* STRUCTURAL-SELECTIVITY STUDY ON SELECTIVE OXIDATION REACTIONS

5.1. SUMMARY

The formation of silicomolybdic acid (SMA, $H_4SiMo_{12}O_{40}$) on silica-supported molybdenum oxide catalysts is studied by *in situ* Raman spectroscopy, TGA measurements, and for the selective oxidation of methane to formaldehyde. The formation of silicomolybdic acid requires exposing the MoO_3/SiO_2 to air saturated with water for several hours at room temperature. The large amount of water deposited on the silica support allows solubilization of part of the silica support in the presence of solvated heptamolybdate species which leads to the formation of silicomolybdic acid. Desorption of water via thermal treatments breaks the silicomolybdic acid into dehydrated or partial hydrated species which are stable up to ca. 573 K. Above 573 K, only isolated and distorted mono-oxo surface molybdenum oxide species is observed by *in situ* Raman spectroscopy. Consequently, the silicomolybdic acid species on SiO_2 should not result in different catalytic behavior than conventional MoO_3/SiO_2 catalysts for reactions taking place above 573 K. Unlike surface molybdenum oxide species, the surface SMA species on SiO_2 are stable during methanol oxidation at 503 K and do not transform into crystalline β-MoO_3 phase. The selective oxidation of methane to formaldehyde (843-883 K) shows no difference between conventional silica-supported molybdenum oxide and silica-supported silicomolybdic acid catalysts. *In situ* Raman spectroscopy studies during methanol oxidation at 573 K reveal that the surface silicomolybdic acid species are not stable and transform into crystalline β-MoO_3.

5.2. INTRODUCTION

Silica-supported molybdenum oxide catalysts have been widely studied [1-10] and the structure of the supported molybdenum oxides is decisive in their catalytic performance [11-21]. However, characterization of the structure of the MoO_3/SiO_2 catalysts by different techniques and under different conditions results in different assignments. Under ambient conditions, the structure of the surface molybdenum oxide species are reported as hydrated surface polymolybdate species ($Mo_7O_{24}^{6-}$) whose structure depends on the surface pH at point of zero charge (PZC) of the catalyst [7]. Formation of silicomolybdic acid from the surface molybdenum oxide species on SiO_2 has also been observed upon exposure to large amounts of water vapor at room temperature [12,14,16]. The silicomolybdic acid is a Keggin-type structure consisting of 12 MoO_6 octahedral surrounding a SiO_4 tetrahedron [22]. Cohesion between the Keggin units is achieved by means of hydrated protons and water molecules [23]. Upon dehydration, the polymolybdate structures are unstable and spread over the silica surface to form isolated surface molybdenum oxide species possessing one terminal Mo=O bond and 4-6 fold oxygen coordination [8,9]. Crystalline molybdenum oxide (MoO_3) is the dominant species at higher loading of molybdenum oxide on SiO_2 and is stable upon dehydration. However, reaction conditions may also alter the nature of the silica-supported molybdenum oxide species. For example, the bulk β-MoO_3 phase readily forms during the oxidation of methanol from the surface dispersed molybdenum oxide species on SiO_2, and this surface β-MoO_3 phase transforms easily into the crystalline α-

MoO_3 phase upon increasing of temperature [9]. Therefore, some questions remain as to whether the polymolybdate species or the surface silicomolybdic acid species is the surface species present on the hydrated SiO_2 surface, and to their stabilities at different temperatures and to its effect on different oxidation reaction environments (particularly, methane oxidation to C_1-oxygenates and methanol oxidation [14,17]). In the present investigation the formation, thermal stability and structural features of silica-supported silicomolybdic acid species under different treatments and different reaction environments were examined by *in situ* Raman spectroscopy in order to clarify the controversies and to better understand this interesting system.

5.3. EXPERIMENTAL SECTION

5.3.1. Sample preparation

The silica-supported molybdenum oxide species were prepared by the incipient-wetness impregnation method with an aqueous solution of ammonium heptamolybdate ($(NH_4)_6Mo_7O_{24}\bullet 4H_2O$). Prior to impregnation, the fumed silica (Cabosil EH-5, 380 m^2/g) was wetted by excess water and further dried in air at 393 K and calcined in air at 773 K to make the handling of silica easier. This wetting procedure does not change the BET surface area of the SiO_2 support. After impregnation, the samples were dried overnight under ambient conditions and at 397 K overnight in air. The dry samples were subsequently calcined in dry air at 773 K for four hours. The silica-supported molybdenum oxide species are referred to as the MoSi series and each specific sample is identified by a number denoting the MoO_3 loading as a weight percent. The experimental procedure for the generation of the silica-supported silicomolybdic acid is based on previous work by Roberge and co-workers [12,16]. However, the transformation process of the surface molybdenum oxide on SiO_2 to the SMA is followed by the first time using *in situ* Raman spectroscopy. Oxygen gas (Linde, 99.99%) was passed through a saturator containing water at room temperature and the water-saturated oxygen flowed through an *in situ* sample cell with a pellet of silica-supported molybdenum oxide catalyst held in the center of the cell at room temperatures for at least 12 hours which results in the SMA series. Identification of specific SMA samples follows a similar nomenclature as the MoSi series.

5.3.2. *In situ* Raman spectrocopy

In situ Raman spectroscopy experiments were performed in order to study the structural changes taking place for the silica-supported molybdenum oxide catalysts under different conditions. These experiments were performed with an *in situ* Raman apparatus consisting of an Ar^+ laser (Spectra Physics, Model 165), a triple grating spectrometer (Spex, Model 1877), a photodiode array detector (EG&G, Princeton Applied Research, Model 1420), and a special designed sample cell. The 514.5 nm line of the Ar^+ laser with 10-100 mW of power is focused on the sample disc in a right-angle scattering geometry. The *in situ* cell was equipped with a spinning sample holder which was generally rotated at ca. 1000 rpm inside a quartz cell which allows working under a controlled atmosphere and temperature. Sample discs of 100-200 mg are held by the cap of the metallic alloy sample holder. A cylindrical furnace surrounding the quartz cell heats the sample and is controlled by an internal thermocouple. The MoO_3/SiO_2 samples had to be calcined at 773 K for at least two hours before the Raman measurement to eliminate the fluorescence from the SiO_2 support. The *in situ* Raman spectra were initially obtained under continuous flow of a He/O_2 gaseous mixture with pressure ratio near 11/6. The Raman spectra of the dehydrated MoSi samples were recorded after *in situ* heating the sample at 773 K for half an hour and cooling to 503 K which is the methanol oxidation reaction temperature employed in the present study. The Raman spectra of the SMA samples were taken under ambient conditions. The Raman spectra under reaction conditions were collected after passing the He/O_2 gaseous mixture through a methanol reservoir at a 273 K water-ice bath for at least one hour. The Raman spectra after the methanol oxidation reaction were taken after reoxidize the reacted catalyst by flowing of the He/O_2 gas at 503 K and 773 K for one hour.

5.3.3. Thermogravimetric analysis

The thermogravimetric analysis was performed on a Cahn 2000 Microbalance operating at a sensitivity of 10 μg. Catalyst samples were heated at 4 K min^{-1} to 773 K in air flowing at 150 ml/min.

5.3.4. Methane oxidation

Measurements of the selective oxidation of methane were carried out at atmospheric pressure in a fixed bed quartz microcatalytic reactor (6 mm o.d.) by cofeeding CH_4 (99.95 % vol.) and O_2 (99.98% vol.) without diluent. The CH_4/O_2 ratio was adjusted to 7 by means of mass flow controllers and the methane residence time was adjusted to 2 gh/mol (referenced to the weight of the dehydrated catalyst). The reactor effluent was analyzed by an on-line Hewlett-Packard Gas Chromatograph 5890 Series-II fitted with a thermal conductivity detector. Chromosorb 107 and Molecular Sieve 5A packed columns were used with a column isolation analysis system.

5.4. RESULTS

5.4.1. Formation of SMA on the SiO_2 support

Fig. 5.1 shows the *in situ* Raman spectra of the 5% MoO_3/SiO_2 catalyst at different temperatures under a flow of oxygen saturated with water vapor (O_2/H_2O). The Raman features at ca. 480, 603, and 804 cm^{-1} are characteristic of the silica support [9]. An intense Raman band is observed at ca. 980 cm^{-1} at 773 K which corresponds to the stretching mode of the terminal bond Mo=O [24] of the dehydrated monomeric surface molybdenum oxide species on the silica support. A weaker Raman band at 360 cm^{-1} is due to the corresponding bending mode of this species (Fig. 5.1a). This Raman spectrum is identical to that obtained for a dehydrated MoO_3/SiO_2 catalyst [7,8]. No significant changes can be observed upon lowering the temperature from 773 K to 443 K (Fig. 5.1a - 5.1d), which suggests that the catalyst remains in a dehydrated state at these temperatures under the flow of water vapor [7,8]. However, at room temperature new Raman bands at 240, 370, 867 and 941 cm^{-1} appear after two hours (Fig. 5.1e). These

Raman bands are characteristic of heptamolybdate species [7] and are formed by the adsorption of water on the silica support, in agreement with previous observations [8]. Further changes are observed in the *in situ* Raman spectra of the MoO_3/SiO_2 sample upon longer exposure to oxygen saturated with water at room temperature for overnight. Under these conditions, new Raman bands are observed at 241, 614, 955, and 975 cm^{-1} which correspond in wavenumber and relative intensity with β-silicomolybdic acid [25] (Fig. 5.1f).

5.4.2. Stability of SMA on SiO_2

Additional *In situ* Raman spectra were recorded by increasing the temperature of the above SMA/SiO_2 sample (Fig. 5.1f) to evaluate the thermal stability of the silica-supported β-silicomolybdic acid in oxygen and oxygen/water environments and are shown in Figs. 5.2 and 5.3, respectively. In both cases, the trends observed are very similar but the SMA/SiO_2 sample in Figs. 5.2 and 5.3 also exhibit a small Raman band at 818 cm^{-1} due to traces of crystalline α-MoO_3. At 443 K, Raman features are observed at ca. 996, and 240 cm^{-1} as well as a shoulder at ca. 977 cm^{-1} (Figs. 5.2b and 5.3b). The 996, 977 and 240 cm^{-1} band is assigned to a dehydrated surface β-silicomolybdic acid species and the shift of the 980 cm^{-1} Raman band to higher frequency is consistent with shortening of the Mo=O bond upon dehydration. The presence of the 240 cm^{-1} Raman band also reveals that the β-silicomolybdic acid species is still present on the SiO_2 surface. Similar features can be observed at 503 K (Figs. 5.2c and 5.3c). At 573 K, the 996 cm^{-1} Raman band has essentially disappeared and the band at ca. 240 cm^{-1} has broadened considerably (Figs. 5.2d and 5.3d). The Raman spectrum at 773 K exhibits a band at ca. 980 cm^{-1} and possesses no 240 cm^{-1} band which is characteristic of isolated surface molybdenum oxide species on silica and no band at 240 cm^{-1} characteristic of β-silicomolybdic acid species (Fig. 5.2e). Thus, the β-silicomolybdic acid species decomposes above 573 K in both dry and wet oxidizing environments.

The *in situ* Raman spectra of the above prepared silica-supported β-silicomolybdic acid sample during methanol oxidations are presented in Fig. 5.4. The Raman bands observed at room temperatures are those previously reported for silicomolybdic acid supported on silica [25]. Under methanol oxidation reaction conditions at 443 and 503 K Raman features at ca. 998, 978, and 235 cm^{-1} are observed (Fig. 5.4b, 5.4c) and assigned to the dehydrated surface β-silicomolybdic acid species.. The strong Raman band at 235 cm^{-1} suggests that methanol is perturbing the vibrations of the silicomolybdic acid species. When the methanol oxidation reaction is operated at higher temperatures (573 K), new changes can be observed in the *in situ* Raman spectra since additional features appear at ca. 838, and 487 cm^{-1} (Fig. 5.4d). These new bands are characteristics of crystalline β-MoO_3, a low temperature phase of bulk MoO_3. The corresponding shift of the 980 cm^{-1} band to 973 cm^{-1} appears to be associated with the formation of isolated surface molybdenum oxide species linked to methoxide species (*9*). Since further treatment in flowing oxygen (Fig. 5.4e) causes the Raman band at 973 cm^{-1} to shift back to 986 cm^{-1} which is characteristic of isolated surface molybdenum oxide species [7,24]. In addition, in the flowing oxygen atmosphere the conversion of the low temperature crystalline β-MoO_3 into the high temperature crystalline α-MoO_3 phase is evidenced by the onset of new Raman bands at 815, 460, 393, 348, and 296 cm^{-1}.

The results from the TGA experiments are presented in Fig. 5.5 in the form of % weight loss for the different samples for samples heated in air. The main feature is the remarkably higher weight loss observed on the SMA series (ca. 45 %) as compared to the MoSi series (<5 %). The difference in weight loss is due to the higher amount of water present on the SMA series. Most of the moisture is desorbed by approximately 443 K. In addition, the SMA series also exhibits a small additional weight loss at ca. 543 K for high molybdenum oxide loadings. This is illustrated by the inset included in Fig. 5.5 for the 5SMA catalyst. This feature becomes less evident as the molybdenum oxide loading decreases and becomes hardly noticeable for low loading SMA samples. This additional weight loss takes place in the same temperature range where the silicomolybdic acid species completely decomposes to isolated surface molybdenum oxide species.

5.4.3. Methane partial oxidation

The results of the selective oxidation of methane are presented in Table 5.1 and Fig. 5.6 for the catalysts 5MoSi and 5SMA. The weight of the 5SMA catalyst was higher than that of 5MoSi in the proportion determined by the TGA experiments due to the presence of moisture so that the molybdenum loading of both catalysts in the reactor (dehydrated) was maintained about the same. In fact, no significant differences in weight were observed between the two catalysts (less than 1%) after reaction. For both catalysts, formaldehyde and carbon monoxide were the main oxidation products and minor amounts of carbon dioxide were also produced. In addition, the conversion and selectivity values were very similar for both catalysts. The selectivity trends presented in Fig. 5.6 indicate that formaldehyde is the main reaction product and that it is further oxidized to carbon monoxide. The almost constant selectivity to carbon dioxide, even at very low conversion levels, appears to indicate that it originates directly from methane rather than from further oxidation of carbon monoxide. These mechanistic observations are in agreement with previous kinetic [29] and isotopic [30] measurements. The most remarkable feature of this plot is the essentially identical selectivity trends for both catalysts. This very similar catalytic behavior indicates that the same active center must be present on both catalysts. This result is expected since under the methane oxidation reaction conditions (863 K) both catalysts possess only dehydrated surface molybdenum oxide species on SiO_2. The slightly higher activity of the 5MoSi catalyst is partial associated with the additional MoO_3 present in this sample.

5.5. DISCUSSION

The hydration/dehydration behavior of the MoO_3/SiO_2 catalysts has been extensively studied [7,8,26] and will not be further discussed in this paper. The results presented above demonstrate that the formation of silicomolybdic acid does take place upon exposure of silica-supported molybdenum oxide to large amounts of water for several hours at room temperature. The presence of water is fundamental for the formation and stabilization of silicomolybdic species, as has previously been demonstrated [12,16,18,27,28]. Initial exposure to air saturated with water at room temperatures has a similar effect to that of exposing silica-supported molybdenum oxide material to ambient humidity. Under these initial conditions, hydrated heptamolybdate ($Mo_7O_{24}^{6-}$) species are formed as demonstrated by *in situ* Raman spectroscopy. These hydrated heptamolybdate species are dissolved in the thin water layer covering the surface of the MoO_3/SiO_2 catalysts [7]. Previous research by Che *et al.* shown that the presence of MoO_3 and SiO_2 stirred in water for a period of time results in the formation of silicomolybdic acid [14]. The same phenomenon is taking place on the surface of the silica support between Mo and Si for the SMA series. TGA measurements reveal the presence of large amounts of water on the SMA series (ca. 45% weight) and significant amounts of water (many layers) which allow solubilization of a portion of the silica support. These conditions are similar to those reported by Che *et al.* [14] and *in situ* Raman spectroscopy directly reveals the formation of silicomolybdic acid.

The silica-supported silicomolybdic acid is not stable at temperatures above 573 K. Initial heating of the SMA series results in dehydration of the materials and the Raman bands characteristic of β-silicomolybdic acid (975, 955, ~630 and 241 cm^{-1}) are no longer present. However, dehydrated or partially hydrated surface silicomolybdic acid species appear to form below 573 K and exhibit Raman bands at 998, 977, and ~235 cm^{-1}. When the sample is heated above ca. 573 K the dehydrated silicomolybdic acid species do not appear to be stable and spread on the silica support as isolated surface molybdenum oxide species (characterized by the Raman bands at ca. 980 and 360 cm^{-1}) [7,8]. Similar behavior can be observed during the decomposition of surface heptamolybdate species by dehydration of the silica-supported molybdenum oxide materials [2,8,26]. In both cases, the same isolated and distorted surface molybdenum oxide species are formed after decomposition.

No catalytic differences are expected between the MoSi and SMA series during reactions above 573 K since silicomolybdic acid is not stable above 573 K and the resulting material is identical to silica-supported molybdenum oxide species. Results presented above for the selective oxidation of methane at 863 K (Table 5.1 and Fig. 5.6) suggested that the same catalyst results under reactions from loading either a MoSi or SMA catalyst into the reactor. The increase in the molybdenum oxide loading results in a higher level of methane conversion as a consequence of the greater number of active sites [10,17,19]. The conversion of methane has a very important effect on the selectivity (Fig. 5.6 and e.g., reference 31) and, consequently, the less selective behavior of the SMA/SiO_2 catalyst may be due to its higher loading of molybdenum oxide rather than to a different active site. The overall lower selectivity towards partial oxidation products also originates from the use of N_2O as oxidant which is less selective than molecular oxygen for methane oxidation [10]. *In situ* Raman studies during methane oxidation over MoO_3/SiO_2 catalysts have shown that the isolated surface molybdenum oxide species are present during reaction [15].

For reactions operating below 573 K, however, the silicomolybdic acid may be present in a dehydrated or partially hydrated state and catalytic differences should be expected between the MoSi and SMA series. The *in situ* Raman spectra during methanol oxidation at 443 K and 503 K (see Figs. 5.4b and 5.4c) show a similar structure as those of the dehydrated surface silicomolybdic acid and no crystalline MoO_3 was detected. Furthermore, this used catalyst recovers the surface SMA species after rehydration in a flow of the H_2O/O_2 gas. These behaviors reveal that the silica-supported silicomolybdic acid is more stable than the silica-supported molybdenum oxide species. The *in situ* Raman spectrum of surface silicomolybdic acid during methanol oxidation at higher temperatures (573 K, Fig. 5.4d) reveals the presence of silicomolybdic acid, surface molybdenum oxide species, and small amounts of β-MoO_3. However, the *in situ* Raman spectra of the 5% MoO_3/SiO_2 catalyst during methanol oxidation at 503 K revealed a complete transformation of the surface molybdenum oxide species to the crystalline β-MoO_3 phase [9]. A very extensive work on the selective oxidation of methanol on silica-supported silicomolybdic acid at 503 K shows a marked acidic character [14,29]. This suggests the silicomolybdic acid species must be more reactive than the surface molybdenum oxide species which accounts for the acidic activity observed by Che *et al.* on silica-supported silicomolybdic acid during the oxidation of methanol [23,29]. *In situ* Raman spectroscopy reveals that treatments of the SMA/SiO_2 catalyst above ca. 573 K break the surface silicomolybdic acid species into isolated surface molybdenum oxide species which are identical to those observed on dehydrated silica-supported molybdenum oxide catalysts. Oxidation of methanol over the silica-supported surface molybdenum oxide species has a redox character [9,23,29] and the redox catalysis observed on the silica-supported silicomolybdic acid after a treatment at 573 K is expected since the acidic silicomolybdic acid species are no longer present at this temperature.

5.6. CONCLUSIONS

Formation of silicomolybdic acid requires adsorption of large amounts of water at room temperature that allow solubilization of silicon and molybdenum oxide species for the formation heteropolyacid. Upon dehydration, silica-supported silicomolybdic acid forms a dehydrated or partially hydrated surface silicomolybdic acid species with an acidic character. At ca. 573 K, the silicomolybdic acid species completely breaks into isolated surface molybdenum oxide species which possesses a redox property during the oxidation of methanol. During the selective oxidation of methane, at ~863 K, the same isolated and distorted mono-oxo surface molybdenum oxide species are present on the silica surface for the silica-supported silicomolybdic acid and surface molybdenum oxide species, independent of the initial presence of silicomolybdic acid. During methanol oxidation at 503 K, the dehydrated silicomolybdic acid species are present on the silica surface which are more stable than the dehydrated molybdenum oxide species on SiO_2 towards the formation of crystalline β-MoO_3. Reaction with methanol at above 573 K also transforms dehydrated silicomolybdic acid species into crystalline MoO_3.

REFERENCES

1. Barbaux, Y., Elamrani, A. R., Payen, E., Gengembre, L., Bonnelle, J. P., and Gryzbowska, B., *Appl. Catal.* **44**, 117 (1988).
2. Liu, T.-C., Forissier, M., Coudurier, G., and Vèdrine, J. C., *J. Chem. Soc., Faraday Trans I*, **85**, 1607 (1989).
3. Ono, T., Anpo, M., and Kubokawa, Y., *J. Phys. Chem.* **90**, 4780 (1986).

4. Cheng, C. P., Schrader, G. L., *J. Catal.* **60**, 276 (1979)
5. Jeziorowski, H., Knözinger, H., Grange, P, and Gajardo, P., *J. Phys. Chem.* **84**, 1825 (1980).
6. Seyedmonir, S. R., Abdo, S., and Howe, R. F., *J. Phys. Chem.* **86**, 1233 (1982).
7. Williams, C. C., Ekerdt, J. C., Jehng, J-M., Hardcastle, F. D., Turek, A. M., and Wachs, I. E., *J. Phys. Chem.* **95**, 8781 (1991).
8. de Boer, M., van Dillen, A. J., Koningsberger, D. C., Vuurman, M. A., Wachs, I. E., and Geus, J. G., *Catal. Lett.* **11**, 227 (1991).
9. Bañares, M. A., Hu, H., and Wachs, I. E., *J. Catal.*, **150**, 407 (1994).
10. Bañares. M. A., Fierro, J. L. G., and Moffat, J. B., *J. Catal.* **142**, 406 (1993).
11. Thomas, R., Moulijn, J. A., de Beer, V. H. J., and Medema, J., *J. Mol. Catal.* **8**, 161 (1980).
12. Stencel, J. M., Diehl, J. R., D'Este, J. R., Makovsky, L. E., Rodrigo, L., Marcinkowska, K., Adnot, A., Roberge, P. C., and Kaliaguine, S., *J. Phys. Chem.* **90**, 4739 (1986).
13. Giordano, N., Meazzo, M., Castellan, A., Bart, J. C., and Ragaini, V., *J. Catal.* **50**, 342 (1977).
14. Rocchiccioli-Deltcheff, C., Amirouche, M., Che, M., Tatibouët, J. M., and Fournier, M. , *J. Catal.* **125**, 2892 (1990).
15. Bañares, M. A., Spencer, N. D., Jones, M., and Wachs, I. E., *J. Catal.* **142**, 206 (1994).
16. Marcinkowska, K., Adnot, A., Roberge, P. C., and Kaliaguine, S., *J. Phys. Chem.* **90**, 4773 (1986).
17. Kasztelan, S., Payen, E., and Moffat, J. B., *J. Catal.* **112**, 320 (1988).
18. Marcinkowska, K., Kaliaguine, S., and Roberge, P. C., *J. Catal.* **90**, 49 (1984).
19. Bañares, M. A., and Fierro, J. L. G., *Catal. Lett.* **17**, 205 (1993).
20. Bañares, M. A., and Fierro, J. L. G., "Catalytic Selective Oxidation" Chap. 27, ACS Symp. Ser. 253. S. T. Oyama and J. W. Hightower, Eds., 1993.
21. Bañares, M. A., and Fierro, J. L. F., *An. Quím.* **87** (2), 223 (1991).

22. Greenwood, N. N., and Earnshaw, A., "Chemistry of the Elements" Pergamon Press, 1989.

23. Tatibouët, J. M., Che, M., Amirouche, M., Fournier, M., and Roccicchioli-Deltcheff, C., *J. C. S. Chem. Commun.* 1260 (1988).

24. Hardcastle, F. D., and Wachs, I E., *J. Raman Spectrosc.* **21**, 683 (1990).

25. Kasprzak, M. S., Leroi, G. E., and Crouch, S. R., *Appl. Spectrosc.* **36**, 285 (1982).

26. Roark, R. D., Kohler, S. D., and Ekerdt, J. G., *Catal. Lett.* **16**, 71 (1992).

27. Castellan, A., Bart, C. J., Vaghi, A., and Giordano, N., *J. Catal.* **42**, 162 (1976).

28. Leyrer, J., Mey, D., and Knözinger, H., *J. Catal.* **124**, 349 (1993).

29. Rocchiccioli-Deltcheff, C., Amirouche, M., Hervé, G., Fournier, M., Che, M., and Tatibouët, J. M., *J. Catal.* **126**, 591 (1990).

30 Spencer, N. D. Pereira, C. J., and Grasselli, R. K., *J. Catal.* **126**, 546 (1990).

31. Bañares, M. A., Rodríguez-Ramos, I., Guerrero-Ruíz, A., and G. Fierro, J. L. G., in "Proceedings, 10th International Congress on Catalysis" (L. Guczi et al., Ed.) Elsevier, Amsterdam, 1131 (1994).

Table 5.1. Methane conversion on silica-supported molybdenum oxide and silicomolybdic acid.

Catalyst	% Conversion		% Selectivity		
	CH_4	O_2	HCHO	CO	CO_2
5SMA	0.7	5.3	71.9	21.3	4.7
5MoSi	0.8	6.8	68.8	26.1	4.4

Reaction conditions: 863 K, CH_4/O_2 = 7 molar, W/F = 2 gh/mol.

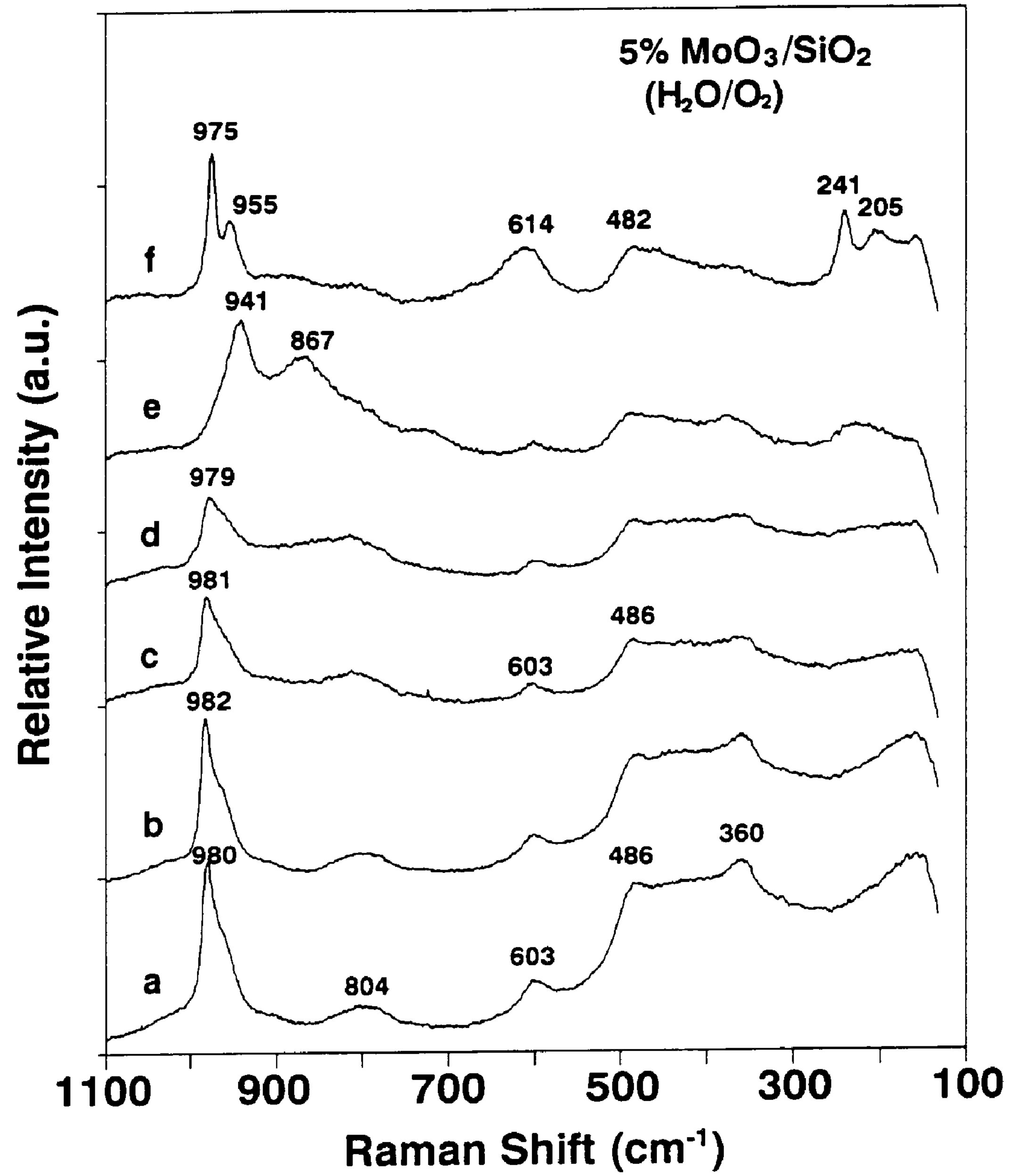

Fig. 5.1. *In situ* Raman spectra of 5MoSi in flowing air saturated with water at different decreasing temperatures: (a) 773 K, (b) 623 K, (c) 503 K, (d) 443 K, (e) room temperature for 2 hours, and (f) room temperature, overnight.

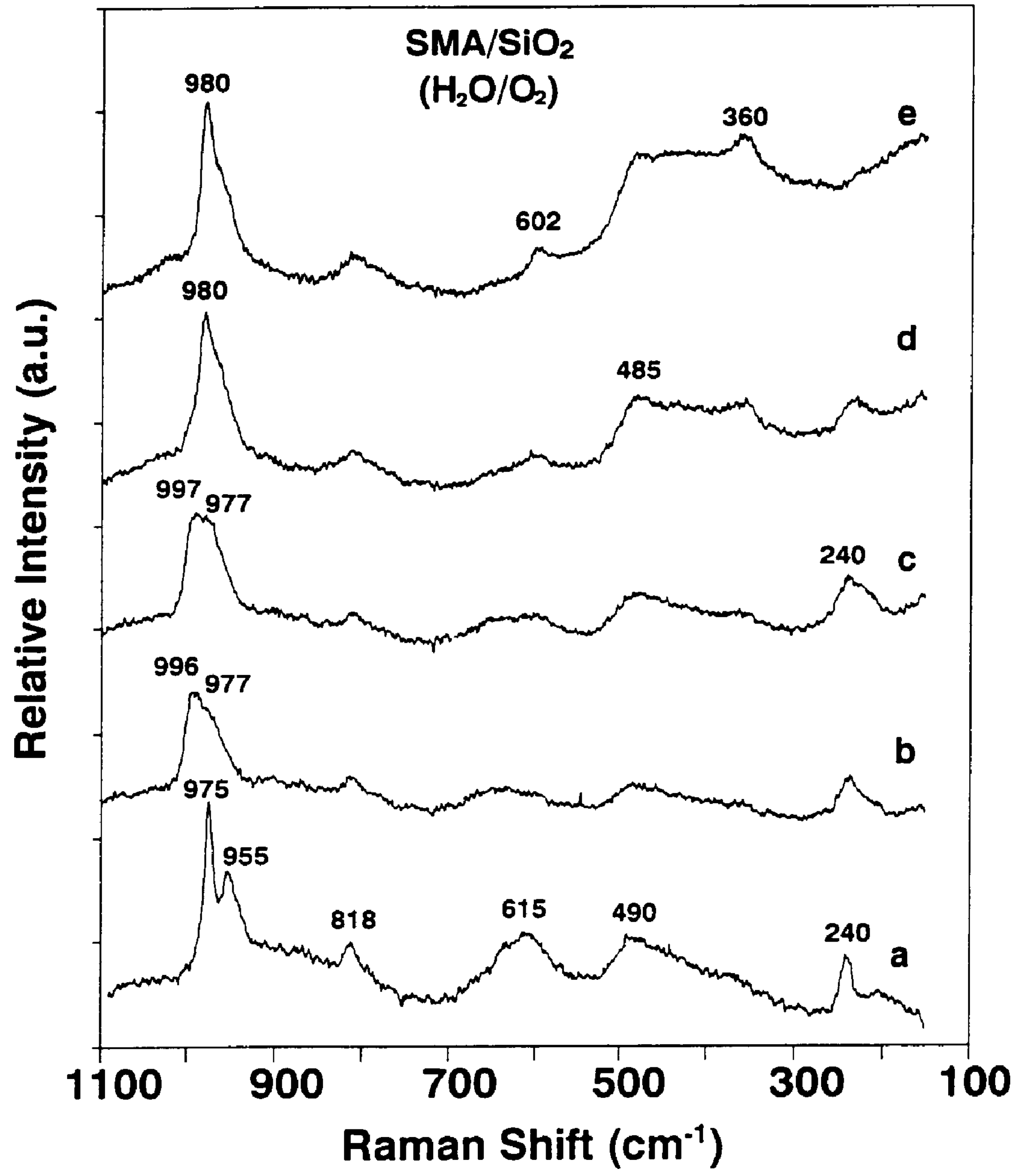

Fig. 5.2. *In situ* Raman spectra of 5SMA in flowing oxygen saturated with water at different increasing temperatures: (a) room temperature, (b) 443 K, (c) 503 K, (d) 573 K, and (e) 773 K.

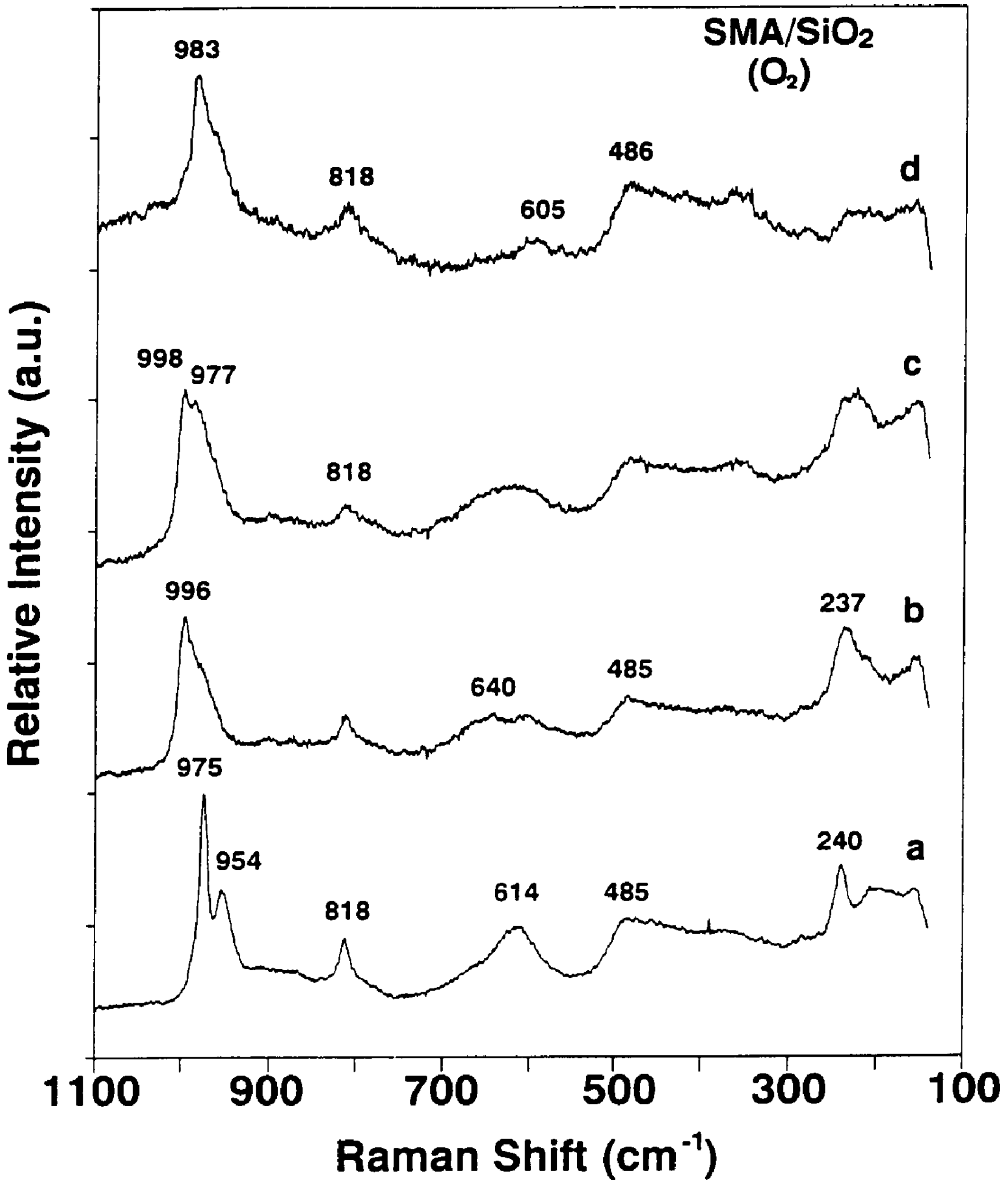

Fig. 5.3. *In situ* Raman spectra of 5SMA in dry oxygen at different increasing temperatures: (a) room temperature, (b) 443 K, (c) 503 K, and (d) 573 K.

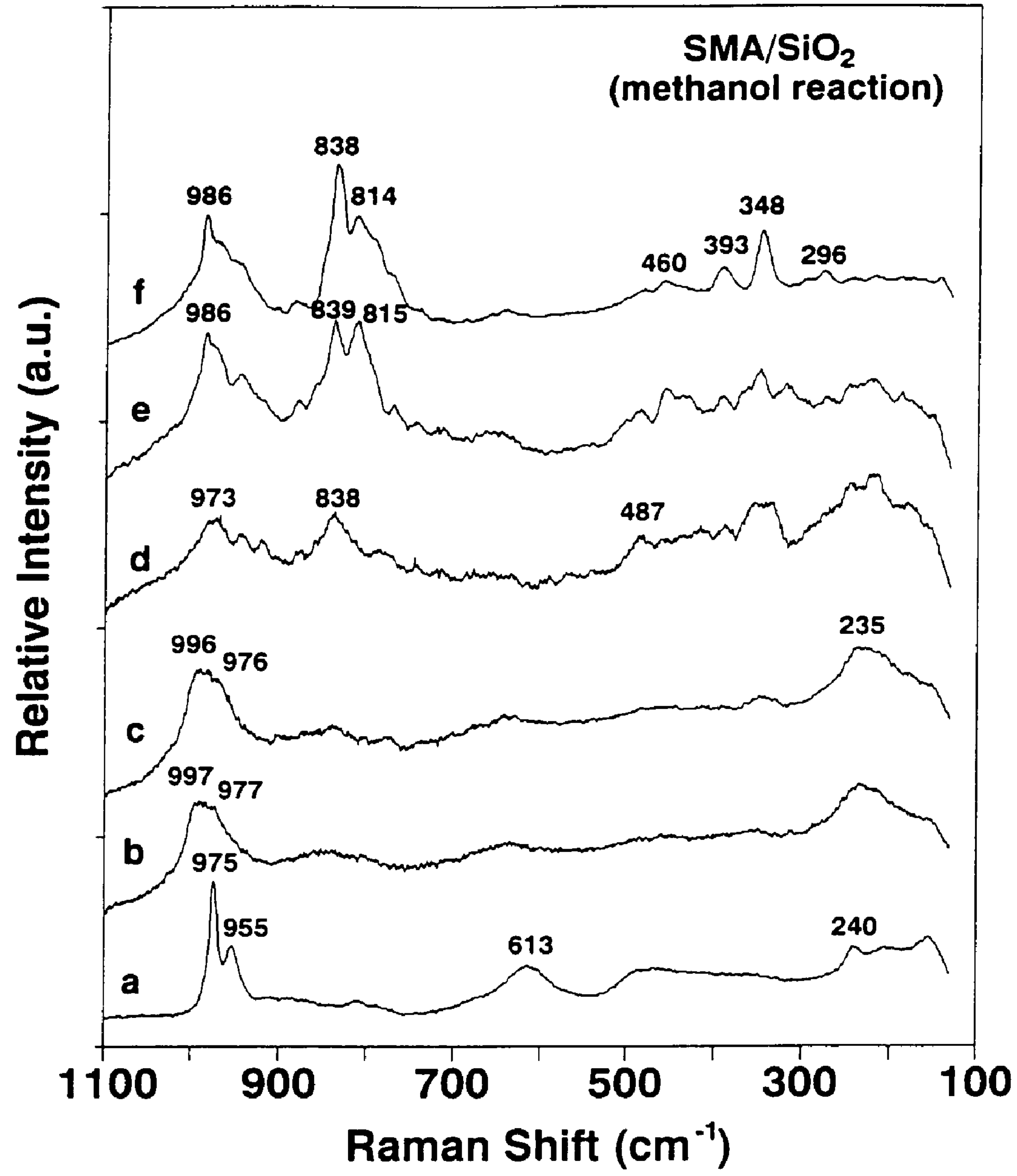

Fig. 5.4. *In situ* Raman spectra of 5SMA during the methanol oxidation reactions at different increasing temperatures: (a) room temperature, ambient, (b) flowing $CH_3OH/He/O_2$ at 443 K, and (c) at 503 K, (d) at 573 K, (e) flowing pure oxygen at 573 K, and (f) at 773 K.

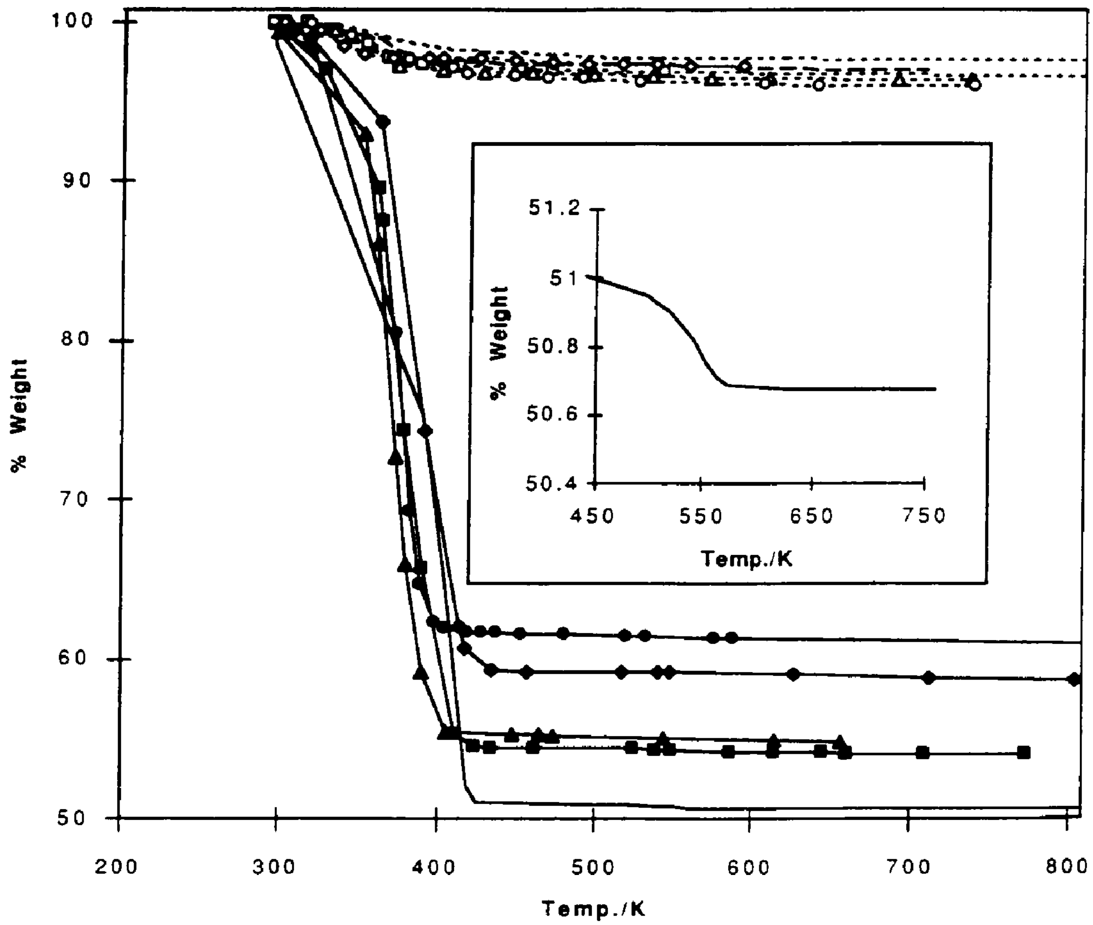

Fig. 5.5. TGA measurements of the weight loss patterns in dry air of the MoSi series (open symbols, dotted lines) and SMA series (closed symbols, solid lines): Square, 1% MoO_3; Diamond, 2% MoO_3; Triangle, 3% MoO_3; Circle, 4% MoO_3; no symbol for 5% MoO_3. The inset is for 5SMA.

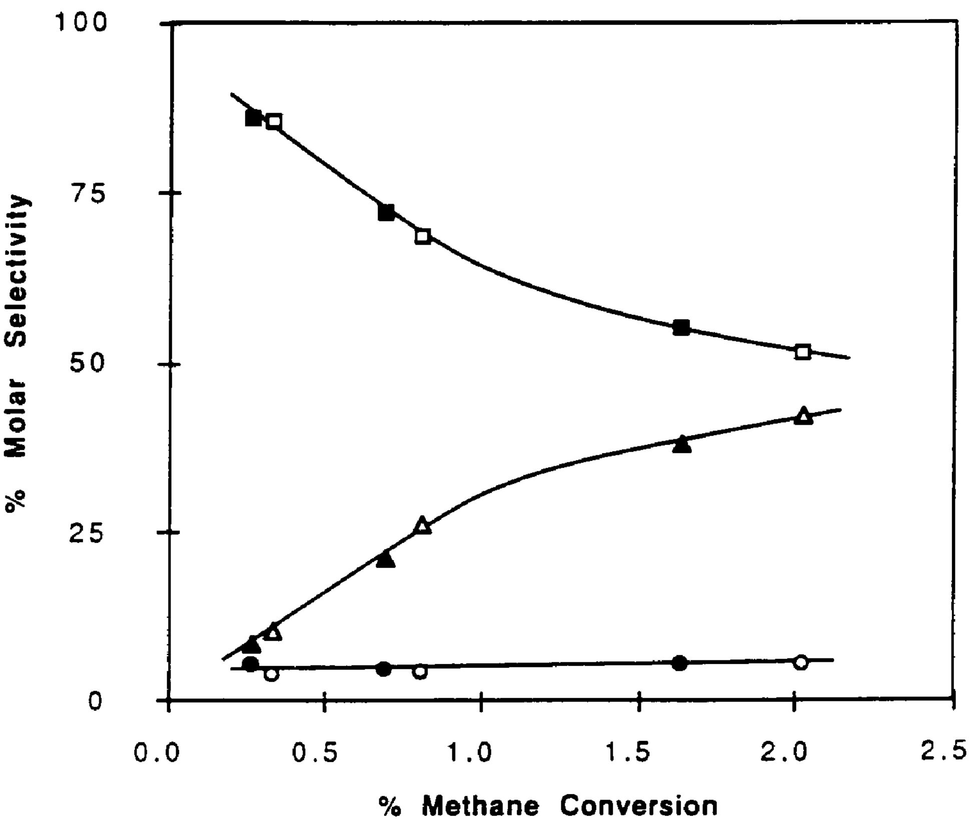

Fig. 5.6. Selectivity *vs.* methane conversion plots for the representative catalysts 5SMA and 5MoSi. Reaction conditions, CH_4/O_2 = 7 molar; W/F = 2 gh/mol; reaction temperature 843-883 K. Closed symbols 5SMA, and open symbols 5MoSi. Square, HCHO; triangle, CO; and circle, CO_2.

CHAPTER 6

CONCLUSIONS

The objective of the current study was to develop the structure-reactivity relationships of supported molybdenum oxide catalysts *via* a fundamental understanding of the molecular structure and the catalytic reactivity of the surface molybdenum oxide species. This objective has been approached along the following line. The structures of the surface molybdenum oxide species were elucidated on different oxide supports (Al_2O_3, TiO_2, ZrO_2, Nb_2O_5, and SiO_2) using Raman and XANES spectroscopies under both ambient and dehydrated conditions. The factors determining the molecular structures of the supported molybdenum oxide species were investigated (molybdenum oxide loading, oxide support, hydration/dehydration condition, as well as preparation method for SiO_2 supported molybdenum oxide catalysts). The catalytic reactivity of the supported molybdenum oxide catalysts were studied for methanol oxidation reaction as a function of the surface molybdenum oxide loading and oxide support. The turnover frequency (TOF) of the surface molybdenum oxide species was found to increase with the molybdenum oxide loading (~ 2-4 fold) and also depended on the specific oxide support (~ 10 fold with $ZrO_2 \sim TiO_2 > Nb_2O_5 > Al_2O_3 > SiO_2$). This final chapter describes the mechanism of the structure-reactivity relationships developed according to the conclusions of the above experimental results.

The commercial catalyst employed for the manufacture of formaldehyde by the oxidation of methanol contains a mixture of iron molybdate ($Fe_2(MoO_4)_3$) and molybdenum oxide (MoO_3) [1]. The Mo atom was found to be the site of catalytic activity [1-3]. A large number of studies have been performed to determine the catalytic behavior for methanol oxidation over MoO_3 single crystal surfaces [1-7], MoO_3 and

$Fe_2(MoO_4)_3$ bulk compounds [1-5], heteropolyanion Keggin units [8,9], and supported molybdenum oxide catalysts [3,7]. These studies were motivated to obtain a fundamental understanding of the kinetics and mechanism of the catalytic reactions through studies of model surface species. The common features in the structures of active surfaces are the easily reducible and reoxidizable Mo (VI) and Mo (V) ions, the terminal Mo=O groups, and the bridging Mo-O-M (M = Mo or support metals) oxygens. The importance of the terminal Mo=O groups or the bridging oxygen in determining the activity of the catalyst are still being argued [5-8].

The main product of methanol oxidation over surface molybdenum oxide supported on TiO_2, ZrO_2, Nb_2O_5, and Al_2O_3 is formaldehyde (HCHO). The basic reaction is the oxidative dehydrogenation of methanol to formaldehyde:

$$CH_3OH + 1/2\ O_2 \rightarrow HCHO + H_2O$$

When the reaction is carried out under excess of oxygen conditions, where reoxidation of the catalyst is fast, the rate expression for the production of formaldehyde is approximately

$$R = k\ [p_{CH3OH}]\ [O_2]^0$$

for all catalysts studied. Where R is the reaction rate, k is the rate constant, and p is the partial pressure of the reactant. It was found that the apparent activation energy is ~80 kJ/mole, and the breaking of a methyl C-H bond is the rate limiting step (shows a strong kinetic isotope effect [2]) for all catalysts studied.

In the current study, the variation of TOFs for methanol oxidation over supported molybdenum oxide catalysts correlated well with the characteristics of the oxide support (e.g., TiO_2, ZrO_2, Nb_2O_5, and Al_2O_3), but not the vibrational frequency of the terminal Mo=O bonds (see chapter 3). This correlation to the support is presumably associated with the properties of the Mo-O-support bonds. Although the activation energy did not change with support for the methanol dehydrogenation to formaldehyde, the supports do have quite different oxygen labilities for their different reduction temperature upon reduced by hydrogen (see Fig. 3.11).

It is generally agreed that the principal pathway of methanol oxidation is: 1) the adsorption of methanol on the surface to form adsorbed surface methoxy species (CH_3O); 2) breaking of a C-H bond by transferring a H to the oxygen in the catalyst; 3) desorption of the product HCHO molecule; and 4) reoxidation of the reduced surface active species by oxygen. The studies of methanol adsorption over MoO_3 single crystal (010) basal plane, which possesses the surface containing the most saturated Mo=O bonds in the layered MoO_3 structure, found no chemisorption of methanol on the (010) layer surface and, thus, hypothesized that methanol adsorption leading to reaction is favored by the coordinatively unsaturated Mo sites (the edge planes) [1,3]. A molecular orbital study of C-H bond breaking during the oxidative dehydrogenation of methanol suggested that bridging oxygens are more labile than terminal oxygens once the metal oxide is reduced [8]. The current study suggests that the bridging oxygens between surface Mo species and oxide support are affecting the pre-exponential factor in this reaction. The pre-exponential factor includes the number of active sites and an entropy term for the activated complex. Since the number of active sites was not found to be a strong function of the oxide support in our studies, the difference in the entropy of the activated complex appears to be responsible for the support dependence. The breaking of the C-H bond was found to be the same for different oxide supports (same activation energy), which suggests that the ease of leaving of another reaction product, H_2O, from the catalyst surface is the determining factor for the different activity of the surface molybdenum oxide species on the different oxide supports. Therefore, a plausible reaction scheme can be drawn as follow:

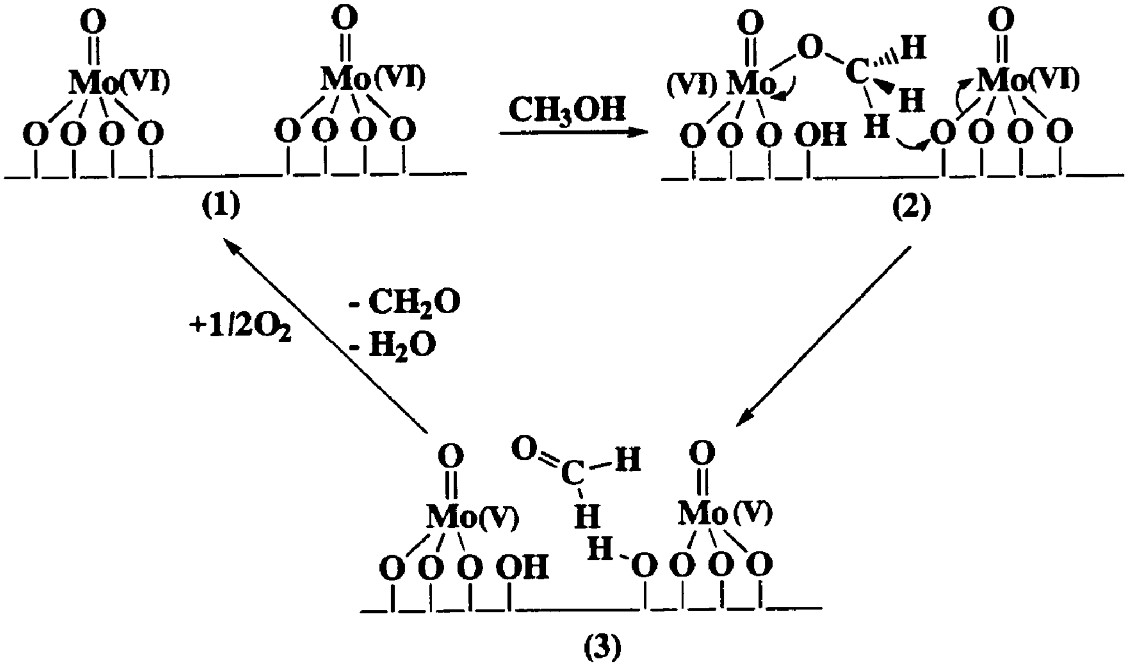

The ZrO_2 and TiO_2 supported molybdenum oxides possess a higher entropy in the transition state complex (2) than that of the Nb_2O_5 and Al_2O_3 supported Mo species and, thus, are more active in the overall oxidative reactions. The increase in entropy may be related to the more labile Mo-O-support oxygen present for ZrO_2 and TiO_2. The increase in TOF with molybdenum oxide loading can also be explained by an increase in the density of accessible electronic states which increase the entropy of activated states.

This study focused on the effect of molybdenum oxide loading and oxide support on the catalytic activity of supported molybdenum oxide catalysts towards the methanol oxidation reaction. However, the current *in situ* Raman approach to the solution of reactivity determining factors is still limited since only a single reactant system and a single reaction condition were studied. The versatile partial oxidation products (methylformate and dimethoxymethane) from methanol partial oxidation under different reaction conditions over molybdenum oxide catalysts is also of great interest for both application and fundamental understanding. In addition, to fully understand the catalytic reaction mechanism over molybdenum oxide containing catalysts requires intensive investigations of different catalyst systems and different reactions since the molybdenum oxide catalyst is such a useful catalyst for many different important reactions.

REFERENCES

1. Chowdhry, U., Ferretti, A., Firment, L. E., Machiels, C. J., Ohuchi, F., Sleight, A. W., and Staley, R. H., *Appli. Surf. Sci.* **19**, 360 (1984).
2. Cheng, W-H, Chowdhry, U., Ferretti, A., Firment, L. E., Groff, R. P., Machiels, C. J., McCarron, E. M., Ohuchi, F., Staley, R. H., and Sleight, A. W., In "*Heterogeneous Catalysis*", Texas A&m Univ. Press, 165 (1984).
3. Machiels, C. J., Cheng, W-H, Chowdhry, U., Farneth, W. E., Hong, F., McCarron, E. M., and Sleight, A. W., *Appli. Catal.* **25**, 249 (1986).
4. Ohuchi, F., Firment, L. E., Chowdhry, U., and Ferretti, A., *J. Vac. Sci. Technol.* **A 2**, 1022 (1984).

5. Chung, J. S., Miranda, R., and Bennett, C. O., *J. Catal.* **114**, 398 (1988).
6. Tatibouët, J. M., and Germain, J. E., *J. Catal.*, **72**, 375 (1981).
7. Tatibouët, J. M., and Germain, J. E., and Volta, J. C., *J. Catal.* **82**, 240 (1983).
8. Weber, R. S., *J. Phys. Chem.* **98**, 2999 (1994).
9. Serwicka, E. M., Broclawik, E., Bruckman, K., and Haber, J., *Catal. Lett.* **2**, 351 (1989).

CURRICULUM VITAE

NAME:	Hangchun Hu
DATE OF BIRTH:	May 15, 1961
PLACE OF BIRTH:	Wenzhou, China
PARENTS:	Cai, Aimei and Hu, Yanfu

EDUCATION

- **Ph. D. in Chemistry**, expected January 1995
  Lehigh University, Bethlehem, Pennsylvania, USA
  DISSERTATION "Molecular Structure-Reactivity Relationships for Supported Molybdenum Oxide Catalysts"

- **M. S. in Chemistry**, May 1991
  University of Notre Dame, Notre Dame, Indiana, USA
  Thesis "Oxidation of Naphthols by Radiolytically Produced OH Radicals"

- **B.S. in Chemistry**, August 1983
  University of Science and Technique of China, Hefei, Anhui, China

WORK EXPERIENCE

- 1/91 - 12/94, Research Assistant at Lehigh University.
  Research: Supported metal oxide catalysts.
- 1/88 - 12/90, Research Assistant at University of Notre Dame.
  Research: Organic free radical reactions.
- 9/83 - 3/87, Research Assistant at University of Science and Technique of China.
  Research: Radiation induced emulsion polymerization.

PUBLICATIONS

1. "Radiation Induced Emulsion Polymerization of 2-Ethylhexyl Acrylate"
   Z. Zhang, H. Hu, and M. Zhang, *J. of Radia. Research and Radia. Processing*, **10**, 129 (1992).
2. "Molecular Design of Supported Metal Oxide Catalysts"
   I. E. Wachs, G. Deo, D. S. Kim, M. A. Vuurman, and H. Hu, *Proc. Int. Congr. Catal. 10th,* A, 543 (1992).
3. "Molecular Design of Supported Metal Oxide Catalysts: an Initial Step to Theoretical Models"
   I. E. Wachs, G. Deo, M. A. Vuurman, H. Hu, D. S. Kim, and J-M. Jehng, *J. Mol. Catal.* **82**, 443 (1993).
4. "Bonding States of Surface Vanadium (V) Oxide Phases on Silica: Structural Characterization by ^{51}V NMR and Raman Spectroscopy"
   N. Das, H. Eckert, H. Hu, I. E. Wachs, J. Walzer, and F. Feher, *J. Phys. Chem.* **97**, 8240 (1993).
5. "Molybdena on Silica Catalysts: Role of Preparation Methods Upon the Structure-Selectivity Properties for the Oxidation of Methanol"
   M. A. Bañares, H. Hu, and I. E. Wachs, *J. Catal.*, **150**, in press (1994).
6. "Surface Structures of Supported Molybdenum Oxide Catalysts: Characterization by Raman and XANES Mo L_3-edge"
   H. Hu, I. E. Wachs, and S. R. Bare, (in preparation).
7. "Catalytic Properties of Supported Molybdenum Oxide Catalysts: An *in situ* Raman and Methanol Oxidation Study"
   H. Hu, and I. E. Wachs, (in preparation).
8. "Modification of V_2O_5/SiO_2 Catalyst by TiO_2 Overlayers: Raman, ^{51}V and ^{1}H NMR, and Methanol Oxidation Studies"
   H. Hu, I. E. Wachs, V. M. Mastikhin, A. V. Nosov, V. V. Terskikh, and K. I. Zamaraev, (in preparation)
9. "Partical Oxidation of Methane by Molecular Oxygen over Supported V_2O_5 Catalysts: A Catalytic and *in situ* Raman Spectroscopy Study"
   Q. Sun, J-M. Jehng, H. Hu, R. G. Herman, I. E. Wachs, and K. Klier, In "*Methane and Alkane Conversion Chemistry*", M. M. Bhasin and D. N. Slocum Eds. Plenum Publishing, (1995).
10. "Genesis and Stability of Silicomolybdic Acid on Silica-Supported Molybdenum Oxide Catalysts: *In situ* Structural-Selectivity Study on selective Oxidation Reactions"
    M. A. Bañares, H. Hu, and I. E. Wachs, *J. Catal.* Submitted.
11. "^{129}Xe NMR Studies of Silica-Supported Metal Oxide Catalysts"
    V. V. Terskikh, V. M. Mastikhin, V. B. Fenelonov, L. G. Okkel, I. E. Wachs, and H. Hu, *J. Chem. Soc., Faraday Trans.*, Submitted.